Universitat de les Illes Balears

DOCTORAL THESIS
2019

B_{12}-RIBOSWITCH FROM *KLEBSIELLA PNEUMONIAE* AS TARGET FOR NEW ANTIBIOTICS. INTERACTION STUDY WITH NATURAL AND SYNTHETIC ADENOSYLCOBALAMIN DERIVATIVES.

Joana Palou Mir

Universitat de les Illes Balears

DOCTORAL THESIS
2019

Doctoral Programme in Chemical Science and Technology

B_{12}-RIBOSWITCH FROM *KLEBSIELLA PNEUMONIAE* AS TARGET FOR NEW ANTIBIOTICS. INTERACTION STUDY WITH NATURAL AND SYNTHETIC ADENOSYLCOBALAMIN DERIVATIVES.

Joana Palou Mir

Thesis Supervisor: Dr. Miquel Barceló Oliver
Thesis tutor: Dr. Àngel Terrón Homar

Doctor by the Universitat de les Illes Balears

B_{12}-Riboswitch from *Klebsiella pneumoniae* as target for new antibiotics. Interaction study with natural and synthetic adenosylcobalamin derivatives.

PhD thesis presented by Mrs. Joana Palou Mir to attain the Doctoral Degree in Chemical Science and Technology

Signature

Mrs. Joana Palou Mir

Pollença, February 12, 2019

Universitat de les Illes Balears

Dr Miquel Barceló Oliver, of University of the Balearic Islands

I DECLARE:

That the thesis titles B_{12}-Riboswitch from *Klebsiella pneumoniae* as target for new antibiotics. Interaction study with natural and synthetic adenosylcobalamin derivatives, presented by Joana Palou Mir to obtain a doctoral degree, has been completed under my supervision and meets the requirements to opt for an International Doctorate.

For all intents and purposes, I hereby sign this document.

Signature

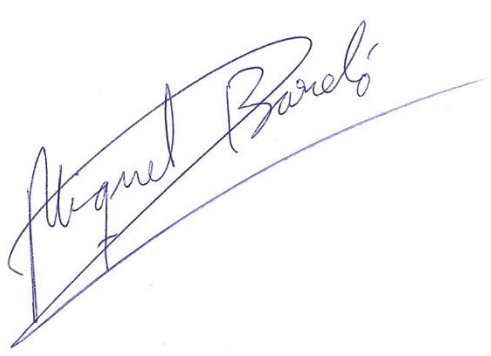

Palma de Mallorca, February 12, 2019

My special thanks go to

Prof. Dr. Miquel Barceló Oliver to give me the opportunity to work and discover the “RNA world”. It has been a good opportunity to gain new skills related with the molecular biology completely unfamiliar at the beginning. I would also like to thank for his help and compression when it was needed in both scientific and personal advice.

Prof. Dr. Roland Sigel from University of Zürich for his inestimable support and giving me the opportunity to be part of the SF lab on two different occasions. I really appreciate the advices given and the good collaboration during all the project.

I would also like to thank all the Chemistry department and SCT of the Universitat de les Illes Balears for the support given to our research and for making all the facilities and equipment available. Furthermore, I would specially like to thank all the Bioinorganic Chemistry area for sharing labs, time and experiences with me.

I would also like to thank:

Prof. Dr. Angel Terrón, thanks for sharing all your knowledge, for your willingness to help in both academic and personal issues and for your cultural chats during the coffee breaks.

Prof. Dr. Angel Garcia Raso, thanks you for your advice with the separation process of the descobaltocobalamin derivatives and your help in the interpretating NMR spectra and for your funny stories.

Prof. Dr. Juan Jesús Fiol thanks for giving the opportunity to teach your students the Protein Data Bank Seminar and for your concise but helpful words when were needed.

Prof. Dr. Antoni Frontera thank you for trying to cheer me up in the difficult moments and in this last period pushing me to write the thesis as soon as possible. Moreover, thank you for all the work done in the English correction of this manuscript.

To all the undergraduate students that have been collaborating with our group during this period, doing their final degree project, that are included as part of this thesis:

Mateu Salom and Xisca Armero Adrover, which collaborate with the initial ITC experiments; Maria Olivia Shweiss who did a hard work with the fluorescence studies and gave me lots of moments of laugh, stories and shared experiences. I would like to thank Marina Bosch Picornell her task with the purple sulphur bacteria, preparing litres and litres of culture and her patience with the chromatographic columns.

Also, thanks to Marc Servera Caldentey for his work done in the ITC during his final degree project and the synthesis of the vitamin B_{12} derivatives done during his master thesis. Maribel, thank you for sharing the lab with me for a little period, introducing me into Yoga and all the laugh and hikes. Yannick, thanks for your constant company, yours pursues along the corridor were not always necessary … but thanks for having always a topic for a chat, music to play on the computer or a joke to make me laugh.

Finally, I would also like to thank Sergi the litres of water brought to the lab with our shared “son” and your jokes, and to Antonia’s reprimands when the lab litters were full.

Thanks to all the SF lab members who have shared with me chats, science discussions, meals and barbeques in May 2014 and summer 2017. I would specially like to thank Dr. Erica Fiorini who introduce me in the protein synthesis and to Dr. Anastasia Musiari who helped me in all the in-line probing experiments. Then, thanks to Dr. Sofia Gallo for teaching me how to work in the radiolab and for all recommendation done during the project. Fabio Amadei, thank you for

making the radiolab more pleasant with your music and to cheer me up when the RNA band was disappeared. And, Elena Alberti, it was a pleasure sharing the lab and the nervous of the last part of your PhD with you.

Family and Friends, thank you so much, without your emotional support my PhD would not have been possible.

I would like to thank my “Chemistry family” which has become bigger along the years. Thank you to the oldest members of the family who started the way with me in the degree: Àngel, Coloma, Espe, Joana, Marga Ferriol, Marga Tortella and Sandra. Also thank to the new member of the family who have been incorporated along the way: Yannick, Maria Barceló, Maria Olivia, Maribel and Marina. Thank you for being there all this time, sharing laughs and a lot of tupper meals.

Espe, thank you so much for sharing this long trip with me. Thank you for all the hours shared in the car, scientific and personal advices, sharing experiences, worrying, laughs and cries, chat from our balcony... Also, thanks for your help in technological critical moments. Joana and Marga, thank you for encoraging me and to be always ready for a dinner or a party in order to give a rest to the brain.

Clara and Laura, thank you because you always have listen me in the difficult moments and you always have found a spot in your diary for a coffee or a walk.

Lastly, but not less important, thanks to all my family for bearing with my bad temper when experiments were not going as expected and giving support to my decisions, although in some cases implied being away from you. Thank you to Xisco and Silvia, Mum and Dad, for encouraging me, without your emotional support I would left the travel on half way. And, Jordi, you have been a very important part of the thesis and the best conclusion I have reached.

Especial gràcies a:

Prof. Dr. Miquel Barceló per haver-me donat l'oportunitat de fer feina i descobrir l'"RNA world". Ha estat una bona oportunitat per adquirir noves habilitats i conèixer tècniques relacionades amb la biologia molecular que eren totalment desconegudes per a mi al principi. També agrair l'ajuda i comprensió rebuda, tan a nivell científic com personal.

Prof. Dr. Roland Sigel de la University of Zürich per el seu suport inestimable durant tot el projecte i per haver-me rebut en dues ocasions al seu laboratori. Agraesc moltíssim els bons consells i la bona col·laboració durant aquest temps.

També agrair a tot el departament de Química i als SCT de la Universitat de les Illes Balears pel suport donat a aquesta recerca i per facilitar-me les seves instal·lacions i equipaments. En especial gràcies a l'àrea de Bioinorgànica per compartir amb mi els laboratoris, temps i experiències.

També m'agradaria donar les gràcies:

Al Prof. Dr. Àngel Terron per compartir tot el seu coneixement amb mi, per tenir la porta del despatx sempre oberta per resoldre qualsevol problema científic o personal i per les xerrades culturals i culinàries dels berenars.

Gràcies també al Prof. Dr. Àngel Garcia Raso per els seus consells amb la columna de separació dels derivats de descobaltocobalamina, la interpretació dels espectres de RMN i les històries gracioses que conta sempre.

Agrair al Prof. Dr. Juan Jesús Fiol haver confiat en mi per a que ensenyés la base de dades Protein Data Bank al alumnes de l'assignatura de Bioinorgànica i per les precises paraules d'ajuda quan han estat necessàries.

Moltes gràcies també al Prof. Dr. Antoni Frontera per animar-me en els moments difícils i sobretot en aquest darrer període per insistir en que escrivís la tesi el més aviat possible. A més, moltíssimes gràcies per tota la feina feta en la correcció d'aquest escrit.

Gràcies a tots els alumnes que han estat col·laborant en el projecte durant tot aquest temps fent els seus treballs final de Grau, que es troben inclosos a aquesta tesi.

Gràcies a en Mateu Salom i na Xisca Armero que van estar treballant en els primers experiments de ITC realitzats amb JP01, gràcies a na Maria Oliva Shweiss per tota la seva tasca feta en els estudis de fluorescència i por tots els moments de rialles, històries i experiències que hem compartit. També vull agrair a na Marina Bosch la seva tasca en el cultiu de bacteris pórpres de sofre i la seva paciència en la purificació per columna.

També m'agradaria agrair a Marc Servera la tasca realitzada en els experiments de ITC durant el seu treball de final de grau i el seu esforç per obtenir altres derivats de B_{12} que s'han usat per fer assajos de fluorescència durant el seu treball final de Màster. Maribel, moltes gràcies per haver compartit amb mi el lab, encara que per poc temps, i també per haver-me introduït al Ioga, per les rialles i les excursions compartides. Yannick, gràcies per la teva constant companyia, les teves persecucions pel passadís no eren sempre necessàries… però gràcies per tenir sempre un tema de conversa, música posada al lab o una broma per fer-me riure.

Finalment també m'agradaria agrair a en Sergi els litres d'aigua que m'ha duit amb el nostre "fill" compartit i a n'Antonia per renyar-me sempre que hi havia les papereres plenes.

Vull agrair també a tots els membres del SF lab amb els qui vaig compartir xerrades, discussions científiques, dinars i barbacoes al maig de 2014 i l'estiu del 2017. M'agradaria agrair especialment a la Dr. Erica Fiorini la seva introducció a la síntesi de proteïnes i a la Dr. Anastasia

Musiari la seva ajuda en els primers experiments de in-line probing. Després, agrair també a la Dra. Sofia Gallo haver-me ensenyat a fer feina al Radiolab i per totes les recomanacions que ens ha fet durant tot el projecte. A Fabio Amadei li don les gràcies per haver fet el radiolab més agradable amb la seva música i per haver-me animant quan la banda d'ARN era inexistent i finalment, gràcies a la Dr. Elena Alberti per haver compartit el laboratori amb mi durant uns mesos i els nervis de la darrera part del seu doctorat.

I com no, moltíssimes gràcies a vosaltres, família i tots amics, ja que sense el vostre suport emocional aquesta tesi tampoc hauria estat possible.

Començaré per la "família de químics" que ha anat sumant membres durant els anys. Aquells que vareu començar el recorregut amb mi durant la carrera, Àngel, Coloma, Espe, Joana, Marga Ferriol, Marga Tortella i Sandra, moltes gràcies pel vostre recolzament, sempre heu fet que segueixi endavant i no tiri la tovallola.

Per altra banda hi ha hagut una sèrie de químics que vos heu anat incorporant durant el camí. Yannick, Maria Barceló, Maria Olivia, Maribel i Marina gràcies per estar al meu costat durant la darrera etapa, compartir rialles i molts de dinars de tuppers.

Espe, moltíssimes gràcies per compartir aquest llarg camí amb mi. Gràcies per totes les anades i vengudes amb cotxe, els teus consells científics i personals, compartir experiències, preocupacions, rialles i plors, les xerrades pel balcó... Agrair-te també l'ajuda en els moments de crisi informàtica. Joana i Marga, moltes gràcies pels ànims, per les sortides i bauxes organitzades per alliberar la ment.

Clara i Laura, moltes gràcies per escoltar-me en els moments difícils i per trobar sempre un buit a l'agenda per anar a posar la ment en blanc amb un cafè o una passejada.

Per últim i no per això menys important, a TOTA la meva família per haver suportat el mal humor en els moments difícils i fer-me costat en totes les decisions preses, encara que a vegades suposaven allunyar-me de vosaltres un temps. Xisco i Silvia, Papa i Mama, gràcies per haver estat al meu costat, sense el vostre suport ho hagués deixat a mig camí. I Jordi, has estat una part molt important d'aquesta tesi, la millor conclusió a la que hagues pogut arribar.

Publication list

Palou-Mir, J.; Musiari, A.; Sigel, R.K.O.; Barceló-Oliver, M.Characterization of the full-lenght btuB riboswitch from Klebsiella pneumoniae. *Journal of Inorganic Biochemistry* **160**, 106-113 (2016).

Barceló-Oliver, M; Palou-Mir, J. Coenzyme B_{12} riboswitch from Klebsiella pneumoniae: an ITC and in-line probing combined study. *Journal of Biological Inorganic Chemistry,* **19**, S769-S770, (2014).

Acronyms list

% I	Inhibition percentatge
5'-UTR	5' untranslated region
A	Adenine
Abs Max	Maximum Absorbance
Abs Min	Minimum Absorbance
Ado	Adenosyl
Ado-Cbi	Adenosylcobinamide
AdoCbl	Adenosylcobalamin, coenzyme B_{12}
APS	Ammonium persulfate
aqCbl	Aquocobalamin
AROs	Antibiotic-resistant organisms
ATP	Adenosine triphosphate
AU	Absorption units
C	Cytosine
ca.	Circa
calc.	calculated
c-AMP-GMP	Cyclic adenosine and guanosine monophosphate
Cbi	Cobinamide
Cbl	Cobalamin
CDC	Centers for Disease Control and Prevention
c-di-AMP	Cyclic di-adenosine monophosphate
c-di-GMP	Cyclic di-guanosine monophosphate
CNCbl	Vitamin B_{12}, Cyanocobalamin
CRISPR	Clustered Regulatory Interspased Short Palindromic Repeats
Dmbz	5,6-dimethylbenzimidazole
DNA	Deoxyribonucleic acid
EDTA	Ethylendiamintetracetic acid
exRNA	Extracelular ribonucleic acid
FIS	Fluorescense intensity signal
FPLC	Fast Protein Liquid Chromatography
G	Guanine
GlcN6P	Glucosamine-6-phosphate
GTP	Guanosine triphosphate
HC	Haptocorrin
HEPES	2-[4-(2-hydroxyethyl)piperazin-1-yl]ethanesulfonic acid
HESI	Heated electrospray ionization
HPLC-HRMS	High performance liquid chromatography-high resolution mass spectrometry
IF	Intrinsic factor
IL	Internal Loop
IMP	Inosinate, Inosine monophosphate
IPTG	Isopropyl β-D-1-thiogalactopyranoside
iRNA	Interference ribonucleic acid
ITC	Isothermal titration calorimetry

J	Junction
Ka	Association constant
KD	Dissociation constant
L	Loop
LB	Lysogeny Broth
Me	Methyl
MeCbl	Methylcobalamin
miRNA	Micro ribonucleic acid
Moco	Molybdenum cofactor
MOPS	3-morpholinopropane-1-sulfonic acid
mRNA	messenger ribonucleic acid
MS	Mass Spectrum
MWCO	Molecular weight cut-off
NCBI	National Center for Biothechnology Information
ncRNA	non-coding ribonucleic acid
Cbi	Neocobinamide
NiCo	Nickel and cobalt
nt.	Nucleotide
OD	Optical dispersion
P	Base paired region
PAGE	Polyacrylamide gel electrophoresis
PCR	Polymerase Chain Reaction
piRNA	Ribonucleic acid associated with Piwi proteins
PNK	Polynucleotide kinase
$PreQ_1$	Prequeuosine-1
RBS	Ribosome Binding Site
RNA	Ribonucleic acid
RNP	Ribonucleoprotein
rRNA	Ribosomal ribonucleic acid
SAH	S-adenosylhomocysteine
SAM	S-adenosylmethionine
SD	Standard deviation
SDS	Sodium dodecyl sulfate
siRNA	Small interfering ribonucleic acid
snoRNA	Small nucleolar ribonucleic acid
snRNA	Small nuclear ribonucleic acid
T	Thymine
TCII	Transcobalamin II
THF	Tetrahydrofolate
Tm	Melting temperature
TEMED	Tetramethylethylenediamine
tmRNA	Transfer-messenger ribonucleic acid
TPP	Thiamine pyrophosphate, vitamin B1
tRNA	Transference ribonucleic acid
TXN	Transcription
U	Uracyl

ULB	Urea loading buffer
UroIII	Uroporphyrinogen
UV	Ultraviolet
vs.	Versus
ZMP	5-amino 4-imidazole carboxamide ribonucleotide
ZTP	5-formamide imidazole-4-carboxamide ribonucleotide

Summary

Today is known that RNA does more functions than previously thought. Riboswitches are RNA molecules situated in the 5'-UTR (untranslated region), which are able to regulate gene expression via changing the RNA conformation upon interaction with a specific metabolite. These molecules have been postulated as good antibiotic targets as they regulate crucial metabolic pathways. Riboswitches consist of two domains; the aptamer where the metabolite is bound and the expression platform, which is the part that finally causes the gene expression regulation. The most common regulation mechanisms used are the transcription termination and the translation inhibition.

A presumable *btuB* riboswitch sequence has been bioinformatically found in the genome of *Klebsiella pneumoniae* and has been proposed as a B_{12} riboswitch candidate. In our study, in-line probing experiments have been performed in order to validate the sequence as a riboswitch. A RNA conformational change has been observed in the RNA sequence upon interaction with AdoCbl. In the gene-on conformation, the ribosome binding site (RBS) is free and the *btuB* gene can be expressed. In contrast, after the metabolite interaction, the RNA is shifted to the gene-off conformation in which the RBS is masked in a base paired region. This fact proves the sequence as a riboswitch and suggests a translation inhibition mechanism.

Then, thermodynamic parameters have been recorded using the isothermal titration calorimetry (ITC) experiments. Two different constructs were used: MB01 which contain the aptamer (214 nt.) and JP01 carrying both the aptamer and the expression platform (243 nt.). Titrations using AdoCbl as titrant were performed for both constructs at different temperatures ranging from 15 °C to 30 °C. Taking the results together we could say that the RNA-AdoCbl interaction is exothermic and follows a 1:1 stoichiometry. The enthalpy obtained at 25 °C is -119±3 kJ/mol for JP01 and -122.7±0.9 kJ/mol for MB01. These enthalpy values are in consonance with a sum of several weak interactions such as H-bond and π staking. The K_D values for MB01 (770±90 nM at 25 °C) are higher than those obtained for JP01 (530±50 mM at 25 °C) in the entire temperature range. Thus, we can conclude that the presence of the expression platform in JP01 stabilizes the interaction of the *btuB* riboswitch with the AdoCbl.

The inhibition translation mechanism was also proved by coupling the riboswitch to a red fluorescent protein (*mCherry*). The protein synthesis was inhibited after increasing amounts of AdoCbl were added to the culture media.

Recently, there is a growing research interest in ligand analogues that are tested for antibiotic potential through riboswitch inhibition. With the aim to synthetize an antivitamin of Cbl, a culture of *Allocromation vinosum* has been anaerobically grown in a deficient cobalt medium. In these conditions, these purple sulphur bacteria are able to synthetize descobaltocobalamins and their derivatives. After cultivating 900 l of bacteria and collecting their cell pellet, we have been able to extract and purify 4mg of descobaltocobalamin and 2 mg of descobaltocobyric acid.

Resum

Avui en dia es sabut que l'ARN pot fer més funcions de les que inicialment li eren assignades. Els ribocommutadors són molècules d'ARN situades a la regió no traduïda de l'extrem 5' (5'-UTR). Aquestes molècules, després d'interaccionar amb el seu metabòlit específic provoquen un canvi conformacional que és el responsable de la regulació génica. Els ribocommutadors s'han postulat com bones dianes per antibiòtics ja que regulen rutes metabòliques crucials. Els ribocommutadors contenen dos dominis, l'aptamer, que és el lloc d'unió del metabòlit, i la plataforma d'expressió, que és la part responsable de la regulació. Els mecanismes de regulació més comuns són la terminació de la transcripció i la inhibició de la traducció.

Un presumible *btuB* ribocommutador ha estat identificat bionformàticament al genoma de *Klebsiella pneumoniae* i postulat com a ribocommutador de B_{12}. Al nostre estudi, s'han realitzat experiments d'in-line probing per tal de validar la seqüencia com a ribocommutador. Un canvi conformacional a l'ARN ha estat detectat després de la interacció del ribocommutador amb el coenzim B_{12}. An la conformació de gen-on, la zona d'unió amb el ribosoma (RBS) està lliure i el gen *btuB* pot esser expressat. Per contra, després de l'interacció amb el metabòlit, la conformació del ARN passa a ser gen-off, on la RBS forma part d'una regió d'aparellament de bases que impedeix l'accés al ribosoma. Aquests fets proven que aquesta seqüència és un ribocommutador de B_{12} i suggereix que el mecanisme de regulació és per inhibició de la traducció.

Per altra banda, els paràmetres termodinàmics han estat calculats mitjançant valoracions de calorimetria isoterma (ITC). Per a aquest experiment es van usar dues seqüències diferents: MB01 que conté només l'aptamer (214 nt.) i la seqüència JP01 que conté l'aptamer i la plataforma d'expressió (246 nt.). A les valoracions calorimètriques s'ha usat AdoCbl com a valorant i s'han fet mesures en un rang de temperatures d'entre 15 °C a 30 °C per a les dues seqüències. Amb els resultats obtinguts es pot dir que la interacció entre l'ARN i AdoCbl és exotèrmica i segueix una estequiometria 1:1. L'entalpia de la interacció a 25 °C és de -119±3 kJ/mol per JP01 i de -122,7±0,9 kJ/mol per MB01. Aquests valors d'entalpia estan d'acord amb que la interacció és el resultat de la suma d'interaccions febles de tipus enllaç d'hidrogen o d'apilament. Els valors de K_D obtinguts per MB01 (770±90 nM a 25 °C) són sempre més elevats que per JP01 (530±50 mM a 25 °C) a tot l'interval de temperatures. Per tant, es pot arribar a la conclusió que la plataforma d'expressió present a la seqüència JP01 té alguna funció en l'estabilització de la interacció del *btuB* riboswitch amb AdoCbl.

El mecanisme de regulació per inhibició de la traducció ha estat validat fent un acoblament del ribocommutador amb una proteïna fluorescent vermella (*mCherry*), ja que la síntesi de la proteïna fluorescent s'inhibeix quan s'incrementa la concentració de cobalamina al medi de cultiu.

Recentment, la recerca en el camp s'ha centrat en la modificació dels metabòlits que regulen els ribocommutadors, ja que s'han postulat com possibles antibiòtics degut a la inhibició de la funció dels ribocommutadors. Amb el propòsit de sintetitzar una antivitamina de cobalamina, s'ha fet créixer un cultiu d'*Allocromatium vinoum* en condicions anaeròbiques i de dèficit de cobalt. En aquestes condicions, aquests bacteris sintetitzen descobaltocobalamines i els seus derivats. Després de fer créixer 900 l de cultiu i recollir les pellets de cèl·lules, hem estat capaços d'extreure i purificar 4 mg de descobaltocobalamina i 2 mg d'àcid descobaltocobíric.

Resumen

Hoy dia es bien sabido que el ARN lleva a cabo más funciones que las que inicialmente se le asignaron. Los riboswitches son moléculas de ARN situadas en la región no traducida del extremo 5' (5'-UTR). Dichas moléculas, después de interaccionar con su metabolito específico, provocan un cambio conformacional que es el responsable final de la regulación génica y, por ello, han sido postulados como buenas dianas para antibióticos, ya que regulan rutas metabólicas essenciales. Los riboswitches contienen dos dominios, el aptámero, donde se une el metabolito y la plataforma de expresión responsable de la regulación. Los mecanismos de regulación más comunes son la terminación de la transcripción y la inhibición de la traducción.

Un presumible *btuB* riboswitch ha sido bioinformáticamente identificado en el genoma de *Klebsiella pneumoniae* y postulado como riboswitch de B_{12}. En nuestro estudio, se han realizado experimentos de in-line probing para validar la secuencia como riboswitch. Un cambio conformacional del RNA ha sido detectado después de la interacción entre el riboswitch con AdoCbl. En la conformación gen-on, la zona de unión con el ribosoma (RBS) está libre y el gen *btuB* puede ser expresado. En cambio, después de la interacción con el metabolito, la conformación del ARN pasa a ser gen-off en la que el RBS forma parte de una región de apareamiento de bases que impide el acceso al ribosoma. Estos echos prueban que esta sequencia es un riboswitch de B_{12} y sugiere un mecanismo de regulación por inhibición de la traducción.

Por otra parte, los parámetros termodinámicos han sido calculados mediante valoraciones calorimétricas isotermas (ITC). Dos secuencias diferentes han sido usadas: MB01 que continene el aptámero (214 nt.) y la secuencia JP01 que contiene el aptámero y la plataforma de expresión (246 nt.) En las valoraciones calorimétricas se ha usado la AdoCbl como valorante y se han realizado diferentes medidas entre 15 °C y 30 °C para ambas secuencias. Con los resultados obtenidos se puede decir que la interacción entre el ARN y la AdoCbl es exotérmica y que sigue una estequiometria 1:1. La entalpía de la interacción a 25 °C es de -119±3 kJ/mol para JP01 y de -122,7±0,9 kJ/mol para MB01. Estos valores de entalpía concuerdan con el hecho de que la interacción se produce a través de la suma de interacciones débiles, como el enlace de hidrógeno o el apilamiento. Los valores de K_D obtenidos para MB01 (770±90 nM a 25 °C) son siempre mayores que los de JP01 (530±50 mM a 25 °C) en todo el intervalo de temperatures. Por tanto, se puede llegar a la conclusión de que la plataforma de expressión presente en la secuencia JP01 tiene alguna función en la estabilización de la interacción del *btuB* riboswitch con AdoCbl.

El mecanismo de regulación por inhibición de la traducción ha sido validado acoplando el riboswitch a una proteína roja fluorescente (*mCherry*) y, de echo, la síntesis de la proteína fluorecente se inhibe cuando se incrementa la concentración de cobalamina en el medio de cultivo.

Recientemente, la investigación en el campo se ha centrado en la modificación de los metabolitos que regulan los riboswitches, ya que se han postulado como posibles antibióticos debido a la inhibición de la función del riboswitch. Con el propósito de sintetitzar una antivitamina de cobalamina, un cultivo de *Allocromatium vinoum* se ha hecho crecer en condiciones anaeróbicas y de décifit de cobalto. En estas condiciones, estas bacterias sintetizan descobaltocobalaminas y sus derivados. Después de cultivar 900 l de cultivo y recoger las pellets de las células, hemos sido capaces de extraer y purificar 4 mg de descobaltocobalamina y 2 mg de ácido descobaltocobírico.

Table of contents

1. Introduction

1.1. Cobalamin derivatives

Thomas Addison described in 1849[1] the pernicious anemia disease, mostly mortal until 1926 when Minot and Murphy discovered that could be cured by eating raw liver[2]. This finding started the research of the active compound responsible for the cure of this disease. It was not until 1948 when Folkers isolated a red crystalline product, vitamin B_{12} or anti-anemia pernicious factor[3]. The structure of the vitamin B_{12} remained unknown until 1954 when Dorothy Crowfoot solved the X-Ray structure of the most complex vitamin[4]. Simultaneously, Barker isolated another crystalline orange product, the coenzyme B_{12}[5], which structure was also solved by Dorothy Crowfoot in 1961[6]. It was then discovered that the active products *in vivo* were adenosylcobalamin and methylcobalamin. The vitamin product isolated by Folkers although is pharmacologically used, was an artefact of the purification process used. After all these new discoveries, the terms corrinoids and cobalamin were coined to describe this family of compounds.

1.1.1. Cobalamin structure

Cobalamins are octahedral cobalt(III) metal complexes with low-spin d^6 electronic configuration. Cobalamins (Cbl) consist of a central cobalt ion, which is equatorially chelated by the nitrogen atoms of the tetradentate corrin macrocycle and two additional axial coordinating ligands[7]. The corrin nucleus consists of four reduced pyrroles linked by three methylene bridges and one direct bond[8], with a total of 14 π-electrons distributed on the 13 carbon atoms. The macrocycle is essential for the stabilization of the Co(I) oxidation state and the Co-C bond[9], crucial for its biological activity. The periphery of the ring is completely saturated with methyl and different amide groups (see Figure 1). Substitution pattern of the corrin moiety is

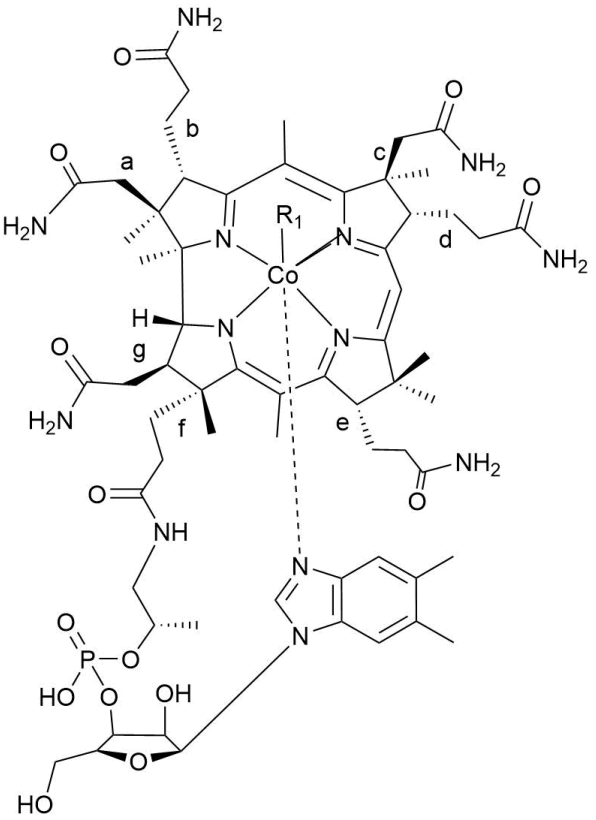

Figure 1.Cobalamin general structure with the Dmbz as apical ligand and all the corrin macrocycle structure.

completely conserved in the naturally occurring B_{12} derivatives. Three acetamide groups (a, c and g) point upward from the corrin plane to the β-site, while the four propionamide side chains (b, d, e and f) point to the α-side[10].

The lower ligand at the α-coordination site is usually an intramolecular 5,6-dimethylbenzimidazole (Dmbz) connected to the f-site chain of the corrin ring via an α-ribazole-phosphodiester moiety[7,11]. When the α-site position is occupied with a ligand linked to the f-chain of the macrocycle, the structure is called base-on. The most common ligand in the α position is the Dmbz, although other ligands such as adenine or modified adenine giving other base-on derivatives have been reported (see Figure 2)[11]. The α-coordination position can be very often filled with a histidine residue of a protein when the coenzyme is attacked at the active site of enzyme, by a nucleobase when interacts with a nucleic acid or even with a water molecule from the solvent. In this case, the cobalamin exhibits a base-off conformation[10,12].

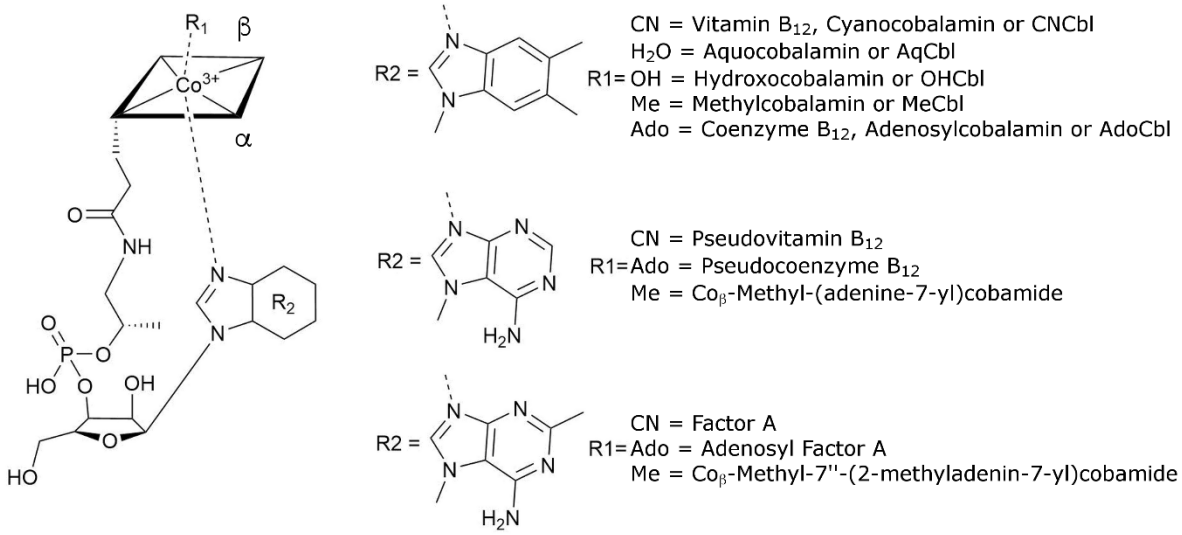

Figure 2. Simplified structure of a cobalamin where R1 and R2 are the ligands changed in the cobalamin families. R2 ligands are Dmbz, adenine and 2-methyladenine while ligand R1 are CN, OH, H_2O, Methyl and 5'-deoxyadenosine.

On the other hand, the coordination ligand of the β-site (upper ligand) is much simpler, ranging from a cyano group to an adenosine (see Figure 2). The AdoCbl and the MeCbl are the active cofactors of the enzymes but they are uptaken and transported as vitamin B_{12}, aqCbl or hydroxoCbl[13].

As mentioned above, a low oxidation state for cobalt is widely stabilized by the σ-donating properties of the macrocycle. This fact allows a rapid substitution of the axial ligand which is exploited in the cofactor B_{12}-dependent enzymatic reactions[9]. In biological systems, cobalamin is found in three oxidation states: i) forming octahedral complexes of Co-(III) (d^6 electrons), ii) square pyramidal complexes are formed when the Co exhibits a Co-(II) oxidation state (d^7

electrons) and iii) square planar complexes in a base off conformation are formed with Co-(I) (d^8 electrons).

The corrinoids are red, red-orange and yellow crystalline substances with an intense absorption band between 300 nm to 600 nm corresponding to the π→π* transition of the corrin nucleus. The intensity of the transitions strongly depends on the apical ligand[8,9]. This family of compounds is soluble in water, stable to heat decomposition but very unstable to light.

Corrinoids lacking of the nucleotide base at the f-chain are called "incomplete" corrinoids which are both natural and artificial B_{12} derivatives as, for instance, the cobyric acid, cobinamide and cobyramide (see Figure 3)[10].

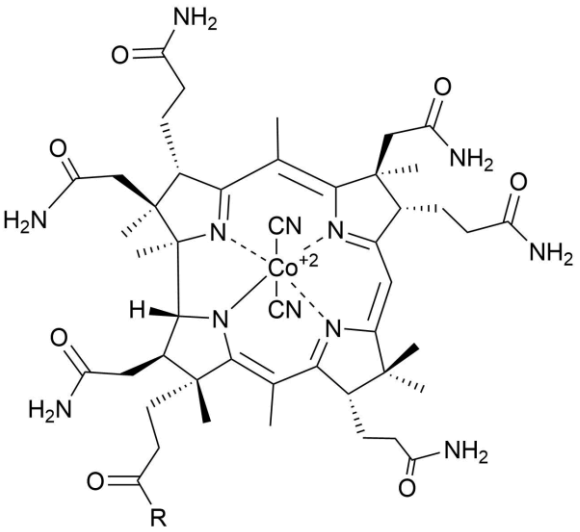

Figure 3. Structure and nomenclature of the incomplete B_{12} derivatives.

1.1.2. Biological function

Due to its nucleophilic characteristic, coenzyme B_{12} and methylcobalamin catalyse isomerization and methyl transference reactions in which the excision and formation of C-C bonds are essential steps. Moreover, the cleavage of the Co-C bond plays an essential role in that reactions.

Organometallic Co-C bond and Cleavage:

A common element of the cobalamin family is the presence of the Co-C bond observed in AdoCbl, MeCbl and other derivatives. The Co-C bond, as mentioned, is stabilized by the corrin macrocycle but can be cleaved in mild acid conditions and by addition of cyanide[14]. Moreover, Co-C is homolytically cleaved after thermo or light exposure[15]. B_{12} derivatives are very light sensitive which complicates their use in biological assays.

Enzymatic functions such as isomerisation, dehalogenation, and methyl transfer rely on the formation and cleavage of the Co-C bond[16,17]. On the one hand, AdoCbl Co-C bond is homolytically cleaved and this process yields the formation of Co(II) species and a 5'-adenosyl radical. On the other hand, MeCbl is heterolytically cleaved yielding nucleophilic Co(I) species[16]. Another heterolytic cleavage of the Co-C has been proposed as the mechanism of heavy metals

detoxification via biomethylation[18]. In this case, the cobalt centre remains as Co(III) and the methyl group is excised as a carbanion. The three Co-C bond cleavage mechanisms are summarized in Figure 4.

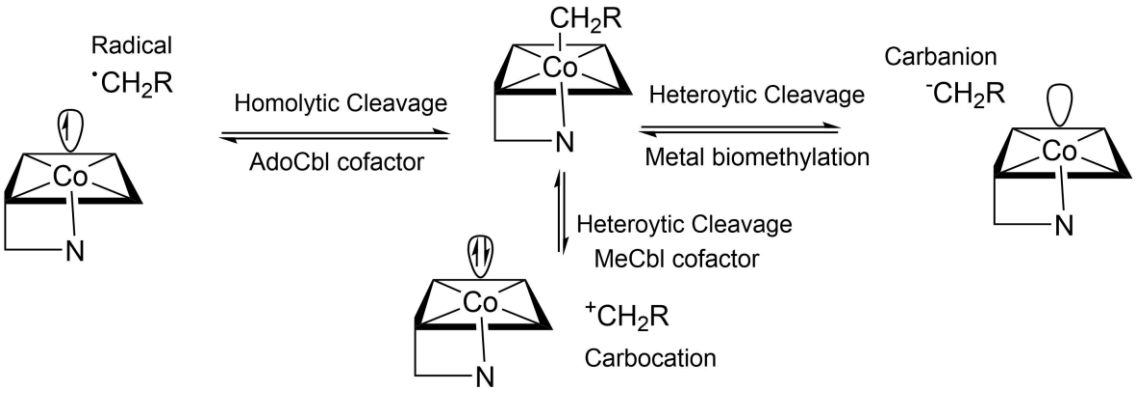

Figure 4. Scheme of the three Co-C bond cleavage possibilities: homolytic cleavage with a radical formation common for the AdoCbl cofactor, heterolytic cleavage with a carbocation formation typical in MeCbl dependent reactions and the heterolytic cleavage with a carbanion formation used for metal biomethylation.

The catalytic activity of the B_{12} depends on the redox chemistry of the cobalt centre. The controlled cleavage of the Co-C bond via the cobalt reduction furnishes highly reactive species and enables this coenzyme to catalyse thermodynamically challenging reactions[16].

Cobalamin enzymatic reactions:

Coenzyme B_{12} and methylcobalamin represent the natural[12] functional cofactors and catalyse rearrangements and methyl transfer reactions[10]. Cobalamins are involved in important processes such as DNA synthesis and regulation, nervous system function and red blood cell formation[16,19].

The methylcobalamin cofactor catalyses the methyl transfer reaction, found in the *methionine synthase*, *methane synthetase* and *DNA-methylase*. The enzyme *methionine synthase* catalyses the methyl transference from the 5-methyl-tetrahydrofolate to the homocysteine, as a result tetrahydrofolate (THF) and methionine are obtained[7]. Thus, a deficit of B_{12} can conduce to a low methionine concentration which is the starting substrate for the synthesis of choline and acetylcholine. These two molecules are involved in the nervous system because they are neurotransmitters. Furthermore, a low concentration of B_{12} causes a low source of THF which is necessary for the purine synthesis, leading to the inhibition of DNA synthesis and cell replication. The inactivation of the *methyltransferase* leads to an insufficient supply of S-adenosyl-methionine and a lack of a proper DNA methylation[12]. Methyl-corrinoids are essential for the formation of methane in Archaea and acetyl CoA synthesis form two CO_2 molecules in autotrophic bacteria[20].

The coenzyme B_{12} is the essential cofactor that catalyses isomerisation, present in the *glutamate mutase*, *methylmalonyl CoA mutase* and *dioldehydrase*. Also, reduction reactions are catalysed by the *ribonucleotide reductase* which is involved in the reduction of the ribonucleotides to deoxynucleotides, essential for the DNA synthesis. The *methylmalonil CoA mutase* enzyme catalyses the isomerization of the methylmalonyl CoA to the succinyl CoA implicated in the degradation of the odd-numbered fatty acids, cholesterol and certain branched-chain amino acid[8,11,12]. For this reason, a deficiency of cobalamin produces a failure of the synthesis of deoxynucleotides and thus, the DNA synthesis and cellular division, and human *mutase* deficiency can produce neuropsychiatric symptoms[11].

In organohalide-respiring bacteria, *reductive dehalogenases* have been found to remove halogen substituents from organic halides. This involves the formation of an halogen-cobalt bond that has been proposed as a new activation mode of the cobalamin-catalysed reactions[21]. Moreover, MeCbl is also involved in detoxification mechanisms via heavy metal methylation[18,20], and a B_{12}-dependent enzyme has been proved to perform the last synthetic step in the Queuosine synthesis, a modified nucleobase present in tRNA[11,22].

1.1.3. B_{12} biosynthesis and chemical synthesis

Although cobalamin is synthesised by Bacteria and Archaea, it is essential to humans in small quantities (1-2µg per day)[9,23]. The correct amounts of vitamin B_{12} uptake depends exclusively on the diet via an elaborate absorption mechanism. Only certain prokaryotes are capable of the *de novo* synthesis of the vitamin B_{12} with an adequate supply of Co[8,24], and Cbls seem to play no metabolic role in plants, fungi or some bacteria.

Biological synthesis

Many authors suggested that B_{12} was synthesized prebiotically and may have been important in the catalysis of the "RNA world". In some bacteria, the biosynthesis begins with an aminoacyl-tRNA molecule, and an RNA molecule is involved in the regulation of the biosynthetic and transport Cbls genes[11].

B_{12} *de novo* synthesis in bacteria[11,13,23]

The B_{12} compound is synthesized from the uroporphyrinogen (UroIII) a common precursor of the heme, siroheme and cobalamin rings. Two distint pathways have been identified to convert the UroIII to the intermediate adenosylcobinamide (Ado-Cbi), which has the fully modified corrin ring with the aminopropanol side-chain added. The main difference between these two pathways is the moment of the cobalt insertion and the oxygen requirements[13,23,25]. *P.*

denistrificants requires molecular oxygen for the synthesis and cobalt is added to the corrin ring at a comparatively late stage. In contrast, *S. typhimurium* and *P. shermanii* are able to synthesize the cobalamin in absence of oxygen and cobalt is added early in the biosynthetic sequence[23]. The *cob* operon contains the genes needed for *de novo* B_{12} synthesis and it can be divided in three major steps[23] (see Figure 5):

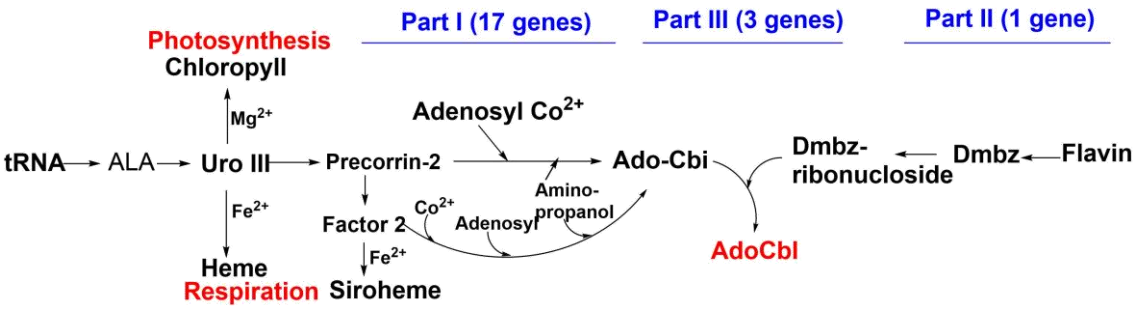

Figure 5. Scheme of the three biosynthetic parts of the AdoCbl.

The first part of the synthesis is the conversion of the UroIII to the Ado-Cbi which consists of at least 20 steps. The cobalt insertion, reduction and adenosylation of the corrin ring occur in this sequence. The methylation and amidation of the periphery of the coring ring are sequentially performed during this synthetic sequence. Several studies have been performed in order to elucidate the peripherical modification sequence of the corrin ring[11,20,23,25,26]. The source of the 1-amino-2-propanol is the threonine which is linked to the cobyric acid intermediate to obtain the Cbi derivative.

The Dmbz is independently synthesized and, although the synthetic pathway remains unknown, it is transformed from a riboflavin precursor. The *CobT* enzyme might also catalyse the ribosyl phosphate transfer.

Finally, the last step is the linkage of the Ado-Cbi and the Dmbz nucleoside. Thus, the aminopropanol group of the Ado-Cbi is activated via phosphorylation followed by a GTP transfer to form Ado-Cbi-GDP catalysed by the *CobU* enzyme. Then *CobS* catalyses the attachment of the aminopropanol activated chain with the Dmbz ribonucleoside at its 3' position yielding the complete AdoCbl[27].

The vitamin B_{12} pharmaceutically used is *in vivo* synthesised using selected bacteria such as *Streptomyces griseus, Pseudomonas denitrificans* and *Propiobacterium freudenreichii* subsp. *Shermanii*[13,23,28].

There are also bacterial species capable, in a deficit of cobalt conditions, to synthesise the organic part of the cobalamin without the metallic atom in the tetrapyrrole centre. The α-(5,6-dimethylbenzimidazole)hydrogenobamide or descobaltocobinamide and the hydrogencobyric

acid or descobaltocobyric acid were isolated from *Chromatiales* bacteria, purple sulphur bacteria such as *Allochromatium vinosum*[29,30], and purple none sulphur bacteria *Rhodopseudomonas spheroides*[31,32].

The uptake of the Cbl into bacterial cells poses two main problems. First, a specific membrane transport system is need due to the cobalamin size, and second, the quantity of compound present in the environment is low, therefore a very high affinity system in needed to enable the Cbl transport to the periplasm.

One system is involved in the Cbl transport across the outer membrane into the periplasm. The *BtuB* transport protein, which acts together with *TonB*, is involved in this first uptake step and presents high affinity for vitamin B_{12} and derivatives including AdoCbl and Cbi. Once bound to the *BtuB,* the Cbl is moved into the periplasm in an energy-dependent manner that requires of the *TonB* protein to drive a proton motive force, which induces the conformational change needed for the transport. The inner membrane transport involves the *BtuC* and *BtuD* proteins, which translocate the Cbl derivatives from the periplasm to the cytoplasm[11].

Both processes, Cbl biosynthesis and transport, are controlled via an RNA sequence that senses AdoCbl and affects both transcriptional and translational regulation of the genes involved, the *cob* operon and the *btuB* gene[11,13].

B_{12} uptake and transformation in Human[7]

Humans depend on diet as B_{12} source and a subsequent uptake and transformation into the cells. Three different proteins are involved in the vitamin B_{12} uptake: intrinsic factor (IF), haptocorrin (HC) and transcobalamin II (TCII). These proteins have a high affinity and selectivity apart from a fast binding kinetics. The combination of the three transporters ensure a high selective transport of B_{12} derivatives.

Once in the cell, vitamin B_{12} is transformed into the active enzyme cofactors AdoCbl and MeCbl. This modification requires the displacement of the β-ligand via homolytic cleavage of the Co-C bond, which is catalysed by the *CblC enzyme*. The cob(II)alamin obtained suffers a subsequent alkylation with ATP yielding the AdoCl. The formation of the MeCbl requeries the reduction to Cob(I)alamin and the methyl group is transferred by s-adenosylmethionine (SAM).

B_{12} chemical synthesis

The chemical synthesis of the vitamin B_{12} has been one of the major challenges of the natural products chemistry. The project was started at the earlies 1960 as a competition between Albert Eschenmoser from the ETH (Switzerland)[33–35] and Robert Burns Woodward from Harvard[36–38].

After four years of hard work, in 1965 both groups came together, and the project was finally acomplished in 1972.

The retrosynthetic scheme of the vitamin B_{12} is shown in the Figure 6. As it can be seen, the first retrosynthetic step is the cobyric acid, since in 1960 Bernhauer demonstrated that the nucleotide chain of the vitamin B_{12} is eliminated via hydrolysis of the amide, and the re-linkage of the f-chain is then possible from the cobyric acid intermediate[39,40]. Hence, the total synthesis of Woodward and Eschenmoser was finished when the cobyric acid intermediate was achieved.

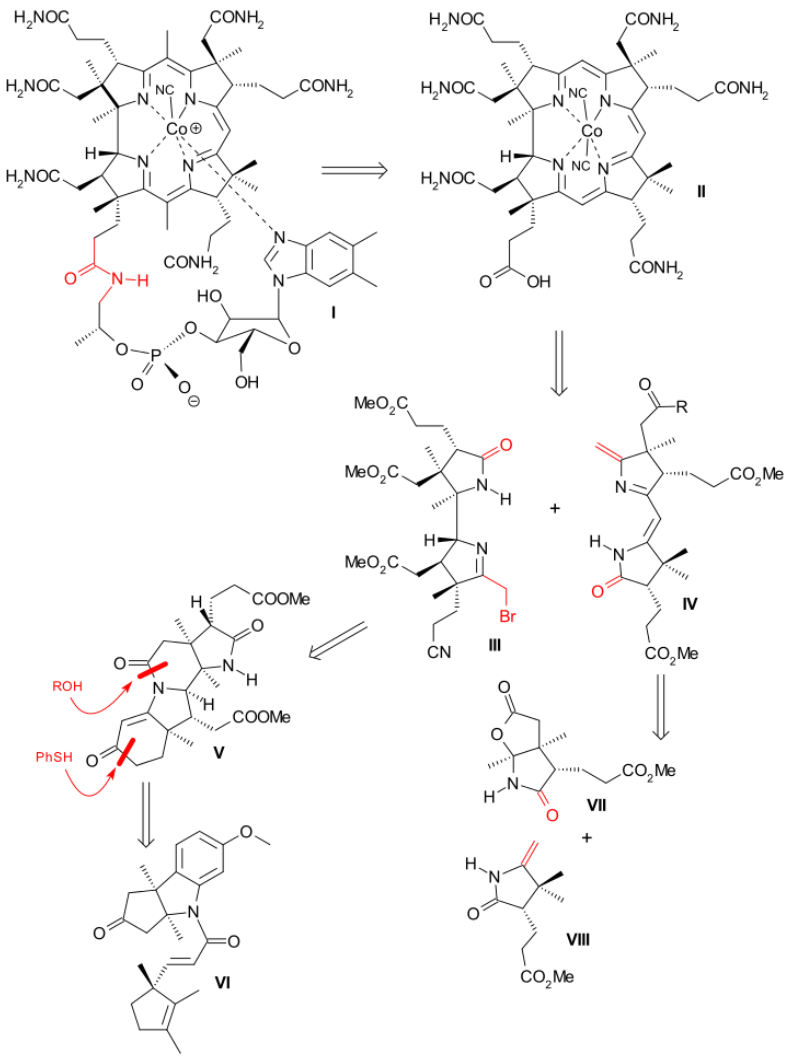

Figure 6. Retrosynthetic scheme (A/B variant) of vitamin B_{12}. I) Vitamin B_{12}: II) Cobyric acid.[a]

In summary, the chemical total synthesis of the vitamin B_{12} was completed in 1972 after more than 10 years of work[10] and more than 70 synthetic steps, in which the Co centre is essential for a correct formation of the corrin macrocycle. It is also important to consider the 9 chiral carbons present in the molecule.

[a] "Vitamin B_{12} retrosynthesis" by V8rik/Dissolution (Rik van der Lingen) is licensed under CC BY-SA 3.0.

1.1.4. Synthesis of derivatives

The synthesis of modified B_{12} derivatives is an active research area as these molecules have been proposed as good cyanide detectors and detoxifying, and their applications in therapy and diagnosis[10]. Also, the design of dysfunctional B_{12} analogues can lead to the development of new classes of antibacterial and antiproliferative agents[9,12].

The high affinity for CN^- of the Co(III) centre of the corrinoids has led to the use of aquocorrinoids for the detection and detoxification of this anion[41,42]. AqCbl is nowadays the most administered pre-clinical antidot for CN^- detoxification[41]. The replacement of the β-ligand by fluorescent moieties has been exploited for investigation of dependent B_{12} enzyme activities and reaction mechanisms as well as to the study of the uptake of the vitamin[43,44] and also in Vitamin B_{12} quantifications[45].

For medical applications, it is very important to consider that the structural changes of the Cbls can affect the binding to the proteins and cell uptake transporter[19]. Modifications at the 5'-OH of the ribose moiety and at the cobalt centre are the best candidates for developing B_{12} derivatives for diagnosis and therapy[7,9,10,19]. A wide variety of modified B_{12}-conjugates have been reported: B_{12} derivatives where the axial ligand has been replaced by inorganic or organic drugs[46–49] (see Figure 7A). The linkage of luminescent molecules at the 5'-OH of the ribose has been explored for the development of luminescent tumour markers[50,51] or drug carriers[19,52,53] (see Figure 7B). The research on antivitamins has been increasing the interest. Antivitamins are defined as compounds that interact with the same receptor as vitamin does but is not able to do the same function thus a different reactivity[7,12,54]. The development of dysfunctional Cbls has focused on the modulation of the redox potential of the cobalt centre by different approaches. The whole f-chain of the corrin moiety has been replaced by a peptide linker with a distinct strength of the intramolecular interaction of

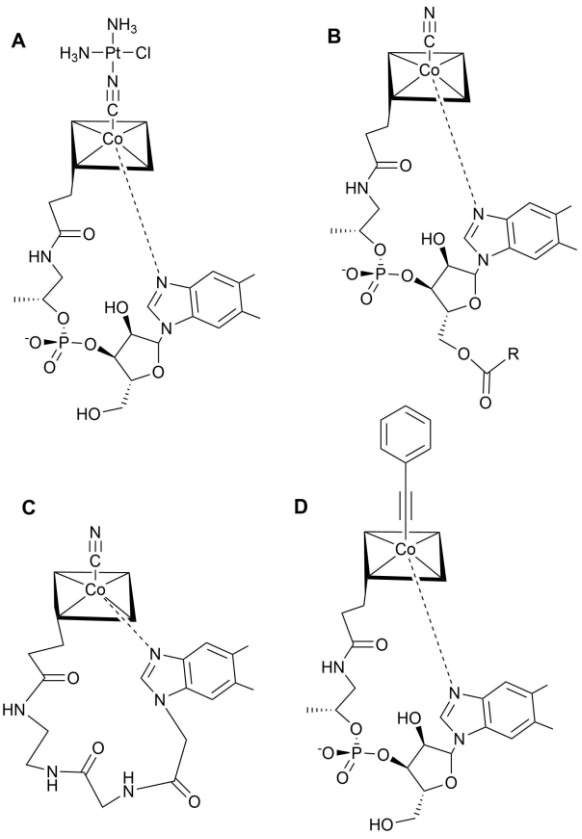

Figure 7. Examples of synthetic derivatives structures. A) ligand replacement by an inorganic drug; B) 5'-OH modification structure; C) f-chain replaced with a peptide linker D) σ-donating ligand as axial ligands.

the Dmbz with the cobalt centre, which has consequences on the redox potential of the complex[9,10,55] (see Figure 7C). B_{12} binding proteins tolerate structural modifications on the β-site, thus modulation of this ligand has also been exploited[9,56]. Strongly σ-donating ligands make the reductive activation more difficult, and analogues with organometallic phenylacetylide and 4-ethylphenyl derivatives have been also reported[9,54] (see Figure 7D). Fluorescent derivatives of cobalamin have been prepared by linking fluorophores to the cobalt centre through a propyl amide spacer, which are suitable for *in vivo* imaging of transcobalamin receptors in cancer cells[56]. Another approach is the linkage of the fluorophore though a cis-platinum bound to the cobalt centre via the cyano group[57].

Finally, in the 70's, after the isolation of the descobaltocobalamins, coordination studies with other metal ions were reported. For instance, zinc and copper derivatives of phenylhydrogenobamide and hydrogencobyric acid, called Currins and Zirrins, were reported by Koppenhagen[58]. Hereafter, analogues of vitamin B_{12} were prepared using the descobaltocobalamins with Zn and Cu. The three compounds were proved to be vitamin B_{12} antimetabolites and supressed the growth of *Lactobacillus leichmanii*[59]. In 1974 Koppenhagen and co-workers, although incompletely characterized, reported rhodium derivates with chloride, water, methyl or 5'adenosyl as apical ligand, whose antiproliferative activity was also tested with *Lactobacillus leichmanii* and *Escherichia coli*[60]. Some of the copper and rhodium derivatives also exhibited an antivitamin effect, competing with the vitamin B_{12} for binding to human transcobalamins[61].

Several strategies to generate metal analogues of the natural corrinoids by removal of the Co centre have been proved without satisfactory results[7,12]. Recently, Kräutler and co-workers reported the synthesis and characterization of the rhodium homologue of coenzyme B_{12} using a combined methodology: the descobaltocobyric acid was biologically synthesized and metal core and axial ligands were chemically introduced[24]. Adenosyl-rhodium-cobalamin has been found to be inactive in the *methionine synthase* and in the dependent *diol dehydratase*s. More surprisingly, crystal structure revealed a better fit of rhodium in the corrin ring in comparison to cobalt[24].

As mentioned before, the light-stability of the Co-C bond has been a handicap in the use of this compound in biological assays. Thus, investigations focusing on the synthesis of light-stable coenzymes have also been reported[54,62,63].

1.2. Central dogma of the Biology

The central dogma of the Biology was postulated by Prof. Dr. Francis Crick in 1958[64] and it can be summarized as: the genetic information only can be stored as DNA, copied in RNA molecules which are an intermediate stage for the final gene product, the proteins[65,66] (see Figure 8).

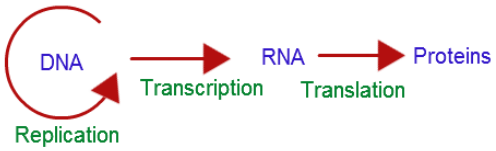

Figure 8. Scheme of the central dogma of the biology.

However, this dogma has always been in question. Nowadays, it is known that some viruses store the genetic information as RNA molecules, that RNA does much more functions than translate information into proteins, and that there are enzymes able to synthesize DNA from an RNA template. All these new discoveries considered together imply a limitation to the dogma postulated by Prof. Dr. Francis Crick.

As it has been delved deeper into the study of eukaryotes, large amounts of non-coding genes have been discovered, as well as different splicing mechanisms and introns or exons identificated. Also, non-coding information found in the DNA genome is transcribed in non-coding RNA that handle different functions, which have opened a new and wide research field.

1.3. RNA architecture and motifs

RNA polymer is constructed by combination of only four different monomers, composed of different bases, the same sugar and phosphate. The combination of these four pieces in distinct conformation allows RNA molecules to exhibit different and complex secondary and tertiary conformations[67] that can lastly be correlated with a wide spectrum of functions. Determining the conformation and stability of RNA secondary and tertiary structures will provide a better understanding of their functions[68]. The presence of a given structure not only depends on the RNA sequence, also temperature and environment are important, therefore knowledge of thermodynamics of the structure is crucial.

1.3.1. RNA monomers, conformations and base interactions.

Nucleic acids, both DNA and RNA, are long biopolymers built as linkage of nucleotides, each composed of a sugar, a phosphate and a nucleobase.

In RNA, four bases built up all different sequences, two of them are purine derivatives, adenine (A) and guanine (G) and the other two are derivatives of pyrimidine, cytosine (C) and uracil (U). This latter, U is the substitute of the DNA thymine (T) during transcription. In each case, N(9) of a purine or N(1) of a pyrimidine is bound to C(1') of the ribose, which is the sugar present in the RNA backbone. The formation of the N-glycosidic bond between the base and sugar give rise to the unit known as nucleoside. A nucleotide is formed when one or more phosphate groups are joined to a nucleoside via a phosphodiester bond. The natural esterification site is the -OH group of ribose C-5' (see Figure 9a).

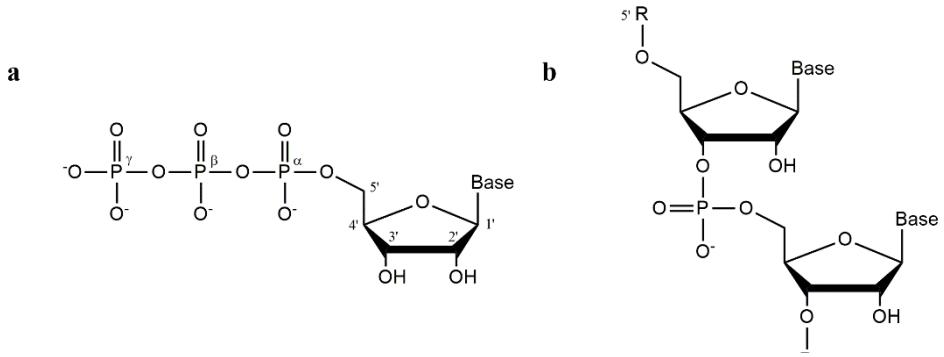

Figure 9. a) Representation of a nucleotide with the ribose link to a base via C-1' and a triphosphate at the O-5'.b) Representation of two nucleotides bond via the phosphodiester bonded. Phosphate group in the 5' position reacts with the 3'-OH group of the next nucleotide so that elongation always run from the 5' to the 3' end.

Sugars in the nucleic acids are linked together through phosphodiester bridges. The 3'-OH group of the sugar moiety of the 5' nucleotide is esterified to a phosphate group of the 3' nucleotide, linked to the 5'-OH of the sugar (see Figure 9b). In this manner the RNA backbone is elongated in the 5' to 3' direction. In addition, due to the presence of the 2'-OH, a 2' to 5' linkage is possible which is involved in the removal of introns and the joining of exons for the formation of mature RNAs[69,70]. The combination of the four nucleotides in a different manner define the primary structure. Then, these single stranded molecules are folded into secondary and tertiary structures where H-bond interactions between bases, different sugars or base conformations, and metal ions interactions play an important role.

The ribose ring can exhibit two pucker, C(2') endo and C(3') endo, conformations (see Figure 10)[71]. A pentose forms a ring with five atoms and at least one of them must be out of the plane. In the C(2') endo pucker, the C(2') atom lies out of the plane on the same side as the base putting apart the two phosphate groups (7 Å). On the other hand, in the C(3') endo pucker, the C(3') atom is the one out of the plane at the base side and phosphate groups are much closer to each

other (5,8 Å). The van der Waals crowding effect, due to the ribose 2'-OH, stabilizes the ribose into the C(3') endo pucker. In the C(3') endo configuration there is an adequate separation between C(2') and C(3') oxygen atoms, while a van der Waals crowding occurs if the ribose is in the C(2') endo pucker conformation. Therefore, RNA molecules are usually found in C(3') conformation. An energetic barrier prevents a pucker change in the RNA double helix and thus justifying the lack of flexibility in the backbone in comparison with the DNA backbone, where the pucker change of deoxyribose is energetically more favourable[70].

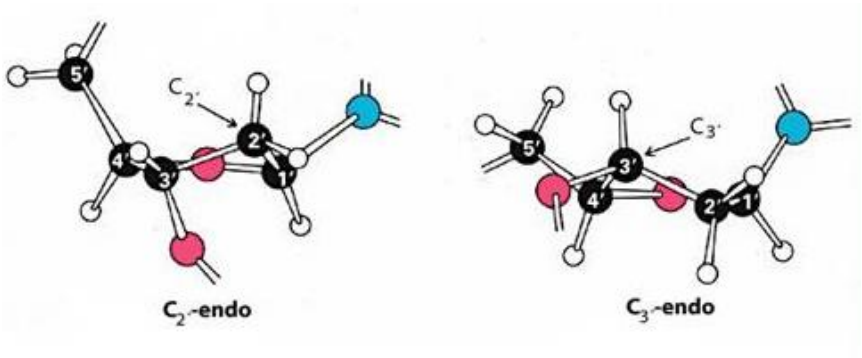

Figure 10. Sugar pucker conformation C2'-endo and C3'-endo[72].[b]

There are small conserved structures often observed as component of motifs or in isolation. The so called structural elements may be observed in several types of motifs, normally implying two or three elements and lack of a characteristic sequence[73]. The U-turns are sharp bends in the backbone with a characteristic staking of the second and third nucleotides present in hairpin and internal loops, while S-turns are two consecutive bends in the backbone where an inverted sugar pucker is observed.

Lots of other structural elements are formed by non-Watson-Crick interactions as A-minor interactions where adenine flips outside a helix and interacts with neighbouring helices, interactions between two coplanar residues forming a dinucleotide platform, and if an additional nucleotide interacts, a base triplet can be formed. Cross-strand stacks can also occur when a base stacks on a base on the opposite strand instead of stacking with adjacent bases on its own strand. The presence of non-canonical base interactions are very important in the folding and RNA structure elements formation. For this reason, several base paring nomenclatures and databases have been developed[73,74]. For their importance and abundance in RNA structures, non-Watson Crick bases pairs will be further emphasised and analysed below.

[b] "DNA sugar puker" by H.M. Sobell is licensed under CC BY 4.0

In large RNA molecules, H-bonds are essential for building up structural motifs and the final functional three-dimensional structure. Contrarily to DNA, large fractions of base interactions are non-canonical Watson-Crick base pairs. Each nucleobase possesses three edges (see Figure 11). The Watson-Crick edge, the Hoogsteen or "C-H" edge and the sugar edge, which involves the 2'-OH group. Two nucleobases can interact with each other via any of the edges, besides, every nucleobase can be in *syn* or *anti* respect to the sugar, leading to 12 distinct families with 168 matching possibilities[75,76]. Even more base triplet possibilities have also been observed such as a stable G·G·A arrangement[65].

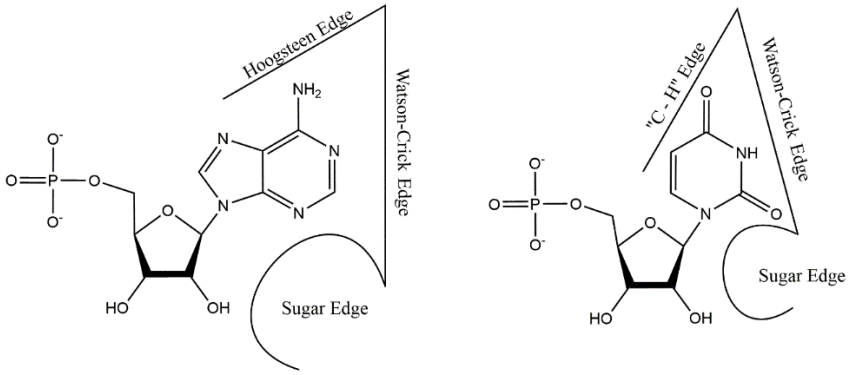

Figure 11. Interaction edges of purine and pyrimidine nucleobases.

Standard Watson-Crick interactions AU and GC represent only 50% of the base paring in large RNAs. The GU wobble base pair is the third most common base pair. The sheared GA pair, AU Hoogsteen, UU wobble and GA Watson-Crick-like pairs are also in high abundance. These seven distinct pairs mentioned represent 90% of the base pairs formed in RNAs[77] (see Figure 12). These pairs are predominant in specific regions: the AU Hoogsteen pair stands out in terms of its intercalative properties and a rare presence between dinucleotide steps. The GA Watson-Crick-like pair as well as the GU wobble pair have a predominant presence in flanking nicks (break in a covalent link between stacked base pairs) in helical domains. Moreover sheared GA pair exists at the ends of helical domains and the UU wobble pair seems to be unable to stack at the end of duplexes. The Watson-Crick GC pairs are more appropriate than AU pairs to terminate helical fragments possibly due to their higher stability. Sequence analysis reveals that non-canonical base pairs have higher stacking affinity with canonical GC and AU pairs rather than with other non-canonical pairs[77].

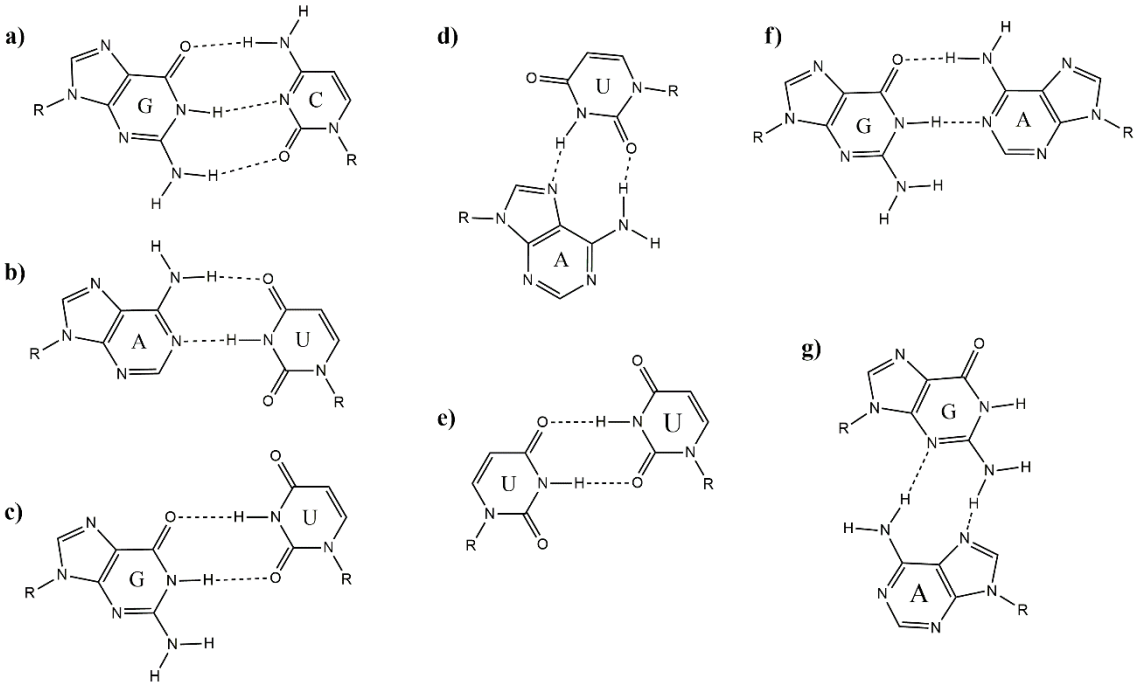

Figure 12. Base pair interactions more abundant in RNA structures; a) and b) canonical Watson-Crick interactions GC and AU; c) wobble GU pair; d) Hoogsteen AU pair; e) wobble UU pair; f) Watson-Crick-like GA pair; g) sheared GA pair[78].

1.3.2. Metal ions in RNA stability and folding

Considering RNA as a polyanion, it seems to be obvious that there is an energetic barrier for the formation of compact structures, and that it needs the presence of a counter-cation. RNA molecules are always associated to certain metal ions which are highly abundant in cells, being the most abundant Na^+ (4,6g/kg bacterial cells), K^+ (115 g/kg bacterial cells), Ca^{2+} (5,1 g/kg bacterial cells) and Mg^{2+} (7 g/kg bacterial cells)[79]. The possitive ions are needed to stabilise, fold and compact the molecule, and frequently they are involved in catalysis.

In RNA folding, negative charges come close, the unspecific binding of monovalent ions (such as Na^+ and K^+) allows the formation of secondary structures while ternary interactions need the specific binding of metal ions with higher valency that are highly directional in the space[80,81]. These metal ions can interact with RNA in several ways: non-specific charge screening ions (diffuse), electrostatically located ions and inner or outer-sphere coordination site bound ions.

The monovalent ions are responsible of the preorganization of the RNA and they are bound to the backbone non-specifically, neutralizing the phosphate negative charge as the main role[82,83]. These abundant diffuse ions remain hydrated and interact with RNA via long range electrostatic interactions. Ions can also interact with RNA surface indirectly via hydrogen-bonding between the first hydration layer[80]. Mg^{2+} is not always essential to stabilize RNA tertiary contacts. Moreover, the RNA can be sensitive to monovalent ion size[84]. Even if monovalent ions are

present in higher concentration, only half Mg^{2+} ions are need to neutralise the same amount of charge[85].

In case of divalent metal ions, the magnesium is the most commonly involved, and it is particularly efficient stabilising compact structures[85]. The Mg^{2+} clamps are formed when Mg^{2+} can interact electrostatically with the adjacent phosphate group of the backbone which is the most common mode of bidentate chelation of Mg^{2+} in RNA. These Mg^{2+} ions bridging two phosphate groups produce a backbone constrain and local rigidity[79,83]. On the other hand, specific metal ion binding sites with high affinity are also required for RNA molecules to fold into the ternary and functional conformation as it has been identified in the T box antiterminator[86]. In riboswitches, Mg^{2+} can facilitate or be necessary for the interaction with the ligand due to the produced pre-folding[87,88]. Furthermore, Mg^{2+} is the most catalytically active cofactor, taking part in the acid-base catalysis found in the active site of ribozymes and ribosomal RNA, catalysing the peptide bond formation, and the transesterification and hydrolysis of the phosphodiester[89]. When a Mg^{2+} is coordinated to a phosphate oxygen, the phosphorous is activated for nucleophilic attack, thus Mg^{2+} increases the rates of RNA hydrolysis[83].

1.3.3. RNA motifs

An RNA motif can be defined as a discrete sequence or combination of base juxtapositions, found in naturally occurring RNAs in unexpectedly high abundance[90]. The different sugar conformations and the distinct base pair possibilities exposed in the previous section 1.3.1 allow RNA to exhibit a wide range of secondary and tertiary structures. It is important to keep in mind that RNA molecules and their structural elements are dynamic and mobile: base pairs can be formed and broken reversibly. Also, base paired regions and helices can be bent and flexed. RNA structural motifs may be bound to water or ions to support their conformations[73].

Structural studies and sequence comparison suggest that RNAs are modular, composed of conserved motifs of secondary and tertiary structure such as: helices, loops, junctions, pseudoknots, mismatches and bulges[68,73,90,91,92,93] (see Figure 13). These motifs are likely to be crucial to both biological function and three-dimensional structure[91], but it is often necessary for individual building blocks of RNA to condense into tertiary structure with the formation of long-range tertiary interactions[93].

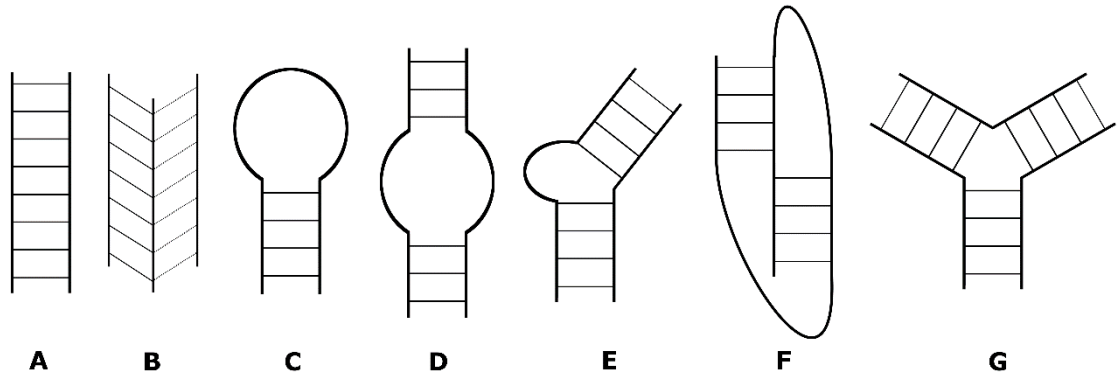

Figure 13. Schematic representation of the RNA common motifs; A)double-stranded helices; B) triple stranded region; C) hairpin loop; D) internal loop; E) mismatched region; F) pseudoknot; G) three way junction.

Double-stranded helices

RNA molecules have at least 50% of their bases in double-stranded helices, as many of their functions require a compact structure. Double-stranded regions in RNA adopt an antiparallel right handed helical conformation, with Watson-Crick base paring leading to an A-form helical geometry, which are the most abundant in RNA natural molecules[73]. In this A-RNA helix, interactions between 2'-OH group and the 4'-O of the next residue play an important role. Sequences of alternating GCGC form left handed Z-form helices.

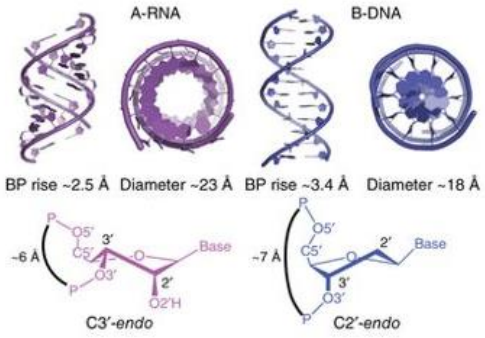

Figure 14. Above comparison between A-RNA form and B-DNA form. Channel in the helix centre can be observed. Below the 3'endo and 2'endo sugar pucker where interphosphate distances are depicted[94] [c]

The C(3') endo sugar pucker adopted by the nucleotides is a distinguishing feature of the A-form helix. This sugar pucker is associated with an interphosphate distance of 5.8 Å, while the interphosphate distance in B-form helices with a C(2') endo sugar pocket is about 7 Å[70,71] (see Figure 14). The A-form helix formation needs about 11 base pairs per turn and the base pairs are displaced towards the minor groove. In this helix form, major groove is very deep and narrow, and the minor groove is wide and shadow, bases are not perpendicular to the helix,

[c] Zhou, H. *et al.* m1A and m1G disrupt A-RNA structure though the intrinsic instability of Hoosteen base pairs. (2016).*Nat. Struct. Mol. Biol.* **23,** 803–810 by permission of Oxford University Press

widening the structure and leading to the formation of a channel in the helix center[65] (see Figure 14).

Hairpin loops

This motif results when a single strand folds to form a double stranded region, leaving some bases unpaired and linking the 3' and 5' ends of a double helix. Hairpin loops are closed by Watson-Crick interactions. The smallest hairpin loop identified has two unbounded bases and the largest may contain about ten unbounded bases. NMR as well as X-ray studies show a 3'endo conformation both in the loop and stem.

Tetraloops are the most common hairpin loops and the most stable sequences are GNRA and UNCG (where N is any nucleotide and R is any purine)[92]. These two tetraloops families have their similarities and all of them present a non-canonical base pair closing the loop. Furthermore, tetraloops are stabilised by: i) internal stacking interactions between nucleobases in the loop; ii) base-phosphate hydrogen bonds and iii) base-ribose hydrogen bonding so, in this case, 2'-OH group plays an important role in the structure and loop stability. RNA A-form helices usually have sugar in 3'endo conformation. On the contrary, in tetraloops the two middle nucleotides exhibit predominantly 2'endo conformation that, in turn, allows to reverse the strand direction in just two nucleotides. Tetraloops of the GNRA family are frequently used in the tetraloop-tetraloop receptor interactions.

Mismatches and Internal loops

Mismatches are an inclusion of residues that are not Watson-Crick paired in at least one strand of the double helix, which yield the distortions of the double helix that are common at the end of helices. These mismatches are stabilized by non-Watson-Crick base pairing, where the two most frequent are the wobble G·U and G·A.

Internal loops can be classified in symmetric and asymmetric. In symmetric internal loops the same number of bases per strand are involved, while in an asymmetric internal loop one strand involves more bases than the other, leading normally to a bulged base[73].

The distortions produced by mismatches may have an important role in the RNA function, providing a specific binding site for other RNA or proteins. The phylogenetic conservation of these regions sustain the hypothesis. Unpaired adenosines flipped outside the helices are common and have importance in the tertiary RNA folding and in molecular recognition[92]. Also, regions with purine-purine pairs widen the major groove of the RNA, increasing the accessibility of numerous functional groups that may play a role in molecular recognition[93].

Bulged loops contain any number of unpaired nucleotides that interrupt one strand of a continuous double helix. These bulged nucleotides are common in predicted structures of large RNAs and can cause its bending depending on size and sequence. NMR studies point out that bulged nucleotides and surrounding base pairs may have a selective influence on the bulged nucleotide position: the nucleotide can be intercalated in the helix or, by contrast, flipped out of the duplex. These bulges are thought to play an essential role in the protein-binding and adenosine is the most predominant bulged nucleobase.

Pseudoknots

Pseudoknots and knots are defined as base pairing between nucleotides separated by regions of secondary structures. By the broad definition, any tertiary interaction which involves base paring is termed a pseudoknot. For this reason, the definition has been restricted to only base-pairing between nucleotides in a hairpin loop with adjacent single stranded regions. A pseudoknot architecture is composed by two stem regions that may be separated by a single stranded region. There are three different paths in forming the pseudoknot, which differ in orientation of the coaxial stack between the two regions[95].

Pseudoknots are motifs with high capacity for molecular recognition, providing binding sites for protein interaction, transcription and translation regulation[93].

Triple Strand Interactions and Junctions

Whenever a helix and a single-strand or loop are nearby, they can interact to form a triple-strand interaction. These ternary interactions serve to fix the relative orientations of helices and are important in the stabilization of three-dimensional structures.

Junction loops are formed by the interaction of three or more double helices, the more common are the three-way junctions and four-way junctions. Coaxial stacking of the helices is a key feature of junction loops and it may occur opposite to the longer junction strand. These structures are commonly stabilized by bridging nucleotides between helices.

Ribose Zipper

Ribose zipper is a tertiary structure motif which shows a strong sequence *bias*, and is found to link a stem or stem-like region with loop regions[91]. When unpaired RNA strands are in proximity, 2'-OH groups of two consecutive ribose on both strands can interact by H-bonding[90] giving as a result an H-bonding network. The capacity of the OH group to act as both, H-bond donor and acceptor, leads to the formation of four different interactions. This kind of arrangement appears

to be particularly significant when interactions between 2'-OH occur linking residues of different chains[93]. It is also important to highlight that the residues involved in the ribose zipper are found to be phylogenetically conserved[91].

1.4. RNA classification and known functions

RNA has been postulated as the initial molecule in life, used as storage of genetic information before DNA. In the initial studies of the cellular biology in the 50's, RNA was believed of low importance. This molecule was thought to just be a messenger (mRNA) of the information between the nucleus and the cytosol, in fact mRNA is the template for protein translation. In the nucleus, the genes to be expressed are transcribed into mRNA by the *RNA polymerase* and this information is then transported to cytosol, where it is finally expressed and translated into a protein. But in the translation process of the mRNA into proteins, two more RNAs have a key role: ribosomal RNA (rRNA) and transference RNA (tRNA). The rRNA is the major component of ribosomes, present in both subunits, which play an important role in both catalysis of the protein synthesis and structure stability of the ribosome. On another note, tRNA is the molecule in commission of transporting the correct activated amino acid to the ribosome, where the peptide-bond is formed, revealing a catalytic activity of the rRNA in the peptide bond formation. There are 50 different tRNA described as they have an anticodon that needs to be complementary to the mRNA codon to introduce the correct amino acid in the protein sequence.

Today, a wide research field stands around RNA, roles of non-coding RNAs and untranslated portions of mRNAs appear to be far more extensive than originally believed[66]. New functions can be now attributed to this biopolymer. The so-called non-coding RNA are RNA molecules that are not translated into protein, which can perform several functions from transcription, catalysis, RNA maturation, RNA modification to gene regulation[96]. In this definition a wide variety of RNA with different functions can be included: transference RNA (tRNA), ribosomal RNA (rRNA), small nuclear RNA (snRNA), RNA associated to Piwi (piRNA), extracellular RNA (exRNA), small interference RNA (siRNA), micro RNA (miRNA), CRISPR, ribozymes, riboswitches…

The catalytical function can include both, self-cleavage or the cleavage of other RNAs. Examples of RNA with these functions are: the Group I and the Group II introns self-cleavage, ribozymes, RNPzymes and the rRNA role in the protein synthesis[65]. Most genes in eukaryotes present introns that must be removed from the mature RNA, intron removal and ligation of exons occur via an esterification reaction in a massive *ribonucleoprotein* (RNP), the spliceosome[97]. *RNase P* is present in the three kingdoms of life and it is essential for tRNA maturation. MRP RNAs, in contrast, are only present in eukaryotes cleaving the RNA primers needed for the DNA

replication[96]. Telomerase RNA is implicated in the catalysis and retro-synthesis of DNA for the homeostatic maintenance of the telomer length[98].

Gene expression and protein translation can also be regulated at RNA level using, for instance, cis-encoded regulatory elements such as riboswitches. Most of the small RNA act as trans-encoded regulators that can form RNA-protein complexes, mimic other nucleic acids structures or interact via base paring with other RNAs[99,100]. These sRNA molecules play important roles in virulence, antibiotic resistance, bacterial stress response and can also reduce the effectiveness of antibiotic therapies[101], making them important candidates for drug targets. The miRNA are small single stranded sequences of about 20 nt. present in animals and plants that are involved in the regulation of translation, post-transcriptional modifications and degradation of mRNA, development and differentiation of metabolic pathways, oncogenic transformation and the replication of certain viruses[102,103]. Interference RNA (iRNA) are also small single strands in complex with the Argonaute protein family. In this case, RNA serves to guide the complex to the appropriate target due to base pairing. A specific example is RNA associated to the Piwi protein (piRNA), this RNA can either repress gene expression via splicing or activate it by preventing the heterochromatin formation. Moreover, these complexes seem also to be involved in transposons silencing pathways[102,103]. The discovery of small nucleolar RNA (snoRNA) and their classification in two subclasses, one related with the 2'-O-ribose methylation and the other implicated in the pseudouridylation, have underlined the implication of RNA molecules in the post-transcriptional modification mainly of rRNA, tRNA and snRNA[104].

In some bacterial and virus systems ncRNAs are used for defence or survival purposes, RNA is capable of manipulating the host cellular machinery for their own purposes (CRISPR and iRNA). The cluster of regulatory interspersed short palindromic repeats (CRISPR) sequence, formed by a repetition of a sequence linked by a short spacer, are identical to plasmid or viral fragments that allow to base pair with the targets and perform their defence purpose[105]. Although RNA is less immunogenic, viral RNPs have much potential to slip the radar of the host and manipulate its metabolism[106]. Also as temperature sensors, the three-dimensional conformation of an RNA can be destabilized when the temperature is increased leading in a conformational change and lastly a protein expression regulation[107]or a protein synthesis activation when the infection temperature is reached[108]. The discovery of the transfer-messenger RNA (tmRNA) that reflects properties of both tRNA and mRNA has pointed out the job of RNA in the quality control of the protein translation; a tmRNA portion transcribed at the C-terminal of a peptide is enough to direct its degradation[109].

Another artificial function related with medicine is the capacity of specific RNA aptamers to sense proteins which can be correlated with health or disease. This fact opens a wide field of research in the use of RNA as diagnosis agents and also for analysis in samples[110].

1.5. Riboswitches

Riboswitches can be defined as RNAs that control gene expression by binding metabolites without the need of protein factors and that are present in species from all three kingdoms of life[67,111,112]. In general, those regulatory elements are situated in the 5'-UTRs of transcript mRNAs and cis-regulate genes related with transport or synthesis of the metabolite thereof[66,113–117] to avoid wasteful energy expenditure or inappropriate physiological responses[118]. It is suggested that riboswitches represent one of the oldest regulatory systems[114,119]. Bacteria use this mechanism to quantify intracellular metabolite concentration and to make appropriate changes and modulation in the expression of relevant genes[120,121]. Their architecture must be complex enough to selectively recognize a metabolite and perform the conformational switch. For this proposal, in a Riboswitch two main domains can be distinguished:

a) The aptamer is the riboswitch part where the metabolite is bound, ranging from 35 to 200 nt.[122]. The combination of only four different monomers leads to a highly specific binding pocket that is widely conserved in evolution. In riboswitches, the sequence is conserved in 50% to 65%, but the secondary structures are conserved across thousands of species[123]. Nucleotides evolutionary conserved directly contact the ligand. Computational analyses of these conserved fragments in bacterial genomes serve as basis for new riboswitch finding and classification. The aptamer can be initially preorganized in some extent before metabolite binding, but the binding must induce at least some structural reorganization or stabilization of the aptamer structures that influence the folding and function of the expression platform.
b) The expression platform of each bacterial riboswitch is usually located downstream of the aptamer and is the riboswitch region that finally causes the gene expression regulation according to the gene-on or gene-off conformations of the aptamer. Sequences of the expression platform can vary, but the most common expression platform in bacteria includes a stem that blocks the ribosome binding site or a transcription terminator.

Riboswitches are very specific and selective to their metabolite, able to discriminate between precursors or metabolite derivatives. The ligand binding pocket specificity includes a

combination of several intermolecular forces and binding principles such as hydrogen bonding, a tight ligand binding pocket and stacking interactions[67,124].

For a correct riboswitch regulation understanding, it is important to recognize that mRNA folding in the transcription context is central for its regulatory function. The aptamer domain is first synthesized by RNA polymerase and folds independently to the expression platform. RNA polymerase stalls for a temporal separation of the two folding events[113], a transcriptional programmed pausing during transcription is required for efficient folding. Folding and ligand binding to the aptamer occur on a similar timescale of the transcription[118].

Riboswitches can be used as tools in research for the gene expression control and the design of artificial aptamers capable of responding to a diversity of chemical effectors[112]. On the other hand, as riboswitches control many fundamental genes and metabolic pathways can be considered as potential targets for drugs[101,112,117,121,125]. As more, there are certain drugs nowadays in use that act at the riboswitch level [101]such as: L-Aminoethyl cysteine and DL-4-Oxalysine[101] that inhibit the synthesis of lysine via the lysine riboswitch, the Pyrithiamine pyrophosphate (DTPP), which acts over a TPP riboswitch, and the Roseoflavin, used for treating tuberculosis, which interacts with a FMN riboswitch[126,101, 127]

There is now a growing research in ligand analogues that are tested for their antibiotic potential throught riboswitch inhibition[101]. Several purine derivatives have also been synthesized and their interaction with a purine riboswitch has been studied in order to prove potential use as drug against the *Clostridioides difficile* [128]. GlcN6P derivatives with a phosphate mimicking group have been tested to activate glms riboswitches[129]. Ribocil is also a FMN riboswitch targeted antibiotic with strong antibacterial effect and less side effects than the previous reported[112] .

1.5.1. Riboswitch classes

After two decades of research in this field a wide diversity of riboswitches has been discovered. Hereafter, known riboswitches are classified according to the metabolite to which thet are bound[121,130,131]. Discrimination of ligand precursors or derivatives is a difficult task achieved due to the highly specific binding pockets formed using different strategies.

Nucleotides:

Several riboswitches able to discriminate between purine derivatives have been discovered. A nucleotide mutation is enough to selectively distinguish an adenine from a guanine. These riboswitches are involved in the synthesis and transport regulation of the metabolites[121,124,132,133]. There are also three different riboswitches that recognize PreQ1[134], a precursor of the queuosine-1 modified purine present in tRNA, and two classes of sensors selective to cyclic purine dinucleotide (c-di-AMP, c-di-GMP and c-AMP-GMP)[120,135–137] (see Figure 15). The c-di-GMP triggers a wide range of physiological changes, c-di-GMP riboswitches are positioned near genes involved in mobility and virulence[138].

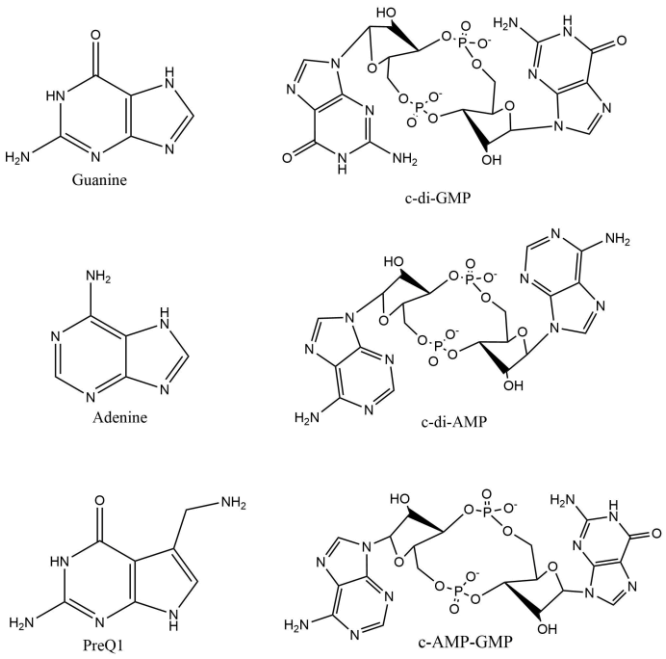

Figure 15 Nucleotide derivatives recognized by riboswitches: guanine, adenine, PreQ1, c-di-GMP, c-di-AMP and c-AMP-GMP.

Metal ions:

Several riboswitches responding to metal ion concentration have been discovered, establishing a precedence for a selective recognition of transition metal ions by RNA elements[139]. NiCo riboswitches can selectively bind Co^{2+} and Ni^{2+} ions with a low-µM affinity in a cooperative manner. It seems to be involved in the detection of toxic levels of these metal ions or in homeostatic regulation[81,140]. Also, an orphan riboswitch widely distributed in bacteria, the yybP-ykoY motif functions as a Mn^{2+} sensor involved in the Mn^{2+} pumps[81,141]. Finally, there are also two riboswitches responding to Mg^{2+}, renamed as M-box, that regulate magnesium homeostasis[142].

Anions:

Despite the inherent electrostatic repulsion, there is a RNA sequence that senses fluoride concentration, which can be related to a defensive mechanism against this anion toxicity[143].

Metal complexes:

Some riboswitches involved in cobalamin regulation[144,116] have been discovered. The first one is involved in regulation of genes related to the metabolite being able to bind AdoCbl or aqCbl[145] depending on the specie. AdoCbl riboswitches are the most widespread class in bacteria. The second cobalamin riboswitch class regulates genes related to the ethanolamine[146].

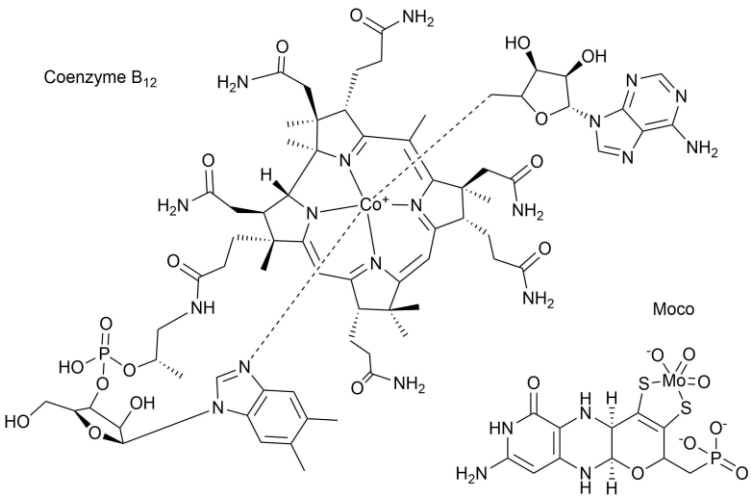

Figure 16. Coenzyme B_{12} and Moco cofactor chemical structure.

Furthermore, a molybdenum cofactor (Moco) riboswitch that regulates genes related to molybdenum and tungsten cofactor metabolism has also been discovered[147].

Amino acids:

The concentration of some amino acids is also regulated via riboswitches. For example, glycine is recognized by a riboswitch consisting of two aptamer domains in tandem regulating the metabolite catabolism[148]. Lysine is also regulated at a riboswitch level, in its synthesis, transport and catabolism[149,150]. These two previously mentioned riboswitches form a tight ligand binding pocket, which could exclusively fit the ligand and hold it by van der Waals interactions[67]. Finally, glutamine can be recognized by two different classes of riboswitches: glnA RNA motif and downstream-peptide motif[151].

Carbon atoms transfers and related molecules:

A wide range of molecules related with the methylation are regulated by riboswitches. A riboswitch that recognizes S-adenosylhomocysteine (SAH)[152] and four riboswitches that regulate S-adenosylmethionine (SAM)[131,152–156] have been characterized and there is a fifth that can recognize both SAH and SAM, although only SAM seems to be biologically relevant[131]. SAM riboswitches, also called S box, are located upstream of genes involved in sulphur metabolism such as cysteine, methionine and SAM. Tetrahydrofolate (THF)[157,158] is bound to two binding pockets of a THF riboswitch aptamer. Finally, riboswitches that respond to ZMP (5-amino-4-

imidazole carboxamide ribonucleotide) and ZTP (5-formamidoimidazole-4-carboxamide ribonucleotide) have been discovered, which are precursors of the IMP (Inosinate) in the *de novo* biosynthesis pathway of purines [122,159] (see Figure 17).

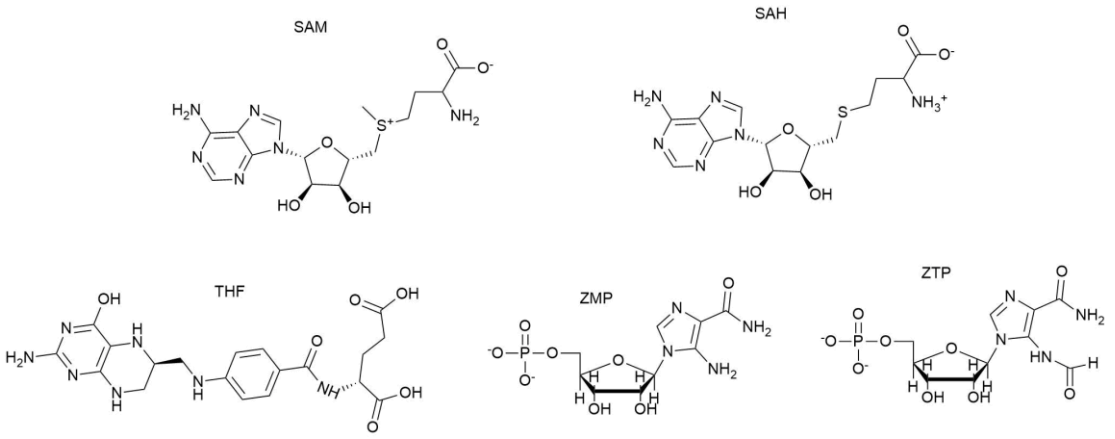

Figure 17. Carbon atom transfers and other related molecules that bind riboswitches: S-adenosulmethionine (SAM), S-adenosylhomocysteine (SAH), tetrahydrofolate (THF), 5-formamidoimidazole-4-carboxamide ribonucleotide (ZMP) and 5-amino-4-imidazole carboxamide ribonucleotide ZTP).

Other cofactors:

Riboswitches can also respond to redox cofactors (see Figure 18) like flavin mononucleotide (FMN), related with the riboflavin (vitamin B_2), implicated in the regulation of genes that encode riboflavin biosynthesis or transport[160]. Glucosamine-6-phosphate synthetase is regulated via riboswitches responding to glucosamine-6-phosphate (GlcN6P)[161,162] and the reversible decarbonization catalysis is controlled by a TPP riboswitch, which binds thiamine pyrophosphate (TPP, vitamin B_1)[163,164]. The TPP riboswitch class appears to be the most widespread identified in most of the taxonomic groups and also found in euryarchaeal, fungal and plant species, and involved in thiamine synthesis, phosphorylation and transport[116].

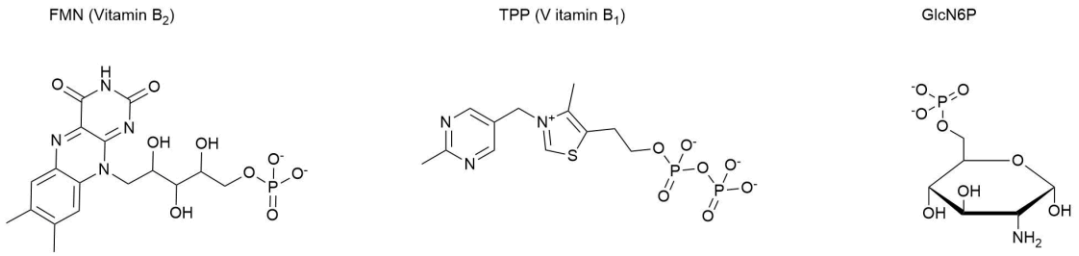

Figure 18. FMN, TPP and GlcN6P chemical structures.

Physico-chemical parameter[d]

There are riboswitches that respond to physico-chemical parameters such as temperature and pH. Riboswitches that respond to temperature are called thermosensors and block translation at low temperature by sequestering the RBS and starting codon. A rise in temperature denatures the RNA structure and translation signals are accessible to ribosomes[108]. Also, a 5'-UTR RNA upstream of the gene alx reacts to alkaline conditions and regulates the gene expression at a translational level[165].

tRNA:

The T-box regulatory elements are used for regulation of amino acid related genes in Gram-positives. The tRNA specific binding depends on an appropiately located codon, the identity of which matches the amino acid specificity of the gene encoded downstream[166].

Orphan riboswitches:

There are some RNA sequences computationally discovered by gene comparison that are postulated to be riboswitches. In some cases, the metabolite related to the sequence has not been identified yet[121,122,118] .

1.5.2. Riboswitch regulation mechanisms

The regulation mechanism depends on both, the riboswitch class and bacteria in which it is present. The riboswitch aptamer must communicate with the expression platform to affect gene expression and it is the conformational change that ensues ligand interaction that thus drives riboswitch function[124]. There are three common mechanisms used by the riboswitches in gene regulation, one of those mechanisms is used in eukaryotes. There are some other more unfrequent mechanisms that are still uncertain nowadays and need further research to be completely understood[167]. Gene expression can be modulated at transcription, translation, splicing and RNA stability levels[108,116,118,121,138].

Transcription termination

Upon metabolite interaction with the riboswitch aptamer, a strong stem followed by uridine residues is formed, which constitute a transcription terminator. This stem is recognized by the rho factor, which causes the transcription interruption and eventually the release of the DNA template and ancient RNA from the RNA polymerase (see Figure 19). There are cases in which

[d] It can be discussed whether they should be classified as riboswitch because they do not specifically bind to a molecule, but they do perform a regulatory function upon changing physiological conditions.

the metabolite binding to the aptamer induces the stability of the anti-terminator stem activating, in this case, the transcription and expression of the corresponding gene. Certain glycine, adenine and lysine riboswitches are examples of positive genetic regulation although most riboswitches that control transcription termination act as negative switches[116]. tRNA riboswitches for instance induce the formation of a terminator stem[166].

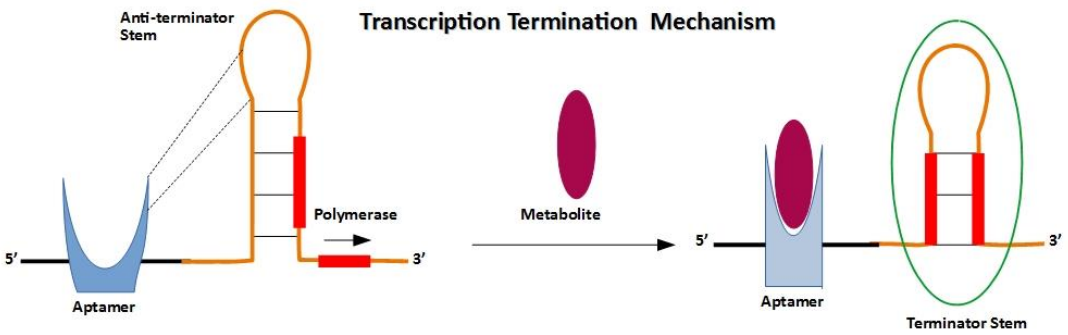

Figure 19. Scheme of the transcription terminator mechanism used by riboswitches.

Translation initiation

In this case, the metabolite binding induces a conformational change that disturbs the access of the ribosome, because a simple motif is formed that sequesters the RBS. The base pair recognition of this sequence consequently prevents the mRNA recognition by the ribosome and inhibits the protein translation (Figure 20).

There are two variants of this regulatory mechanism. In some riboswitches, the RBS is buried by the aptamer without the involvement of the expression platform, and thus blocking the ribosome access and a negative regulation. There are other cases in which riboswitches induce a transcription terminator located close to the open reading frame. These kinds of riboswitches with dual expression platform can both attenuate transcription and, if termination does not occur, could inhibit transcription[116]. With this mechanism, gene activation can also be induced if metabolite binding stabilizes the pseudoknot with the anti-RBS, giving access to ribosome binding in the RBS. Metabolite-dependent inhibition of the ribosome binding has been proven *in vitro* for the *E. coli* AdoCbl riboswitch[168].

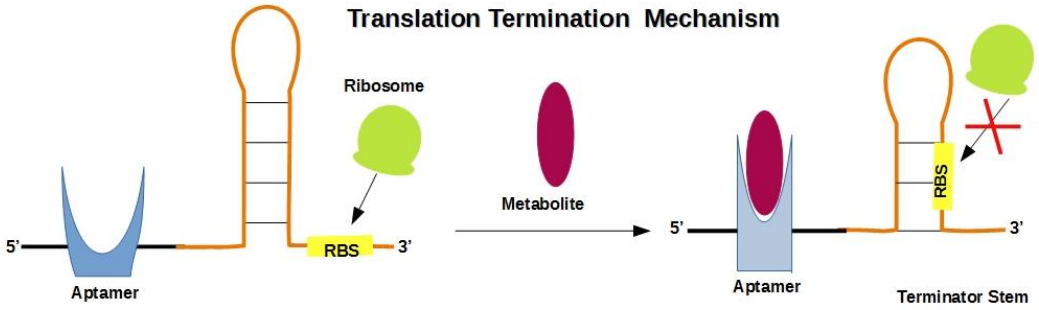

Figure 20. Scheme of the translation termination mechanism used by masking the RBS.

Splicing

This regulation mechanism is the most common in eukaryotes. The genetic control is induced by a complex cascade of events. TPP riboswitch found in eukaryotes is in 5'-end introns of immature mRNA. Ligand recognition of the sequence modulates the intron splicing, generating an alternative-processed mRNA[116] that contains internal stop codons, which either causes translation of aberrant peptides or premature translation termination[138] (Figure 21). Also, c-di-GMP riboswitches are located adjacent to group I self-splicing introns that exhibit this kind of regulatory mechanism. The metabolite c-di-GMP binding induces a conformational change that allows GTP to attack the 5'-intron splice site and, subsequently intron self-excision, bringing together two distant halves of the RBS sequence and thus generating a translatable mRNA[138].

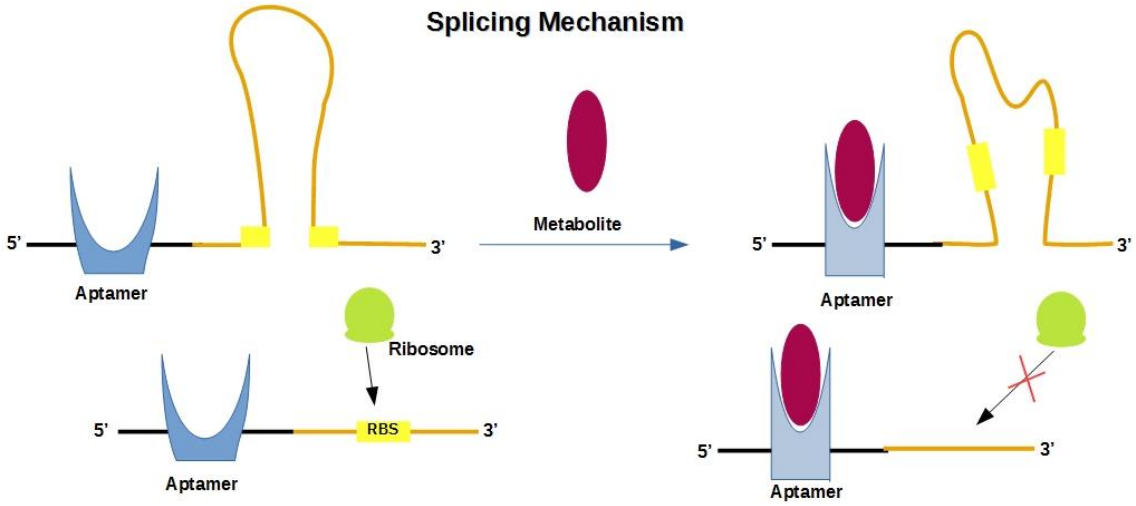

Figure 21. Sheme of the most common splicing mechanism in eukaryotes.

Transcription interference or antisense

This kind of Riboswitches is located downstream and on opposite orientation of the regulated gene (see Figure 22). Regulation in this case can be done at transcription termination and translation initiation levels. The SAM-I riboswitch is an example of a riboswitch that acts with this mechanism and regulates the transformation of methionine to cysteine. At low concentration of SAM, transcription of the full length antisense mRNA may cause inhibition or degradation of the sense mRNA while, at high SAM levels, the metabolite binds to the riboswitch aptamer causing the terminator stem formation and the premature termination of the antisense transcript[116]. The regulation may be caused also by competition between *RNA polymerase* to initiate at convergent promoters or the transcription of the mRNA versus the riboswitch-linked RNA.

There are also evidences of trans regulation in *SreA* and *SreB* SAM-riboswitches from *Listeria monocytogenes*. The SAM-riboswitch transcript can base pair the 5'-UTR of the regulated mRNA gene and inhibits the translation[138].

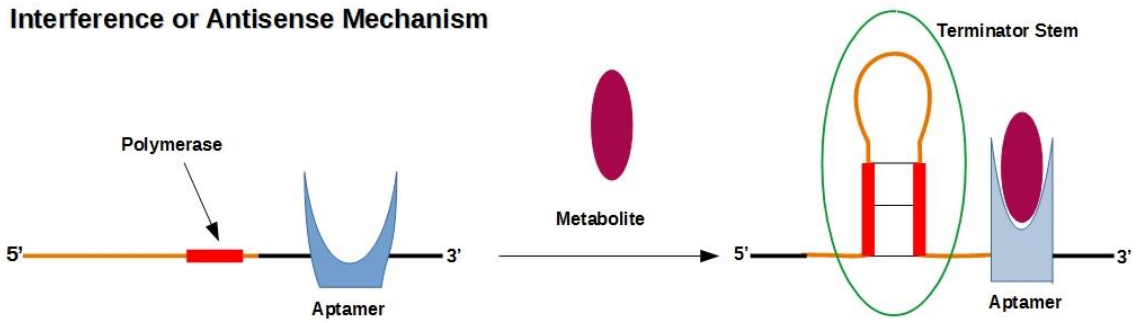

Figure 22. Scheme of the interference or antisense mechanism for the riboswitches located downstream of the regulated gene.

Self-cleaving

Riboswitches that respond to this mechanism have a ribozyme activity, like *GlmS* riboswitch (see Figure 23). In the presence of the metabolite, a self-cleavage of the 5-end is induced. The gene regulation with this mechanism is related to the different mRNA stability prior and after 5' end excision. In Gram-positive bacteria, mRNA is 5'-end capped to protect it from *RNAse J*, so that, mRNA degradation is promoted after self-cleavage.

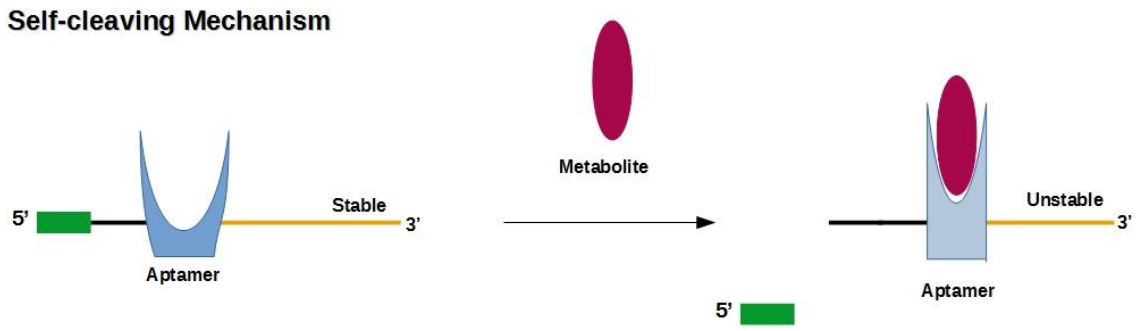

Figure 23. Scheme of the self-cleaving mechanism of the GlmS riboswitch.

Tandem

Several riboswitches have been found in tandem, where two aptamers regulate a single gene. The 88% of the mRNA regulated by glycine present two aptamer domains. Binding of two molecules makes riboswitch more sensitive to smaller changes in ligand concentration than a single aptamer[116] (see Figure 24). Tandem arrangements of TPP and AdoCbl are less common, where each aptamer appears to act independently over the same expression platform. *L. monocytigenes* SAM riboswitch functions only at a temperature permissive for infection, when the adjacent RNA thermosensor is unfolded[138].

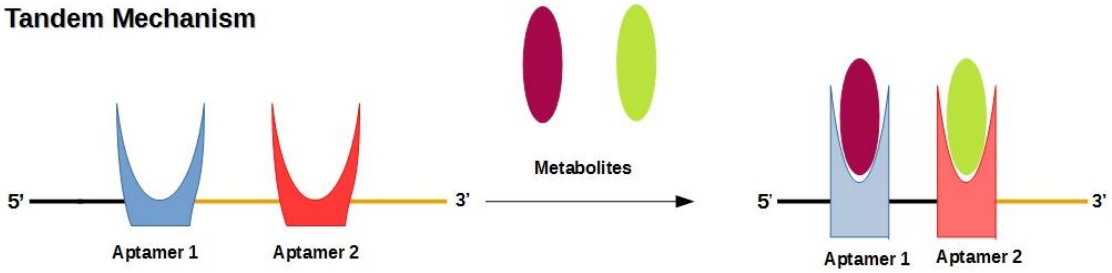

Figure 24. Scheme of the tandem riboswitch containing two aptamers for regulation a single gene.

1.6. B_{12} Riboswitches

Fragments of the RNA located in the 5'-UTRs of genes related to B_{12} were discovered and were called B_{12}-box[169]. Afterwards the function of these fragments was identified and the term Cbls riboswitch was coined[170]. These riboswitches contain the B_{12} box motif sequence and 10 additional base pairing sequences highly evolutionary conserved where 57 nucleotides are conserved in 90% of the cobalamin riboswitches[116,171,172]. Cobalamin riboswitches are the largest riboswitches identified (more than 200 nt.), with a consensus domain that contains a three-way and a four-way junction and some peripheral more variable regions[173] (see Figure 25).

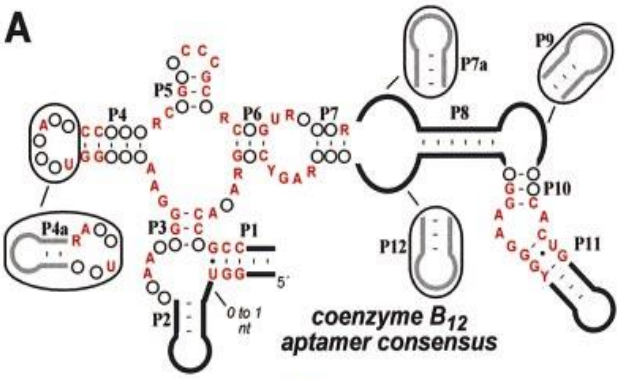

Figure 25. Consensus structure of a cobalamin riboswitch aptamer. Continuous lines depict parts of a variable length. Nucleotides depicted in red are the most evolutionary conserved[172] [e].

Coenzyme B_{12} or adenosyl cobalamin riboswitches are widespread[13,111,173] through diverse bacterial species, moreover ranking from 1 to 13 representatives per genome have been identified after computational genomic comparison studies[174]. This riboswitch class is widespread in all taxonomic groups of bacteria where Gram-positives seem to exhibit regulation at a transcriptional level while Gram-negatives use a translational regulation via the RBS sequestration[114,171]. In rare instances, both transcriptional and translational regulation can be simultaneously controlled[114].

This riboswitch is primarily used for regulation of genes expressing cobalamin synthesis proteins[172,175], porphyrin and cobalt transport[13,121,169,171,174,176] and, in isolated instances, B_{12} riboswitches regulate expression of proteins for glutamate fermentation, succinate fermentation, ethanolamine[146], coenzyme B_{12} independent *ribonucleotide reductase*, and the fatty-acid desaturase[117,171].

The *btuB* riboswitches from *E. coli* and *S. typhimurium* and the *cob* operon riboswitch in *S. typhimurium* have been widely studied[171]. The *btuB* riboswitch in *E. coli* was the first validated riboswitch to interact with a metabolite in absence of protein factors[170].

1.6.1. B_{12} riboswitch subclasses.

The cobalamin riboswitch compresses two different subfamilies BI and BII[171], distinguished by the peripheral extensions surrounding the common core. The secondary structure of both classes contains a central four-way junction between P3 and P6, forming the core of the receptor domain responsible for the cobalamin binding and the T-loop mediated tertiary interactions[111,145]. Although cobalamin riboswitches from distinct species differ notably in the

[e] Nahvi, A., Barrick, J. E. & Breaker, R. R. Coenzyme B12 riboswitches are widespread genetic control elements in prokaryotes. (2004) *Nucleic Acids Res.* **32,** 143–150 by permission of Oxford University Press

peripheral regions, the ligand binding mechanism seems to be common, relying on a kissing loop formation between the L5 and L13 loops, which is another shared element in this riboswitch class[115,145].

Cobalamin riboswitches of the class BI have the P8-P12 extension and they are very selective in the AdoCbl recognition. The 5'-adenosyl moiety is in direct contact with nucleotides in the J6/3 (junction between P6 and P3) and IL11/10 (internal loop between P11 and P10) pulls J6/3 off the four-way junction away from the J3/4 (junction between P3 and P4), to provide space for the β-moiety[111].

In the cobalamin subclass BII two subgroups can be also distinguished:

Methylcobalamin and aquocobalamin are also reported to be recognized by different riboswitches[115,145], while they are unable to recognize AdoCbl. Marine cyanobacterial and *environmental metagenomes* samples from the ocean surface seem to lack the P6 extension and they bind with much higher selectivity to AqCbl rather than AdoCbl, probably due to an adaptation to the environment as the cobalamin derivative available is AqCbl owing to the rapid photolysis of AdoCbl[145]. These cobalamin riboswitches have been classified as BIIa, which include both the four-way junction and the T-loop but lack the P8-P12 extension[111].

The BIIb subclass has been coined after the discovery of a new AdoCbl riboswitch that seems to regulate the expression of genes related to the ethanolamine degradation. In this case, the binding of the metabolite increases the stability of the mRNA so the mRNA synthesis is promoted, giving an example of positive regulation[146]. These riboswitches also lack the P8-P12 but significantly differ in the nucleotide composition of the J6/3 binding core and interact with high selectivity with AdoCbl in contrast to the BIIa class[111].

1.6.2. Metabolite recognition in Cobalamin Riboswitches

The specificity and the selectivity of the ligand recognition by these RNA sequences are important to fully understand their mechanism of action and gene modulation. Thus, big efforts have been made to answer this question using different approaches and using several techniques. At the beginning, in-line probing and assays with ligand derivatives were used due to the difficulties in the crystallization of these large macromolecules.

AdoCbl riboswitches usually rely on the ligand-dependent formation of a pseudoknot between a specific C-rich loop and sequences outside the aptamer core to exert gene control[116]. RNA uses molecular recognition on the adenosyl moiety, the dimethyl benzimidazole moiety and the cobinamide ring[170]. Most probably, the riboswitch aptamer forms a single ligand-binding

pocket[172], although this riboswitch class carries the largest aptamer domain identified, this is in consonance with the large and chemically sophisticated metabolite which is recognised[121].

To provide a good selectivity and the corresponding response, a precise binding pocket needs to be formed for AdoCbl in order to preclude the genetic switch from being triggered by another metabolite[170]. The riboswitch seems to be more sensitive to the lack of the voluminous β-moiety whereas modifications at the 2'-OH of the ribose moiety are tolerated[170].

Gallo and co-workers demonstrated that apical ligands have influence on the binding affinity to the riboswitch,have a K_D of 90nM for AdoCbl while a K_D of 300 µM is reported for vitamin B_{12} lacking the apical ligand[177]. The H-bonding pattern and the electrostatic environment provided for the corrin ring are essential for the correct rearrangement and switch of the *btuB* riboswitch of *E. coli*[177,178]. Although a single change in a functional group does not prevent binding, the riboswitch does not undergo the correct structural rearrangement. The base-on or base-off conformation of the cobalamin derivative has much less influence on the affinity than the presence of the voluminous axial ligand[177].

The crystal structures of B_{12} riboswitches interacting with the metabolite give an important insight of how the ligand is recognized with high specificity and selectivity[145,173]. Peselis et. al. reported a riboswitch structure in complex with AdoCbl. Hydrophobic packing, hydrogen bonds and electrostatic interactions seem to contribute to the recognition. The side chains of the ligand create a surface complementary to the pocket. The β-side of the ligand is positioned in the minor groove of the P3 and the Watson-Crick face of the adenosyl moiety interacts with the Hoogsteen edge of the conserved A157[173]. Acetamide and propionamide moieties of the corrin ring also interact via several H-bonds with bases and backbones of the surrounding nucleotides. Johnson and co-workers have also reported crystal structures of two different cobalamin riboswitches that are shown in Figure 26[145]. In both structures, cobalamin is sandwiched between the minor grooves of the P3-P6. Staking of four purines forms a surface, the β-axial ligand of AdoCbl is projected directly to this surface while the corrin ring is perpendicular to this surface. The ligand selectivity is driven by a complex interplay between the binding core and the peripheral regions[13,111]. In the envAqCbl the cavity of the adenosyl moiety is occluded justifying the selectivity for derivatives with small β ligands. In the TteAdoCbl structure the adenosyl moiety is recognized by base pairing with the Hoogsteen face of the A162[145]. In both structures, the Dmbz and the aminopropyl linker interact with a ribose phosphate from the backbone of L5 and L13 via van der Waals interactions.

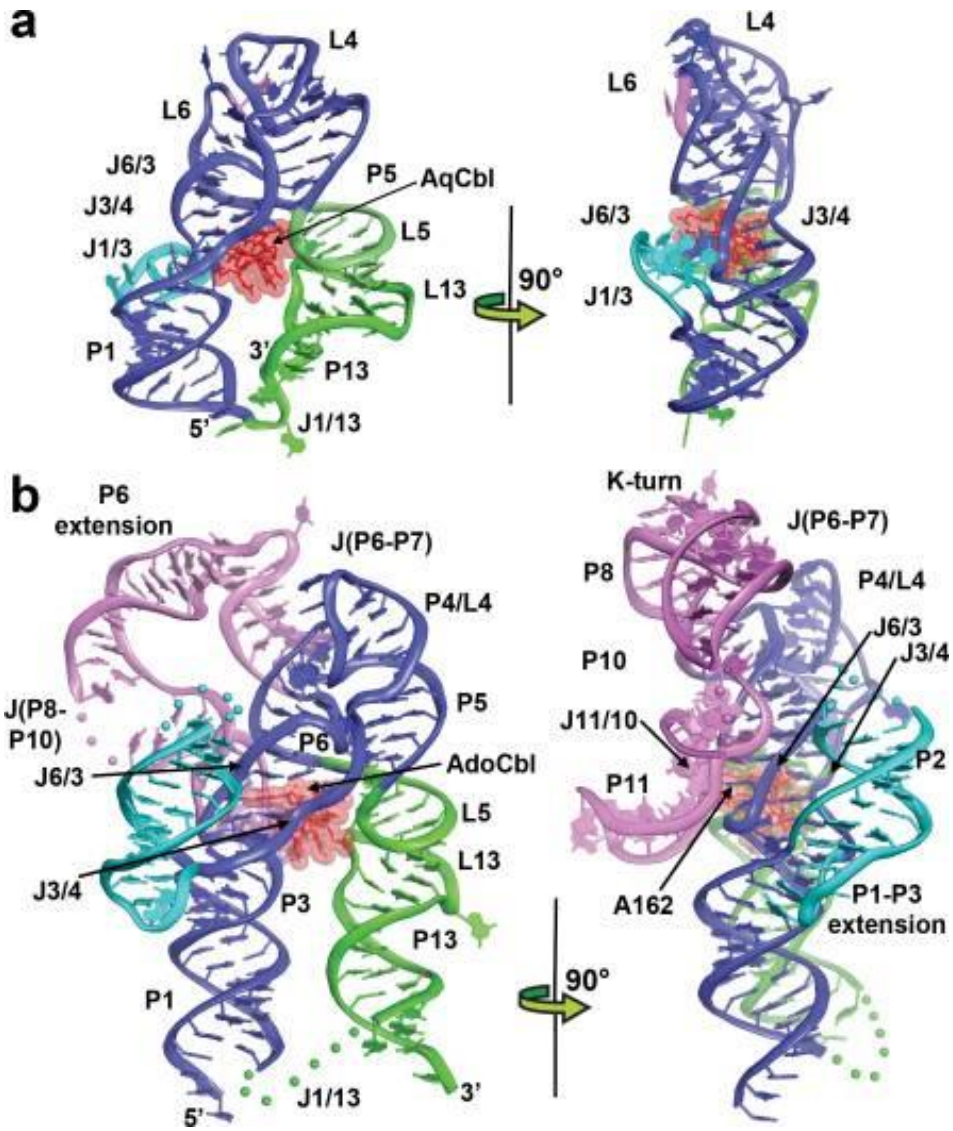

Figure 26. Crystal structures of: a) env8AqCb. b) TteAdoCbl. Coloured regions represent the core aptamer domain (blue), regulatory Kissing loop interaction (green) and peripheral domains (magenta and cyan). Ligands (red) are represented by van der Waals spheres. Disordered regions are represented by spheres[145,f].

1.6.3. *btuB* riboswitch

Gram-negative bacteria express an outer membrane protein involved in the active transport of the cobalamin, due to its molecular weight it cannot trespass the membrane. In the transport of cobalamin, B-twelve-uptake (*btu*), the first step implicates the *btuB* membrane protein. The expression of the *btuB* gene encoding the outer membrane cobalamin transporter is highly regulated at a riboswitch level[168]. The expression of this protein is repressed in presence of cobalamin, the ribosome binding to the *btuB* RNA is inhibited in *E. coli* with a half-maximal inhibition at 0.3 μM AdoCbl and the B_{12} box seems to be implicated in the RBS sequestration[168]. Crystal structures of the *btuB* riboswitch from *E. coli* show a kissing loop interaction which is in

[f] Johnson, J. E., Reyes, F. E., Polaski, J. T. & Batey, R. T. B12 cofactors directly stabilize an mRNA regulatory switch. *Nature* **492,** 133–137 (2012) by permission of Springer Nature

the proximity of the bound metabolite. The kissing loop is not essential for the metabolite binding; however it improves the ligand binding efficiency and is required for the expression platform conformational change necessary for the gene regulation[115]. As already mentioned, the *btuB* riboswitches of *E. coli* and *S.typhimurium* have been widely studied and characterized.

1.7. Antibiotic resistance

Infection diseases have been one of the major causes of human mortality and morbidity[179]. The discovery of the penicillin at the early 1900's made possible several medicine practices that are routinely used today and have improved human quality of life. Immunosuppression associated with transplantation or with anticancer therapy, extensive surgery and even catheterization are possible due to effective antibacterial therapies[179]. Nevertheless, thanks to their rapid evolution, bacteria have quickly developed an antibiotic resistance mechanism. The number of multidrug-resistant bacteria is increasing and antibiotic resistance is listed as one of the greatest threats to human health[180,181,182]. According to the Center for Disease Control and Prevention (CDC), the antibiotic-resistant organisms (AROs) cause 2 millions of infections and 23000 deaths per year in USA[183]. The research for new antibiotics is a need that represents one of the largest therapeutics research areas.

During a long period no novel antibiotic classes have been reported. The long "innovation gap" goes from 1962 with the application of quinolones and streptogramin, until 2000 with the introduction of oxazolinidones[182]. The known antibiotic families target essential cellular processes such as: DNA replication, transcription, translation, tetrahydrofolate synthesis and cell walls synthesis[182,184]. As RNAs are central to many of these processes they are nowadays though to be the best targets for new antibiotics research. New insights in RNA structure and functions facilitate the development of these new antibiotics targeting RNA[125].

In an attempt to break the resistance cycle, maximizing the specificity and efficacy will be an important goal in future drug development. There is also an increasing interest in species-specific drugs capable of targeting pathogens, while leaving the host natural microbiota unperturbed[101].

1.7.1. Klebsiella pneumoniae

Klebsiella pneumoniae, also known as Friedlander bacillus, is an immobile Gram-negative bacterium present in human skin, digestive and respiratory system. Also, it is a common hospital-acquired pathogen causing urinary infections, nosocomial pneumonia, liver abscess, meningitis and intraabdominal infections typical to immunosuppressed patients or patient with long clinical stays[185,186]. *K. pneumoniae* has been known to cause pneumonia since more than

100 years ago causing fever, breath difficulties and chest pain.It is a Gram-negative bacterium with an outer membrane difficult to penetrate. This fact makes it possible that multiple kinds of antibiotics can be expelled by efflux pumps[182].

Epidemic analyses reveal that there is more than one strain of this bacterium involved in this infection development. This pathogen has developed resistance to the most common antibiotics in use such as ampicillin and amoxicillin due to the development of wide-spectrum beta lactamases[186], being also resistant to cephalosporins and ceftazidime. Also, straining resistant to carbapenems[187] has been detected, making these bacteria resistant to almost all known antibiotics, classifying *K. pneumoniae* as a superbug[188].

2. Aim of the project

The discovery of riboswitches almost two decades ago opened a wide research field which is in continuous growing, due to the discovery of new riboswitch families responding to a broad diversity of metabolites, as already mentioned in section 1.5.1. The interest in these regulatory molecules, which are mainly present in bacteria, has grown as they are good target candidates for the development of new antibiotics.

This work is focused on the interaction of the *btuB* riboswitch from *K. pneumoniae* and its binding molecules, the cobalamins. The validation of this candidate riboswitch sequence and the investigation of the role and influence of the expression platform in the rearrangement of the structure upon cobalamin binding are also studied in this thesis. For this reason, a sequence of 216 nt. is compared, which only contains the aptamer part with a 243 nt. sequence containing both the aptamer and the expression platform.

Furthermore, this work is also focused on the *in vivo* regulation of the system and on the synthesis of cobalamin derivatives lacking the metal core. This derivative would not presumably perform the natural biological function but would maintain the structure roughly invariable and, thus the affinity to the riboswitch would be likely maintained.

Part I is focused on the validation of the sequence as a riboswitch and the characterization of the secondary structure and the thermodynamic parameters of the interaction. The main question to answer is if the expression platform plays an important role in the affinity and switching of the sequence.

Part II is dedicated to the biosynthesis of descobaltocobalamins in *Allocromatium vinosum* and further purification and characterization of the products.

3. PART I: Characterization of the *btuB* Riboswitch from *Klebsiella pneumoniae* and Interactions with Corrins

3.1. Introduction to PART I

3.1.1. In-line probing principle

In-line probing is one of the most common techniques used to elucidate secondary structures of large RNA molecules. The technique allows the study of structural rearrangements and switch validation without the need of RNA sequence or structure modifications. The RNA is 5' dephosphorylated followed with a re-phosphorylation with ^{32}P, thus a labelled sample is obtained, which gives high resolution to the method while using very little amount of sample.

The principle of this technique is the self-cleavage of the phosphodiester bond, which links two nucleotides in a RNA sequence. The principal mechanism by which an RNA phosphodiester linkage is spontaneously cleaved involves an internal nucleophilic attack by the 2'-oxygen on the adjacent phosphorous centre[170]. This leads to the formation of a 2',3'-cyclic phosphate and the excision of the P-O bond (see Figure 27)[189,190]. The reaction follows a S_N2 mechanism and is proportional to the "in-line character" of the phosphate linkage. Thus, the reaction is promoted when the incoming 2'-OH group and the 5'-oxygen leaving group are situated opposite to each other[191].

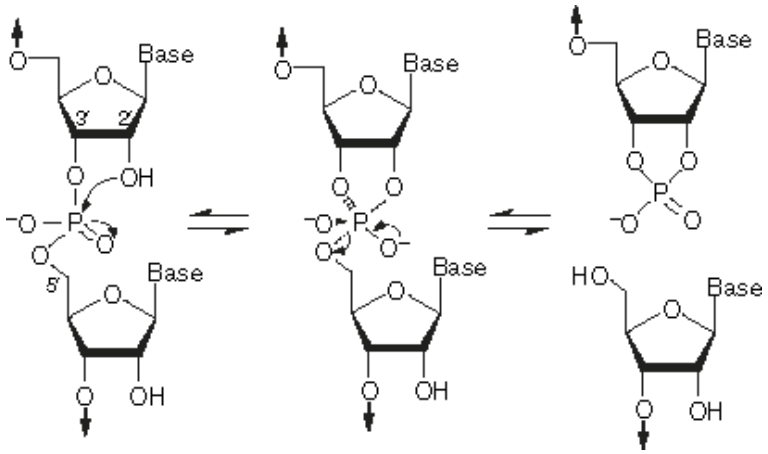

Figure 27. Mechanism of the self-cleavage reaction. The 2'-OH group attacks the bridging phosphate group. A pentacoordinate intermediate is formed followed by the excision of a phosphate group and the 5'-OH leaving group[189g].

[g] Regulski, E. E. & Breaker, R.R., In-line Probing Analysis of Riboswitches. Methods Mol. Biol. (2008) 419, 53-67 by permission of Springer Nature.

The self-cleavage due to the presence of the ribose 2'-OH group in RNA is the most important reason of its reduced stability in physiological medium. The cleavage of the bond is catalysed in the presence of divalent ions such as Mg^{2+} or in acid or alkaline medium[189].

RNA linkages that are formed by nucleotides involved in stable base-paired structures rarely undergo spontaneous cleavage because they rarely adopt an in-line conformation, while nucleotides located in relatively unstructured regions or in certain ternary-structured regions experience a higher level of spontaneous cleavage[170].

In-line probing is an ideal method to detect structural changes in RNA of different sizes. It is frequently applied in the study of the structural changes in riboswitches upon interaction with the metabolite effector or related derivatives[115,121,128,148,170,177,178].

3.1.2. Isothermal Titration Calorimetry principle

The isothermal titration calorimetry or ITC is a technique used to determine all the thermodynamic parameters of a molecular interaction in solution performing a single experiment. Another advantage of the technique is that can be readily applied to almost any RNA-ligand complex without any labelling and in a broad range of temperatures, pH and ionic concentrations[192]. The experiment involves incremental addition of one species (a titrant) to its binding partner (titrate) while monitoring the energy input required to maintain the sample and reference cells at the same temperature[193]. The titration thermogram represents the heat absorbed or released vs. time. The integration of area of the individual peaks allows to calculate the enthalpy, stoichiometry and association constant of the interaction. Furthermore, with these values other thermodynamic parameters can then be additionally calculated.

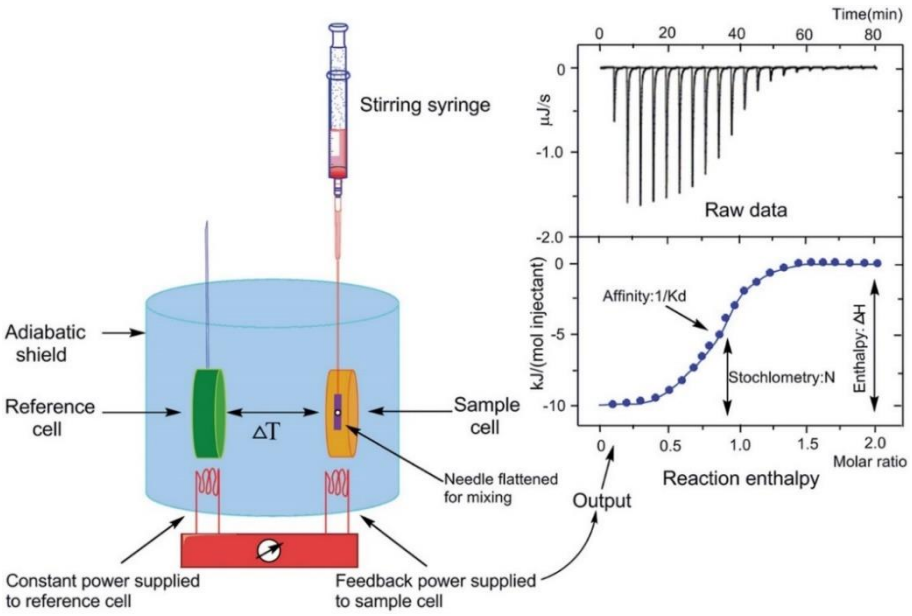

Figure 28. Schematic functioning of the Isothermal Titration Calorimetry. Left: scheme of the parts of an ITC instrument. Right: titration thermogram were the heat per unit of time is represented after each injection of ligand. Then the heat realized or absorbed in each injection vs. the ratio between total ligand concentration and total sample concentration is represented.[194,h]

This method has been applied quite extensively to investigate the interaction of a macromolecule with small ligands such as drugs or metal ions but also interactions between big biomolecules. It has been applied for the study of protein-protein interaction or interactions between protein and nucleic acids[194–197]. Although this technique has been widely used in the study of protein interactions, it took long until its application in nucleic acids interaction studies. This is probably because large amounts of sample were required by older instruments before more sensitive instruments became available (modern instruments can measure heat powers as low as 0.1 μW)[197]. ITC has been applied in the study of the interaction of DNA and small metal complexes and the interaction of DNA with proteins has been also widely investigated[193]. ITC has been applied successfully in the study of the interaction of the natural purine riboswitch[198, 199], of the fluoride riboswitch[143], of the TPP riboswitch[197], of the B_{12} riboswitch[111] and of the synthetic aptamer which responds to tetracycline[200].

The ITC methodology allows also to obtain a complete kinetic information ranging from a single binding molecule to the complex RNA folding using the kinITC method. The kinetic information is enclosed in the peak shape, enabling the calculation of the kinetic constant and the activation enthapies of the process [197].

[h] CC-BY 2015, C., Zhang, S. & Huang, H. Choosing a suitable method for the identification of replication origins in microbial genomes. *Front. Microbiol.* **6,** 1–18 (2015).

3.1.3. Aim of the subproject

Previous studies have characterized the *btuB* riboswitch from *E. coli* and *S. typhimurium* in detail using constructs carrying the whole aptamer part of the riboswitch. The aim of this part is the validation and characterization of a new Cbls riboswitch candidate. The *btuB* riboswitch from *K. pneumoniae* was selected because it represents a step further in the evolutionary philogenic tree. This species has been catalogued as a super bug as aforementioned in section 1.7.1, so research for new antibiotics specific to this bacteria is needed. The objectives of this part were:

- Validation of the candidate sequence as a cobalamin riboswitch.
- Characterization of the secondary structure, including the gene-on and gene-off conformations.
- Collection of the thermodynamic parameters for the interaction and comparison of the 216nt. sequence containing the aptamer with the 246nt. sequence carrying the whole expression platform.
- Monitoring the in vivo regulation of the *btuB* riboswitch in the presence of cobalamin derivatives using a mCherry fluorescent protein coupled to the riboswitch promoter.

3.2. Experimental section

All reagents used were purchased from Sigma-Aldrich, Promega, Scharlab and VWR and were used without additional purification. All reagents were p.a. grade or higher.

3.2.1. Plasmids preparation

3.2.1.1. pMB01 design

The complete genome from *Klebsiella pneumoniae*, subspecies *pneumoniae*, strain MGH 78578 was extracted from the National Center for Biotechnology Information (NCBI) with GenBank code CP000647.1. The gene of the *btuB* membrane protein was located between the positions 4660313-4662169 and the 5'-UTR of the AdoCbl dependent *btuB* riboswich was postulated to start at position 4660061[144]. Some modifications of the sequence (*Table 1*) were performed to optimize further steps of the study and to obtain RNA constructs of distinct length:

Table 1. pMB01 sequence from the 5'-end to 3'end. In red *T7-RNA polymerase* promotor followed by the three G introduced to have good transcription yields. In blue the three nucleotides mutated from the native form to have a *XhoI* restriction site in the starting codon position and in green the two nucleotides mutated from the native form to have a *HindIII* restriction site.

TAA TAC GAC TCAC TATA GGGA CCGG TCCT GTGA GTTA AAAG GGAA CCCA GTGG AAAT CTGG GGCT GACG CGCA GCGG TAAG GAAG GTGA GAAA TGAG CGCA CTCG GTGC AGAC ACTG CGGC TAGC CGTG GGAA GTCA TTAT TTCT TGAA ACAG CCTC CAAG CCCG AAGA CCTG CCGG AATA CGTC GCAC TGGG TTTT ATCG TCGC GAGC AACT GATA AAAC CTGC GGCA **AG**CT TTTT CTGT TTCG GATG CTTT TACT **CGA**G

- The 5'-long tail was cut and three G were added to have a good transcription starting point[65]. The 5'-end of the RNA sequence was changed to 5'-GGGA.
- At the 3'-end, the RBS and the staring codon of the protein were included. Just at the starting codon position, a mutation was introduced and $A_{241}T_{242}G_{243}$ were changed to CGA in order to have a restriction point for the enzyme *XhoI*: C'TCGA_G.
- The originals T_{213} and C_{214} were also mutated to A_{213} and G_{214}, so a restriction site for *HindIII* (A'AGCT_T) was introduced just after the riboswitch aptamer.

The sequence designed (pMB01) was synthesized by GenScript (USA) and subcloned in a commercial pET-21b(+), which already contained an ampicillin resistance gene and the *T7-polymerase* promotor and terminator. The scheme of the pMB01 plasmid can be found in Appendix 1.

3.2.1.2. pJP01 design and preparation

For the study of the riboswitch sequence containing the RBS and the starting codon, the restriction site for *HindIII* was removed from the sequence using a point mutation protocol[201]. The A_{213} and G_{214} of the plasmid pMB01 were changed to the native T_{213} and C_{214}. The primers used for the point mutation were:

JP01_1: 5'-GAT AAA ACC TGC GGC A**TC** CTT TTT CTG TTT CGG-3'

JP01_2: 5'-CCG AAA CAG AAA AAG **GA**T GCC GCA GGT TTT ATC-3'

The nucleotides to be changed with the point mutation are highlighted in the above primer sequences.

The PCR (Polymerase Chain Reaction) reaction mixture was prepared in a 200 µl PCR tube. The final volume of the reaction was 50 µl and the concentrations used in the mixture were: 11 µg/ml vector (pMB01 dam methylated as it was grown in a *E. coli XL1blue* or *DH5α* strain), 0.2 µM of each primer (JP01_1 and JP01_2), 0.2 mM of each dNTP, 1X of *Pfu* buffer, 1 mM $MgSO_4$ and 2.5 U of *Pfu DNA Polymerase*.

The PCR product was obtained after a starting step of 5 min at 95°C followed by 18 cycles of melting 30 s at 95°C, annealing for 1 min at 55°C and elongation for 7 min at 68°C, additional 5 min of elongation at 68°C was added to the last cycle.

In order to digest the pMB01 vector, 40 U of *DpnI* were added to the PCR reaction mixture that was incubated 1h at 37°C without shaking. The result was a plasmid based on pET-21b(+) with the entire Riboswitch sequence and only one restriction site for *XhoI* on the startng codon, giving a RNA construct of 243 nt. long. The scheme of the pJP01 plasmid can be found in Appendix 1.

3.2.1.3. pJP02 design and preparation

Plasmid pJP01 was modified to introduce a *HindIII* restriction site after the *XhoI* one situated on the starting codon. The goal was to have a linearized plasmid with two different restriction enzymes to include a sequence in between.

To include the new *HindIII* restriction site in the sequence, the point mutation protocol was followed[201]. The primers used for the PCR reaction were:

JP02_1: 5'-CTC GAG CAC CAC CA**A GCT T**AC CAC TGA GAT CC-3'

JP02_2: 5'-GGA TCT CAG TGG T**AA GCT** TGG TGG TGC TCG AG-3'

The nucleotides to be changed with the point mutation are highlighted in the above primer sequences.

Duplicate reactions were prepared in PCR thin wall tubes of 200 µl. The final volume of the reaction mixture was 50 µl. The concentrations used in the reaction mixture were: 4.8 µg/ml of vector (pJP01 dam methylated), 0.25 µM of each of the primers (JP02_1 and JP02_2), 0.4 µM of each dNTP, 1X *Pfu* buffer, 1 mM $MgSO_4$ and 2.5 U *Pfu DNA polymerase* enzyme.

The PCR and DpnI digestion conditions were performed as for section 3.2.1.2. The scheme of the pJP02 plasmid can be found in Appendix 1.

3.2.1.4. pmCherry design and preparation

Roger Tsien very kindly supplied us the plasmid pRSETb-mCherry (see Appendix 1) which already carries a *HindIII* restriction site at end of *mCherry* gene. The plasmid was modified to introduce a *XhoI* restriction site at the start codon of protein gene sequence. Again, the point mutation protocol[201] was used with slight modifications. Primers used for this PCR follow:

CIRERA_F: 5'-CGA TAA GGA TCC CGC CAC **TCG A**GT GAG CAA GGG CGA GG-3'

CIRERA_R: 5'-CCT CGC CCT TGC TCA C**TC GA**G TGG CGG GAT CCT TAT CG-3'

The nucleotides to be changed with the point mutation are highlighted in the above referenced primer sequences.

Two reactions were prepared in PCR thin wall tubes of 200 µl. The final volume of the reaction mixtures was 50 µl, as well. The concentrations used in the reaction mixtures were: 4.1 µg/ml of vector (pRSETb-mCherry dam methylated), 0.2 µM of each of the primers (CIRERA_F and CIRERA_R), 0.4 µM of each dNTP, 1X *Pfu* buffer, 1 mM and 5 mM $MgSO_4$ and 2.5 U *Pfu DNA polymerase* enzyme.

The temperature ramp program was just modified at one point: elongation of the chain was performed at 68 °C for 4 minutes instead of 7 minutes because of the length of the plasmid, and 18 cycles were also performed. The PCR reaction mixture was then incubated at 37 °C and 300 rpm for 1h with 20 U *DpnI*. The scheme of the pmCherry plasmid can be found in Appendix 1.

3.2.1.5. pJP03 design and preparation

pJP03 (see Appendix 1) was obtained after a ligation of the double digested pJP02 vector and the double digested insert of pmCherry containing the *mCherry* gene sequence. The procedure followed for the ligation was:

-Vector (pJP02 double digested): 14 µg plasmid (pJP02), 1X R buffer, 50U of *XhoI* in a final volume of 100 µl. The mixture was incubated at 37 °C for 4h. After that time, the enzyme was inactivated at 80 °C for 20 min. Afterwards, 50 U of *HindIII* were added to the mixture and R buffer was adjusted to maintain 1X buffer concentration. The mixture was incubated at 37 °C overnight and lastly, *HindIII* was inactivated at 80 °C for 20 min. Reaction mixtures were analysed by 1% agarose gel in 1X TAE (40mM, 1mM EDTA, pH = 8.3) to ensure the entire digestion. The digested plasmid was cut out from the gel, and lastly, extracted and purified from the gel pieces using the DNA Gel extraction kit from OMEGA Bio-TeK.

-Insert (pmCherry double digested): four reaction mixtures were set up with the following concentrations: 10 µg pmCherry, 1X R buffer, 20 U *HindIII* and 20 U *XhoI* in a final volume of 40 µl. Reaction mixtures were incubated at 37 °C for 4 h. Straightaway, 9 U *FastAP* and 1X F*astAP* Buffer in a final volume of 50 µl were added and incubated for 15 min more at 37 °C. Finally, the enzymes of the reaction mixture were inactivated at 80 °C for 20 min. The digested fragments were then purified in 2% agarose gel in 1X TAE. The insert of ≈ 700 nt was cut out from the gel and lastly, extracted and purified from the gel pieces using the DNA Gel extraction kit from OMEGA Bio-TeK as well.

-Ligation: The final step in the construction of the recombinant pJP03 was the connection of the insert (from pmCherry) into a compatibly double digested vector backbone (pJP02). Several insert:vector rations for the ligation mixtures were tried to optimize the conditions. The final and successful conditions used for ligation were: 1X Rapid Ligation Buffer, 1.8 nM Vector, 10 nM insert (≈ 6:1 ratio) and 5 U of *T4 Ligase* in a final volume of 20 µl. Reaction mixture was incubated for 5 min at 22 °C.

3.2.1.6. pJP04 design and preparation

Restriction site for *XhoI* in pJP03 was deleted to restore the native sequence and the start codon of the protein. The restored starting codon will allow the pJP04 plasmid to be translated *in vivo* and, *mCherry* should be expressed according to the riboswitch regulation. For this purpose, a point mutation was performed over pJP03, using the subsequent primers;

JP04_1: 5'-GTT TCG GAT GCT TTT AC**A ATG G**TG AGC AAG GGC GAG GAG-3'

JP04_2: 5'-CTC CTC GCC CTT GCT CAC **CAT T**GT AAA AGC ATC CGA AAC-3'

The nucleotides to be changed with the point mutation are highlighted in the primer sequences shown above.

Point mutation protocol conditions, such as the concentrations of primers, plasmid or $MgSO_4$,

the type of DNA polymerase or temperature program, were changed with no positive results. Finally, it was decided to perform the mutation externally, by Genscript, USA. The scheme of the pJP0 plasmid can be found in Appendix 1.

3.2.2. Large-Scale Plasmid Preparation

Competent Cell Transformation: The plasmids were transformed into chemically competent cells of *E. coli DH5α or BL21* strains. Heat-shock transformation was carried out using 100 µl competent cell aliquots thawn on ice. 2-10 µl of the PCR reaction mixture or 1 µl of stock plasmid (depends on concentration) were added. The mixture was softly shacked and kept on ice for 10 min, at 37 °C for more 3 min and on ice for 3 min. 500 µl LB medium (25 g/l without antibiotic) were added to the mixture and the cells were grown by incubation at 37 °C and 400 rpm for 30 min. The tubes containing cells were centrifuged 2 min at 800 rpm. 500 µl of supernatant were discarded. Cells were resuspended in the remaining supernatant (50-100 µl) and subsequently were spread on culture plates. Petri dishes with LB-agar (25 g/l LB, 15 g/l agar and 100 µg/ml ampicillin were plated with 50 µl cell suspension distributed homogeneously on the plate surface. Plates were incubated at 37 °C over-night.

Small liquid cultures: A single colony from the Petri dish was selected, picked with a sterile pipette tip and dropped into a culture tube containing 6 ml LB (100 µg/ml ampicillin). Cells were grown by incubation at 37 °C and shaking at 220 rpm for 6 h. Aliquots of the mixture were mixed with 50% glycerol and stored at -80 °C as stock. If necessary for sequencing, small culture was harvested by centrifugation at 12000 rpm and 4 °C for 15 min and the plasmid was purified using the Plasmid DNA Mini Kit form OMEGA Bio Labs.

Large liquid cultures: 400 ml LB medium (100 µg/mL ampicillin) were inoculated with 5 ml of the small culture. Cells were grown overnight by incubation at 37 °C and shaking at 220 rpm. The cells were harvested by centrifugation at 15000x*g* and 4 °C for 15 min and the plasmid was isolated and purified using the Plasmid DNA Maki Kit from OMEGA Bio Labs.

3.2.3. RNA T7 – polymerase production

Plasmid p911, carrying the *T7 RNA polymerase* encoded gene[202] as well as the genes for ampicillin and chloramphenicol resistance, were kindly given by Prof. Roland K.O. Sigel from University of Zürich. 2 µl of plasmid were transformed into chemically competent cells (*E. coli BL21*) as explained in section 3.2.2.

These cells were plated in Petri dishes containing ampicillin (100 µl/ml) and chloramphenicol (34 µg/ml) and incubated at 37 °C overnight. A single colony was selected with a pipette tip and transferred into a 40 ml LB medium (100 µl/ml ampicillin and 34 µg/ml chloramphenicol). Cells were grown by incubation at 37 °C and 180 rpm overnight. 15 ml of the previous culture were added to two 800 ml cultures that were incubated for 3-4 more hours. OD_{600} of the cultures was checked using UV-vis spectrophotometer (Ultrospec 7000 de GE Healthcare Life sciences). Cells were kept growing until OD_{600} reached 0.5-0.7. When the cell growth was optimal, the protein production was induced by addition of 0.4 mM IPTG as final concentration and then the cells were kept in the incubator for additional 4 h.

Subsequently, cells were harvested by centrifugation at 6000 rpm, 4 °C for 15 min; the supernatant was refused and cell pellet was stored at -80 °C overnight.

The cell pellets were resuspended in 20 ml of Lysis Buffer (0.05 M $Na_2HPO_4 \cdot 12H_2O$, 0.3 M NaCl, 0.02 M Imidazole, pH=7.5, sterile-filtered and degassed for 30 min) and transferred into 50 ml centrifuge tubes. Tubes were kept on ice and sonicated in 6 cycles of 30 s, with 30 s of repose to avoid sample degradation. After sonication, the samples were centrifuged at 15500 rpm, 4 °C for 45 min. Supernatant was transferred to new tubes and kept on ice while the pellets were refused.

Supernatant was slowly sterile-filtred with 0.22 µm filter to prepare the sample to perform FPLC (Fast Protein Liquid Chromatography). An ÄKTAprime plus from GE Healthcare Life sciences with a His-Trap FF, nickel Sepharose 6 column was used for the *T7 RNA polymerase* purification. The process can be divided in 5 steps:

-Purge of the system: injection of ethanol 20% at 10 ml/min flow for 5 min. Then the flow was stopped and the column was connected to the system. UV lamp was set at 280 nm and maximum pressure at 0.3 MPa. Then the entire system was rinsed with degassed water for 10 min at 5 ml/min flow.

-Column equilibration: Lysis Buffer was injected at 5 ml/min flow for 2-3 min and then 2-3 min of Elution Buffer (0.05 M $Na_2HPO_4 \cdot 12H_20$, 0.3 M NaCl, 0.5 M Imidazole, pH=7.5, sterile-filtered and degassed for 30 min) to end up with other 2-3 min with Lysis buffer.

-Sample injection: the sample was injected at 1 ml/min flow. The sample volume was about 20 ml. The UV absorption increased to 3000 mAU, subsequently to the end of the sample injection, Lysis buffer was injected at 1 ml/min flow until UV absorption was back to the initial value (30 mAU).

-Elution: a gradient from 0% to 100% Elution Buffer at 1 ml/min flow for 40 min was injected. Fractions of 6 ml were automatically collected. *T7-RNA polymerase* was eluted at the beginning of the gradient as it was shown by an increase of the absorption.

-Wash: 5 ml/min flown for 10 min with Elution Buffer, 10 min with Lysis Buffer, 10 min of NaCl 1.5 M, 10 min NaOH 1M and lastly, 10 min water. Subsequently, the flow was reduced to 1 ml/min and water was injected for 1 h. Finally, the flow was increased to 5 ml/min and ethanol 20% was injected for 10 min, then the column was disconnected and stored at 4 °C.

The FPLC fractions containing the *T7 RNA polymerase* were transferred to a dialysis membrane previously rehydrated in water for 3 h. Dialysis membrane was sealed with a clip once it contained the *T7 RNA polymerase* fraction, disposed in 2 l Dialysis Buffer (50 mM Tris-HCl, pH=8, 100 mM NaCl, 2 ml β-mecaptoetanol) and shaked for 2 h at 4 °C. Afther 2 h, the Dialysis Buffer was removed and 3 l of new Dialysis Buffer were used. Dialysis membranes containing the samples were shaken at 4 °C overnight.

Once the sample was dialyzed, it was concentrated to a final volume of 10 ml by centrifugation at 3000 rpm, 4 °C for 20 min using a VivaSpin 20 (10000 MWCO from GE Healthcare Life Science). Once the T7 was concentrated, aliquots of 1 ml sample: glycerol (1:1) were prepared, well mixed and stored at -20 °C.

The purity of the *T7- RNA polymerase* obtained was analysed with a SDS-PAGE gel in Tris-Tricine buffer (Tris-Tricine buffer 3X: 3M Tris-HCl, pH=8.45 and 0.3% (m/v) SDS). Along the process different fractions were stored at 4°C for further analysis: 1) cells prior addition of IPTG; 2) cell after incubation with IPTG; 3) supernatant of the cell pellet; 4) supernatant after sonication; 5) sample after the FPLC prior dialysis; 6) and 7) samples after dialysis and VivaSpin.

The SDS-PAGE gel was prepared using the following procedure (see Figure 29):

i) the SDS running gel solution (14% acrylamide (32:1), 1X Tris-Tricine buffer and 0.5% glycerol) was mixed with APS 10% and TEMED and loaded in the gel plates. The plate was not filled up with the SDS running solution, the last centimetre was filled with isopropanol and left until complete polymerization of the gel.

ii) After polymerization, the isopropanol was removed, and this centimetre of gel plate was filled with the SDS stacking gel solution (4% acrylamide (32:1), 1X Tris-Tricine buffer) mixed with the APS 10% and TEMED and the combs for the lines formation were introduced.

iii) When the gel was completely polymerized, it was placed in the gel cassette, cathode chamber was filled with cathode buffer (0.1 M Tris, 0.1 M Tricine and 0.1% (m/v) SDS, pH=8.25) and the tank was filled with anode buffer (0.2 M Tris-HCl, pH=8.9).

iv) 40 µl samples 1) to 7) were heated to 95 °C and were shaken for 5 min followed by addition of 40 µl of Tricine Sample Buffer (100 mM Tris-HCl, pH=6.8, 24% (m/v) glycerol, 8% (m/v) SDS, 5% (v/v) β-mercaptoethanol and 0.22% (m/v) bromophenol blue).

v) 15 µl of the sample mixture was loaded to each pocket and the gel was run at 90 V for 30 min and at 120 V for 1 h. A protein ladder was also loaded into the gel.

vi) The gel was revealed using the Coomassie blue method. The gel was covered by 1 cm of Coomassie Staining solution (10% (v/v) acetic acid, 44% (v/v) methanol and 0.1% (v/v) of Coomassie blue in water) and was shacken overnight. Subsequently, the Coomassie staining solution was replaced with the Coomassie Destaining (10% (v/v) acetic acid, 25% (v/v) methanol in water) and left shaking for 4 h. Afterward, protein bands could be observed directly by eye.

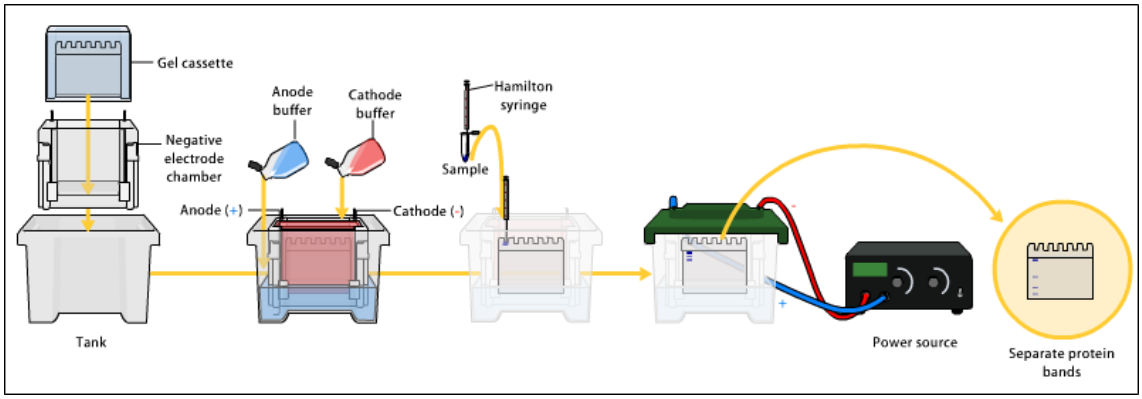

Figure 29. Scheme of the steps and procedure for the SDS-Page for protein analysis[i]

[i] "SDS-PAGE Electrophoresis" by Bensaccount is licensed under CC BY 3.0

Transcription trials with increasing amounts of the newly synthesized protein were made to know the concentration/activity ratio and the amount of *T7-polymerase* to be added for further transcription reactions.

Transcription trial experiments of 50 µl were prepared with: 5 mM NTP, 1X TXN buffer (40 mM Tris-HCl, pH=7.5, 2 mM Spermidine and 5 mM DTT), 0.01% Triton-X-100, 15 µg/ml digested plasmid, 30 mM $MgCl_2$ and increasing amounts of *T7-polymerase*: 10, 20, 30, 40, 50, 60, 70, 80, 90 and 100 µl/ml. Reaction mixtures were incubated at 37 °C and 300 rpm for 5 h and consequently centrifuged during 1 min at 6000 rpm. 40 µl supernatant were mixed with 40 µl of ULB (23.6 M urea, 16.7% Sucrose, 0.17% xylene cyanole and 0.17% bromophenol blue, 83 mM Tris-HCl, pH=7.5 and 1.7 mM EDTA). The mixture was loaded into a PAGE 10% denaturalized gel and it was run for 2.5 h at 24 W. Finally, RNA bands were visualized using a UV lamp.

3.2.4. Preparation of the RNA

3.2.4.1. Preparation of MB01

The reaction conditions used for the linearization of plasmid pMB01 were: 100 µg plasmid, 1X R buffer, 200 U *HindIII* in a final volume of 400 µl. Reaction mixtures were incubated for 4 h at 37 °C. Subsequently, restriction enzyme was deactivated at 80 °C for 20 min. Agarose gel was run to ensure the total linearization of the plasmid.

The construct MB01, a sequence of 214 nt. corresponding to the aptamer of the *btuB* riboswitch was prepared by *in vitro* transcription with the homemade *T7 RNA polymerase*. *In vitro* transcription conditions were: 20 µg/ml digested plasmid (pMB01), 5 mM each NTP, 0.01% triton-X-100, 30 mM $MgCl_2$, 1X TXN Buffer and 40-70 µl/ml of *T7 RNA polymerase* (depending on the batch). Reaction mixture was incubated for 5 h at 37 °C and 300 rpm. After incubation, tubes were centrifuged for 2 min at 4 °C and 6000 rpm. After centrifugation, supernatant was transferred into new tubs and ethanol precipitated; 2.5 volumes of ice cold ethanol 100% and 250 mM NaCl were added and stored at -20 °C overnight. The precipitated RNA was centrifuged 30 min at 4 °C and 12000x*g*, supernatant was discarded, and RNA pellet was dried in the Vacuum Concentrator Plus, Eppendorf. Once the pellet was dried, RNA was resuspended in the minimum amount of water and purified by denaturing PAGE (10% w/v, 7 M urea) run at 40 W/gel for 5 h approximately[203,204]. RNA band was located by UV shadowing at 254 nm, excised and extracted from the gel using Crush and Soak methodology[204]: gel band was crushed in small pieces and stored at -20 °C overnight, 3 volumes of crush and soak buffer (10 mM MOPS, pH=6, 1 mM EDTA and 250 mM NaCl) were added, vortexed and shaken at 4 °C for 2.5 h, vortexing the sample for 30 s every 30 min. Lastly, samples were centrifuged for 15 min at 4 °C and 12000x*g* and

supernatant containing RNA was ethanol precipitated as previously explained. Dried RNA pellets were resuspended in ddH_2O and concentrated by *Vivaspin* (10000 MWCO) Centrifugation. RNA concentration was quantified spectroscopically by UV from absorbance at 260nm yielding ≈ 1.5 mg per 24 ml reaction.

3.2.4.2. Preparation of JP01

The reaction conditions used for the linearization of plasmid pJP01 were: 100 µg plasmid, 1 X R buffer, 200 U *XhoI* in a final volume of 400 µl. Reaction mixtures were incubated 3 h at 37 °C. Subsequently, restriction enzyme was deactivated at 80 °C for 20 min. Agarose gel was run to ensure the total linearization of the plasmid.

The construct JP01, a sequence of 243 nt. corresponding to the whole *btuB* Riboswitch (aptamer and expression platform until starting codon), was prepared by *in vitro* transcription with the homemade *T7 RNA polymerase* using the same conditions and steps explained for MB01 in 3.2.4.1 yielding ≈1.65 mg of RNA per 24 ml of TXN reaction.

3.2.5. Native gels

To evaluate the optimal Mg^{2+} concentration needed to fold RNA, native gels were used. Samples of 5 µM JP01, 100 mM KCl and 100 mM HEPES, pH=7.5 in a final volume of 10 µl were prepared. Magnesium concentrations used were: 1) 0, 1, 5, 10, 20 and 30 mM $MgCl_2$; 2) 0, 10, 20, 50, 100 and 200 mM $MgCl_2$; 3) 0, 0.25, 0.5, 0.75, 1, 1.5 and 2 mM $MgCl_2$; 4) 0, 1, 3, 5, 10, 20 and 50 mM $MgCl_2$.

The RNA was mixed with KCl and water, annealed at 90 °C for 45 s, subsequently HEPES and $MgCl_2$ were added and incubated 15 min at room temperature. Samples were then analysed in a native PAGE (6% w/v) and run for 3 h at 10 W/gel and 4 °C.

To evaluate conformational changes in the presence of AdoCbl, samples with 10 mM, 20 mM and 30 mM $MgCl_2$ were prepared with 0 or 0.5 mM AdoCbl. Preparation sample procedure was analogous to the cited above. After AdoCbl addition, sample were incubated for 15 more min at room temperature and lastly analysed by native PAGE (6% w/v). In presence of AdoCbl no observable differences were detected.

3.2.6. UV Melting curves

Melting curves were recorded for JP01 in water, with 100 mM KCl and an RNA concentration of *ca.* ≈0.18 µM. RNA in the presence of KCl was annealed for 45 s at 90 °C. 3 ml samples were filled into a 5 ml cuvette and covered with 0.5 ml paraffin oil to avoid sample evaporation. Additionally, cuvette was capped, and the cap was fixed with parafilm. A heating and cooling

cycle was performed between 10 to 93 °C. Absorption at 260 nm was recorded over the given temperature range and it was done for duplicate.

The same experiments were performed with addition of 5 mM $MgCl_2$, and with 5 mM $MgCl_2$ in presence of 100 µM of AdoCbl, after annealing using the same temperature range and recording the absorbance at 260 nm in duplicate.

3.2.7. In-line probing experiments

3.2.7.1. 5'-End Labelling of the RNA

Both constructs, MB01 and JP01, were 5'-labelled with ^{32}P-γ-ATP (150 µCi/µl, 3000 Ci/mmol, PerkinElmer) following the same procedure[189]. 240 pmol of RNA were dephosphorylated by mixing 1X Multicore Buffer, 20 U *TSAP* in a final volume of 50 µl. The reaction mixture was incubated at 37 °C, 300 rpm for 30 min. Immediately afterwards, the RNA was purified by phenol/chloroform extraction using the following procedure: to the 50 µl of sample, 2.5 µl of NaCl 5 M were added, consecutively 52.5 µl of phenol were added and vortexed to mix. The mixture was centrifuged for 3 min at 10000 rpm in order to separate the phases. The aqueous phase was stored and a second extraction with 50 µl of ME buffer (10 mM MOPs, pH=6, and 1 µM EDTA) was performed to the organic phase.

The aqueous phases were combined and 100 µl of chloroform were added and subsequently vortexed and centrifuged. The aqueous phase was transferred to a new tube and a second extraction with chloroform was performed. After the extraction, the RNA was precipitated with ethanol overnight, centrifuged during 30 min at 4°C and 13200 rpm, the supernatant was discarded, and the RNA pellet was dried in the concentrator for 20 min and finally, resuspended in 8 µl ME buffer.

Dephosphorylated RNA was mixed with 4 µl of ^{32}P-γ-ATP, 4 U of T4 polynucleotide kinase (PNK) and 1X PNK Buffer in a final volume of 20 µl. The sample was incubated at 37 °C and 300 rpm for 30 min. Reaction mixture was purified by denaturing PAGE (5% w/v, 7 M Urea) run at 20 W for 2.5 h. RNA was visualized using Storage Phosphor Screen and subsequently scanned and digitalized with Typhoon FLA 9500 GE Healthcare Life Sciences. The RNA band was excised and extracted from the gel using the crush and soak methodology explained in section 3.2.4. RNA pellets were then dissolved in ddH_2O and the concentration was quantified by scintillation counting and spectroscopically from absorbance at 260 nm using a Picodrop CUBE.

3.2.7.2. In-line probing titrations

In-line probing experiments were performed using ^{32}P-5'-labelled RNA (≈2.5 nM ^{32}P-labelled RNA). RNA was annealed for 45 s at 90 °C prior to the addition of 50 mM Tris-HCl, pH=8.3, 100 mM KCl, 20 mM $MgCl_2$ and the corresponding concentration of the B_{12} derivative (see below) in an overall volume of 10 µl. The RNA was incubated with increasing amounts of the corresponding B_{12} derivative for 40 h at room temperature in the dark. The cleavage bands were separated by denaturing PAGE (10% w/v, 7 M) and quantified using ImageQuant TL 8.1 de GE Healthcare Life Sciences.

OH^- Ladder:

The alkaline hydrolysis cleavage ladder was prepared by mixing ^{32}P-labelled RNA (same concentration as the corresponding experiment) with 0.2 M $NaHCO_3$, pH=9, in an overall volume of 10 µl, and incubated for 5 min at 90 °C.

T1 Ladder:

The T1 cleavage ladder, a G sequencing ladder catalysed by *ribonuclease T1* (restriction enzyme that cuts the sequence after G) was prepared by mixing ^{32}P-labelled RNA (same concentration as the corresponding experiment) with sodium citrate 25 mM, pH=5, and 1 U *T1 ribonuclease* in colourless FLB (10 mM EDTA in formamide) in an overall volume of 10 µl. The sample was incubated at 55 °C and 300 rpm for 15 min.

Blank:

The ^{32}P-labelled RNA was diluted in water to the same concentration as the corresponding experiment. The sample did not contain Mg^{2+}.

The titration experiments were performed under conditions as described above. Both constructs MB01 and JP01 where incubated with increasing concentrations of AdoCbl and Vitamin B_{12}. The same titration conditions for one B_{12} derivative were used for both RNA constructs.

AdoCbl titrations: titrations were done by addition of AdoCbl to a final concentration of 0, 50 nM, 100 nM, 200 nM, 300 nM, 400 nM, 500 nM, 1 µM, 2,5 µM, 10 µM, 50 µM, 100 µM and 500 µM.

Vitamin B_{12} titrations: titrations were done by addition of Vitamin B_{12} to a final concentration of 0, 1 µM, 2.5 µM, 10 µM, 50 µM, 100 µM, 250 µM, 500 µM, 750 µM, 1 mM and 2.5 mM.

3.2.8. Isothermal titration calorimetry (ITC)

ITC system (Nano-ITC low volume, TA Instruments) was cleaned out with SDS 2% solution (≈200 ml), subsequently, reference and titration cells were filled with SDS 2% solution and heated to 80 °C for 1 h. Lastly, in both cells, ethanol 70% was injected, rinsed with ddH_2O and measurement temperature was set and stabilized overnight.

For optimal results is extremely important to have the same buffer concentration in all solutions used in an ITC experiment in order to avoid errors due to dilution heat. For these reason, stock 10X ITC buffer (1 M HEPES-KOH, pH=7.5, 1 M KCl and 50 mM $MgCl_2$) was added in the needed amount to prepare all ITC solutions.

To perform an ITC experiment, 1 ml ITC Buffer 1X, 500 µl AdoCbl (150-250 µM, protected from light to avoid degradation) in ITC Buffer 1X and 250 µl RNA (15-20 µM, RNA solution was annealed at 90 °C for 45 s and kept on ice prior ITC Buffer addition) in 1X ITC Buffer were needed. Exact concentration of AdoCbl and RNA solution was spectroscopically measured. All solutions were degassed at the experiment temperature for 15 min prior to be injected. Reference cell was filled with 250 µl of 1 X ITC Buffer, titration cell with 250 µl RNA solution and 50 µl were loaded in the titration syringe.

Blank experiments were also performed. In this case, titration cell was also filled with 1X ITC Buffer to record dilution heat, which needs to be subtracted to the experimental heat. Titration parameters used were: 17 injections of 3.03 µl with a collection time of 300s between injections.

ITC experiments were recorded for at 15, 17.5, 20, 22.5, 25, 27.5 and 30 °C for JP01 and 15, 20, 25 and 30 for MB01. Experiments at all the conditions were run in triplicate.

Titrations using Vitamin B_{12} as titrant were tried without any satisfactory result. The reaction heat was too low to be distinguished from background and dilution heat.

3.2.9. Fluorescence studies by coupling the *btuB* Riboswitch with *mCherry* protein.

M9 medium

The M9 medium was used due to the absence of cobalamins, while LB can contain uncertain quantities of cobalamin from the yeast extract. 5X M9 salts solution contained $Na_2HPO_4{\cdot}7H_2O$ (64 g/l), KH_2PO_4 (15 g/l), NaCl (2.5 g/l) and NH_4Cl (5 g/l) dissolved in water and autoclaved.

For M9 supplemented medium (M9 medium), sterile M9 salts were diluted to 1X final concentration and supplemented with the following nutrients that were sterilized by filtration

prior to use: glucose (0.4%), $MgSO_4$ (2 mM), $CaCl_2$ (100 µM), DL-alanine (100 µg/mL), L-arginine (22 µg/mL), glycine (100 µg/mL), L-histidine (22 µg/mL), L-leucine (20 µg/mL), L-isoleucine (20 µg/mL), L-methionine (20 µg/mL), L-proline (30 µg/mL), L-threonine (80 µg/mL), L-valine (40 µg/mL), L-lysine (88 µg/mL), L-cysteine (22 µg/mL), L-phenylalanine (20 µg/mL), L-tyrosine (20 µg/mL), L-tryptophan (20 µg/mL), L-serine (100 µg/mL), L-asparagine (100 µg/mL), L-glutamine (100 µg/mL), L-aspartic acid (100 µg/mL), L-glutamic acid (100 µg/mL), Niacin (1 µg/mL), calcium pantothenate (1 µg/mL), pyridoxine-HCl (1 µg/mL), thiamine-HCl (1 µg/mL) and biotin (500 ng/mL).

Cells incubation

Plasmid pJP04 was transformed into *BL21 (DE3)* cells according to the protocol described in 3.2.2. Small culture was centrifuged at 1000*xg* for 1 min. Supernatant was discarded and pellet was resuspended in 4.2 ml of M9 medium.

Then, the corresponding amount of B_{12} derivative was added to the sample according to the Table 2. Culture tubes containing M9 medium with different cobalamin concentrations were inoculated with 100 µl of bacterial culture in M9 (resuspended pellet), final volume of each sample was 4.1 ml. A blank sample without any cobalamin derivative was also prepared.

Samples were incubated for 8 h at 37 °C and 210 rpm. After 4 h incubation, IPTG to 0.4 mM was added. 3 ml of each culture was transferred into plastic fluorescence cuvettes and optical dispersion was measured at 650 nm (OD_{650}). It was attempted to equalize the samples dispersion values by addition of M9 medium (differences on dispersion ranged 5%).

Table 2. Fluorescence studies performed with the mCherry protein. The cobalamin derivatives used were adenosylcobalamin (AdoCbl), vitamin B_{12} (Vit B_{12}), cobinamide (Cbi) and neocobinamide (Neocbi) with diferent concentratiosn.

Tube	1	2	3	4	5	6	7	8	9	10
[AdoCbl] µM	0	0.1	1	10	30	50	100	250	500	750
[Vit B_{12}] µM	0.1	1	10	30	50	100	250	500	750	1000
[Cbi] µM	0.1	1	10	30	50	100	250	500	750	1000
[Neocbi] µM	0.1	1	10	30	50	100	250	500	750	1000

Finally, fluorescence of samples was measured using a Varian Cary Eclipse fluorimeter. Samples were excitated at 560 nm and emission was registered from 580 to 900 nm. Experiments were done in triplicate preparing new cultures every time.

The Cbi and Neocbi derivatives were synthesised by Marc Servera as part of his Master thesis entitled “Preparació de derivats de cobalamina i estudi de la seva interacció amb el ribocommutador de *K. pneumoniae*”.

3.3. Results and discussion.

For the full characterization of the full-length riboswitch from *Klebsiella pneumoniae* in-line probing, native gels and isothermal titration calorimetry were performed. The native gel provides information of the secondary structure of the RNA with or without interacting with the effective biomolecule. Native gels give a slight insight in the RNA folding in the presence of metal ions and the ITC provides a full characterization of the thermodynamic parameters of the interaction.

3.3.1. Native gels

Native gels were performed to evaluate magnesium effect on the RNA folding and consequently, on the secondary structure.

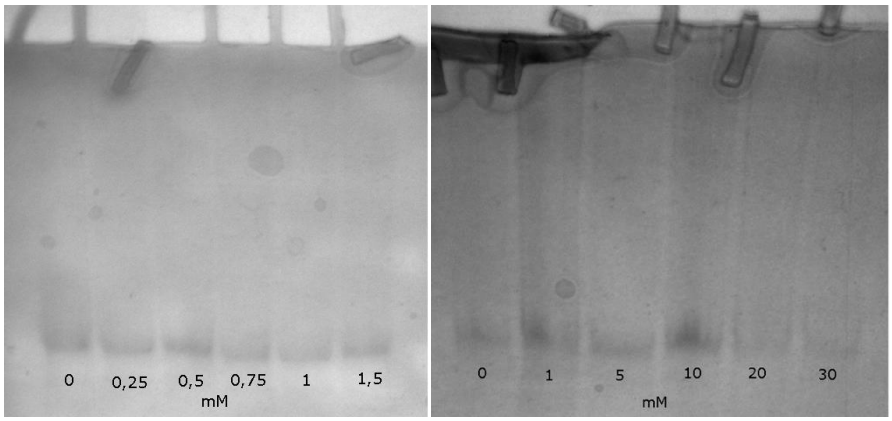

Figure 30. Native gel of JP01 titrated with increasing Mg^{2+} concentration.

Samples with magnesium concentration lower than 10 mM showed a broader band than samples with higher magnesium concentration. Therefore, due to sample aggregation, less RNA was migrating through the gel. Also, a small migration difference can be observed between 1 mM Mg^{2+} and 5 mM Mg^{2+}.

It can be seen in Figure 30 that samples containing from 0 to 0.5 mM magnesium migrated less in the gel than samples with higher magnesium concentration. This can be correlated with P. K. Choudhary et. al. result with *btuB* riboswitch of *E. coli*. In that case, raising the concentration of Mg^{2+} to 0.5 mM makes a noticeable conformational change to a more compact structure. This fact explains the increment of the RNA migration in the gel[87].

After native gels analysis we conclude that the optimal magnesium conditions for our construct were between 1 and 5 mM Mg^{2+} to ensure correct folding but avoiding aggregation.

Native gels analyses in the presence of AdoCbl were also performed trying to observe conformation changes in the RNA folding upon addition of coenzyme B_{12}. Unfortunately, conformational changes caused by the coenzyme B_{12} binding to the *btuB* riboswitch could not be observed with this technique, suggesting that they are quite subtle.

3.3.2. UV melting curves

To investigate the temperature stability of the RNA conformation in the presence of Mg^{2+}, thermal denaturation experiments were performed with and without the presence of the metal ion. In order to compare all the experiments, the dissociation fraction (α) was calculated as in Equation 1:

$$\alpha = (Abs\,\max - Abs\;x)\;/(Abs\,\max - Abs\,\min) \qquad \textit{Equation 1}$$

Where Abs max is the maximum absorbance, Abs min is the minimum absorbance and Abs x is the absorbance corresponding to the temperature.

The α obtained was plotted vs. temperature for both cases. The heating curves were less reproducible than the cooling curves due to the dependence of the heating system and condensation at the cuvette at low temperatures. For this reason, absorption data for the cooling process is the one used in the plot (Figure 31).

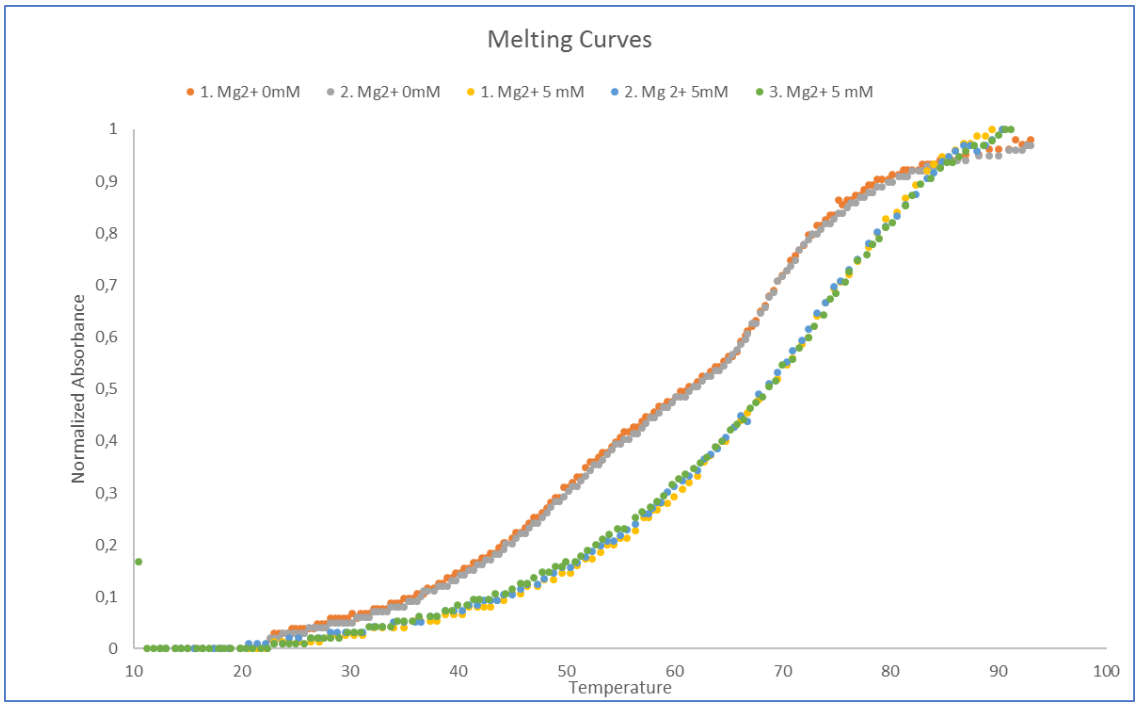

Figure 31. Melting temperature curves. Grey and Orange doted curves represent the RNA in absence of magnesium while doted curves in blue, yellow and green respresent the samples with 5 mM Mg^{2+}.

As can be observed in Figure 31, the curve in absence of magnesium shows two different steps, thus the RNA exhibits two unfolding steps. Although the two different steps can be observed in the graph, it has not been possible to fit the curve to obtain two corresponding melting temperatures. In presence of magnesium, only one transition is observed because only one secondary structure is likely stabilized in presence of the cation.

The melting temperature (Tm) can be defined as the temperature at which $\alpha = 0.5$[205], the interpolation in the curve at this value allows to calculate the Tm for both conditions (Table 3):

Table 3. Melting temperatures obtained in absence of magnesium and with 5 mM magnesium for the JP01 construct.

Experiment	Tm (°C) 0mM Mg^{2+}	Tm (°C) 5 mM Mg^{2+}
1	55.4	68.2
2	55.4	68.4
3	55.0	68.6
Average	55.3±0.2	68.4±0.2

The melting temperature for the RNA in absence of magnesium was 55.3 ± 0.2 °C while increases up to 68.4 ± 0.2 °C in presence of 5 mM Mg^{2+}. Thus, as it can be observed in the plot, the addition of 5 mM Mg^{2+} leads to a significative stabilization of the RNA conformation (~ 13 °C). Furthermore, in absence of the metal ion, the RNA seems to lose the conformation in two different steps while only one step was seen in presence of magnesium.

3.3.3. In-line probing

3.3.3.1. Evaluation of the titration experiments

Evaluation of the gels

As explained in section 3.2.7.2, in-line probing experiments were performed with both RNA constructs used in this study (JP01 and MB01) and with both B_{12} derivatives (AdoCbl and Vitamin B_{12}). Several titrations were incubated and loaded onto gels for analysis, however a poor resolution of the T1 ladder was observed in most of the gels apart from two, which were further analysed. They correspond to the JP01 construct titrated with AdoCbl and will be named as Gel A and Gel B hereafter.

Evaluation of changing bands:

The evaluation of the in-line probing gels A and B of JP01 (see Appendix 2) with increasing amounts of AdoCbl led to the observation of a total of 18 changing bands as it can be observed in the Figure 32, where the cleavage sites were depicted with green flags. Cleavage sites were numbered from 1 to 15 and bands 2', 4' and 8' were treated together with 2, 4, 8 respectively

due to their proximity in the sequence and same concentration dependent behaviour. The band number and their corresponding position in the sequence are shown in Table 4.

Table 4. Band numbers and their nucleotide position in the sequence.

Band	Nucleotide position
1	39
2	49
2’	53
3	58
4	70
4’	71

Band	Nucleotide position
5	78
6	81
7	90
8	104
8’	107
9	114

Band	Nucleotide position
10	120
11	133
12	148
13	166
14	184
15	208

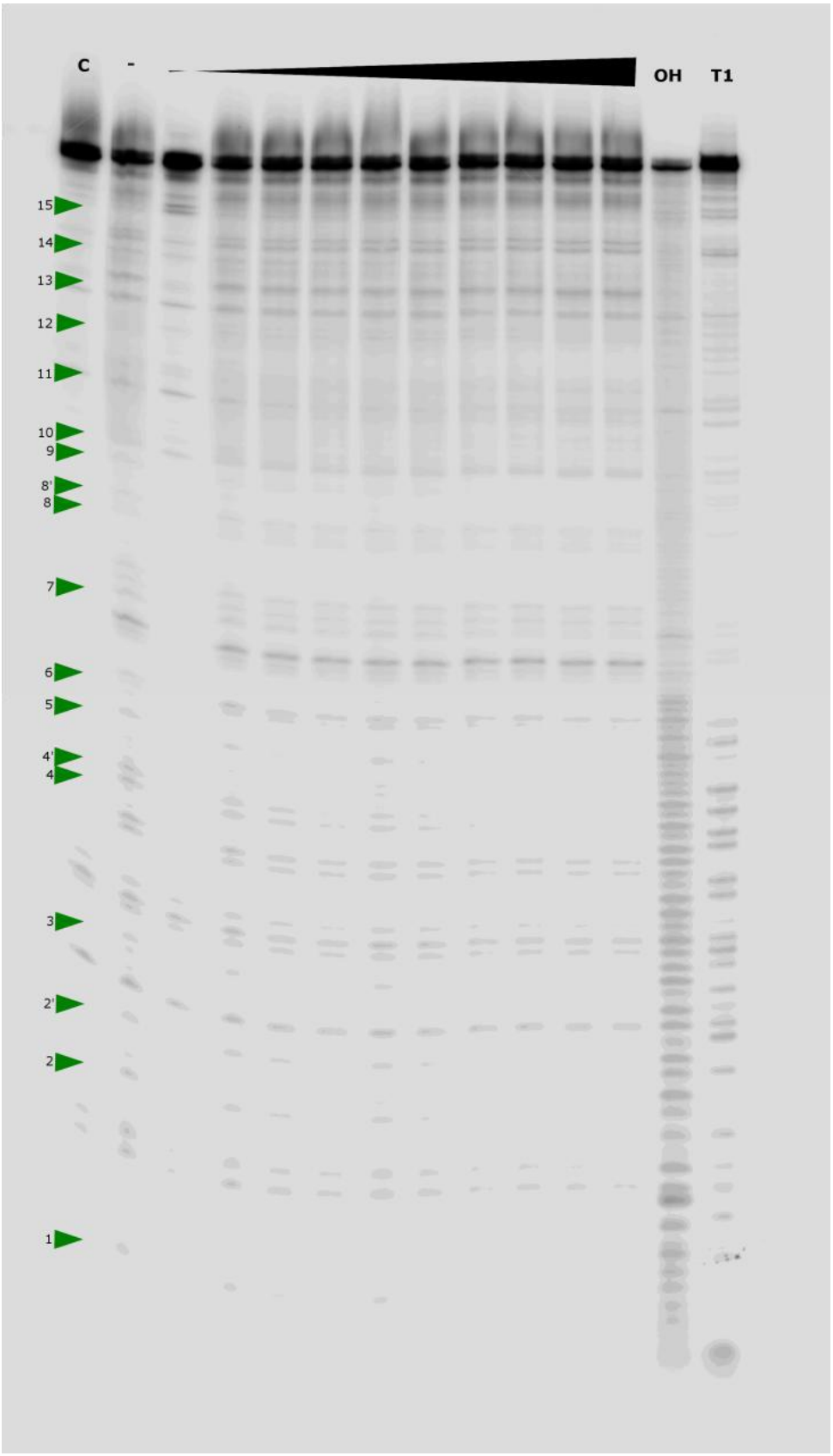

Figure 32. Gel B. Concentration dependent in-line probing experiment with JP01 and AdoCbl. Lane C is unreacted RNA. Lane – shows the cleavage patern of the RNA in the absence of AdoCbl. AdoCbl has been increased from left to right (A to K pockets) and OH and T1 are the ladders after alkaline and RNase T1 digestion. Green flags represent the 18 changing bands detected.

Background correction:

Correction of bands intensity deriving from deviations in the loaded volume were adressed by evaluation of two different constant regions (see Figure 33.

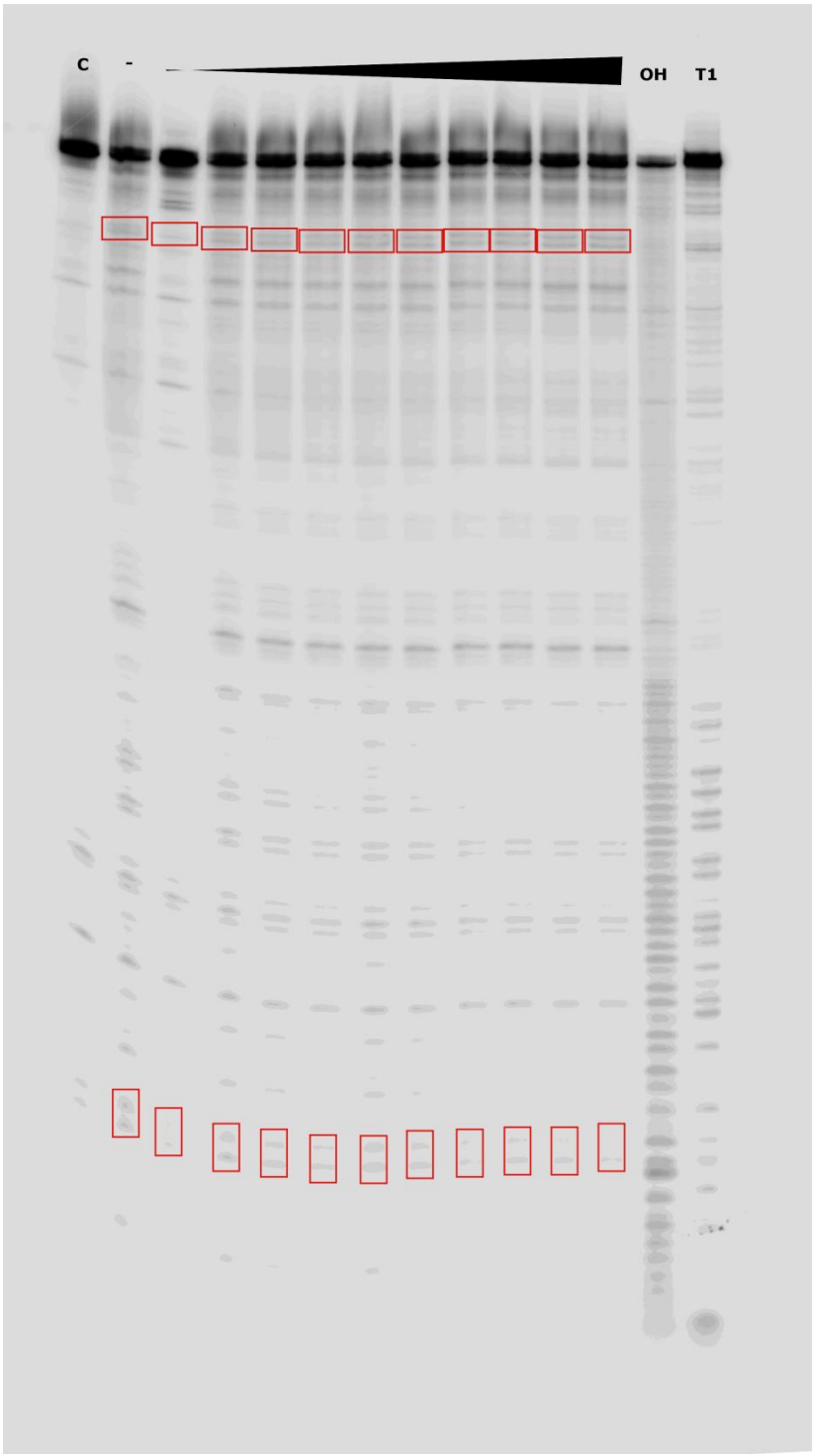

Figure 33. Gel B. Concentration dependent in-line probing experiment with JP01 and AdoCbl. The red squares depict the two regions selected (Zone 1 and Zone 2 from top to bottom) to correct the background.

The intensity of the two zones, depicted with red squares in Figure 33, were normalized dividing a single pocket intensity by the maximal intensity of the zone giving the R factor of the single zone (R1 and R2). Then, the R factor for each line was calculated by the average of the R factors of a single zone and are gathered in Table 5. Calculations for gel A are shown in Appendix 2.

Table 5. R factors calculation for intensity correction of gel B

Pocket	Zone 1		Zone 2		R factor
	Intensity 1	R1	Intensity 2	R2	
A	3632	0.886	321.9	0.847	0.867
B	3974	0.970	314.8	0.828	0.899
C	3616	0.882	331.0	0.871	0.877
D	3890	0.949	320.5	0.843	0.896
E	3296	0.804	257.0	0.676	0.740
F	3087	0.753	296.0	0.779	0.766
G	4098	1.000	380.0	1.000	1.000
H	3862	0.945	271.2	0.714	0.828
I	3409	0.832	239.0	0.629	0.730
J	3967	0.968	297.8	0.783	0.876
K	3459	0.844	243.9	0.642	0.743

Intensity correction of the single bands and fitting for Ka calculation

After the calculation of the R factor, the intensity of each band was corrected by dividing the intensity by the correction factor of the corresponding line giving the corrected intensity (I_{corr}) of each band (see Table 6).

Changes of each cleavage site were quantified by plotting the intensities of the single band after background correction ($I_{corr}/10^3$) vs. AdoCbl concentration using the software OriginLab. Experimental data were fitted to a 1:1 binding isotherm[206] (Equation 2).

$$y = dF + (dB - dF).\frac{\sqrt{\left(cRNA + x + \frac{1}{K_a}\right) - \left(cRNA + x + \frac{1}{Ka}\right)^2 - 4 \cdot cRNA \cdot x}}{2 \cdot cRNA} \quad \textit{Equation 2}$$

Where y corresponds to the $I_{corr}/10^3$, x to the AdoCbl concentration, dF is the RNA free fraction, dB is the RNA bound to AdoCbl fraction, Ka corresponds to the association constant of the

process and cRNA is the total concentration of RNA that was constant in all experiments ($2.6 \cdot 10^{-8}$ M). Figure 34 shows the data for the first changing band of the gels A and B and the calculated parameter after fitting the data to the 1:1 binding isotherm.

Calculation of the other bands and their fittings for both gels are shown in Appendix 2.

Table 6. Intensity correction calculations for band 1 of gel B. Depicted in blue data omitted in the fit.[9].

Pocket	I	R average	I corrected	[AdoCbl] µM
A	236.30	0.866	272.68	0
B	232.55	0.899	232.55	0.05
C	223.38	0.877	254.82	0.1
D	192.62	0.896	214.92	0.2
E	153.63	0.740	207.54	0.3
F	167.51	0.766	218.71	0.4
G	201.10	1.000	223.68	0.5
H	134.15	0.828	162.01	1
I	119.55	0.730	163.68	2.5
J	130.70	0.876	149.24	10
K	109.21	0.743	147.00	100

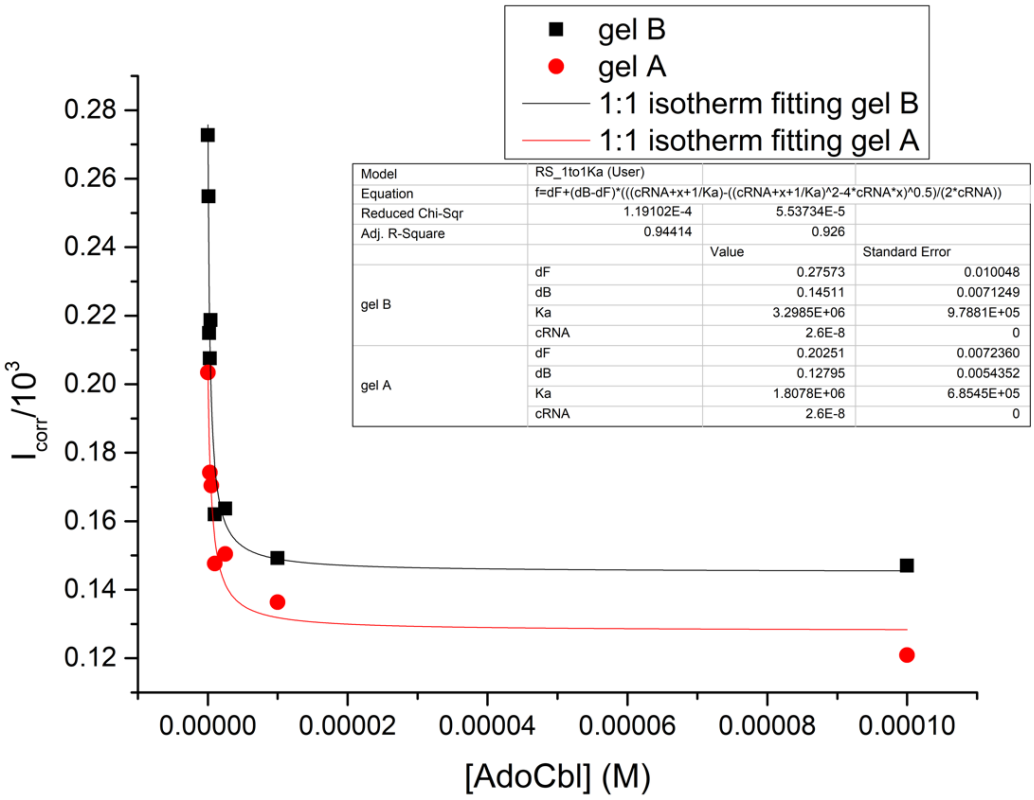

Figure 34. Plot of the corrected intensities vs AdoCbl concentration of site 1 of both gels A and B fitted to the 1:1 isotherm.

A Ka value was obtained for each cleavage site after fitting the data to the isotherm. These Ka values with their standard deviation are summarized in Table 7. The Ka of the process was calculated as the average of the Ka for the individual cleavage sites and the standard deviation calculated using the propagation of uncertainty method. Finally, the dissociation constant was calculated as the inverse of Ka. Obtained values are shown in Table 7.

Table 7. Association constant of the AdoCbl to every individual cleavage site with the corresponding standard deviation and the Ka, log Ka and KD of the overall interaction.

Site	K(AdoCbl)	Site	K(AdoCbl)
1	2.6E+06 ± 7E+05	**8**	9E+06
2	1.1E+07 ± 9E+06	**8'**	7E+06 ± 6E+06
2'	3E+06 ± 2E+06	**9**	3.270E+06 ± 7E+03
3	1.3E+06	**10**	2.2E+06
4	9E+06 ± 6E+06	**11**	1.1E+07 ± 8E+06
4'	4E+06 ± 2E+06	**12**	3.3E+06 ± 1.3E+06
5	1.23E+06	**13**	2.5E+06 ± 1.2E+06
6	2.18E+07	**14**	2.7E+06
7	6E+06 ± 5E+06	**15**	5.4E+06 ± 1.5E+06
$K_{mitjana}$(AdoCbl)	6E+06 ± 5E+06		
log $K_{mitjana}$	6.77 ± 0.37		
K_D	170 ± 140 nM		

It should be recalled that the sequence used in these experiments, JP01, included both the aptamer and the expression platform. The dissociation constant obtained after the calculations and fitting of the data agreed with the K_D values obtained for the well-studied *btuB* riboswitches from *E. coli* and *S. thypimurium* found in Table 8.

Table 8. Bibliographic values of the dissociation constant with AdoCbl for the well-studied btuB riboswitches.The constructs already studied do not carry the expression platform.

btuB riboswitch from	KD	sequence
Escherichia coli	89 nM[177] 300 nM[172]	202 nt
Salmonella thypimurium	400 nM[172]	206 nt

Evaluation of the relative intensity changes

Then, the intensity of each cleavage site was evaluated to understand the influence of the metabolite in each individual part of the RNA. To perform the evaluation, the parameter dF and dB obtained after the data fitting to the isotherm were used and calculations are shown in Table 9.

Table 9. Calculations of the relative intensity changes of the cleavage sites. Data from both gels are presented in the table.

	B	A	B	A	B	A	B	A	B	A	B	A	B	A
DECREASING	**dF**		**dB**		**y = error(dB)**		**f = 1/dF**		**dB(new) = dB*f**		**Decrease = -[1-dB(new)]**		**Corrected error=(f^2*y2)^0.5**	
1	0.276	0.203	0.145	0.128	0.007	0.005	3.627	4.938	0.526	0.632	-0.474	-0.368	0.026	0.027
2	0.500	0.254	0.175	0.135	0.007	0.011	2.000	3.942	0.350	0.533	-0.650	-0.467	0.015	0.041
2'	0.354	0.213	0.204	0.125	0.010	0.004	2.828	4.700	0.576	0.588	-0.424	-0.412	0.028	0.018
3		0.221		0.160		0.005		4.518		0.721		-0.279		0.023
4	0.664	0.412	0.320	0.212	0.014	0.012	1.507	2.428	0.483	0.514	-0.517	-0.486	0.021	0.029
4'	0.524	0.397	0.260	0.189	0.018	0.010	1.908	2.521	0.495	0.477	-0.505	-0.523	0.035	0.024
5		0.227		0.179		0.001		4.408		0.791		-0.209		0.003
6	0.559		0.433		0.005		1.789		0.775		-0.225		0.008	
7	0.816	0.529	0.624	0.392	0.014	0.007	1.225	1.890	0.764	0.740	-0.236	-0.260	0.017	0.013
9	0.672	0.565	0.409	0.267	0.016	0.009	1.488	1.770	0.608	0.473	-0.392	-0.527	0.024	0.016
11	2.317	1.968	1.833	1.464	0.025	0.040	0.432	0.508	0.791	0.744	-0.209	-0.256	0.011	0.021
12	1.900	1.567	1.033	0.817	0.042	0.034	0.526	0.638	0.544	0.521	-0.456	-0.479	0.022	0.022
14	3.679		2.447		0.049		0.272		0.665		-0.335		0.013	
INCREASING	**dF**		**z = error(dF)**		**dB**		**b = 1/dB**		**dF(new) = dF*b**		**Increase = 1-dF(new)**		**Corrected error=(b^2*z^2)^0,5**	
8	0.382		0.016		0.526		1.900		0.726		0.274		0.030	
8'	0.567	0.392	0.008	0.007	0.718	0.486	1.392	2.058	0.789	0.807	0.211	0.193	0.010	0.014
10	1.200		0.034		1.525		0.656		0.787		0.213		0.022	
13	2.594	1.814	0.080	0.062	3.282	2.346	0.305	0.426	0.790	0.773	0.210	0.227	0.024	0.026
15	6.407	3.989	0.369	0.790	8.451	7.332	0.118	0.136	0.758	0.544	0.242	0.456	0.044	0.108

When the intensity of the band decreased, a new dB was calculated dividing dB by the dF. Finally, the diminution of intensity was obtained as the negative value of 1 minus the dB previously calculated. Contrarily, when the intensity of the band increases a corrected dF was calculated by dividing the dF value by the dB and the relative increase of the intensity was finally obtained as 1 minus the dF corrected (see equations in Table 9).

The relative increments and diminutions of the intensity were then plotted vs the cleavage site in order to visualize the local changes that were produced upon interaction of the metabolite (see Figure 35).

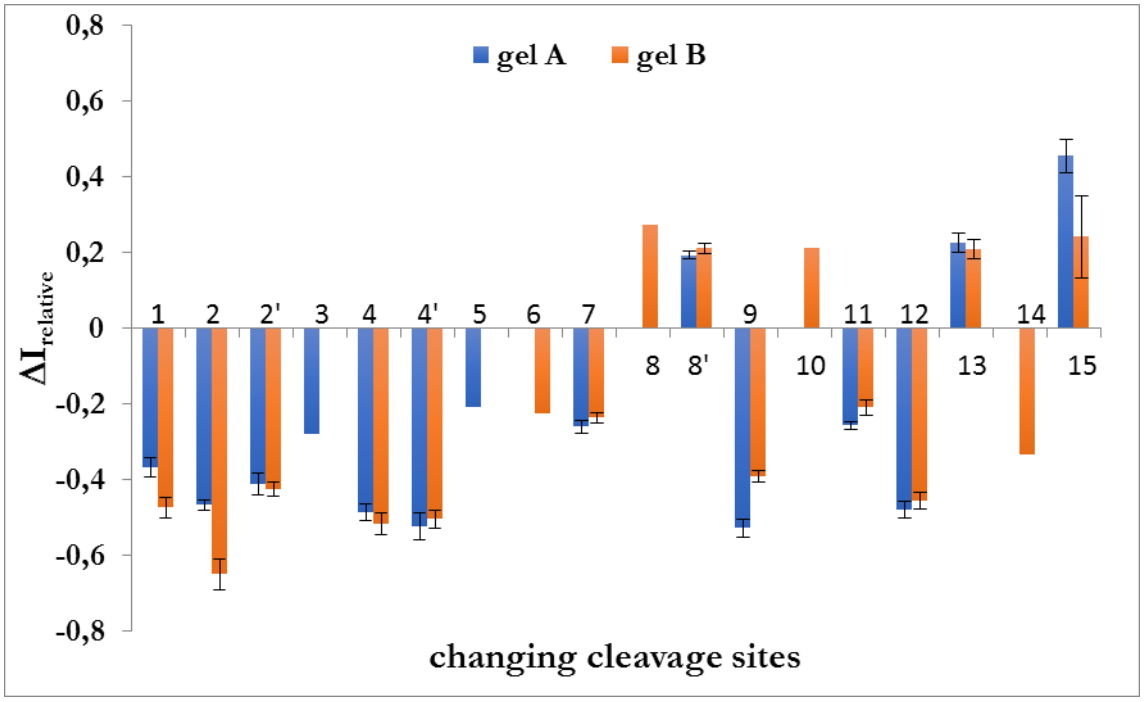

Figure 35. Plot of the relative intensity increases and decreases for every cleavage sites of both gels.

Due to the structural requirements of the self-cleavage reaction, those bands whose intensity have changed with the addition of the coenzyme B_{12} have undergone a change in their local structure. While small structural changes are the possible origin of such intensity changes, also larger changes like a switch from double-to-single stranded region (giving flexibility to the backbone) upon B_{12} biding or vice versa are feasible.

It can be observed in Figure 35 that bands 3 and 5 were only observable in gel A, while bands 6, 8, 10 and 14 were only present in gel B. It has been already mentioned that in-line probing is a widely used technique to analyse the changes in the RNA secondary structure. The technique can be also used to estimate the association constant of the interaction process as shown in Table 7.

In the in-line probing experiments, a band intensity increase implies a major cleavage probability in this RNA region, thus 8, 8', 10, 13 and 15 sites were involved in a conformational change to a more flexible zone upon the RNA interaction with AdoCbl. In contrast, the decrease of the band intensity implies a loss of cleavage in the zone that can be related with a major rigidity or a base paring formation in the proximity of the cleavage site when the RNA interacts with the AdoCbl.

It has been already mentioned that the *btuB* riboswitches exhibit a negative regulation of protein expression after binding to the metabolite. The cleavage sites identified from the in-line probing experiments allow the postulation of a secondary structure for the gene-on conformation of the *btuB* riboswitch from *K. pneumoniae* (Figure 36). In this conformation the RBS depicted in green is accessible to the ribosome and the *btuB* protein can be synthetized. The Figure 36 has been represented in consonance with the consensus structure of the most conserved regions[172] and the energy of the non-conserved parts of the riboswitch was minimized using the RNAfold web server. The yellow flags in the figure represent the position for the changing bands found in the in-line probing experiments.

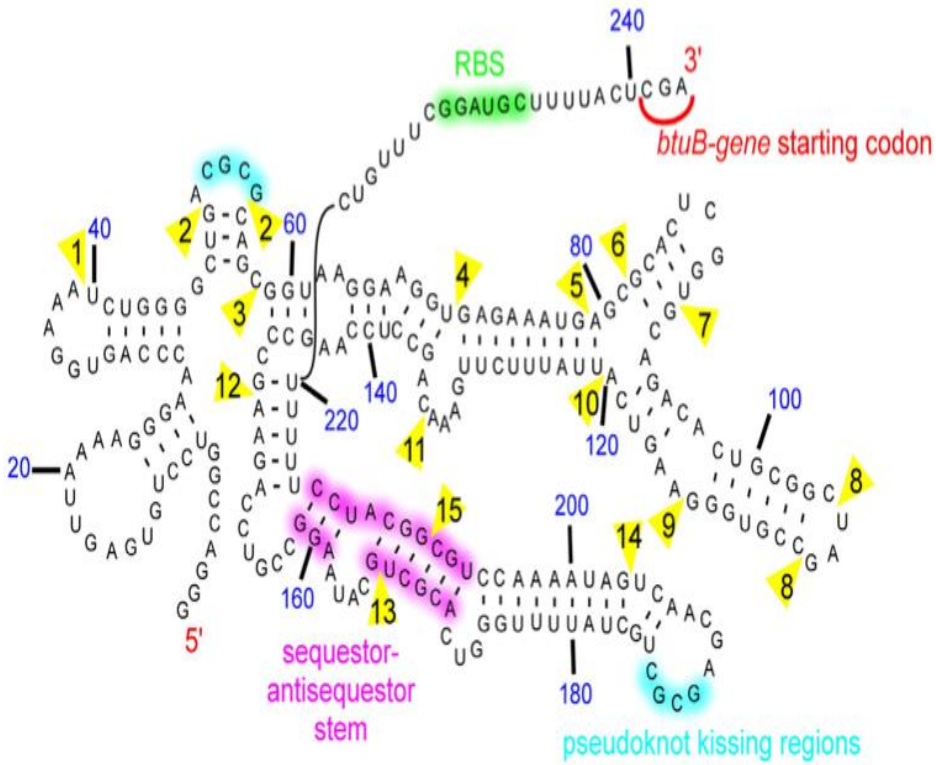

Figure 36. Secondary structure of the btuB riboswitch from K. pneumniae in its gene-on conformation, unbound to the AdoCbl metabolite. Yellow flags depict the changing band positions found in in-line probing.

In contrast, the riboswitch interaction with the AdoCbl leads to the gene-off conformation, which is represented in the Figure 37. In this conformation the RBS is masked in the RBS-

sequestor hairpin depicted in green. Thus, the *btuB* riboswitch upon the AdoCbl binding inhibits the synthesis of the *btuB* protein. In the figure, cleavage sites found in the in-line probing experiments are also depicted by yellow flags.

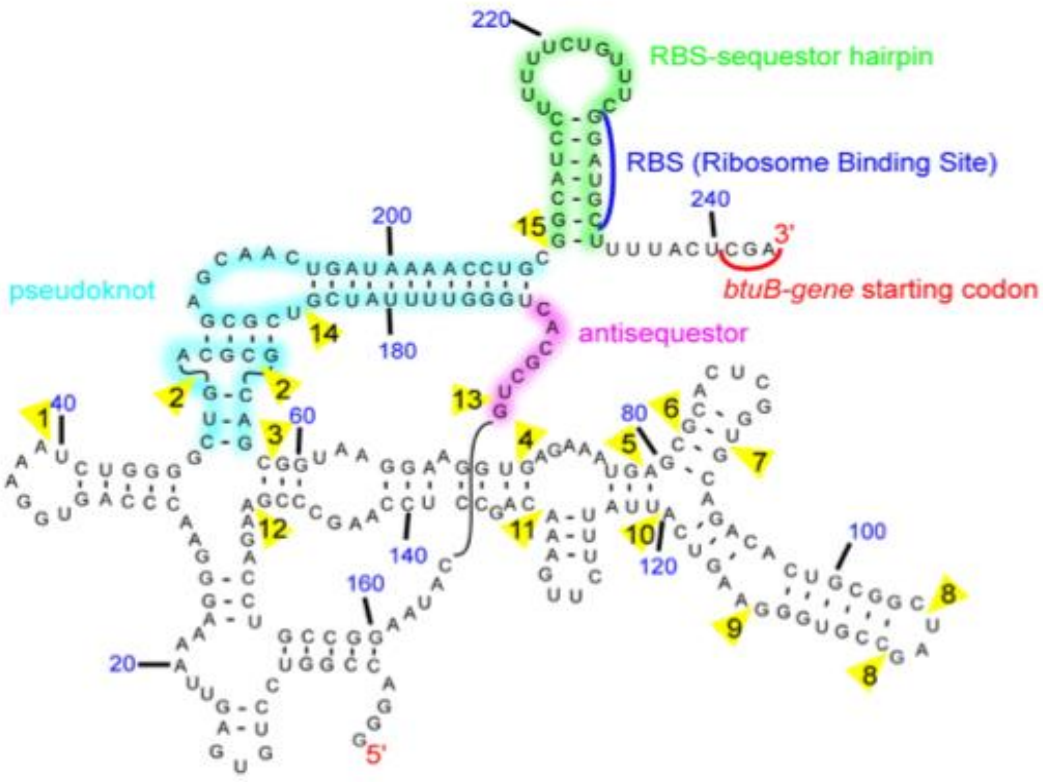

Figure 37. Secondary structure of the btuB *riboswitch from K. pneumniae in its gene-off conformation, upon binding to the AdoCbl metabolite. Yellow flags depict the changing band positions found in in-line probing.*

The comparison of the gene-on and gene-off conformations of the *butB* riboswitch from *K. pneumoniae* and the relative changes of intensity represented in Figure 35 shows that they are in agreement. For instance, the bands corresponding to cleavage sites 2 and 2' decrease their intensity when the AdoCbl concentration increases. Those bands are situated in a flexible zone in the gene-on conformation whereas in the gene-off conformation they form part of a rigid base pair region implicated in the formation of the pseudoknot. On the other hand, bands 13 and 15 increase their cleavage upon interaction of the AdoCbl. These two bands are situated in the sequester-antisequestor stem depicted in pink in the gene-on conformation, which is a rigid motif due to the base pair formation in the region. Upon interaction with the coenzyme B_{12}, the RNA is shifted to the gene-off conformation in which the antisequester region, where the cleavage site is situated, is single stranded having more flexibility and probability to be cleaved. The same occurs for the band 15 which is placed as a linkage between two stems.

The cleavage intensity of some other bands is more difficult to interpret from the comparison of the two conformational structures. However, it is necessary to keep in mind that some changes in the bands intensities can be directly influenced by the direct interaction of the metabolite with a specific RNA region, which can change the local flexibility of the sequence.

The results presented are consistent with those from the well-studied B_{12}-riboswitches from *E. coli* and *S. typhimurium*. Although being of different primary sequence, the affected cleavage sites appear at similar locations on the secondary structures and are consistent with the regulatory function of the sequence. The comparison of the cleavage sites obtained for *K. pneumoniae* with the 8 main sites found by Nahvi et al. in the *btuB* riboswitch from *E. coli* and later 9 sites found by Gallo et al. is shown in Figure 38. Seven of these cleavage sites found in *E. coli* match with those found in *K. pneumoniae* in secondary structure localization as observed by comparing Figure 37 to Figure 38. The equivalent cleavage sites are summarized in Table 10. The site 1 from *E. coli*, if present in *K. pneumoniae* could not be identified due to experimental limitations. The site 2 in *E. coli* was not present in the *K. pneumoniae* structure probably because of the distinct difference in size of the P8 region. This is intriguing because it implies that the local structures at these sites are equivalent to each other in both riboswitches.

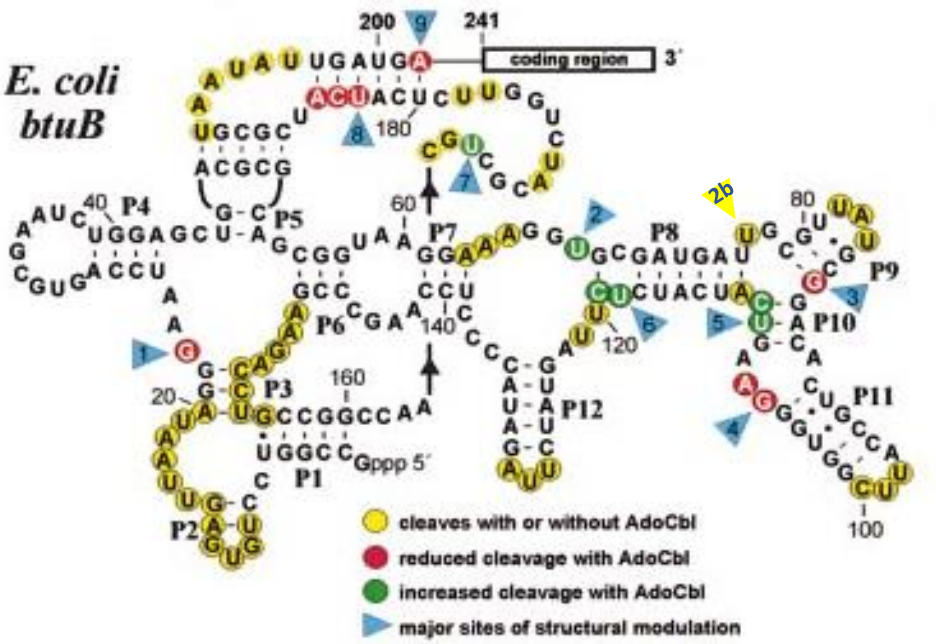

Figure 38. Secondary structure model for the btuB riboswitch from E.coli of 202 nt. length. Depicted with blue flags the cleavage sites identified with the in-line probing experiments. [172] *Depicted with a yellow flag a new evaluated cleavage site*[177.j]

[j] Nahvi, A., Barrick, J. E. & Breaker, R. R. Coenzyme B_{12} riboswitches are widespread genetic control elements in prokaryotes. (2004) *Nucleic Acids Res.* **32,** 143–150 by permission of Oxford University Press

Table 10. Comparison of the equivalent cleavage sites from E.coli and K. Pneumoniae.

Cleavage site *E. coli*	Cleavage site *K. pneumoniae*
2 (68 nt)	4 (71 nt)
2b (77 nt)	5 (78 nt)
3 (87 nt)	7 (90 nt)
4 (106 nt)	9 (115 nt)
5 (110 nt)	10 (120 nt)
7 (164 nt)	13 (166 nt)
8 (183 nt)	14 (184 nt)
9 (202 nt)	15 (208 nt)

It is also important to note that the *btuB* riboswitch from *K. Pneumoniae* presents some additional cleavage sites that are not present in previous studied sequences such as sites 1, 2, 3, 6, 8 and 12.

3.3.4. Isothermal Titration Calorimetry

ITC was used to measure the heat evolved or absorbed during the RNA-B_{12} interaction. The experiments allow a characterization of the thermodynamic parameters of the interaction, yielding the enthalpy (ΔH), entropy (ΔS), stoichiometry (n) and the association constant (Ka) in a single experiment. Moreover, from these data, also Gibbs energy and the dissociation constant of the process can also be calculated.

In the experiments at a certain temperature, the raw heat vs time was recorded for both experiments, with B_{12} as titrant and RNA as a titrate (Figure 39) and the dilution experiment where the buffer was used as titrate (Figure 40). Then, the dilution heat was subtracted from the experimental heat, to yield the value of the heat which corresponds only to the interaction between the RNA and the B_{12} derivatives.

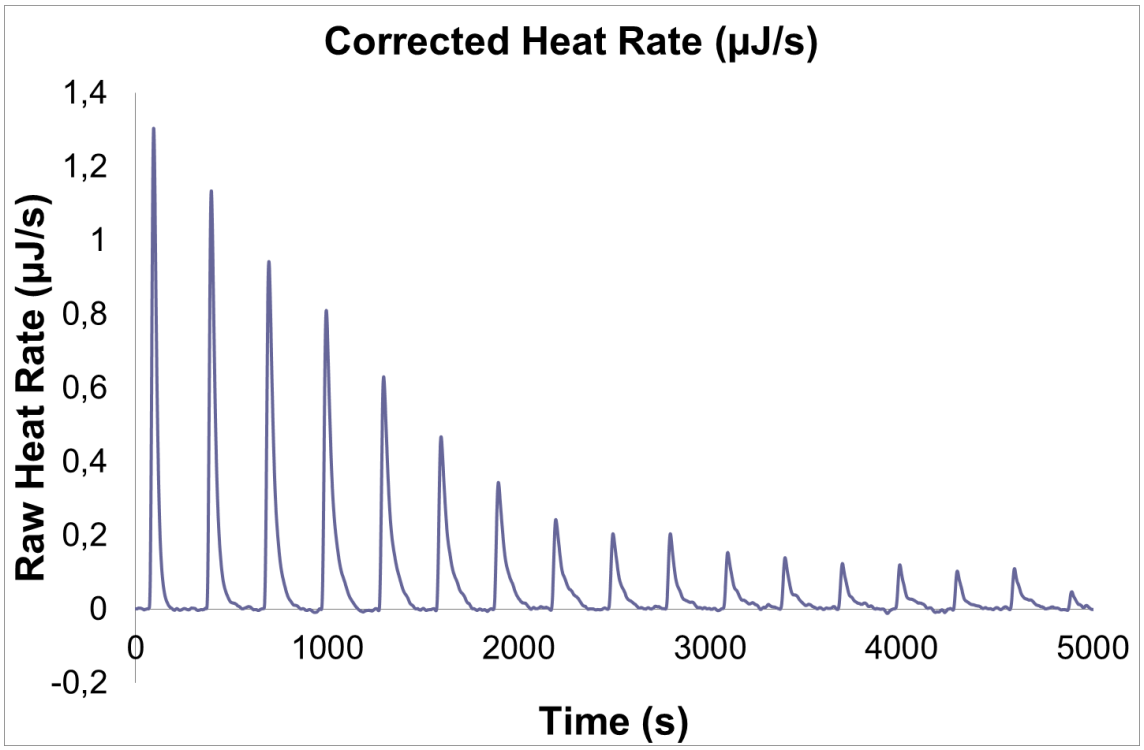

Figure 39. Plot of the Raw Heat (µJ/s) vs. time (s) in an AdoCbl titration at 25°C with JP01. Every peak corresponds to the heat released after a titrant injection.

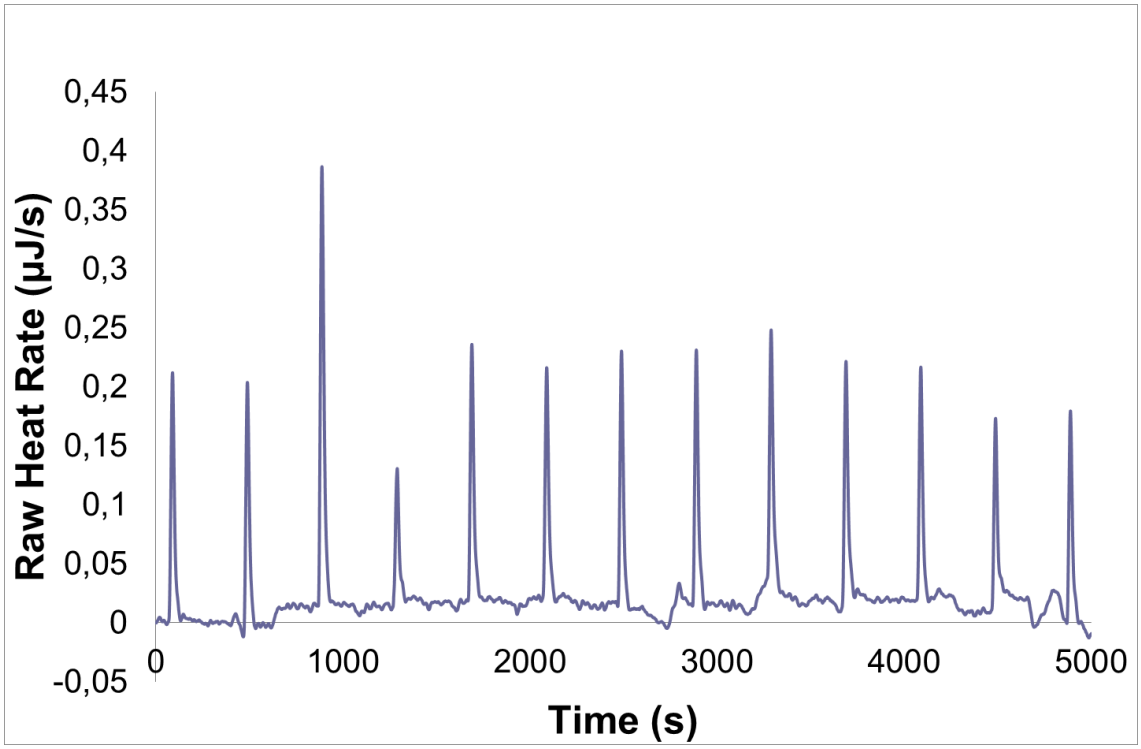

Figure 40. Plot of the Raw Heat (µJ/s) vs. time (s) after addition of buffer at 25°C with JP01 dilution experiment. Every peak corresponds to the heat released after a titrant injection.

The individual heat of every injection was obtained by integrating the area below of the corrected peak. Corrected peak areas were plotted vs. concentration of coenzyme B_{12} (injection) and the resulting curve fitted to an independent 1:1 process using the software included with the calorimeter (NanoAnalize Software v3.1.2, TA Instruments).

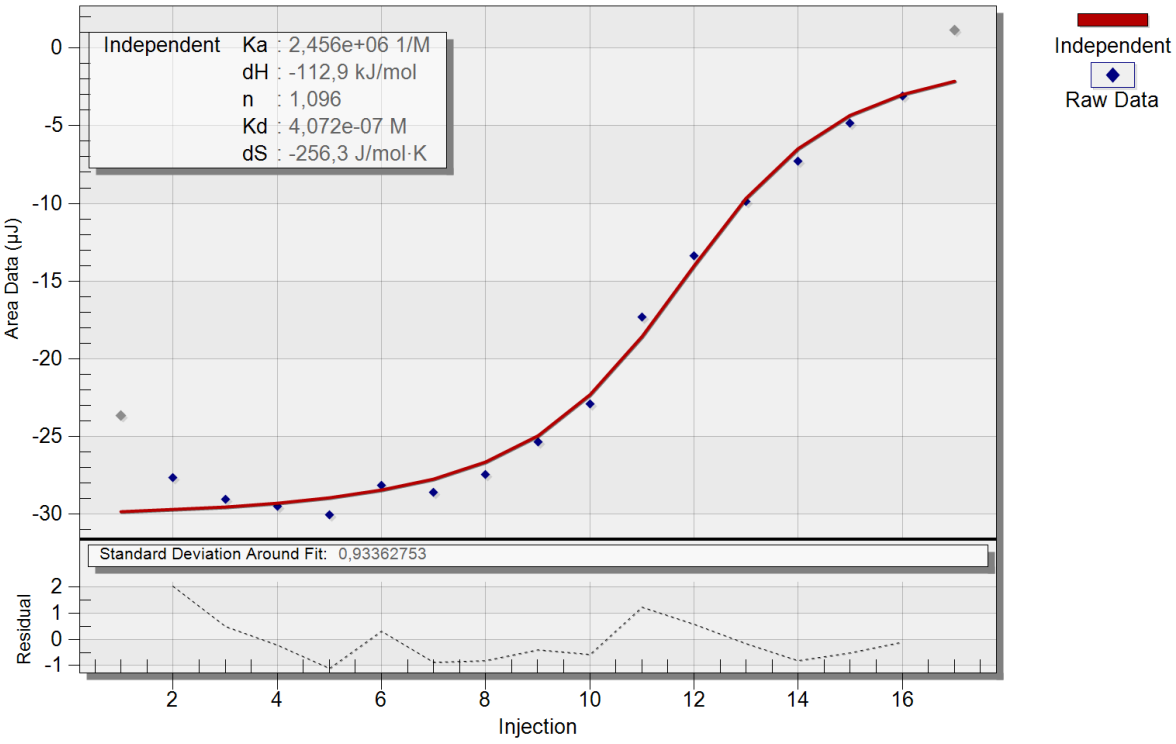

Figure 41. Peak areas corresponding to the heat released after injection plotted vs. cobalamin concentration (injection) and the fitting to a 1:1 independent process.

Experiments at different temperatures, between 15 °C and 30 °C, for both RNA constructs, JP01 and MB01, were recorded. Arithmetical means from the data at each temperature studied are shown in Table 11 for the JP01 construct and the Table 12 shows the results for the MB01.

Table 11. ITC experiments results with JP01 having AdoCbl as titrant. Values given are the mean of three titration experiments with standard deviation. Results at 300.65K and 295.65 are mean of 4 and 5 experiments respectively.

T (K)	Ka	log Ka	ΔH (kJ/mol)	n	ΔS (J/K·mol)	K_D (nM)
303.15	1.0E+6±2E+5	5.99±0.09	-132±5	0.91±0.08	-321±16	1000±200
300.65	1.7E+6±3E+5	6.23±0.07	-120±15	0.72±0.09	-280±50	600±100
298.15	1.8E+6±2E+5	6.27±0.05	-119±3	1.0±0.3	-281±9	530±50
295.65	2.6E+6±6E+5	6.41±0.09	-100±10	0.84±0.18	-230±30	390±80
293.15	4.76E+6±1.7E+5	6.67±0.02	-83±3	0.86±0.2	-160±10	210±8
290.65	3.4E+6±8E+5	6.52±0.09	-75±11	0.68±0.04	-130±50	300±60
288.15	5.4E+6±3E+5	6.73±0.02	-60±6	0.82±0.03	-80±18	185±9

Table 12. ITC experiments results with MB01 having AdoCbl as titrant. Values given are the mean of three experiments with standard deviation.

T (K)	Ka	log Ka	ΔH (kJ/mol)	n	ΔS (J/K·mol)	K_D (nM)
303.15	7.5E+5±7E+4	5.88±0.04	-151±4	0.65±0.02	-385±14	1300±130
298.15	1.3E+6±1.5E+5	6.11±0.05	-122.7±0.9	0.72±0.06	-294±3	770±90
293.15	1.8E+6±4E+5	6.25±0.09	-95±5	0.78±0.09	-204±16	570±110
288.15	9.0E+6±1.3E+6	6.95±0.06	-61±11	0.86±0.17	-70±40	110±16

As it can be extracted from the results in Table 11 and Table 12, the interaction between the butB riboswitch from *K. pneumoniae* follows a 1:1 stoichiometry (n≈1) for both constructs, although the n values obtained for the MB01 are lower than those obtained for JP01. From the ITC experiments it can be deduced that the interaction exhibits an exothermic enthalpy change that increases in absolute value when the temperature increases. The enthalpy at 298.15 K was -119±3 kJ/mol for JP01 and -122.7±0.9 kJ/mol for MB01. In Figure 42 the enthalpy changes for both constructs are represented vs. temperature for an easier comparison:

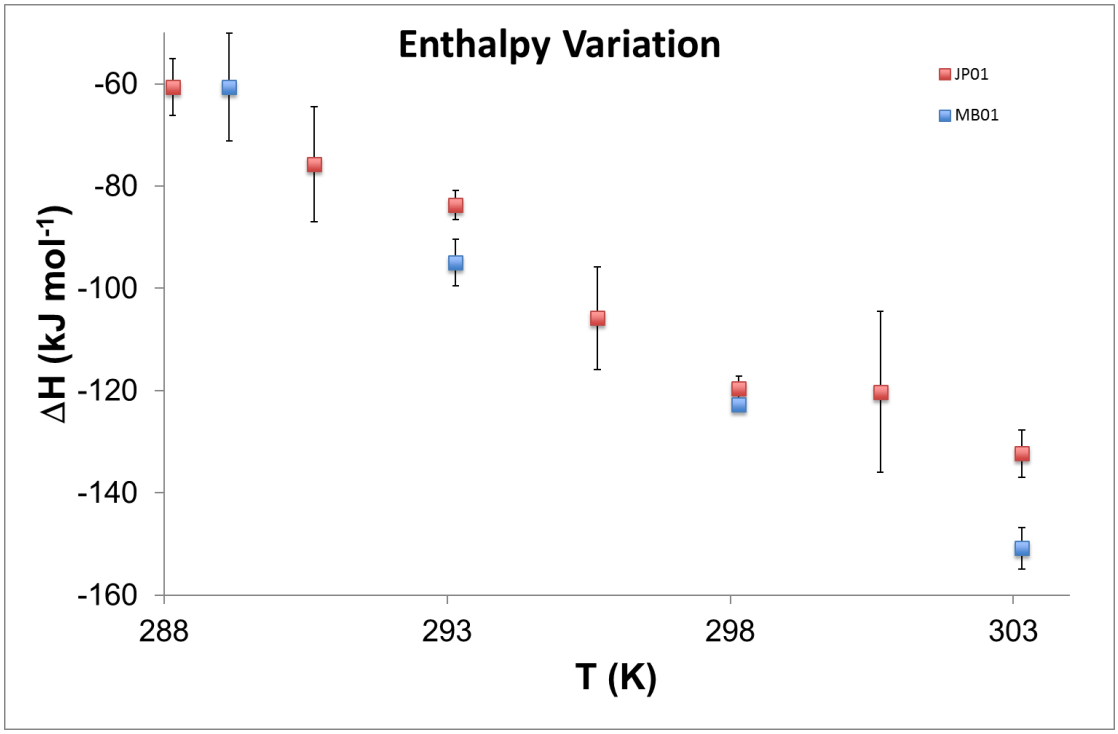

Figure 42. Plot of the Enthalpy change versus temperature. In blue squares values obtained for MB01 and in red squares data for JP01

As it can be appreciated in Figure 42, the variation of the enthalpy can be considered equivalent for both constructs. The enthalpy of the interaction was exothermic, and its absolute value increased upon a temperature raise. From the enthalpy change value, it can be assumed that the interaction with the coenzyme B_{12} was not covalent (a higher enthalpy value would be

expected), but that a sum of several weaker interaction like H-bonds (≈ 20 kJ/mol) or π-staking were involved in the interaction.

The entropy of the process was at 298.15 K, -281±9 J/K·mol for JP01 and -294±3 J/K·mol for MB01. The variation of the entropy vs. temperature was equivalent for both constructs. A negative entropy change implies a more organized system after interaction with the coenzyme B_{12}. The conformational changes from the Gene-on conformation to the Gene-off form implicate the pseudoknot formation, which causes a more conformationally restricted form of the *btuB* riboswitch in addition to the complex formation between the RNA and B_{12}.

From the ITC data, the Ka and log Ka were also obtained and from these results, the K_D was calculated as K_D= 1/Ka. The plot of the variation of the K_D vs. temperature is shown in Figure 43 for both constructs.

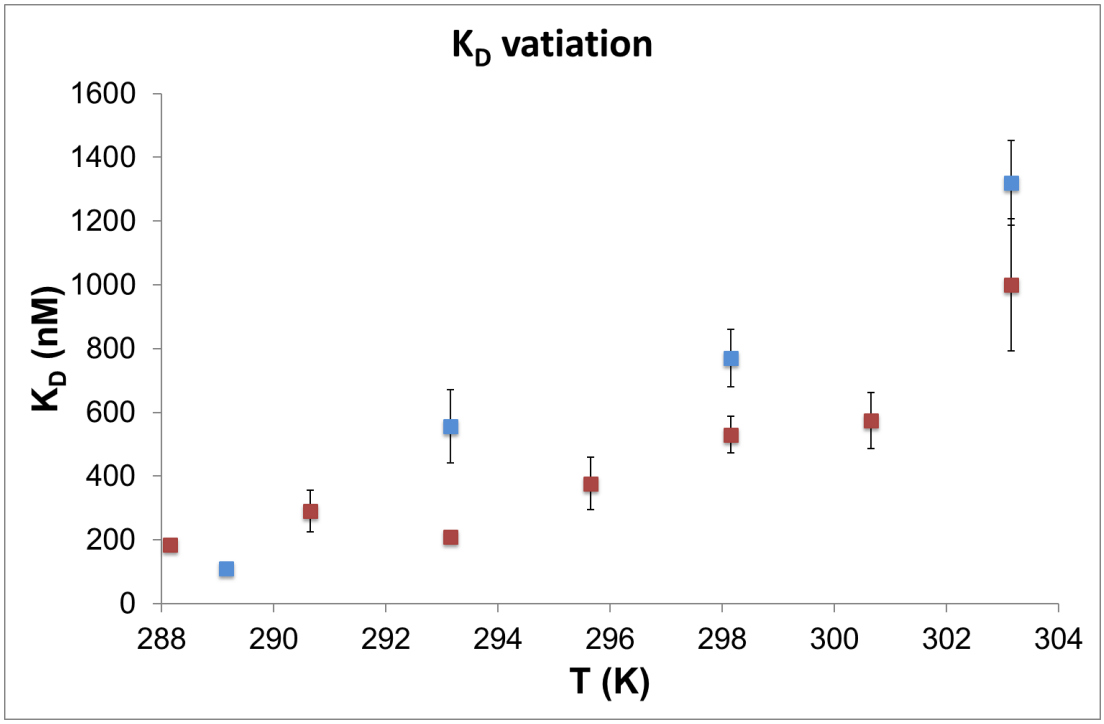

Figure 43. Plot of the variation of the K_D vs temperature. In blue squares the dissociation constants calculated for MB01 and in red squares the results for JP01.

The K_D for JP01 at 298.15 K was 530±50 nM and 770±90 nM for MB01. In this case, the dissociation constant of the MB01 was in general higher than the dissociation constant for the JP01. A higher dissociation constant implicates a lower complex formation. Thus, the presence of the expression platform present in JP01 construct plays an important role in the complex formation providing stability.

The thermodynamic parameters show a distinct variation with temperature, which is due to the non-negligible changes in the heat capacity (ΔCp= dΔH/dT). The van't Hoff (Equation 3) and Gibbs-Helmholtz (Equation 4) plots to study the temperature dependence of the system are represented in Figure 44 and Figure 45 respectivelly.

$$van't\ Hoff:\ lnK = -\frac{\Delta H}{RT} + \frac{\Delta S}{R} \qquad \textit{Equation 3}$$

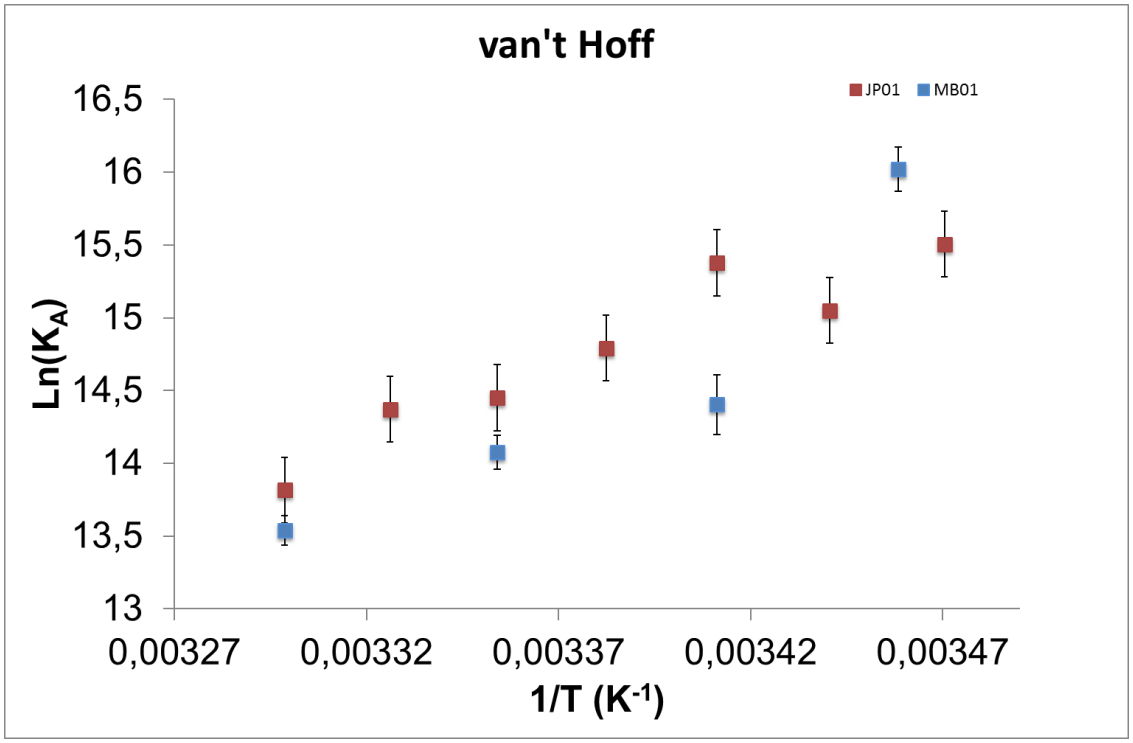

Figure 44. Plot of the van't Hoff equation for JP01 and MB01 data.

$$Gibbs - Helmoltz:\ \Delta G = \Delta H - T\Delta S$$ *Equation 4*

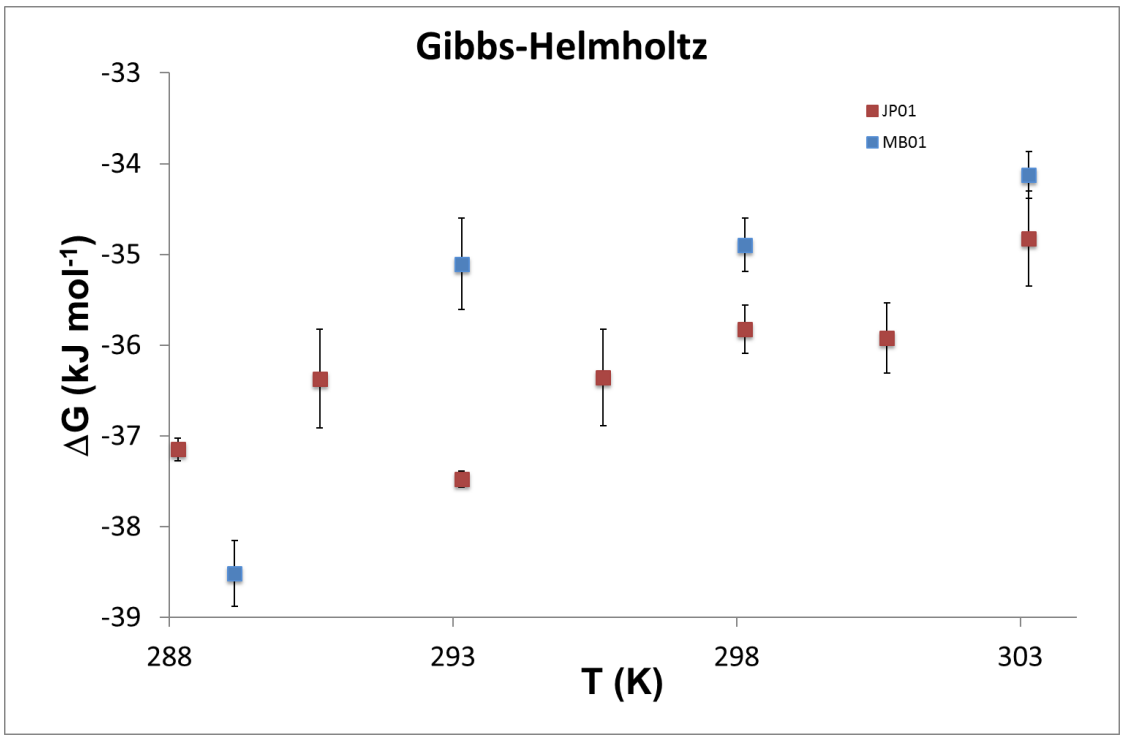

Figure 45. Plot of the Gibbs-Helmoltz equation for JP01 and MB01.

Both representations (van't Hoff and Gibbs-Helmholtz) are linear when ΔCp equals zero. The non-linearity of the plots (Figure 44 and Figure 45) suggests the need of using an extra term to consider the ΔCp and the curve is fitted with a second order polynomial curve. However, in our case, data shown in Figure 44 and Figure 45 cannot be fitted with a second order polynomial curve. This fact suggests a more complex dependence on temperatures, or even a mechanistic change dependent on temperature.

3.3.5. Fluorescence studies by coupling the *btuB* Riboswitch with *mCherry* protein.

Colonies transformed with pJP04 were rosy coloured, fact that confirmed that plasmid pJP04 was correctly designed and cells containing this construct expressed correctly the *mCherry* fluorescent and coloured protein.

The fluorescence of cultures, grown as explained in 3.2.9, corroborates the expression of *mCherry* proteins. Cells grown in a cobalamin free medium (M9) presented an emission fluorescence maximum at 606 nm. Keeping in mind that, according to literature, the *mCherry* absorption maximum is at 560 nm and emission fluorescence maximum is situated at 610 nm[207], and the fact that factors such as pH can shift the peak by several nm, the maximum emission peak at 606 nm can be attributed to *mCherry* fluorescence in the same way that the absorption.

In Figure 46, a decrease in fluorescence intensity upon addition of coenzyme B_{12} can be observed. Fluorescence intensity depends on the fluorophore concentration that, in this construct, is regulated by the *btuB* riboswitch. A higher Coenzyme B_{12} concentration increases the maximum ratio of *btuB* riboswitch in the gene off conformation, which results in a lower *mCherry* translation and thus in a lower fluorescent signal.

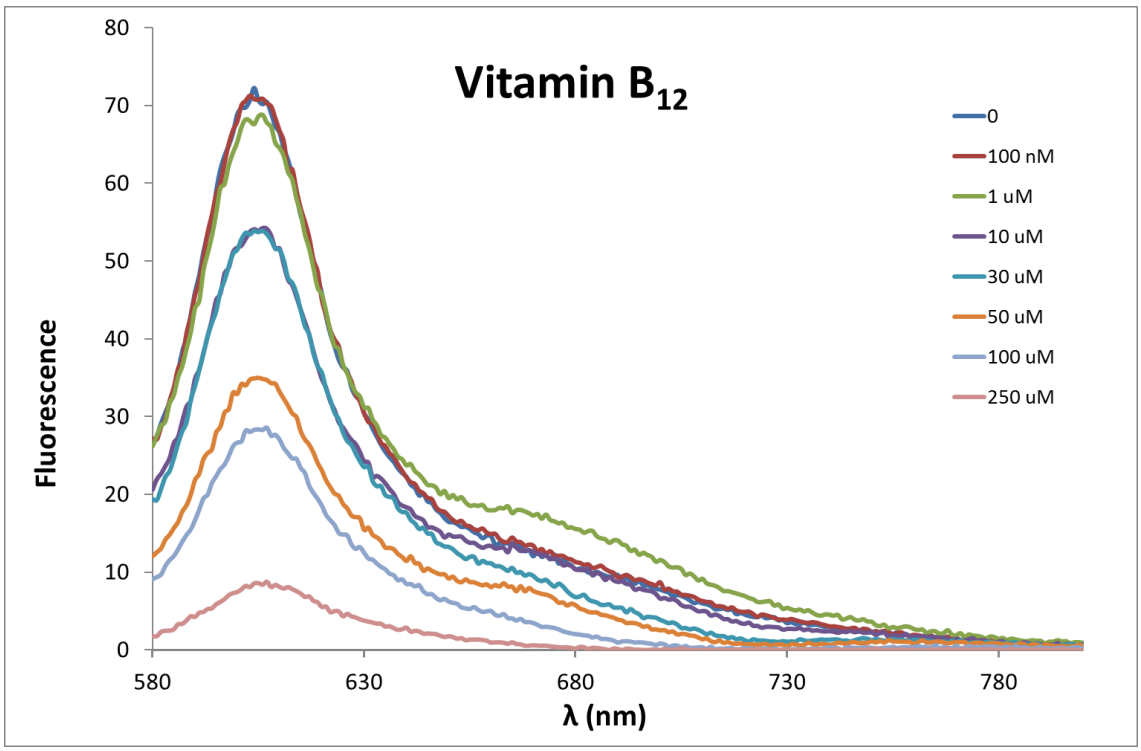

Figure 46. Fluorescence emission spectrum of BL21 E. Coli cells containing pJP04 after 8h incubation with increasing amounts of coenzyme B_{12}.

The same trend was found when cell cultures were incubated with increasing amounts of cyanocobalamin. The fact that fluorescence intensity decreases while the cobalamin concentration increases is thereby attributed to the regulatory function of the riboswitch.

In addition, differences in fluorescence intensity signal (FIS) can be noted for equal concentration of B_{12} derivatives (see Table 13 and Table 14). Fluorescence intensity diminishes faster for cyanocobalamin than for adenosyl cobalamin.

Table 13. Average value of three fluorescense experiments with adenosylcobalamin.

[AdoCbl] (nM)	log [AdoCbl]	FIS	% Inhibition	SD
0		117.3	0.0	0.0
10^2	2.0	114.0	2.1	6
10^3	3.0	104.8	10.7	1.9
10^4	4.0	90.5	23.0	7
$3{\cdot}10^4$	4.5	75.1	35.8	3
$5{\cdot}10^4$	4.7	65.5	44.3	4
10^5	5.0	46.8	59.8	7
$2.5{\cdot}10^5$	5.4	19.7	83.2	1.4
$5{\cdot}10^5$	5.7	8.5	92.7	0.9
$7.5{\cdot}10^5$	5.9	5.1	95.6	0.3
[AdoCbl] (nM)	log [AdoCbl]	FIS	% Inhibition	SD

Table 14. Average value of three fluorescence experiments with vitamin B_{12}.

[vit B_{12}] (nM)	log [vit B_{12}]	FIS	% Inhibition	SD
0		117.3	0.0	0
10^2	2.0	120.0	-1.9	7
10^3	3.0	119.3	-1.4	8
10^4	4.0	93.2	20.5	3
$3{\cdot}10^4$	4.5	71.1	39.6	4
$5{\cdot}10^4$	4.7	55.4	52.7	3
10^5	5.0	37.3	68.0	6
$2.5{\cdot}10^5$	5.4	7.8	93.2	2
$5{\cdot}10^5$	5.7	3.9	96.6	1.3
$7.5{\cdot}10^5$	5.9	4.0	96.6	1.1
10^6	6.0	1.3	98.9	0.5

Inhibition percentage of fluorescence correlates with the inhibition of the protein *mCherry* translation was calculated. It was calculated using Equation 5, where F_0 is the fluorescence intensity signal for the cobalamin free cell culture and F is the fluorescence signal of the corresponding sample. Experiments were all done in triplicate. The average of the %I and the standard deviation (SD) (see Table 13 and Table 14) for both cyanocobalamin and adenosylcobalamin were calculated to plot the inhibition percentage against the logarithm of the cobalamin concentration.

$$\%I = \frac{F_0 - F}{F_0} \cdot 100 \qquad \textit{Equation 5}$$

Inhibition values were square adjusted to a sigmoidal curve (Figure 47) using the SOLVER tool, included in Microsoft Excel, considering a sigmoidal curve as Equation 6:

$$y = \frac{a}{1 + e^{b+cx}} + d \qquad \textit{Equation 6}$$

The coefficient values were calculated by minimizing the value of the sum of squared errors $(y_{est}-\dot{y})^2$ where y_{est} was the curve value and $\dot{y}$ the average of experimental values.

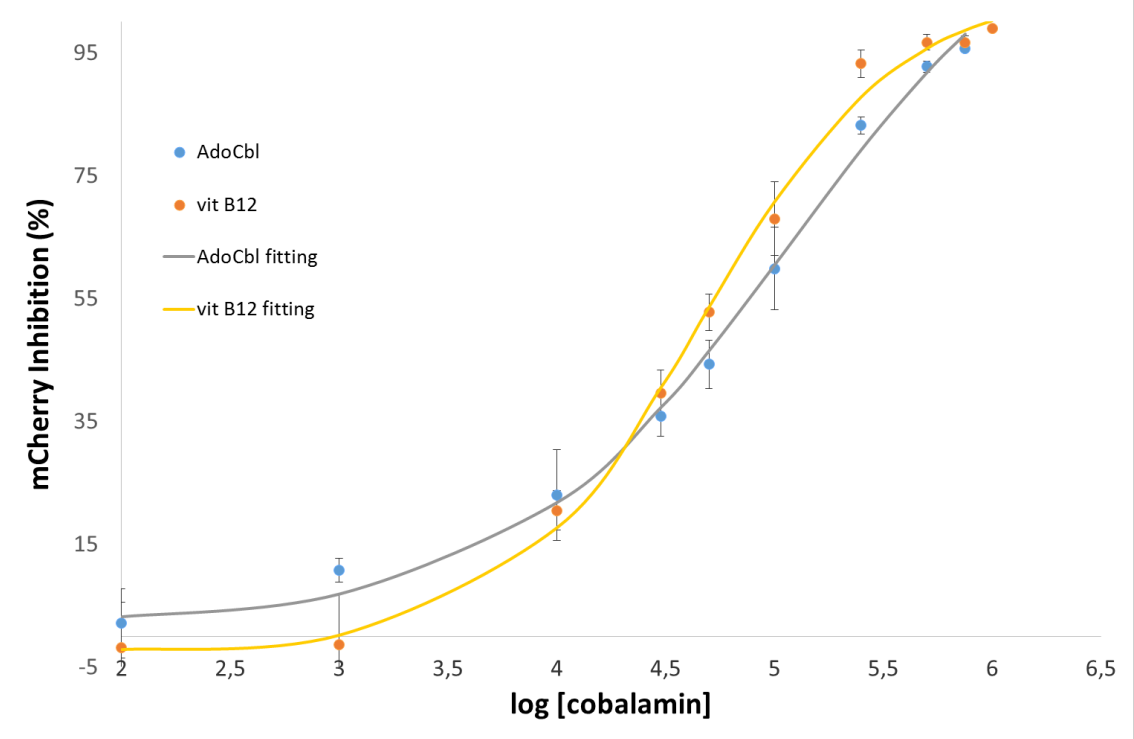

Figure 47. Representation of the inhibition percentage (I%) against the logarithm of cobalamin concentration (nM). Points show the average of three experimental values and lines, the adjusted sigmoidal curves.

With the resulting equation obtained after adjustment, cobalamin concentration values that results in 50% *mCherry* inhibition were calculated: $[AdoCbl]_{50}$ = 60 ± 7 µM and $[CNCbl]_{50}$ = 44 ± 4 µM. It should be emphasized that for the same concentration (750 µM) the coenzyme B_{12} inhibits the protein expression in a 95.6% while vitamin B_{12} shows an inhibition of 96.6%. These results are not consistent with thermodynamic parameters found for the ligand-RNA interactions process. Affinity constants for adenosylcobalamin are much higher in all temperatures that cyanocobalamin affinity constant. However, vitamin B_{12} can be taken up much more easily from the environment by bacteria than adenosylcobalamin. In the end, vitamin B_{12} can be easily transformed to the coenzyme in vivo in the cell, likely explaining the observed differences.

Fluorescence for the cobinamide and neocobinamide was also recorded and the fluorescence emission spectra from 580 nm to 900 nm have been plotted in Figure 48. For both derivatives

the fluorescence spectrum recorded was equivalent, thus only the plot for the cobinamide is shown.

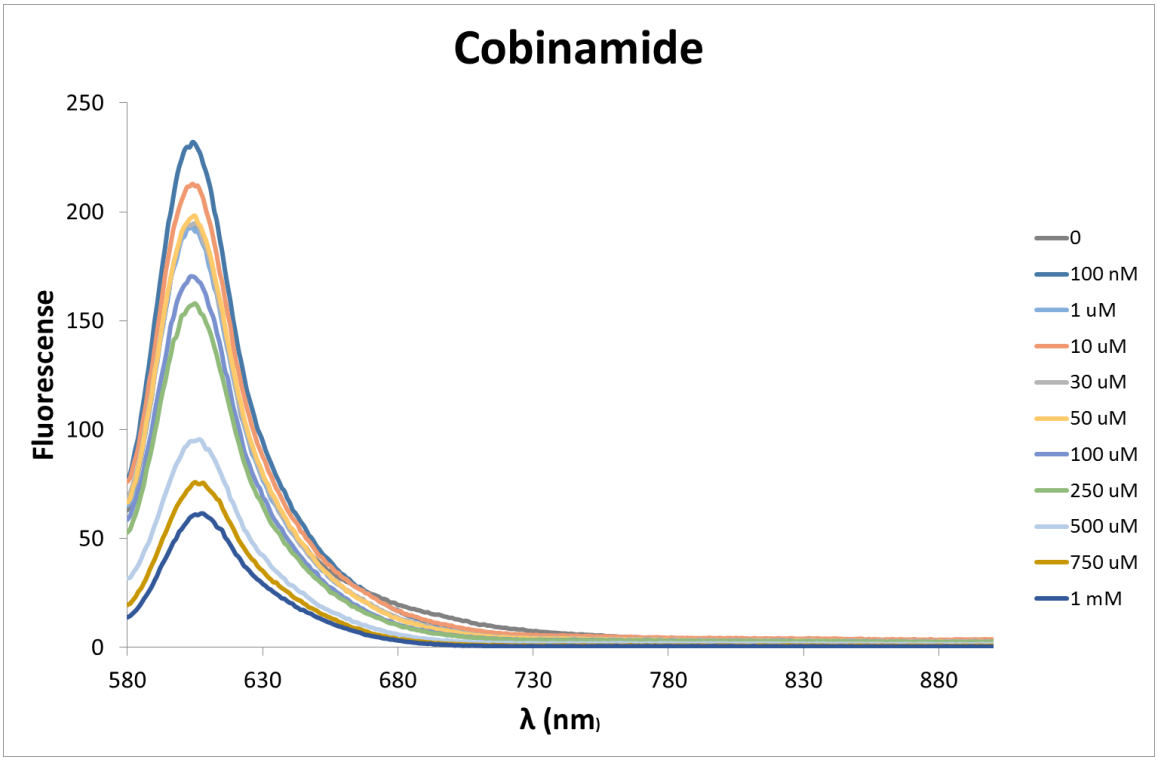

Figure 48. Fluorescence emission spectrum of BL21 E. Coli cells containing pJP04 after 8h incubation with increasing amounts of cobinamide.

It can be observed in the Figure 48 that upon increasing the concentration of the Cbi and Neocbi derivatives the fluorescence was quenched. Thus both derivatives were taken-up and were able to interact with the riboswitch and furthermore were able to switch the RNA to the gene-off conformation in order to negatively regulate the synthesis of the protein.

The experiments were made for duplicate and average of the results of the two experiments are summarized in Table 15 and Table 16 for both derivatives, cobinamide and neocobinamide, where % of inhibition was calculated using Equation 5.

Table 15. Average value of two fluorescence experiments with cobinamide.

[Cbi] nM	log[Cbi]	FIS	% Inhibition	SD
0	0	204.5	0.0	0.0
10^2	2.0	221.9	-17.3	0.3
10^3	3.0	150.0	6.8	0.2
10^4	4.0	212.6	-4.0	0.2
$3{\cdot}10^4$	4.5	200.1	2.1	0.5
$5{\cdot}10^4$	4.7	188.0	8.0	0.4
10^5	5.0	173.6	15.1	0.0
$2.5{\cdot}10^5$	5.4	161.9	20.8	0.2
$5{\cdot}10^5$	5.7	101.8	50.2	0.1
$7.5{\cdot}10^5$	5.9	85.6	58.2	0.1
10^6	6.0	64.7	68.4	0.0

Table 16. Average value of two fluorescence experiments with neocobinamide.

[Neocbi] nM	log[Neocbi]	FIS	% Inhibition	SD
0	0	204.5	0.0	0.0
10^2	2.0	186.2	8.9	0.2
10^3	3.0	201.3	1.5	0.0
10^4	4.0	193.9	5.2	0.1
$3{\cdot}10^4$	4.5	184.9	9.6	0.3
$5{\cdot}10^4$	4.7	181.7	11.1	0.3
10^5	5.0	170.3	16.7	0.3
$2.5{\cdot}10^5$	5.4	132.2	35.4	0.4
$5{\cdot}10^5$	5.7	105.0	48.7	0.0
$7.5{\cdot}10^5$	5.9	84.6	58.7	0.2
10^6	6.0	63.0	69.2	0.1

The % inhibition was calculated with Equation 5 and plotted vs the logarithm of the concentration of cobalamin and adjusted to a sigmoidal curve (Equation 6) as explained above for vitamin B_{12} and coenzyme B_{12}.

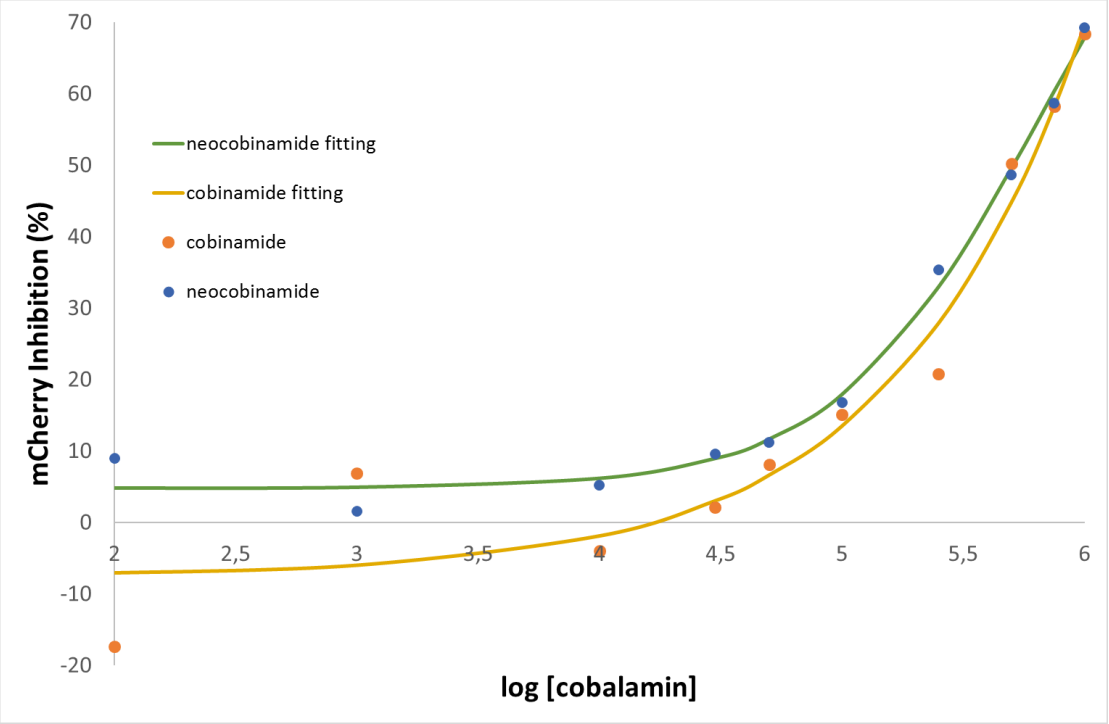

Figure 49. Representation of the inhibition percentage (I%) agaist the logarithm of cobinamide and neocobinamide concentration (nM). Points show the average of two experimental values and lines, the adjusted sigmoidal curves.

With the resulting equations obtained after adjustment, cobinamide and neocobinamide concentration values that result in 50% *mCherry* inhibition were calculated: $[Cbi]_{50}$ = 563 ± 68 µM and $[Neocbi]_{50}$ = 508 ± 45 µM. From the inhibition 50% values we can affirm that both derivatives (Cbi and Neocbi) behaviour was pretty much identical.

It is important to notice that the maximal concentration used was 1 mM and only inhibited around the 70% of the expression, while the same concentration with other derivatives was nearly 100%. Assuming an equal up-take mechanism and efficiency for the four derivatives used, we could conclude that the concentration values that results in 50% *mCherry* inhibition for the complete derivatives (AdoCbl and $VitB_{12}$) were 10 times lower than values for the incomplete derivatives (Cbi and Neocbi). These results are in consonance with other results in bibliography which conclude that the corrin ring is essential for the *btuB* riboswitch recognition and is enough to switch the RNA structure (the four derivatives were able to switch the RNA structure), but axial ligands are the responsible of the affinity (complete derivatives show a lower 50% inhibition concentration than incomplete derivatives).

4. PART II: Synthesis of descobaltocorrinoids

4.1. Introduction to PART II

4.1.1. Descobaltocobalamin derivatives: synthesis and purification

As already exposed in section 1.1.3, there are certain bacterial species capable, in a deficit of cobalt conditions, to synthesize the organic cobalamin moiety without the metallic atom in the tetrapyrrole centre[208]. Descobaltocobalamin derivatives have been isolated from *Ch*romatiales bacteria, purple sulphur bacteria such as *Allochromatium vinosum*[29,30], and purple none sulphur bacteria *Rhodopseudomonas spheroides*[31,32].

These compounds were then extracted and purified from the cell pellets. The extraction was commonly performed in a solid-liquid extraction, using commonly ethanol or acetate buffer, followed by a chromatographic column purification to isolate the distinct derivatives extracted[14,29,209,210]. Chromatographic methodology has been widely used in the purification of cobalamin derivative mixtures from both synthetic and biosynthetic typology[20,25,46,62,211].

4.1.2. Aim of the subproject

The main aim of this second part of the thesis is to obtain an antivitamin derivative and to synthesize descobaltocobalamin derivatives in which structural changes are supposed to be minimum. Thus affinity to the Cbls protein transporters and riboswitches is expected to be maintained. Furthermore, the lack of the cobalt centre will prevent the redox reactivity of the molecule and consequently its biological function. The concret aims of this subpart were:

- Biosynthesis of descobaltocobalamins and their extraction and purification.
- Characterization of the descobaltocobalamin derivatives obtained.
- Studies of the coordination chemistry of the descocaltocobalamin derivatives with other metal ions in an oxidation state (+3)

4.2. Experimental section

Allochomatium Vinosum is a purple sulphur bacteria that grows under anaerobic conditions. This bacterial strain naturally synthesizes descobaltocorrinoids when it is grown in a medium where cobalt is absent[208,212].

4.2.1. Media Composition and preparation

To obtain descobaltocobalamin a medium with no cobalt content was used[208]:

-Solution I: 7.02 g NaCl, 1.61 g NH_4Cl, 0.544 g KH_2PO_4, 0.986 g $MgSO_4 \cdot 7H_20$, 0.146 g $CaCl_2 \cdot 2H_2O$, 20 ml HCl 6N, 20 ml Malic acid 161 g/l, pH=7, 2 ml Solution III and 1.6 ml Solution IV were dissolved in 1.2 l MilliQ water and autoclaved for 20 min at 121 °C.

-Solution II: 24.93 g Na_2CO_3 and 0.114 g $Na_2S \cdot 9H_2O$ were dissolved in 0.9 l MilliQ water and autoclaved for 20 min at 121 °C.

-Solution III: 2.86 g H_3BO_3, 1.48 g $MnCl_2 \cdot 2H_2O$, 0.222 g $ZnSO_4 \cdot 7H_2O$, 0.079 g $CuSO_4 \cdot 5H_2O$, 0.145 g $Na_2MoO_4 \cdot 2H_2O$, 0.023 g NH_4VO_3 and 0.049g $Co(NO_3)_2 \cdot 6H_2O$ was dissolved in 1 l MilliQ and autoclaved water. Stored at 4 °C.

-Solution IV: 4 g EDTA (acid form) and 2.65 g KOH were dissolved in 46.5 ml MilliQ water. 3.43 g $FeSO_4 \cdot 7H_2O$ were dissolved in 91 ml MilliQ water. Once solved, solutions were mixed and let to react with air bubbling overnight.

-Media: 600 ml Solution I and 300 ml Solution II were mixed. pH was adjusted to 7.6 and 20 mg/l dimethylbenzimidazole were added, finally MilliQ autoclaved water was added to a final 1 l volume. Air of the solution was removed by bubbling N_2 into the solution.

4.2.2. Cell grown and descobaltocorrinoid extraction

Cell cultures were made in 2.2 l bottle with frosted tap. Cells were grown in a phototropic chamber (Binder KBW400 90020-0180) at 30±1 °C and light from Osram lumilux Cool daylight of 24 w/m^2 or 9000 lx for 72±2 h. After this period, cells were harvested by centrifugation at 3214x*g* for 15 min at 4 °C. Cell pellets were washed with NaCl 0.9%(w/v) and stored at -20 °C for further steps. Approximately 16 g of cell pellet were obtained from every 9 l of culture.

Stock cell culture was prepared by lyophilization of 4 ml culture pellets resuspended in 1 ml sucrose 10% (w/v). Once lyophilized, sample was stored at -20 °C.

The compounds of interest were ethanol extracted from the cell pellets in the darkness to avoid degradation. A mixture of ethanol: water: acetic acid (180:20:1) was prepared and *ca.*≈ 100 g of cell pellets were resuspended in *ca.*≈ 600 ml of the extraction solution and vortexed until

complete resuspension. Cell suspension was then centrifuged 10 min at 3214x*g*, the blue-green supernatant was collected in a 1 l round-bottomed flask and rotaevaporated at 35 °C until complete ethanol evaporation. To ensure the total elimination of ethanol, 20 ml of MilliQ water were added and evaporated again. The final volume of the sample was ca.≈ 100 ml, where a brownish precipitate appeared while solution was concentrating.

The pH of the final solution was adjusted to 3 by addition of HCl 6M and centrifuged for 5 min at 3214x*g* at room temperature. The supernatant was collected in a clean flask and pH adjusted to 7 by addition of NaOH 5M. The final yellow-orange solution was lyophilized for further concentration and stored at -20 °C before purification.

4.2.3. Descobaltocorrinoids purification

First purification was performed using a C-18 reverse phase column. 3 g of C-18 were used to pack the chromatographic column, resulting in a 4 cm long and 1.5 cm diameter column. Solvents used for purification were water (A) and acetonitrile 90% (v/v) (B). The chromatographic column was run using overpressure.

- Chromatographic column packing and preparation: 3g of C-18 were dissolved in 10 ml B and inserted in a 10 ml glass column of 1.5 cm diameter and left to deposit by gravity. Once chromatographic column was packed, solvent was gradually changed to A. 50 ml of A were passed through the chromatographic column prior to sample loading.

- Sample purification: Samples were dissolved in a minimum amount of water (25 ml) and centrifuged for 10 min at 10.000*xg* prior to the chromatographic column loading. Pellet formed was discarded and only the liquid phase was loaded to the chromatographic column. A solvent gradient to 30% B was used to separate JPM_1 fraction from JPM_2 fraction. Both fractions were concentrated until dryness in concentrator and stored at 4 °C for further purification.

-JPM_1 purification: the JPM_1 fractions of 10 extractions were solved in a minimum water and purified on a C-18 chromatographic column using a gradient from 10% to 30% B. In the purification, 5 different fractions were collected: JPM1_1 (pallid pink) was eluted at 10% B, JPM1_2 (orange) was eluted at 22.5% B, JPM1_3 (yellow) fraction was eluted at 25% B, JPM1_4 (orange) was eluted at 25% B and finally JPM1_5 (yellow) fraction eluted at 27.5% B.

-JPM_2 purification: JPM_2 fraction of 10 extractions were solved in a minimum water and purified on a C-18 chromatographic column using a gradient from 0% to 20%B. From the JPM2 sample 7 fractions were distinguished: at 2.5% B JPM2_1 (yellow) fraction was eluted, at 5% B JPM2_2 (yellow) was collected, JPM2_3 (pink) was eluted at 7.5% B and JPM2_4 (intense pink)

was eluted at 10% B. Fraction JPM2_5 (pink) was collected at 15% B, samples JPM2_6 (yellow) and JPM2_7 (pink) were eluted at 17.5% B and 20% B, respectively.

-All samples were concentrated until dryness in the concentrator at room temperature and stored at 4 °C.

- MS spectrum: 2 mg of sample were dissolved in 1 ml water. Then, 1 µl of the previous solution was taken and diluted in 1 ml methanol. The MS used was a Q-exactive Orbitrap (Thermo Fisher Scientific). A heated electrospray ionization (HESI) source in positive ion mode was used for the ionization of target compounds. The key parameters were as follows: spray voltage, 3.9 kV; sheath gas flow rate, 6 arbitrary units; and capillary temperature, 320 °C.

4.3. Results and discussion

To obtain the descobaltocorrinoids, a culture medium without cobalt was prepared and cells were grown and collected. Afterwards, the descobaltocorrinoids were extracted and separated by chromatographic columns. The results of the extractions and the experiments for the identification of the fractions obtained are explained below.

4.3.1. Cell grown and descobaltocorrinoids extraction

In total, 1600 g of cell pellets were processed, which correspond to 900 l of culture media. Fractions of 160 g were extracted thus 10 descobaltocorrinoids extractions were performed, followed by their respective chromatographic columns for separation of JPM1 and JPM2 fractions.

Finally, the fractions of JPM1 and JPM2 obtained from the different chromatographic columns were combined for the last purification step, giving 7 fractions of the JPM2 and 5 fractions for JPM1.

4.3.2. Descobaltocorrinoids purification

In the purification process, several bands were eluted from the chromatographic column. Bands with a red coloration, which could correspond to the descobaltocobalamin and descobaltocobiric acid were analysed using a HPLC-HRMS.

For JPM_1, bands corresponding to JPM1_1, JPM1_2 (Figure 50) and JPM1_4 were analysed.

For JPM_2, bands corresponding to JPM2_3, JPM2_4, JPM2_5 and JPM2_7 were analysed.

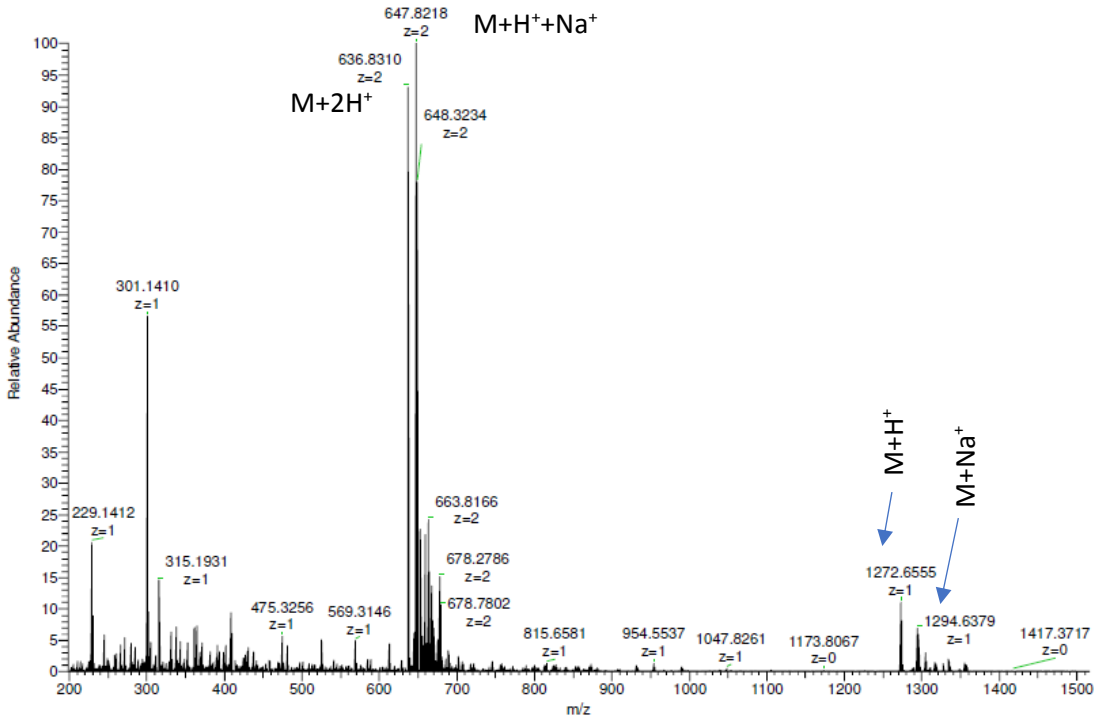

Figure 50. Mass spectrum of the JPM1_2 fraction, which corresponds to the descobaltocobalamin.

In the mass spectrum of the fraction JPM1_2 several peaks were assigned as shown in Figure 50: m/z of 1272.6555 corresponds to M+H$^+$(calc. for $C_{62}H_{91}N_{13}O_{14}P^+$ 1272.6541), peak at 1294.6379 corresponds to M+Na$^+$ (calc. for $C_{62}H_{90}N_{13}O_{14}PNa^+$ 1294.6360) and with z=2 peaks 636.8310 and 647.8218 were assigned to M+2H$^+$ (calc. for $C_{62}H_{92}N_{13}O_{14}P^{2+}$ 636.8307) and M+H$^+$+Na$^+$ (calc. for $C_{62}H_{91}N_{13}O_{14}PNa^{2+}$ 647.8216) respectively.

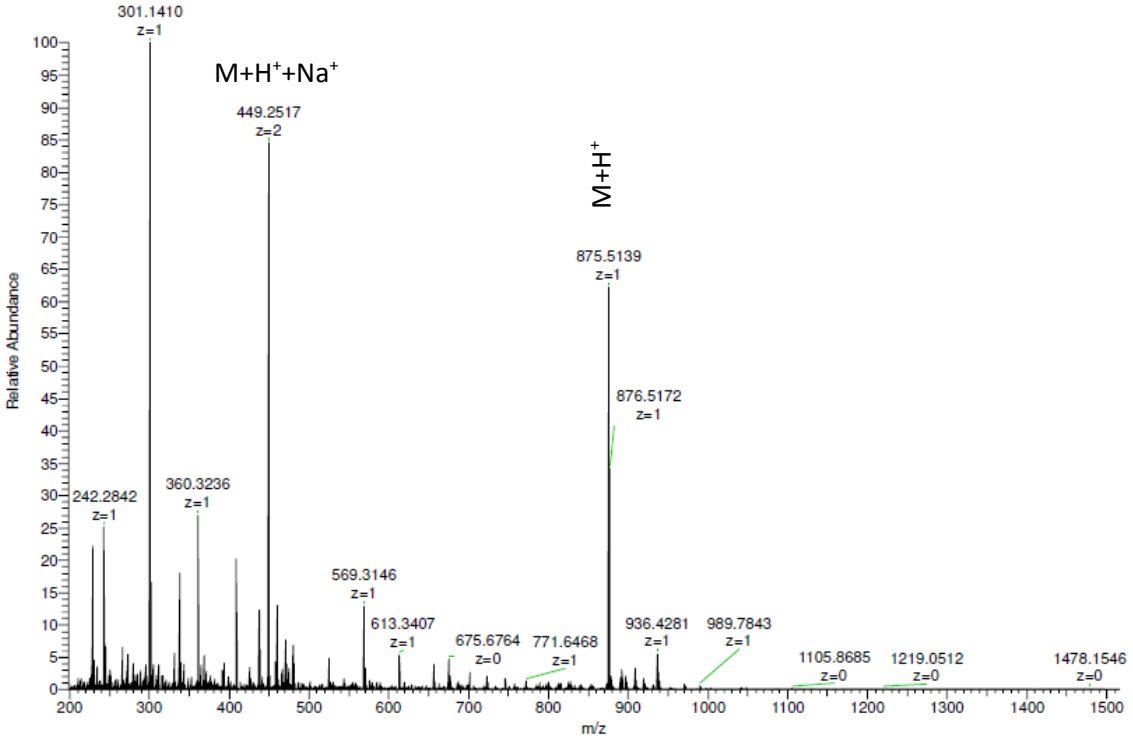

Figure 51. Mass spectrum of the JPM2_5 fraction which correspond to the descobalocobyric acid.

In the mass spectrum of the fraction JPM2_5 several peaks were assigned as shown in Figure 51: m/z of 875.5139 corresponds to $M+H^+$(calc. for $C_{45}H_{67}O_8N_{10}^+$ 875.5138) and with z=2 peaks 449.2517 assigned to $M+H^++Na^+$ (calc. for $C_{45}H_{67}O_8N_{10}Na^{2+}$ 449.2515) respectively.

In both mass spectra the peak 301.1410 correspond to dibutylphthalate (calc. for $C_{16}H_{22}NaO_4^+$ 301.1410) and 229.1412 to (2)-trimethyl (3-phenylpent-3-en-1-yn-1-yl)silane (calc. for $C_{15}H_{21}Si^+$ 229.1407), contaminants from plastic material used in the synthesis like Eppendorf tubes or septums.

Despite the presence of the plastic contaminants, 4 mg of descobaltocobalamin and 2 mg of descobaltocobyric acid were obtained in high purity.

.

5. Conclusions and Outlook.

The project addresses the verification of the computationally found sequence of a *btuB* riboswitch in *Klebsiella pneumoniae* genome and, if so, how the B_{12}-responding riboswitch interacts with the metabolite.

After the native gels and the UV melting experiments, it was observed that the presence of magnesium is essential for the RNA folding. The melting temperature determined for a sample in absence of magnesium is 55.3±0.2 °C. That temperature is increased to 68.4±0.2 °C upon magnesium addition to 5mM. From these results it is concluded that a concentration between 5 and 20 mM is needed for a correct RNA folding. Concentrations below 5 mM do not ensure the correct RNA folding while concentrations above 20 mM implicate the aggregation of the sample.

The in-line probing tritation studies with the *btuB* riboswitch from *K. pneumoniae* give insights in the RNA structural rearrangements, after interaction with coenzyme B_{12}, by showing intensity changes at 15 cleavage sites within the 243 nt. long sequence. This rearrangement, produced upon the coenzyme B_{12} binding to the RNA, validates the computationally found sequence as a riboswitch of the B_{12} family. Taken together, these results allow to postulate a secondary structure of the *btuB* riboswitch from *K. pneumoniae,* both in gene-on and gene-off conformations. In proposed the gene-off conformation, the RBS was masked in a double strand region, thus concluding that this riboswitch gene regulation is due to an inhibition of the translation initiation mechanism. In order to estimate a K_D, the intensity of the gel bands was background corrected. The corrected intensity was fitted to a 1:1 binding isotherm, yielding to a Ka for an individual band. The Ka of the process was calculated as the average of individual Kas. Finally, the K_D value of 170 ± 140 nM was estimated for the interaction between the *btuB* riboswitch and the coenzyme B_{12}.

ITC experiments have been performed to thermodynamically characterize both sequences, JP01 and MB01, which differ in the expression platform. It is concluded that both sequences show the same behavior upon interaction with AdoCbl. Moreover, after the thermodymamic characterization of both sequences, JP01 and MB01, which differ in the expression platform, it is concluded that both sequences showed the same behaviour. The interaction process is exothermic with an entalphy of -119±3 kJ/mol for JP01 and -122.7±0.9 kJ/mol for MB01 at 298.15 K. The entropy change is also negative, as can be expected in a process where two molecules interact in the formation of a complex. The results were fitted to a 1:1 isotherm, thus concluding that the process follows a 1:1 stoichiometry from the n values obtained. The K_D

values obtained are 530±50 nM and 770±90 nMfor JP01 and MB01 respectively at 298 K which are in consonance with other K_D found in bibliography for other B_{12} riboswitches studied.

ITC experiments using Vitamin B_{12} as a titrant were performed. Nevertheless, the heat released could not be distinguished from the dilution heat. Thus, quantitative results could not be extracted. Although it can be affirmed that the vitamin B_{12} interaction with the *btuB* riboswitch is weaker compared with the one observed with AdoCbl.

The regulation mechanism of the riboswitch has been in vivo evaluated by coupling a red fluorescence protein (*mCherry*) to the riboswitch sequence. The cells have been incubated with a gradient of cobalamin derivatives in the media. Then, their fluorescence have been measured.

The fact that the fluorescence intensity decreases upon increasing amounts of B_{12} derivatives gives a proof of the protein synthesis inhibition via riboswitch regulation. According to the fact that the *mCherry* protein is the responsible for the sample fluorescence, lower amount of this protein leads to a fluorescence decrease.

The fluorescence experiments also corroborate prior studies, which concluded that the corrin ring is essential for the RNA recognition but the apical moieties of the B_{12} are essential for increasing the affinity. That trend is also observable in the fluorescence experiments. On one hand the neocobinamide and the cobyric acid derivatives are capable of partially inhibiting the synthesis of the *mCherry* protein in the used condition. On the other hand, the complete B_{12} derivatives, the vitamin B_{12} and coenzyme B_{12}, are able to fully inhibit the protein synthesis using much lower concentrations.

Finally, in the last part of the thesis it has been possible to obtain the descobaltocobalamin and the descobaltocobyric acid from cultures of *Allochromatium Vinosum*. The extraction procedure followed has been less efficient than expected. Hundreds of liters of bacteria have been processed and only 4 mg of descobaltocobalamin and 2 mg of descobaltocoyric acid have been obtained.

One of the aims of the project was the synthesis of new B_{12} derivatives using the descobaltocobalamin products obtained. Although the isolation of these products in quite high purity was achieved, the small amounts obtained and the tedious obtention proces made it impossible.

During the writing of this thesis, one of the objectives was achieved by one of our competitors. In particular, Kraütler and coworkers were able to synthesize the descobaltorhodiumcobalamin[24] using a more efficient methodology.

6. Literature

1. Addison, T. Anemia-Disease of the Supra-renal Capsules. *London Med. Gaz.* **43**, 517–518 (1849).

2. Minot, G. R; Murphy, W. P. Treatment of pernicious anemina by a special diet. *J. Am. Med. Assoc.* **87**, 470–476 (1926).

3. Rickes, E. L.; Brink, N. G.; Koniuszy, F. R.; Wood, T. R.; Folkers, K. Crystalline Vitamin B_{12}. *Science* (80) **107**, 396–397 (1948).

4. Brink, C.; Hodgkin, D. C.; Linosey, J.; Picworth, J.; Robertson, J. H.; White, J. G. Structure of vitamin B_{12}: X-ray crystallographic evidence on the structure of vitamin B_{12}. *Nature* **174**, 1169–1171 (1954).

5. Barker, H. A.; Weissbach, H.; Smyth, R. D. A coenzyme containing pseudovitamin B_{12}. *Proc. Natl. Acad. Sci. U. S. A.* **44**, 1093–1097 (1958).

6. Lenhert, P. G.; Hodgkin, D. C. Structure of the 5,6-dimethylbenzimidazolylcobamide coenzyme. *Nature* **192**, 937–938 (1961).

7. Zelder, F.; Sonnay, M.; Prieto, L. Antivitamins for medicinal applications. *ChemBioChem* **16**, 1264–1278 (2015).

8. Combs, G. F.; McClung, J. P. "Vitamin B_{12}" *The vitamins: Fundamental aspects in Nutrition and Health* (5th Edition), Academic press, 431–451 (2017)

9. Zelder, F. Recent trends in the development of vitamin B_{12} derivatives for medicinal applications. *Chem. Commun.* **51**, 14004–14017 (2015).

10. Proinsias, K.; Giedyk, M.; Gryko, D. Vitamin B_{12}: Chemical modifications. *Chem. Soc. Rev.* **42**, 6605–6619 (2013).

11. Roth, J. R.; Lawrence, J G.; Bobik, T. A. Cobalamin (Coenzyme B_{12}): Synthesis and Biological Significance. *Annu. Rev. Microbiol.* **50**, 137–181 (1996).

12. Kräutler, B. Antivitamins B_{12}- A Structure- and Reactivity-Based Concept. *Chem. Eur. J.* **21**, 11280–11287 (2015).

13. Fang, H.; Kang, J.; Zhang, D. Microbial production of vitamin B_{12}: A review and future perspectives. *Microb. Cell Fact.* **16**, 15 (2017).

14. Weissbach, H.; Toohey, J.; Barker, H. A. Isolation and Properties of B_{12} Coenzymes Containing Benzimidazole or Dimethylbenzimidazole. *Proc. Natl. Acad. Sci. U. S. A.* **45**, 521–525 (1959).

15. Hogenkamp, H. P. C. The Photolysis of Methylcobalamin. *Biochemistry* **5**, 417–422 (1966).

16. Giedyk, M.; Goliszewska, K.; Gryko, D. Vitamin B_{12} catalysed reactions. *Chem. Soc. Rev.* **44**, 3391–3404 (2015).

17. Kepp, K. P. Co-C dissociation of adenosylcobalamin (Coenzyme B_{12}): Role of dispersion, induction effects, solvent polarity, and relativistic and thermal corrections. *J. Phys. Chem. A* **118**, 7104–7117 (2014).

18. Ridley, W. P.; Dizikes, L. J.; Wood, J. M. Biomethylation of toxic elements in the enviroment. *Science* **197**, 329-332 (1977).

19. Jackowska, A.; Chromiński, M.; Giedyk, M.; Gryko, D. 5'-Vitamin B_{12} derivatives suitable for bioconjugation via the amide bond. *Org. Biomol. Chem.* **16**, 936–943 (2018).

20. Stupperich, E.; Stainer, I.; Rühlemann, M. Isolation and analysis of bacterial cobamides by high-performance liquid chromatography. *Anal. Biochem.* **155**, 365–370 (1986).

21. Payne, K. A. P.; Quezada, C. P.; Fisher, K.; Dunstan, M. S.; Collins, H. S.; Levy, C.; Hay, S.; Rigby, S. E. J.; Leys, D. Reductive dehalogenase structure suggests a mechanism for B_{12}-dependent dehalogenation. *Nature* **517**, 513–516 (2015).

22. Miles, Z. D.; McCarty, R. M.; Molnar, G.; Bandarian, V. Discovery of epoxyqueuosine (oQ) reductase reveals parallels between halorespiration and tRNA modification. *Proc. Natl. Acad. Sci. U.S.A.* **108**, 7368–7372 (2011).

23. Raux, E.; Schubert, H. L.; Warren, M. J. Biosynthesis of cobalamin (vitamin B_{12}): A bacterial conundrum. *Cell. Mol. Life Sci.* **57**, 1880–1893 (2000).

24. Widner, F. J.; Lawrence, A. D.; Deery, E.; Heldt, D.; Frank, S.; Gruber, K.; Wurst, K.; Warren, M. J.; Kräutler, B. Total Synthesis, Structure, and Biological Activity of Adenosylrhodibalamin, the Non-Natural Rhodium Homologue of Coenzyme B_{12}. *Angew. Chemie Int. Ed. Engl.* **55**, 11281–11286 (2016).

25. Kiuchi, F.; Leeper, F. J.; Battersby, A. Biosynthesis of porphyrins and related macrocycles, part 43. Isolation and characterization of intermediates of coenzyme B12 biosynthesis, a

cobyrinic acid triamide, the a,c-diamide and their Co-(5'-deoxy-5'-adenosyl) derivatives, from *Propionibacterium shermanii. Chem. Biol.* **2**, 527–532 (1995).

26. Blanche, F.; Thibaut, D.; Couder, M.; Muller, J. C. Identification and Quantitation of corrinoid precursors of Cobalamin from *Pseudomonas denitrificants* by High-Performance Liquid Chromatography. *Anal. Biochem.* **189**, 24–29 (1990).

27. Maggio-Hall, L. A.; Claas, K. R.; Escalante-Semerena, J. C. The last step in coenzyme B_{12} synthesis is localized to the cell membrane in bacteria and archaea. *Microbiology* **150**, 1385–1395 (2004).

28. Martens, J. H.; Barg, H.; Warren, M. J.; Jahn, D. Microbial production of vitamin B_{12}. *Appl. Microbiol. Biotechnol.* **58**, 275–285 (2002).

29. Toohey, J. I. A vitamin B_{12} compound containing no cobalt. *Proc. Natl. Acad. Sci. U. S. A.* **54**, 934–942 (1965).

30. Toohey, J. I. Cobalt-free corrinoid compounds from photosynthetic bacteria. *Fed. Proc.* **25**, 1628–1632 (1966).

31. Kamikubo, T.; Sasaki, K.; Hayashi, M. Formation of cobalt-free corrinoids in *Rhodopseudomonas spheroides. J. Nutr. Sci. Vitaminol. (Tokyo).* **23**, 179–185 (1977).

32. Dresow, B.; Schlingmann, G.; Ernst, L.; Koppenhagen, V. B. Extracellular Metal-free Corrinoids from *Rhodopseudomonas spheroides. J. Biol. Chem.* **255**, 7637–7644 (1980).

33. Eschenmoser, A. Roads to corrin. Q. *Rev. Chem. Soc.* **24**, 366–415 (1970).

34. Eschenmoser, A. Organishe Naturstoffsynthese heute Vitamin B_{12} als Beispiel. *Naturwissenschaften* **61**, 513–525 (1974).

35. Eschenmoser, A.; Wintner, C. E. Natural Product Synthesis and Vitamin B_{12}. *Science* **196**, 1410–1420 (1977).

36. Woodward, R. B. Recent Advances in the Chemistry of Natural Products. *Pure Appl. Chem.* **25**, 283–304 (1971).

37. Woodward, R. B. The total synthesis of vitamin B_{12}. *Pure Appl. Chem.* **33**, 145–178 (1973).

38. Woodward, R. B. Recent advances in the chemistry of natural products. *Pure Appl. Chem.* **17**, 519–547 (1968).

39. Friedrich, W.; Gross, G.; Bernhauer, K.; Zeller, P. Synthesen auf dem Vitamin B_{12}-Gebiet. 4. Mitteilung Partialsynthese von Vitamin B_{12}. *Helv. Chim. Acta* **43**, 704–712 (1960).

40. Bonnett, R.; Godfrey, J. M.; Redman, D. G. Cobyric Acid and Related Compounds from Vitamin B_{12}. *J. Chem. Soc*. (C) 1163–1166 (1969).

41. Broderick, K. E.; Potluri, P.; Zhuang, S. Cyanide detoxification by the cobalamin precursor cobinamide. *Exp. Biol. Med.* **231**, 641–649 (2006).

42. Zelder, F. H.; Männel-Croisé, C. Recent Advances in the Colorimetric Detection of Cyanide. *Chim. Int. J. Chem.* **63**, 58–62 (2009).

43. Jacobsen, D. W.; Holland, R. J.; Montejano, Y.; Huennekens, F. M. Cryptofluorescent analogs of cobalamin coenzymes: synthesis and characterization. *J. Inorg. Biochem.* **10**, 53–65 (1979).

44. Rosendahl, M. S.; Omann, G. M.; Leonard, N. J. Synthesis and biological activity of a profluorescent analogue of coenzyme B_{12}. *Proc. Natl. Acad. Sci. U.S.A* **79**, 3480–3484 (1982).

45. Watanabe, F.; Abe, K.; Takenaka, S.; Fujita, T.; Nakano, Y. Method for Quantification of total vitamin B_{12} in foods using a highly fluorescent vitamin B_{12} derivative. *J. Agric. Food Chem.* **45**, 4661–4663 (1997).

46. Rossier, J.; Hauser, D.; Kottelat, E.; Rothen-Rutishauser, B.; Zobi, F. Organometallic cobalamin anticancer derivatives for targeted prodrugs via transcobalamin-mediated uptake. *Dalt. Trans.* **46**, 2159-2164 (2017).

47. Clardy, S. M.; Allis, D. G.; Fairchild, T. J.; Doyle, R. P. Vitamin B_{12} in drug delivery: breaking through the barriers to a B_{12} bioconjugate pharmaceutical. *Expert Opin. Drug Deliv.* **8**, 127–140 (2011).

48. Ruiz-Sánchez, P.; König, C.; Ferrari, S.; Alberto, R. Vitamin B_{12} as a carrier for targeted platinum delivery: in vitro cytotoxicity and mechanistic studies. *J. Biol. Inorg. Chem.* **16**, 33–44 (2011).

49. Zobi, F.; Blacque, O.; Jacobs, R. A.; Schaub, M. C.; Bogdanova, A. Y. 17 e- rhenium dicarbonyl CO-releasing molecules on a cobalamin scaffold for biological application. *Dalt. Trans.* **41**, 370–378 (2012).

50. Lee, M.; Grissom, C. B. Design, synthesis, and characterization of fluorescent cobalamin analogues with high quantum efficiencies. *Org. Lett.* **11**, 2499–2502 (2009).

51. Fedosov, S.; Grisson, C. B.; Fedosova, N. U.; Moestrup, S. K.; Nexø, E. Application of fluorescent cobalamin analogue for analysis of the binding kinetics.A study emplooying recombinant human transcobalamin and intrínsec factor. *FEBS J.* **273**, 4742–4753 (2006).

52. Viola-Villegas, N.; Rabideau, A. E.; Bartholomä, M.; Zubieta, J.; Doyle, R. P. Targeting the cubilin receptor through the vitamin B_{12} uptake pathway: cytotoxicity and mechanistic insight through fluorescent Re(I) delivery. *J. Med. Chem.* **52**, 5253–5261 (2009).

53. Vortherms, A. R.; Kahkosko, A. R.; Rabideau, A. E.; Zubieta, J.; Andersen, L. L.; Madsen, M.; Doyle, R. P. A water soluble vitamin B_{12}-Re(I) fluorescent conjugate for cell uptake screens: use in the confirmation of cubilin in the lung cancer line A549. *Chem. Commun.* **47**, 9792–9794 (2011).

54. Chromiński, M.; Lewalska, A.; Gryko, D. Reduction-free synthesis of stable acetylide cobalamins. *Chem. Commun.* **49**, 11406–11408 (2013).

55. Zhou, K.; Oetteri, R. M.; Brandl, H.; Lyatuu, F. E.; Buckel, E.; Zelder, F. Chemistry and Bioactivity of an Artificial Adenosylpeptide B_{12} Cofactor. *ChemBioChem* **13**, 2052–2055 (2012).

56. Smetlzer, C. C.; Cannon, M. J.; Rinson, R. P.; Munger, J. D.; West, F. G.; Grissom, C. B. Synthesis and Characterization of fluorescent Cobalamin (cobalafluor) derivatives for imaging. *Org. Lett*. **3**, 799–801 (2001).

57. Ruiz-Sánchez, P.; Mundwiler, S.; Alberto, R. Syntheses of fluorescent vitamin B_{12}-Pt(II) Conjugates and their Pt(II) release in a spectroelectrochemical assay. *Chimia* **61**, 190–193 (2007).

58. Koppenhagen, V. B.; Pfiffner, J. J. Currins and Zirrins, Two New Classes of Corrin Analogues. *J. Biol. Chem.* **245** 5865–5867 (1970).

59. Koppenhagen, V. B.; Pfiffner, J. J. α-(5,6-dimethylbenzimidazolyl)hydrogenobamide and its copper and zinc analogues. *J. Biol. Chem.* **246**, 3075–3077 (1971).

60. Koppenhagen, V. B.; Elsenhans, B.; Wagner, F.; Pfiffner, J. J. Methylrhodibalamin and 5' deoxyadenosylrhodibalamin, the rhodium analogues of methylcobalamin and cobalamin coenzyme. *J. Biol. Chem*. **249**, 6532–6540 (1974).

61. Carmel, R.; Koppenhagen, V. B. The effect of rhodium and copper analogs of cobalamin on human cells in vitro. *Arch. Biochem. Biophys.* **184**, 135–140 (1977).

62. Gallo, S.; Freisinger, E.; Sigel, R. K. O. Towards the synthesis of light-stable coenzyme B_{12} analogues. *Inorganica Chim. Acta* **360**, 360–368 (2007).

63. Zhu, B. H.; Liu, Z. H.; Yan, H.; Liu, J.; Chen, H. The coenzyme B_{12} analogs-ribosylcobalamins: synthesis, characterization, and photolysis studies. *J. Inorg. Biochem*. **65**, 45–52 (1997).

64. Crick, F. H. C. On Protein Synthesis. *Symp. Soc. Exp. Biol.* 12, 138–163 (1958).

65. Neidle, S. "RNA structures and their diversity", *Principles of Nucleic Acid Structure*, Academic press 204–248 (2008).

66. Wakeman, C. A.; Winkler, W. C.; Dann, C. 3rd. Structural features of metabolite-sensing riboswitches. *Trends Biochem. Sci.* **32**, 415–424 (2007).

67. Peselis, A.; Serganov, A. Themes and variations in riboswitch structure and function. *Biochim. Biophys. Acta - Gene Regul. Mech.* **1839**, 908–918 (2014).

68. Wyatt, J. R.; Tinoco Jr., I. "RNA estructural elements and RNA function", *The RNA world*, edited by Gesteland, R. F.; Atkins, J. F. Cold Spring Harbor Laboratory Press 465–496 (1993).

69. Berg, J. M.; Tymoczko, J. l.; Stryer, L. *Biochemistry 5th Edition*, W. H. Freeman and Company (2001).

70. Rich, A. The Era of RNA Awakning: structural biology of RNA in the early years. *Q. Rev. Biophys.* **42**, 117–137 (2009).

71. Rich, A. The double helix: A tale of two puckers. *Nat. Struct. Biol.* **10**, 247–249 (2003).

72. Sobell, H. M. Premeltons in DNA. *J. Struct. Funct. Genomics* **17**, 17–31 (2016).

73. Hendrix, D. K.; Brenner, S. E.; Holbrook, S. R. RNA structural motifs: Building blocks of a modular biomolecule. *Q. Rev. Biophys*. **38**, 221–243 (2005).

74. Nagaswamy, U.; Voss, N.; Zhang, Z.; Fox, G. E. Database of non-canonical base pairs found in known RNA structures. *Nucleic Acids Res.* **28**, 375–376 (2000).

75. Šponer, J. E.; Špačková, N.; Kulhánek, P.; Leszczynski, J.; Šponer, J. Non-Watson-Crick base pairing in RNA. Quantum chemical analysis of the cis Watson-Crick/sugar edge base pair family. *J. Phys. Chem. A* **109**, 2292–2301 (2005).

76. Roy, A.; Panigrahi, S.; Bhattacharyya, M.; Bhattacharyya, D. Structure, stability, and dynamics of canonical and noncanonical base pairs: Quantum chemical studies. *J. Phys. Chem. B* **112**, 3786–3796 (2008).

77. Olson, W. K.; Esguerra, M.; Xin, Y.; Lu, X.-J. New information content in RNA base pairing deduced from quantitative analysis of high-resolution structures. *Methods* **47**, 177–186 (2009).

78. Desiraju, G.R.; Steine, T. *The weak hydrogen bond in structural chemistry and biology*, International Union of Crystallography and Oxford University Press, 399-404 (1999).

79. Pan, T.; Long, D. M.; Uhlenbeck, O. C. "Divalent metal ions in RNA folding and catalysis" *The RNA world*, edited by Gesteland, R. F.; Atkins, J. F. Cold Spring Harbor Laboratory Press 271–302 (1993).

80. Draper, D. E. RNA folding: Thermodynamic and molecular descriptions of the roles of ions. *Biophys. J.* **95**, 5489–5495 (2008).

81. Peselis, A.; Gao, A.; Serganov, A. Cooperativity, allostery and synergism in ligand binding to riboswitches. *Biochimie* **117**, 100–109 (2015).

82. Woodson, S. A. Metal ions and RNA folding: A highly charged topic with a dynamic future. *Curr. Opin. Chem. Biol.* **9**, 104–109 (2005).

83. Bowman, J. C.; Lenz, T. K.; Hud, N. V; Williams, L. D. Cations in charge: Magnesium ions in RNA folding and catalysis. *Curr. Opin. Struct. Biol.* **22**, 262–272 (2012).

84. Lambert, D.; Leipply, D.; Shiman, R.; Draper, D. E. The Influence of Monovalent Cation Size on the Stability of RNA Tertiary Structures. *J. Mol. Biol*. **390**, 791–804 (2009).

85. Hayes, R. L.; Noel, J. K.; Whitford, P. C.; Mohanty, U.; Sanbonmatsu, K. Y.; Onuchic, J. N. Reduced model captures Mg^{2+}-RNA interaction free energy of riboswitches. *Biophys. J.* **106**, 1508–1519 (2014).

86. Jack, K. D.; Means, J. A.; Hines, J. V. Characterizing riboswitch function: Identification of Mg^{2+} binding site in T box antiterminator RNA. *Biochem. Biophys. Res. Commun.* **370**, 306–310 (2008).

87. Choudhary, P. K.; Sigel, R. K. O. Mg^{2+}-induced conformational changes in the *btuB* riboswitch from *E . coli. RNA* **20**, 1–10 (2013).

88. Yamauchi, T.; Miyoshi, D.; Kubodera, T.; Nishimura, A.; Nakai, S.; Sugimoto, N. Roles of Mg^{2+} in TPP-dependent riboswitch. *FEBS Lett.* **579**, 2583–2588 (2005).

89. Warf, M. B.; Berglund, J. A. Role of RNA structure in regulating pre-mRNA splicing. *Trends Biochem. Sci.* **35**, 169–178 (2010).

90. Moore, P. B. Structural Motifs in RNA. *Annu. Rev. Biochem.* **68**, 287–300 (1999).

91. Holbrook, S. R. RNA structure: The long and the short of it. *Curr. Opin. Struct. Biol.* **15**, 302–308 (2005).

92. Leontis, N. B.; Westhof, E. Analysis of RNA motifs. *Curr. Opin. Struct. Biol.* **13**, 300–308 (2003).

93. Pyle, A. M.; Green, J. B. RNA folding. *Curr. Opin. Struct. Biol.* **5**, 303–310 (1995).

94. Zhou, H.; Kimsey, I. J.; Nikolova, E. N.; Sathyamoorthy, B.; Grazioli, G.; McSally, J.; Bai, T.; Wunderlich, C. H.; Kreutz, C.; Andricioaei, I.; Al-Hashimi, H. M. m1A and m1G disrupt A-RNA structure though the intrinsic instability of Hoogsteen base pairs. *Nat. Struct. Mol. Biol.* **23**, 803–810 (2016).

95. Tomizawa, J. "Evolution of funcional structures of RNA", *The RNA world*, edited by Gesteland, R. F.; Atkins, J. F. Cold Spring Harbor Laboratory Press 419–447 (1993).

96. Bompfünewerer, A. F.; Flamm, C.; Fried, C.; Fritzsch, G.; Hofacker, I. L.; Lehmann, J.; Missal, K.; Mosig, A.; Müller, B.; Prohaska, S. J.; Stadler, B. M. R.; Stadler, P. F.; Tazer, A.; Washietu, S.; Witwer, C. Evolutionary patterns of non-coding RNAs. *Theory Biosci.* **123**, 301–369 (2005).

97. Will, C. L.; Lührmann, R. "Spliceosome structure and function" *RNA worlds: from lives origins to diversity in gene regulation*, edited by Atkins, J. F.; Gesteland, R. F.; Cech, T. R. Cold Spring Harbor Laboratory Press 181–204 (2011).

98. Blackburn, E. H.; Collins, K. "Telomerase: an RNP ensyme synthesizes DNA" *RNA worlds: from lives origins to diversity in gene regulation*, edited by Atkins, J. F.; Gesteland, R. F.; Cech, T. R. Cold Spring Harbor Laboratory Press 205–214 (2011).

99. Vogel, J. A rough guide to the non-coding RNA world of Salmonella. *Mol. Microbiol.* **71**, 1–11 (2009).

100. Storz, G.; Opdyke, J. A.; Zhang, A. Controlling mRNA stability and translation with small, noncoding RNAs. *Curr. Opin. Microbiol.* **7**, 140–144 (2004).

101. Colameco, S.; Elliot, M. A. Non-coding RNAs as antibiotic targets. *Biochem. Pharmacol.* **133**, 29–42 (2017).

102. Nilsen, T. W. RNA 1997-2007: A Remarkable Decade of Discovery. *Mol. Cell* **28**, 715–720 (2007).

103. Joshua-Tor, L.; Hannon, G. J. “Ancestral roles of small RNAs: an ago-centric perspective” *RNA worlds: from lives origins to diversity in gene regulation*, edited by Atkins, J. F.; Gesteland, R. F.; Cech, T. R. Cold Spring Harbor Laboratory Press 243–254 (2011).

104. Hüttenhofer, A.; Schattner, P.; Polacek, N. Non-coding RNAs: Hope or hype? *Trends Genet.* **21**, 289–297 (2005).

105. Jore, M. M.; Brouns, S. J. J.; van der Oost, J “RNA in defense: CRISPRs protect prokaryotes against Mobile genètic elements” *RNA worlds: from lives origins to diversity in gene regulation*, edited by Atkins, J. F.; Gesteland, R. F.; Cech, T. R. Cold Spring Harbor Laboratory Press 231–242 (2011).

106. Steitz, J.; Borah, S.; Cazalla, D.; Fok, V.; Lytle, R.; Mitton-Fry, R.; Riley, K.; Samji, T. “Noncoding RNPs of viral origin” *RNA worlds: from lives origins to diversity in gene regulation*, edited by Atkins, J. F.; Gesteland, R. F.; Cech, T. R. Cold Spring Harbor Laboratory Press 165–180 (2011).

107. Johansson, J.; Mandin, P.; Renzoni, A.; Chiaruttini, C.; Springer, M.; Cossart, P. An RNA thermosensor controls expression of Virulence Genes in Listeria monocytogenes. *Cell* **110**, 551–561 (2002).

108. Bastet, L.; Dubé, A.; Massé, E.; Lafontaine, D. A. New insights into riboswitch regulation mechanisms. *Mol. Microbiol.* **80**, 1148–1154 (2011).

109. Gottesman, S. The Small RNA Regulators of *Escherichia coli* : Roles and Mechanisms. *Annu. Rev. Microbiol.* **58**, 303–328 (2004).

110. Zhu, X.; Wang, X. X.; Zhang, C.; Wang, X. X.; Gu, Q. A riboswitch sensor to determine vitamin B_{12} in fermented foods. *Food Chem.* **175**, 523–528 (2015).

111. Polaski, J. T.; Webster, S. M.; Johnson, Jr. J. E.; Batey, R. T. Cobalamin riboswitches exhibit a broad range of ability to discriminate between methylcobalamin and adenosylcobalamin. *J. Biol. Chem.* **292**, 11650–11658 (2017).

112. Aghdam, E. M.; Hejazi, M. S.; Barzegar, A. Riboswitches: From living biosensors to novel targets of antibiotics. *Gene* **592**, 244–259 (2016).

113. Gilbert, S. D.; Batey, R. T. Riboswitches: Fold and Function. *Chem. Biol.* **13**, 805–807 (2006).

114. Santillán, M.; Mackey, M. C. Dynamic behaviour of the B_{12} riboswitch. *Phys. Biol.* **2**, 29–35 (2005).

115. Lussier, A.; Bastet, L.; Chauvier, A.; Lafontaine, D. A. A kissing loop is important for *btuB* riboswitch ligand sensing and regulatory control. *J. Biol. Chem.* **290**, 26739–26751 (2015).

116. Barrick, J. E.; Breaker, R. R. The distributions, mechanisms, and structures of metabolite-binding riboswitches. *Genome Biol.* **8**, R239 (2007).

117. Warner, D. F.; Savvi, S.; Mizrahi, V.; Dawes, S. S. A riboswitch regulates expression of the coenzyme B12- independent methionine synthase in *Mycobacterium tuberculosis*: Implications for differential methionine synthase function in strains H37Rv and CDC1551. *J. Bacteriol.* **189**, 3655–3659 (2007).

118. Garst, A. D.; Batey, R. T. A switch in time: Detailing the life of a riboswitch. *Biochim. Biophys. Acta - Gene Regul. Mech.* **1789**, 584–591 (2009).

119. Nudler, E.; Mironov, A. S. The riboswitch control of bacterial metabolism. *Trends Biochem. Sci.* **29**, 11–17 (2004).

120. Serganov, A.; Patel, D. J. Molecular recognition and function of riboswitches. *Curr. Opin. Struct. Biol.* **22**, 279–286 (2012).

121. Winkler, W. C.; Breaker, R. R. Regulation of Bacterial Gene Expression By Riboswitches. *Annu. Rev. Microbiol.* **59**, 487–517 (2005).

122. Meyer, M. M.; Hammond, M. C.; Salina, Y.; Roth, A.; Sudarsan, N.; Breaker, R. R. Challenges of ligand identification for riboswitch candidates. *RNA Biol.* **8**, 5–10 (2011).

123. Sanbonmatsu, K. Y. Towards structural classification of long non-coding RNAs. *Biochim. Biophys. Acta - Gene Regul. Mech.* **1859**, 41–45 (2016).

124. Soukup, J. K.; Soukup, G. A. Riboswitches exert genetic control through metabolite-induced conformational change. *Curr. Opin. Struct. Biol.* **14**, 344–349 (2004).

125. Hong, W.; Zeng, J.; Xie, J. Antibiotic drugs targeting bacterial RNAs. *Acta Pharm. Sin. B* **4**, 258–265 (2014).

126. Lee, E. R.; Blount, K. F.; Breaker, R. R. Roseoflavin is a natural antibacterial compound that binds to FMN riboswitches and regulates gene expression. *RNA Biol.* **6**, 187–194 (2009).

127. Mulhbacher, J.; St-Pierre, P.; Lafontaine, D. A. Therapeutic applications of ribozymes and riboswitches. *Curr. Opin. Pharmacol.* **10**, 551–556 (2010).

128. Yan, L.-H.; Le Roux, A.; Boyapelly, K.; Lamontagne, A.-M.; Archambault, M.-A.; Picard-Jean, F.; Lalonde-Seguin, D.; St-Pierre, E.; Najmanovich, R. J.; Fortier, L-C.; Lafontaine, D.; Marsault, E. Purine analogs targeting the guanine riboswitch as potential antibiotics against *Clostridioides difficile. Eur. J. Med. Chem.* **143**, 755–768 (2017).

129. Fei, X.; Holmes, T.; Diddle, J.; Hintz, L.; Delaney, D.; Stock, A.; Renner, D.; McDevitt, M.; Berkowitz, D. B.; Soukup, J. K. Phosphatase-inert glucosamine 6-phosphate mimics serve as actuators of the *glms* riboswitch. *ACS Chem. Biol.* **9**, 2875–2882 (2014).

130. Garst, A. D.; Edwards, A. L.; Batey, R. T. "Riboswitches: structures and mechanisms" *RNA worlds: from lives origins to diversity in gene regulation*, edited by Atkins, J. F.; Gesteland, R. F.; Cech, T. R. Cold Spring Harbor Laboratory Press 79–92 (2011).

131. Weinberg, Z.; Wang, J. X.; Bogue, J.; Yang, J.; Corbino, K.; Moy, R. H.; Breaker, R. R. Comparative genomics reveals 104 candidate structured RNAs from bacteria, archaea, and their metagenomes. *Genome Biol.* **11**, R31 (2010).

132. Serganov, A.; Yuan, T.-R.; Pikovskaya, O.; Polonskaia, A.; Malinina, L.; Phan, A. T.; Hobartner, C.; Micura, R.; Breaker, R. R.; Patel, D. J. Structural basis for discriminative regulation of gene expression by adenine- and guanine-sensing mRNAs. *Chem. Biol.* **11**, 1729–1741 (2004).

133. Batey, R. T.; Gilbert, S. D.; Montange, R. K. Structure of a natural guanine-responsive riboswitch complexed with the metabolite hypoxanthine. *Nature* **432**, 411–415 (2004).

134. McCown, P. J.; Liang, J. J.; Weinberg, Z.; Breaker, R. R. Structural, functional, and taxonomic diversity of three preq1riboswitch classes. *Chem. Biol.* **21**, 880–889 (2014).

135. Nelson, J. W.; Breaker, R. R. The lost language of the RNA World. *Sci. Signal.* **10**, eaam8812 (2017).

136. Lee, E. R.; Baker, J. L.; Weinberg, Z.; Sudarsan, N.; Bearker, R. R. An Allosteric Self-Splicing Ribozyme Triggered by a Bacterial Second Messenger. *Science* **329**, 845–848 (2010).

137. Jones, C. P.; Ferré-D'Amaré, A. R. Crystal structure of a c-di-AMP riboswitch reveals an internally pseudo-dimeric RNA. *EMBO J*. **33**, 2692–2703 (2014).

138. Serganov, A.; Nudler, E. A decade of riboswitches. *Cell* **152**, 17–24 (2013).

139. Saunders, A. M.; DeRose, V. J. Beyond Mg^{2+}: Functional interactions between RNA and transition metals. *Curr. Opin. Chem. Biol.* **31**, 153–159 (2016).

140. Furukawa, K.; Ramesh, A.; Zhou, Z.; Weinberg, Z.; Vallery, T.; Winkler, W. C.; Breaker, R. R. Bacterial Riboswitches Cooperatively Bind Ni^{2+} or Co^{2+} Ions and Control Expression of Heavy Metal Transporters. *Mol. Cell* **57**, 1088–1098 (2015).

141. Price, I. R.; Gaballa, A.; Ding, F.; Helmann, J. D.; Ke, A. Mn^{2+}-Sensing Mechanisms of yybP-ykoY Orphan Riboswitches. *Mol. Cell* **57**, 1110–1123 (2015).

142. Dann 3rd, C. E.; Wakeman, C. A.; Sieling, C. L. Baker, S. C.; Irnov, I.; Winkler, W. C. Structure and Mechanism of a Metal-Sensing Regulatory RNA. *Cell* **130**, 878–892 (2007).

143. Ren, A.; Rajashankar, K. R.; Patel, D. J. Fluoride ion encapsulation by Mg^{2+} ions and phosphates in a fluoride riboswitch. *Nature* **486**, 85–89 (2012).

144. Vitreschak, A. G.; Rodionov, D. A.; Mironov, A. A. Regulation of the vitamin B_{12} metabolism and transport in bacteria by a conserved RNA structural element. *RNA* **9**, 1084–1097 (2003).

145. Johnson Jr., J. E.; Reyes, F. E.; Polaski, J. T.; Batey, R. T. B_{12} cofactors directly stabilize an mRNA regulatory switch. *Nature* **492**, 133–137 (2012).

146. Fox, K. A.; Ramesh, A.; Stearns, J. E.; Bourgogne, A.; Reyes-Jara, A.; Winkler, W. C.; Garsin, D. A. Multiple posttranscriptional regulatory mechanisms partner to control ethanolamine utilization in *Enterococcus faecalis. Proc. Natl. Acad. Sci.* **106**, 4435–4440 (2009).

147. Regulski, E. E.; Moy, R. H.; Weinberg, Z.; Barrick, J. E.; Yao, Z.; Ruzzo, W. L.; Breaker, R. R. A widespread riboswitch candidate that controls bacterial genes involved in molybdenum cofactor and tungsten cofactor metabolism. *Mol. Microbiol.* **68**, 918–932 (2008).

148. Sherman, E. M.; Esquiaqui, J.; Elsayed, G.; Ye, J. D. An energetically beneficial leader-linker interaction abolishes ligand-binding cooperativity in glycine riboswitches. *RNA* **18**, 496–507 (2012).

149. Serganov, A.; Huang, L.; Patel, D. J. Structural insights into amino acid binding and gene control by a lysine riboswitch. *Nature* **455**, 1263–1267 (2008).

150. Garst, A. D.; Héroux, A.; Rambo, R. P.; Batey, R. T. Crystal structure of the lysine riboswitch regulatory mRNA element. *J. Biol. Chem.* **283**, 22347–22351 (2008).

151. Ames, T. D.; Breaker, R. R. Bacterial aptamers that selectively bind glutamine. *RNA Biol.* **8**, 82–89 (2011).

152. Edwards, A. L.; Reyes, F. E., Héroux, A.; Batey, R. T. Structural basis for recognition of S -adenosylhomocysteine by riboswitches. *RNA* **16**, 2144–2155 (2010).

153. Poiata, E.; Meyer, M. M.; Ames, T. D.; Breaker, R. R. A variant riboswitch aptamer class for S-adenosylmethionine common in marine bacteria. *RNA* **15**, 2046–2056 (2009).

154. Corbino, K. A.; Barrick, J. E.; Lim, J.; Welz, R.; Tucker, B. J.; Puskarz, I.; Mandal, M.; Rudnick, N. D.; Breaker, R. R. Evidence for a second class of S-adenosylmethionine riboswitches and other regulatory RNA motifs in alpha-proteobacteria. *Genome Biol.* **6**, R70 (2005).

155. Winkler, W. C.; Nahvi, A.; Sudarsan, N.; Barrick, J. E.; Breaker, R. R. An mRNA structure that controls gene expression by binding S-adenosylmethionine. *Nat. Struct. Biol.* **10**, 701–707 (2003).

156. Lu, C.; Smith, A. M.; Fuchs, R. T.; Ding, F.; Rajashankar, K.; Henkin, T. M.; Ke, A. Crystal structures of the SAM-III/SMK riboswitch reveal the SAM-dependent translation inhibition mechanism. *Nat. Struct. Mol. Biol*. **15**, 1076–1083 (2008).

157. Ames, T. D.; Rodionov, D. A.; Weinberg, Z.; Breaker, R. R. A Eubacterial Riboswitch Class that Senses the Coenzyme Tetrahydrofolate. *Chem. Biol.* **17**, 681–685 (2010).

158. Trausch, J. J.; Ceres, P.; Reyes, F. E.; Batey, R. T. The structure of a tetrahydrofolate sensing riboswitch reveals two ligand binding sites in a single aptamer. *Structure* **19**, 1413–1423 (2011).

159. Trausch, J. J.; Marcano-Velázquez, J. G.; Matyjasik, M. M.; Batey, R. T. Metal Ion-Mediated Nucleobase Recognition by the ZTP Riboswitch. *Chem. Biol.* **22**, 829–837 (2015).

160. Serganov, A.; Huang, L.; Patel, D. J. Coenzyme recognition and gene regulation by a flavin mononucleotide riboswitch. *Nature* **458**, 233–237 (2009).

161. Cochrane, J. C.; Lipchock, S. V.; Strobel, S. A. Structural investigation of the Glms ribozyme bound to its catalytic cofactor. *Chem. Biol.* **14**, 97–105 (2007).

162. Roth, A.; Weinberg, Z.; Chen, A. G. Y.; Kim, P. B.; Ames, T. D.; Breaker, R.R. A widespread self-cleaving ribozyme class revealed by bioinformatics. *Nat. Chem. Biol.* **10**, 56–60 (2014).

163. Cressina, E.; Chen, L., Abell, C.; Leeper, F. J.; Smith, A. G. Fragment screening against the thiamine pyrophosphate riboswitch thiM. *Chem. Sci.* **2**, 157–165 (2011).

164. Kubodera, T.; Watanabe, M.; Yoshiuchi, K.; Yamashita, N.; Nishimura, A.; Nakai, S.; Gomi, K.; Hanamoto, H. Thiamine-regulated gene expression of Aspergillus oryzae thiA requires splicing of the intron containing a riboswitch-like domain in the 5'-UTR. *FEBS Lett.* **555**, 516–520 (2003).

165. Nechooshtan, G.; Elgrably-Weiss, M.; Sheaffer, A.; Westhof, E.; Altuvia, S. A pH-responsive riboregulator. *Genes Dev.* **23**, 2650–2662 (2009).

166. Henkin, T. M. "RNA-dependent RNA switches in bacteria" *Riboswitches,* Methods in Molecular Biology vol.540, edited by Servanov, A. Humana Press 207–214 (2009).

167. Breaker, R. R. "Riboswitches and the RNA world" *RNA worlds: from lives origins to diversity in gene regulation*, edited by Atkins, J. F.; Gesteland, R. F.; Cech, T. R. Cold Spring Harbor Laboratory Press 63–77 (2011).

168. Nou, X.; Kadner, R. J. Adenosylcobalamin inhibits ribosome binding to *btuB* RNA. *Proc. Natl. Acad. Sci.* **97**, 7190–7195 (2000).

169. Franklund, C. V; Kadner, R. J. Multiple transcribed elements control expression of the *Escherichia coli btuB* gene. *J. Bacteriol.* **179**, 4039–4042 (1997).

170. Nahvi, A.; Sudarsan, N.; Ebert, M. S.; Zou, X.; Brown, K. L.; Breaker, R. R. Genetic control by a metabolite binding mRNA. *Chem. Biol*. **9**, 1043–1049 (2002).

171. Vitreschak, A. G.; Rodionov, D. A.; Mironov, A. A.; Gelfand, M. S. Regulation of the vitamin B_{12} metabolism and transport in bacteria by a conserved RNA structural elements. *RNA* **9**, 1084–97 (2003).

172. Nahvi, A.; Barrick, J. E.; Breaker, R. R. Coenzyme B_{12} riboswitches are widespread genetic control elements in prokaryotes. *Nucleic Acids Res*. **32**, 143–150 (2004).

173. Peselis, A.; Serganov, A. Structural insights into ligand binding and gene expression control by an adenosylcobalamin riboswitch. *Nat. Struct. Mol. Biol*. **19**, 1182–1184 (2012).

174. Kazanov, M. D.; Vitreschak, A. G.; Gelfand, M. S. Abundance and functional diversity of riboswitches in microbial communities. *BMC Genomics* **8**, 347 (2007).

175. Ravnum, S.; Andersson, D. I. An adenosyl-cobalamin (coenzyme-B_{12})-repressed translational enhancer in the *cob* mRNA of *Salmonella typhimurium. Mol. Microbiol.* **39**, 1585–1594 (2001).

176. Nou, X.; Kadner, R. J. Coupled Changes in Translation and Transcription during Cobalamin-Dependent Regulation of *btuB* Expression in *Escherichia coli. J. Bacteriol.* **180**, 6719–6728 (1998).

177. Gallo, S.; Oberhuber, M.; Sigel, R. K. O.; Kräutler, B. The corrin moiety of coenzyme B_{12} is the determinant for switching the *btuB* riboswitch of *E. coli*. *ChemBioChem* **9**, 1408–1414 (2008).

178. Gallo, S.; Mundwiler, S.; Alberto, R.; Sigel, R. K. O. The change of corrin-amides to carboxylates leads to altered structures of the B_{12}-responding *btuB* riboswitch. *Chem. Commun.* **47**, 403–405 (2011).

179. Martínez, J. L.; Baquero, F. Emergence and spread of antibiotic resistance: setting a parameter space. *Upsala J. Med. Sci.* **119**, 68–77 (2014).

180. Blair, J. M. A.; Webber, M. A.; Baylay, A. J.; Ogbolu, D. O.; Piddock, L. J. V. Molecular mechanism of antibiotic resistance. *Nat. Rev. Microbiol.* **13**, 42–51 (2015).

181. Denys, G. A.; Relich, R. F. Antibiotic Resistance in Nosocomial Respirtory Infections. *Clin Lab Med* **34**, 257–270 (2014).

182. Fabbretti, A.; Gualerzi, C. O.; Brandi, L. How to cope with the quest for new antibiotics. *FEBS Lett.* **585**, 1673–1681 (2011).

183. Rocha, C.; Reunolds, N. D.; Simons, M. P. Resistencia emergente a los antibióticos: una amenaza global y un ploblema crítico en el cuidado de la salud. *Rev. Peru Med. Exp. Salud Pública* **32**, 139–145 (2015).

184. Cuddy, P. G. Antibiotic Classification: Implications for Drug Selection. *Crit. Care Nurs. Q.* **20**, 89–102 (1997).

185. Ko, W.-C.; Paterson, D. L., Sagnimeni, A. J.; Hansen, D. S.; Von Gottberg, A.; Mohapatra, S.; Casellas, J. M.; Goossens, H.; Mulazimoglu, L.; Trenholme, G.; Klugman, K. P.; McCormack, J. G.; Yu, V. L. Community-acquired Klebsiella pneumoniae bacteremia: global differences in clinical patterns. *Emerg. Infect. Dis.* **8**, 160–6 (2002).

186. Rosen, D. A.; Hilliard, J. K.; Tiemann, K. M.; Todd, E. M.; Morley, S. C.; Hunstad, D. A. Klebsiella pneumoniae FimK promotes virulence in murine pneumonia. *J. Infect. Dis.* **213**, 649–658 (2016).

187. Wickiser, J. K.; Winkler, W. C.; Breaker, R. R.; Crothers, D. M. The speed of RNA transcription and metabolite binding kinetics operate an FMN riboswitch. *Mol. Cell* **18**, 49–60 (2005).

188. Shon, A. S.; Russo, T. A. Hypervirulent Klebsiella pneumoniae: The next superbug? *Future Microbiol.* **7**, 669–671 (2012).

189. Regulski, E. E.; Breaker, R. R. In-line probing analysis of riboswitches. *Methods Mol. Biol.* **419**, 53–67 (2008).

190. Weeks, K. M. Advances in RNA structure analysis by chemical probing. *Curr. Opin. Struct. Biol.* **20**, 295–304 (2010).

191. Soukup, G. A.; Breaker, R. R. Relationship between internucleotide linkage geometry and the stability of RNA. *RNA* **5**, 1308–1325 (1999).

192. Gilbert, S. D.; Batey, R. T. "Monitoring RNA-ligand interaction using Isothermal titration calorimetry" *Riboswitches,* Methods in Molecular Biology vol.540, edited by Servanov, A. Humana Press 97–114 (2009)

193. Feig, A. L. Application of Isothermal Titration Calorimetry in RNA Biochemistry and Biophysics. *Biopolymers.* **87**, 295-301 (2007).

194. Song, C.; Zhang, S.; Huang, H. Choosing a suitable method for the identification of replication origins in microbial genomes. *Front. Microbiol*. **6**, 1049 (2015).

195. Kumar, G. S.; Basu, A. The use of calorimetry in biophysical characterization of small molecule alkaloids binding to RNA structures. *Biochim. Biophys. Acta* **1860**, 930–944 (2016).

196. Todd, M. J.; Gomez, J. Enzyme Kinetics determined usig calorimetry: a general assay for enzyme activity? *Anal. Biochem.* **296**, 179–187 (2001).

197. Burnouf, D.; Ennifar, E.; Guedich, S.; Puffer, B.; Hoffmann, G.; Bec, G.; Disdier, F.; Baltzinger, M.; Dumas, P. KinITC: a new method for obtaining joint thermodynamic and kinetic data by isothermal titration calorimetry. *J. Am. Chem. Soc.* **134**, 559–565 (2012).

198. Gilbert, S. D.; Stoddard, C. D.; Wise, S. J.; Batey, R. T. Thermodynamic and Kinetic Characterization of Ligand Binding to the Purine Riboswitch Aptamer Domain. *J. Mol. Biol.* **359**, 754–768 (2006).

199. Gilbert, S. D.; Mediatore, S. J.; Batey, R. T. Modified pyrimidines specifically bind the Purine Riboswitch. *J. Am. Chem. Soc.* **128**, 14214–14215 (2006).

200. Müller, M.; Weigand, J. E.; Weichenrieder, O.; Suess, B. Thermodynamic characterization of an engineered tetracycline-binding riboswitch. *Nucleic Acids Res.* **34**, 2607–2617 (2006).

201. Prof. Dr. Eva Freisinger. Point Mutation Protocol. Personal Communication

202. Gallo, S.; Furler, M.; Sigel, R. K. O. *In vitro* transcription and purification of RNAs of different size. *Chimia* **59**, 812–816 (2005).

203. Martins, R.; Queiroz, J. A.; Sousa, F. Ribonucleic acid purification. *J. Chromatogr. A* **1355**, 1–14 (2014).

204. Zhang, C.; Papakonstantinou, T. "Purification of nucleic acids from gels" *Handbook of Nucleic Acids Purification vol.23*, Edited by Liu, D. CRC press 537–554 (2002).

205. Marky, L. A.; Breslauer, K. J. Calculating thermodynamic data for transitions of any molecularity from equilibrium melting curves. *Biopolymers* **26**, 1601–1620 (1987).

206. Sigel, R. K. O.; Freisinger, E.; Lippert, B. Effects of N7-methylation, N7-platination, and C8-hydroxylation of guanine on H-bond formation with cytosine: Platinum coordination strengthens the Watson-Crick pair. *J. Biol. Inorg. Chem.* **5**, 287–299 (2000).

207. Molino, J. V. D.; de Carvalho, J. C. M.; Mayfield, S. Evaluation of secretion reporters to microalgae biotechnology: Blue to red fluorescent proteins. *Algal Res.* **31**, 252–261 (2018).

208. Aron, D. I.; Das, V. S. R.; Anderson, J. D. "Metabolism of photosynthetic bacteria I. Effects of carbon sourse and hydrogen gas on biosynthetic patterns in chromatium" *Sutdies on microalgae and photosynthetic Bacteria*. *A collection of papers* edited by the Japanese Society of plant physiologists, University of Tokio Press 529–545 (1963).

209. Barker, H. A.; Smith, R. D.; Weissbach, H.; Toohey, J. I.; Ladd, J. N.; Volcani, B. E. Isolation and propierties of Crystalline cobamide coenzymes containing benzimidazole or 5,6-dimethylbenzimidazole. *J. Biol. Chem.* **235**, 480–488 (1960).

210. Barker, H. A.; Smith, R. D.; Weissbach, H.; Munch-Petersen, A.; Toohey, J. I.; Ladd, J. N.; Volcani, B. E.; Marilin Wilson, R. Assay, Purification, and Properties of the Adenosylcobinamide coenzyme. *J. Biol. Chem.* **235**, 181–190 (1960).

211. Butler, P. A.; Murtaza, S.; Kräutler, B. Partial Synthesis of CoαCoβ-dicyano-176-norcobinamide. *Monats. Chem.* **137**, 1579–1589 (2006).

212. Pfenning, N.; Trüper, H. G. “The family Chromatiaceae” *The prokaryotes 2nd Edition*, edited by Balows, A.; Trüper, A. G.; Dworkin, M.; Harder, W.; Schleifer, K.-H. Springer science+business media 3200–3221 (1992).

7. Appendices

Appendix 1. Plasmids schemes

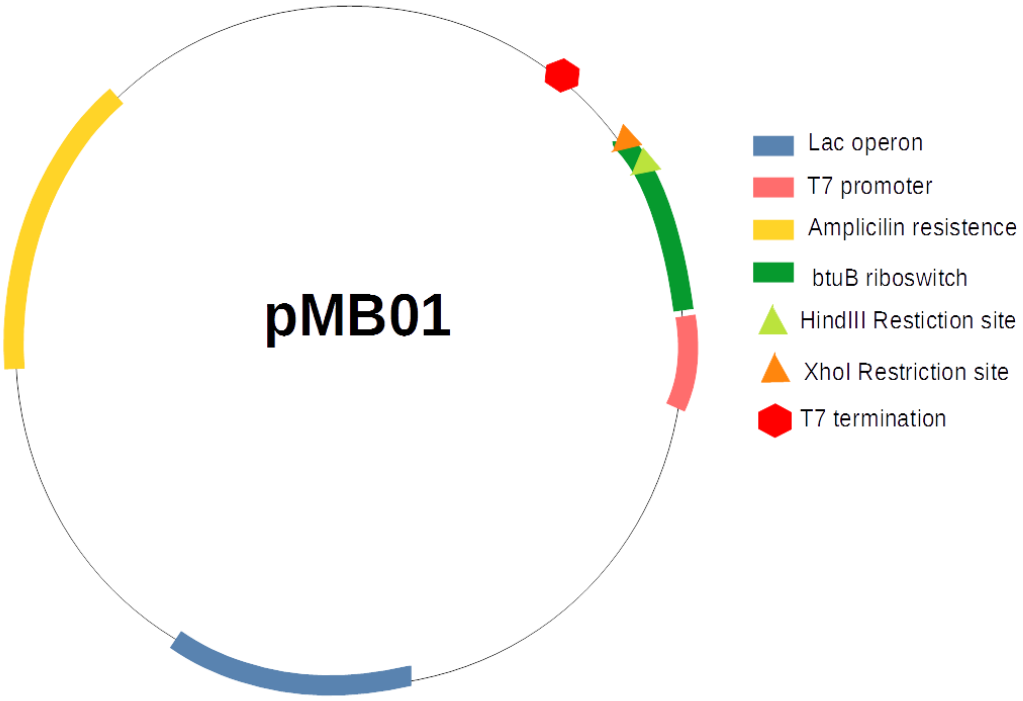

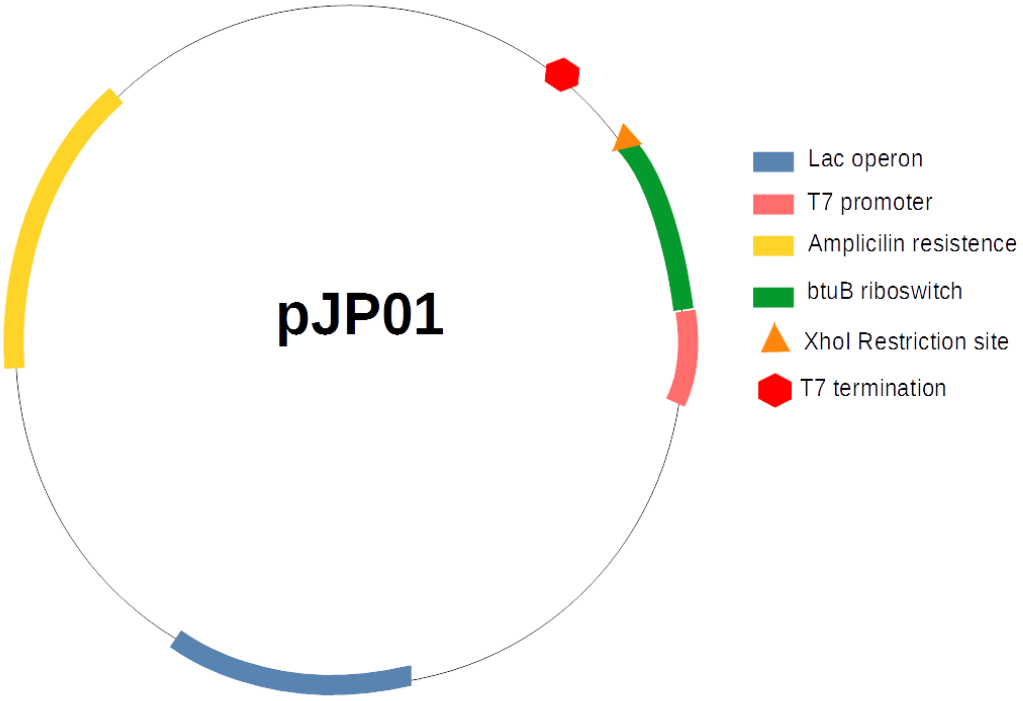

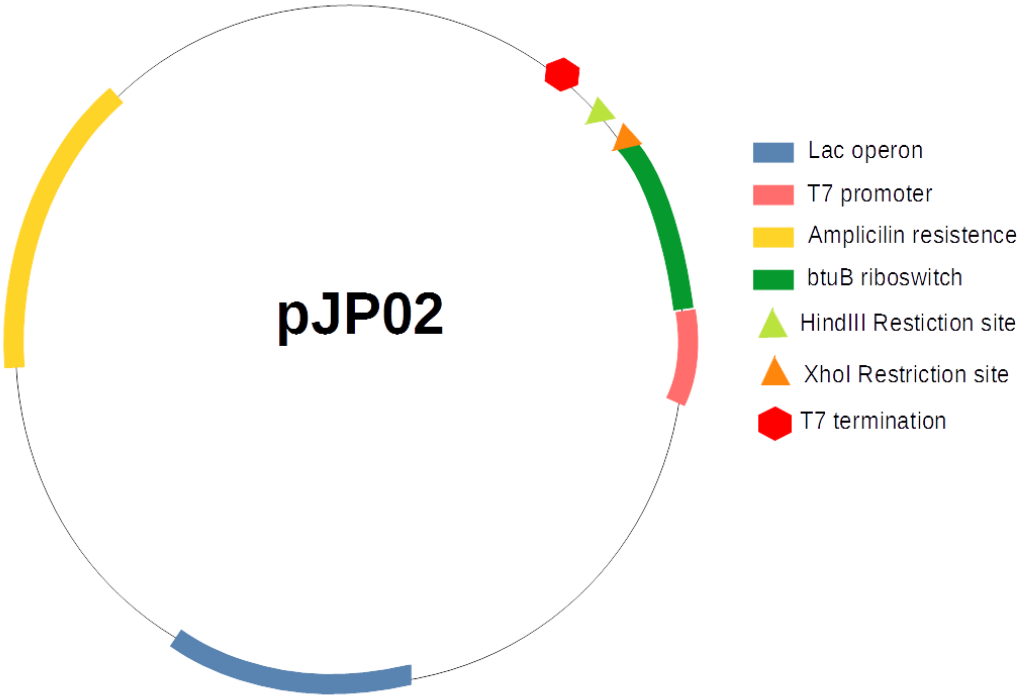
pJP02
Lac operon
T7 promoter
Amplicilin resistence
btuB riboswitch
HindIII Restiction site
XhoI Restriction site
T7 termination

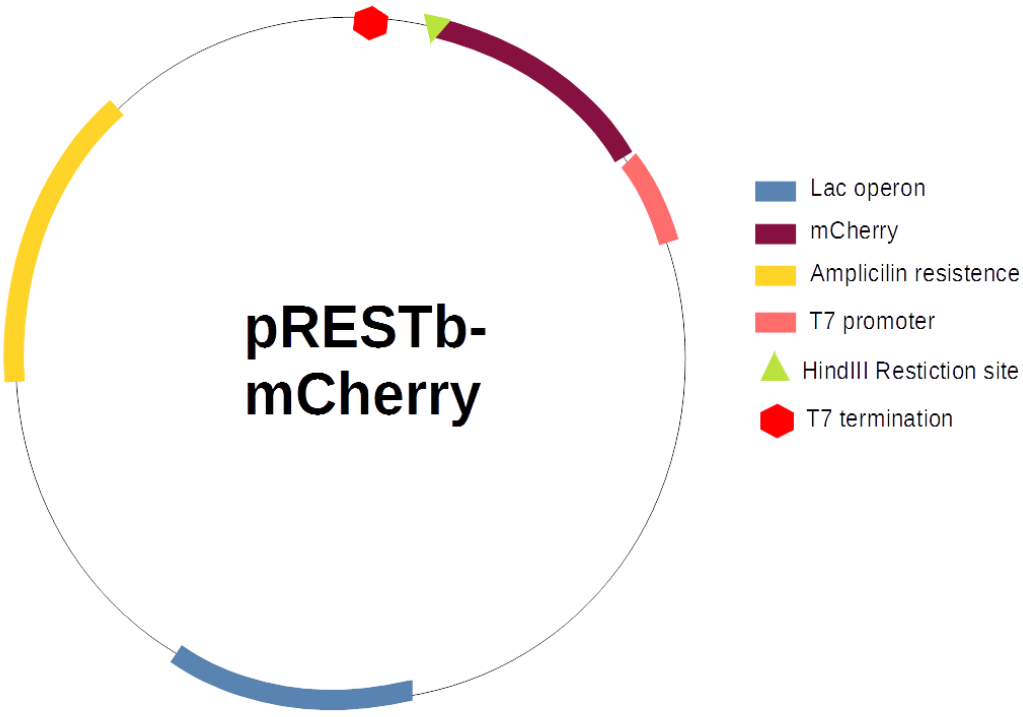
pRESTb-
mCherry
Lac operon
mCherry
Amplicilin resistence
T7 promoter
HindIII Restiction site
T7 termination

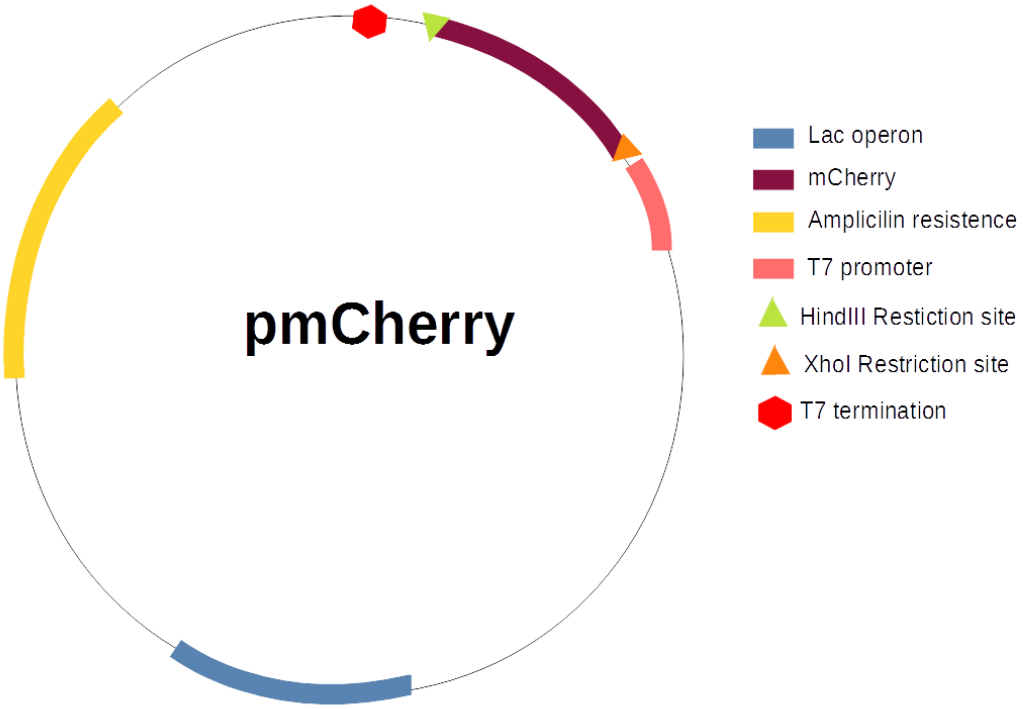
pmCherry
Lac operon
mCherry
Amplicilin resistence
T7 promoter
HindIII Restiction site
XhoI Restriction site
T7 termination

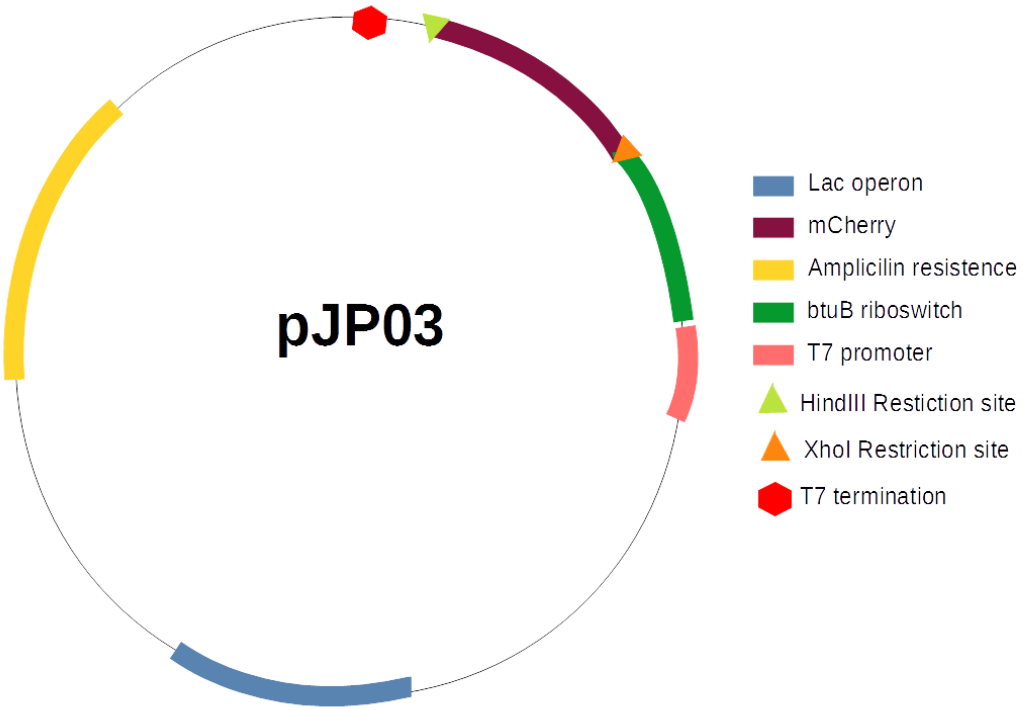
pJP03
Lac operon
mCherry
Amplicilin resistence
btuB riboswitch
T7 promoter
HindIII Restiction site
XhoI Restriction site
T7 termination

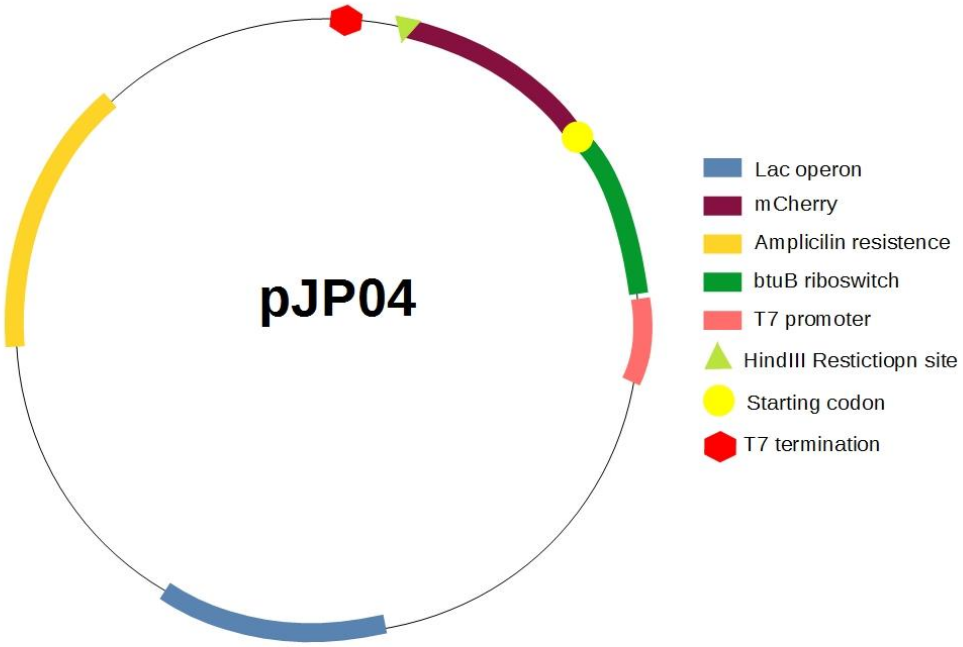
pJP04
Lac operon
mCherry
Amplicilin resistence
btuB riboswitch
T7 promoter
HindIII Restictiopn site
Starting codon
T7 termination

Appendix 2. In-line probing gels and bands fitting to the 1:1 isotherm.

Gel A

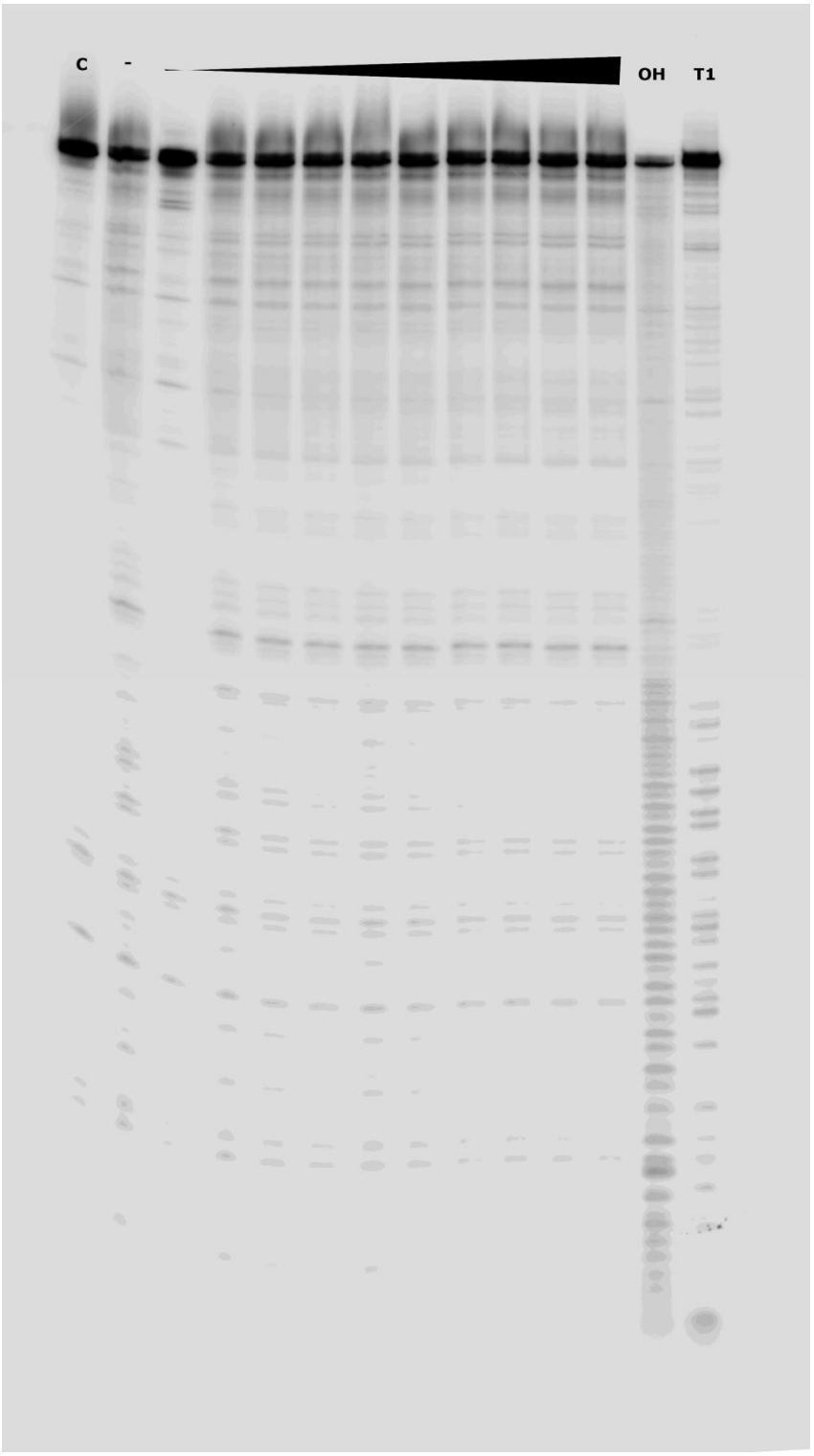

Gel B

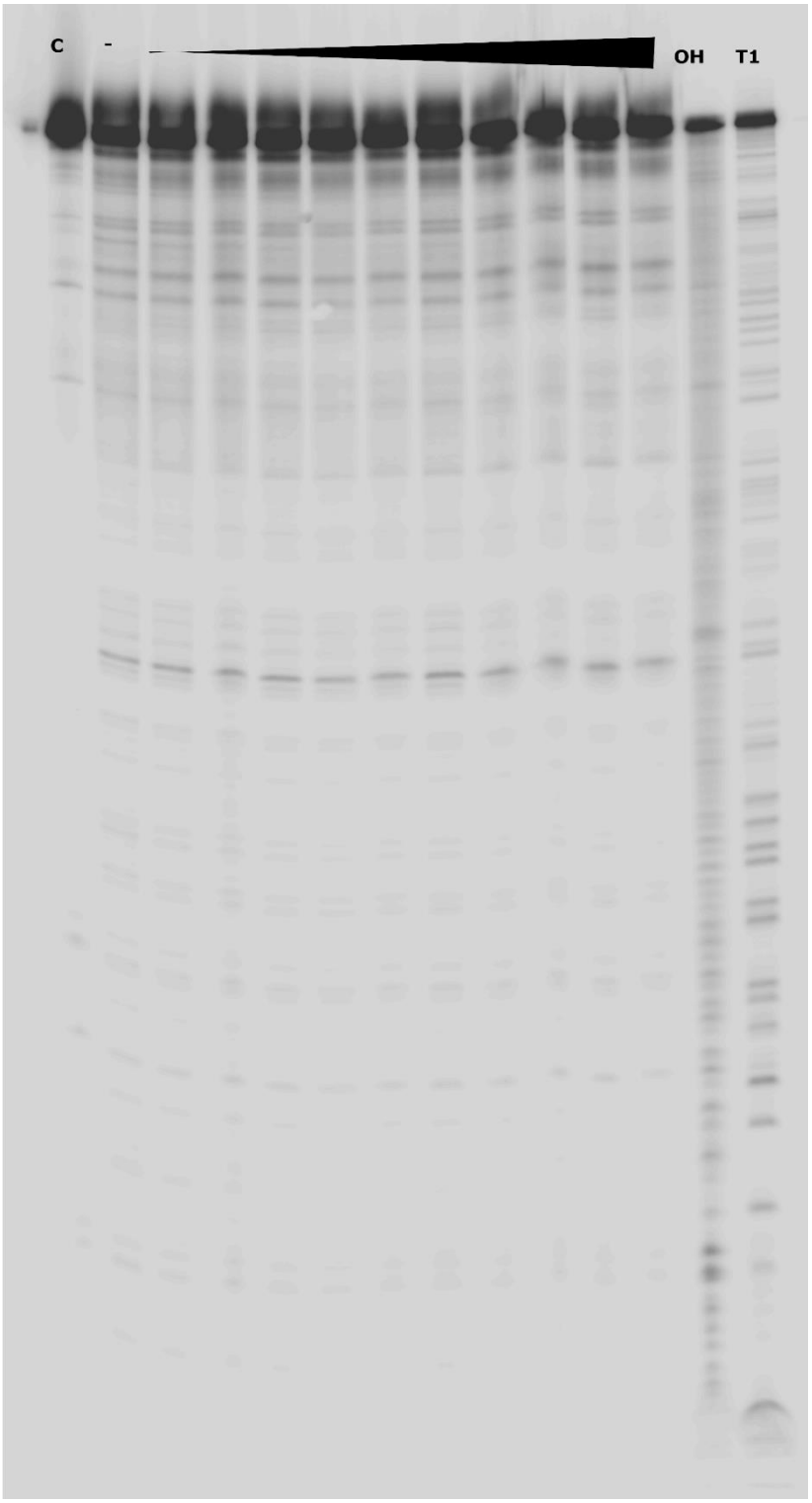

Background zones of the gels and R calculation

Gel A

Pocket	Zone 1		Zone 2		R average
	Intensity 1	R_1	Intensity 2	R_2	
A	3021.63	0.981	337.65	1.000	0.990
B	1028.43	0.334	132.97	0.394	0.364
C	2608.70	0.847	286.06	0.847	0.847
D	2833.97	0.920	265.13	0.785	0.853
E	2717.19	0.882	237.10	0.702	0.792
F	2993.00	0.971	326.04	0.966	0.969
G	2824.82	0.917	258.80	0.766	0.842
H	2760.38	0.896	209.27	0.620	0.758
I	2847.65	0.924	236.38	0.700	0.812
J	2902.98	0.942	217.41	0.644	0.793
K	3081.05	1.000	201.99	0.598	0.799

Gel B

Pocket	Zone 1		Zone 2		R average
	Intensity 1	R_1	Intensity 2	R_2	
A	3631.73	0.886	321.87	0.847	0.867
B	3974.10	0.970	314.81	0.828	0.899
C	3615.65	0.882	331.02	0.871	0.877
D	3889.87	0.949	320.48	0.843	0.896
E	3296.41	0.804	256.95	0.676	0.740
F	3086.57	0.753	295.92	0.779	0.766
G	4098.29	1.000	380.03	1.000	1.000
H	3862.15	0.942	271.22	0.714	0.828
I	3409.18	0.832	239.02	0.629	0.730
J	3967.42	0.968	297.75	0.783	0.876
K	3459.07	0.844	243.90	0.642	0.743

Intensity corrected values for the bands and the 1:1 isotherm fitting.

Band 1

Pocket	[AdoCbl] μM	$I_{corrected}$ Gel B	$I_{corrected}$ Gel A	$I_{Corrected}/10^3$ Gel B	$I_{Corrected}/10^3$ Gel A
A	0	272.69	203.44	0.273	0.203
B	0.05	-	-	-	-
C	0.1	254.82	-	0.255	-
D	0.2	214.92	-	0.215	-
E	0.3	207.54	174.24	0.208	0.174
F	0.4	218.71	-	0.219	-
G	0.5	-	170.40	-	0.170
H	1	162.01	147.65	0.162	0.148
I	2.5	163.68	150.46	0.164	0.150
J	10	149.24	136.36	0.149	0.136
K	100	147.00	120.91	0.147	0.121

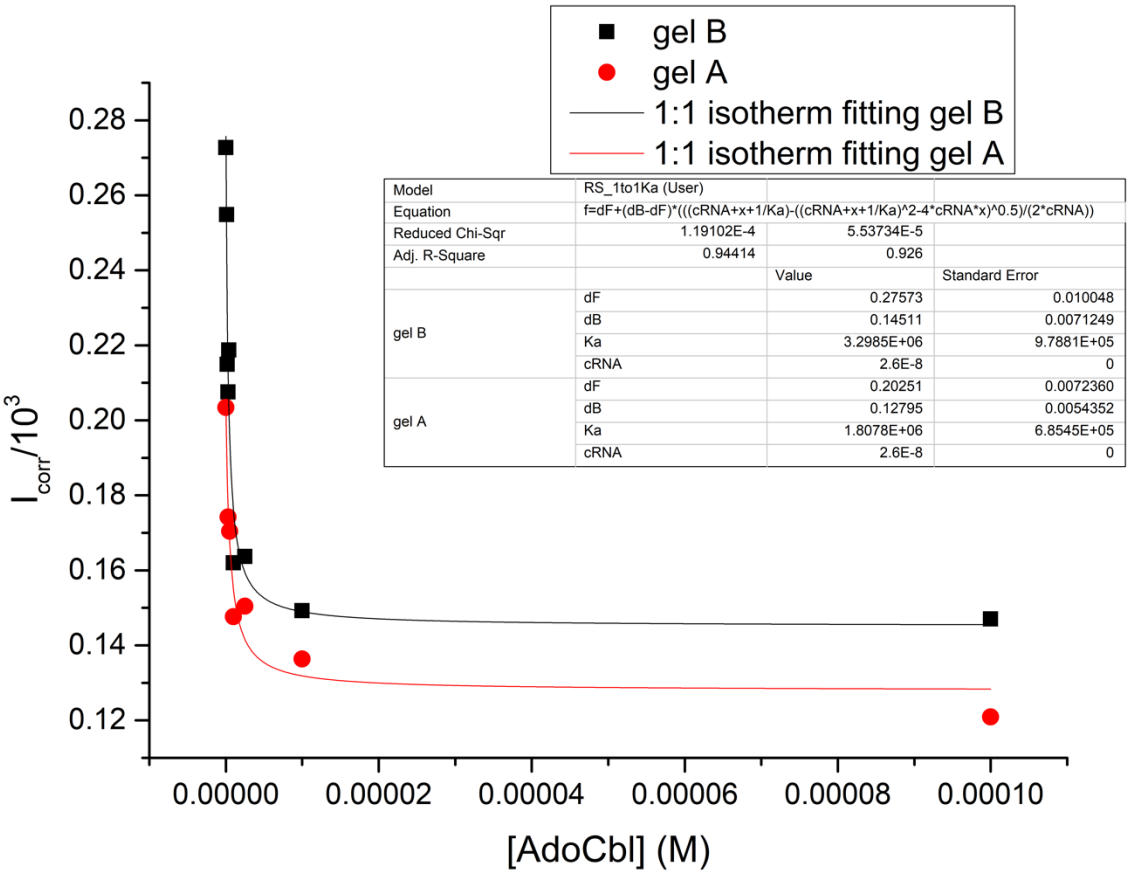

Band 2

Pocket	[AdoCbl] µM	$I_{corrected}$ Gel B	$I_{corrected}$ Gel A	$I_{Corrected}/10^3$ Gel B	$I_{Corrected}/10^3$ Gel A
A	0	338.55	-	0.339	-
B	0.05	312.40	235.50	0.312	0.236
C	0.1	236.54	208.99	0.237	0.209
D	0.2	217.44	188.47	0.217	0.188
E	0.3	229.01	228.90	0.229	0.229
F	0.4	225.38	188.77	0.225	0.189
G	0.5	187.54	160.95	0.188	0.161
H	1	187.23	162.28	0.187	0.162
I	2.5	171.10	142.61	0.171	0.143
J	10	159.35	129.93	0.159	0.130
K	100	147.00	120.91	0.147	0.121

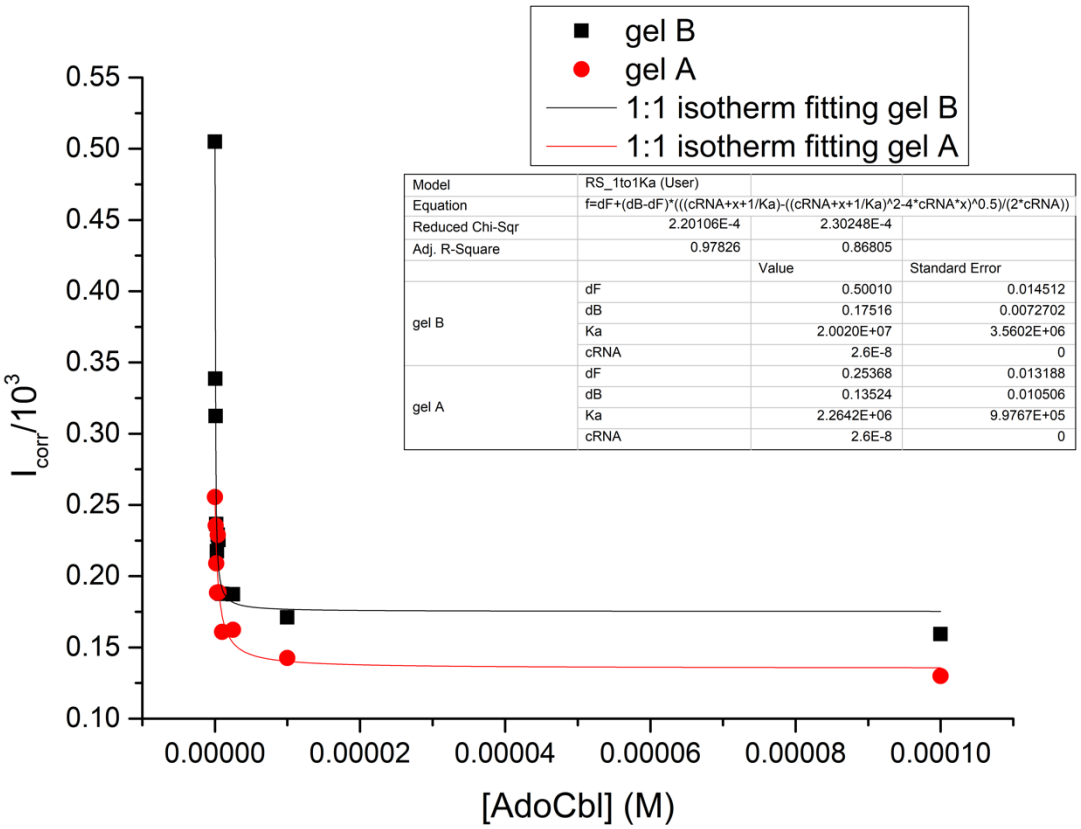

Band 2'

Pocket	[AdoCbl] μM	$I_{corrected}$ Gel B	$I_{corrected}$ Gel A	$I_{Corrected}/10^3$ Gel B	$I_{Corrected}/10^3$ Gel A
A	0	362.76	210.14	0.363	0.210
B	0.05	312.95	-	0.313	-
C	0.1	320.62	-	0.321	-
D	0.2	264.92	204.54	0.265	0.205
E	0.3	254.49	190.19	0.254	0.190
F	0.4	282.07	-	0.282	-
G	0.5	266.33	179.91	0.266	0.180
H	1	223.60	161.84	0.224	0.162
I	2.5	224.92	152.10	0.225	0.152
J	10	205.68	134.99	0.206	0.135
K	100	194.33	123.27	0.194	0.123

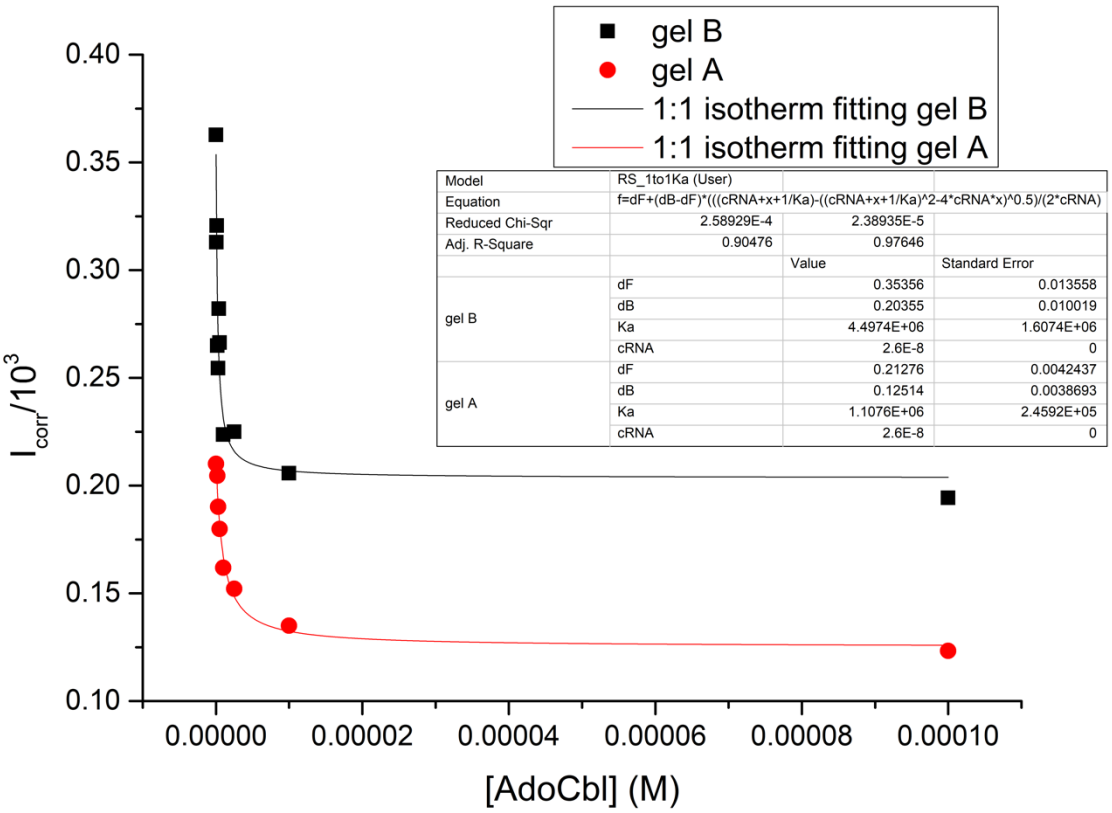

Model	RS_1to1Ka (User)		
Equation	f=dF+(dB-dF)*(((cRNA+x+1/Ka)-((cRNA+x+1/Ka)^2-4*cRNA*x)^0.5)/(2*cRNA)		
Reduced Chi-Sqr	2.58929E-4	2.38935E-5	
Adj. R-Square	0.90476	0.97646	
		Value	Standard Error
gel B	dF	0.35356	0.013558
	dB	0.20355	0.010019
	Ka	4.4974E+06	1.6074E+06
	cRNA	2.6E-8	0
gel A	dF	0.21276	0.0042437
	dB	0.12514	0.0038693
	Ka	1.1076E+06	2.4592E+05
	cRNA	2.6E-8	0

Band 3

Pocket	[AdoCbl] μM	$I_{corrected}$ Gel B	$I_{corrected}$ Gel A	$I_{Corrected}/10^3$ Gel B	$I_{Corrected}/10^3$ Gel A
A	0	-	226.76	-	0.227
B	0.05	-	207.86	-	0.208
C	0.1	-	-	-	-
D	0.2	-	215.39	-	0.215
E	0.3	-	204.09	-	0.204
F	0.4	-	-	-	-
G	0.5	-	195.79	-	0.196
H	1	-	180.18	-	0.180
I	2.5	-	181.08	-	0.181
J	10	-	162.60	-	0.163
K	100	-	158.68	-	0.159

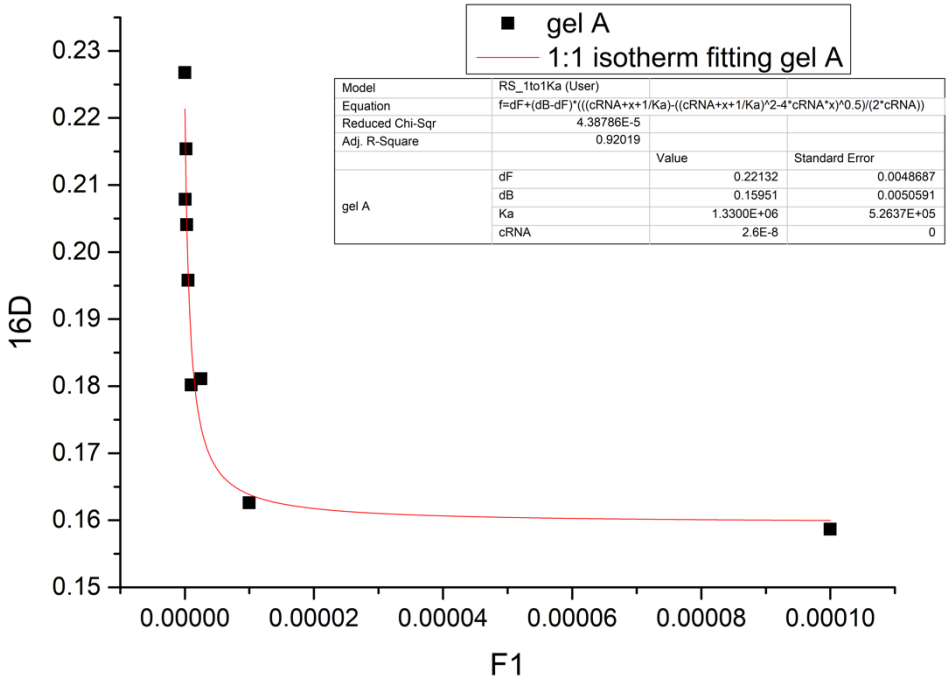

Band 4

Pocket	[AdoCbl] μM	$I_{corrected}$ Gel B	$I_{corrected}$ Gel A	$I_{Corregida}/10^3$ Gel B	$I_{Corregida}/10^3$ Gel A
A	0	667.14	402.09	0.667	0.402
B	0.05	510.40	-	0.510	-
C	0.1	512.89	389.99	0.513	0.390
D	0.2	393.98	361.65	0.394	0.362
E	0.3	360.26	307.58	0.360	0.308
F	0.4	374.20	325.89	0.374	0.326
G	0.5	385.09	296.76	0.385	0.297
H	1	-	265.46	-	0.265
I	2.5	350.41	244.63	0.350	0.245
J	10	316.26	-	0.316	-
K	100	305.92	213.62	0.306	0.214

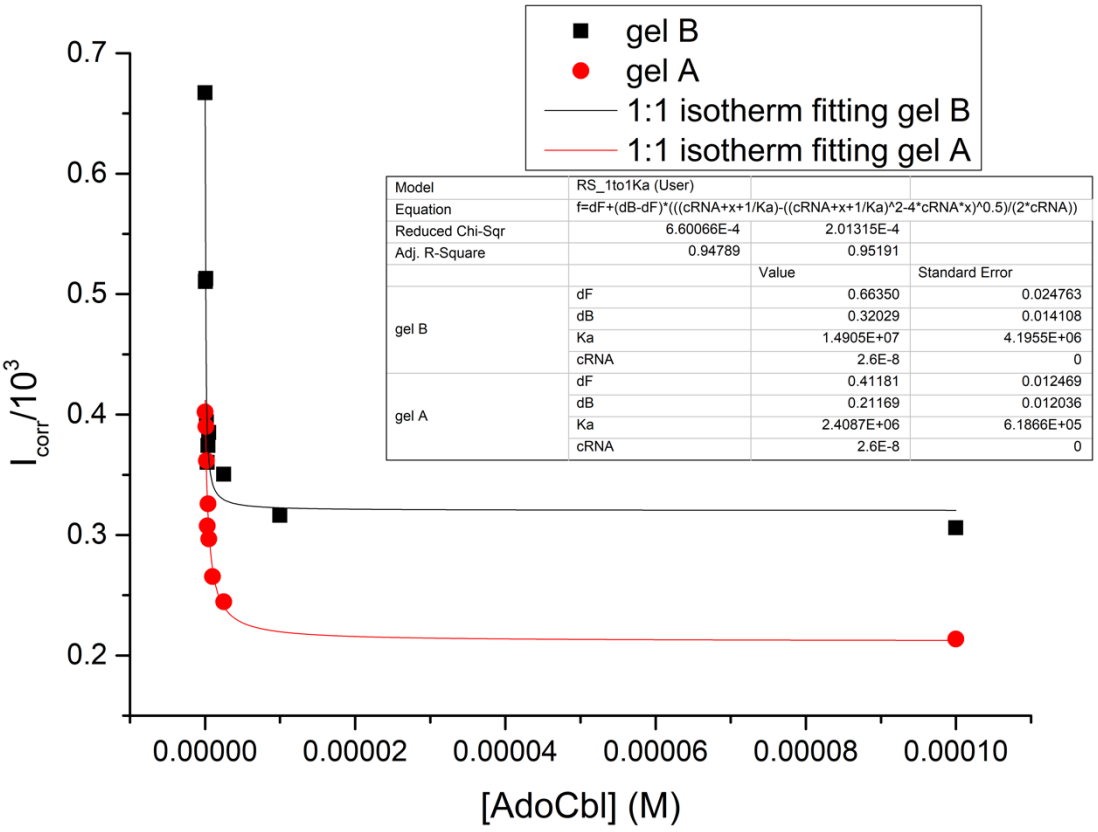

Model	RS_1to1Ka (User)		
Equation	f=dF+(dB-dF)*(((cRNA+x+1/Ka)-((cRNA+x+1/Ka)^2-4*cRNA*x)^0.5)/(2*cRNA))		
Reduced Chi-Sqr	6.60066E-4	2.01315E-4	
Adj. R-Square	0.94789	0.95191	
		Value	Standard Error
gel B	dF	0.66350	0.024763
	dB	0.32029	0.014108
	Ka	1.4905E+07	4.1955E+06
	cRNA	2.6E-8	0
gel A	dF	0.41181	0.012469
	dB	0.21169	0.012036
	Ka	2.4087E+06	6.1866E+05
	cRNA	2.6E-8	0

Band 4'

Pocket	[AdoCbl] μM	$I_{corrected}$ Gel B	$I_{corrected}$ Gel A	$I_{Corregida}/10^3$ Gel B	$I_{Corregida}/10^3$ Gel A
A	0	543.33	387.86	0.543	0.388
B	0.05	433.26	-	0.433	-
C	0.1	440.11	367.81	0.440	0.368
D	0.2	357.89	333.02	0.358	0.333
E	0.3	350.43	290.72	0.350	0.291
F	0.4	360.16	298.02	0.360	0.298
G	0.5	348.69	273.40	0.349	0.273
H	1	297.91	232.89	0.298	0.233
I	2.5	295.61	-	0.296	-
J	10	-	211.01	-	0.211
K	100	228.12	182.80	0.228	0.183

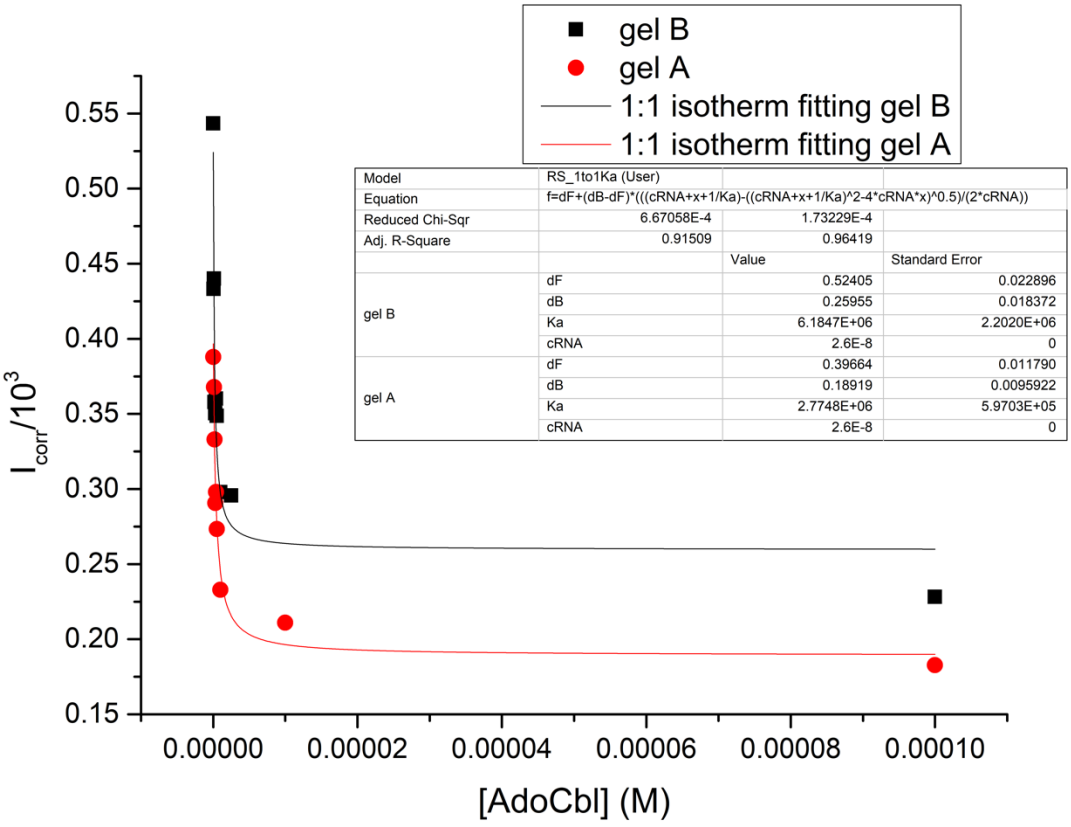

Model	RS_1to1Ka (User)		
Equation	f=dF+(dB-dF)*((((cRNA+x+1/Ka)-((cRNA+x+1/Ka)^2-4*cRNA*x)^0.5)/(2*cRNA))		
Reduced Chi-Sqr	6.67058E-4	1.73229E-4	
Adj. R-Square	0.91509	0.96419	
		Value	Standard Error
gel B	dF	0.52405	0.022896
	dB	0.25955	0.018372
	Ka	6.1847E+06	2.2020E+06
	cRNA	2.6E-8	0
gel A	dF	0.39664	0.011790
	dB	0.18919	0.0095922
	Ka	2.7748E+06	5.9703E+05
	cRNA	2.6E-8	0

Band 5

Pocket	[AdoCbl] μM	$I_{corrected}$ Gel B	$I_{corrected}$ Gel A	$I_{Corrected}/10^3$ Gel B	$I_{Corrected}/10^3$ Gel A
A	0	-	227.06	-	0.227
B	0.05	-	-	-	-
C	0.1	-	222.43	-	0.222
D	0.2	-	217.64	-	0.218
E	0.3	-	212.78	-	0.213
F	0.4	-	-	-	-
G	0.5	-	209.27	-	0.209
H	1	-	201.56	-	0.202
I	2.5	-	191.48	-	0.191
J	10	-	-	-	-
K	100	-	179.56	-	0.180

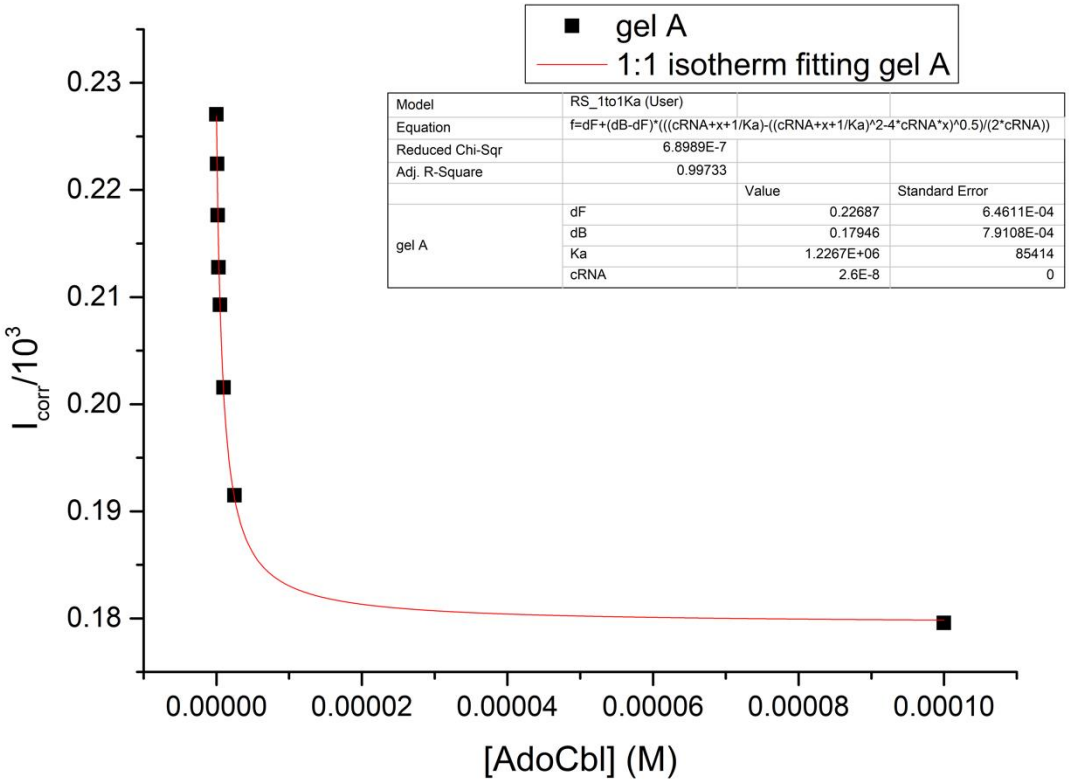

Band 6

Pocket	[AdoCbl] μM	$I_{corrected}$ Gel B	$I_{corrected}$ Gel A	$I_{Corrected}/10^3$ Gel B	$I_{Corrected}/10^3$ Gel A
A	0	557.10	-	0.557	-
B	0.05	511.33	-	0.511	-
C	0.1	469.24	-	0.469	-
D	0.2	-	-	-	-
E	0.3	448.80	-	0.449	-
F	0.4	447.90	-	0.448	-
G	0.5	-	-	-	-
H	1	-	-	-	-
I	2.5	440.28	-	0.440	-
J	10	-	-	-	-
K	100	431.68	-	0.432	-

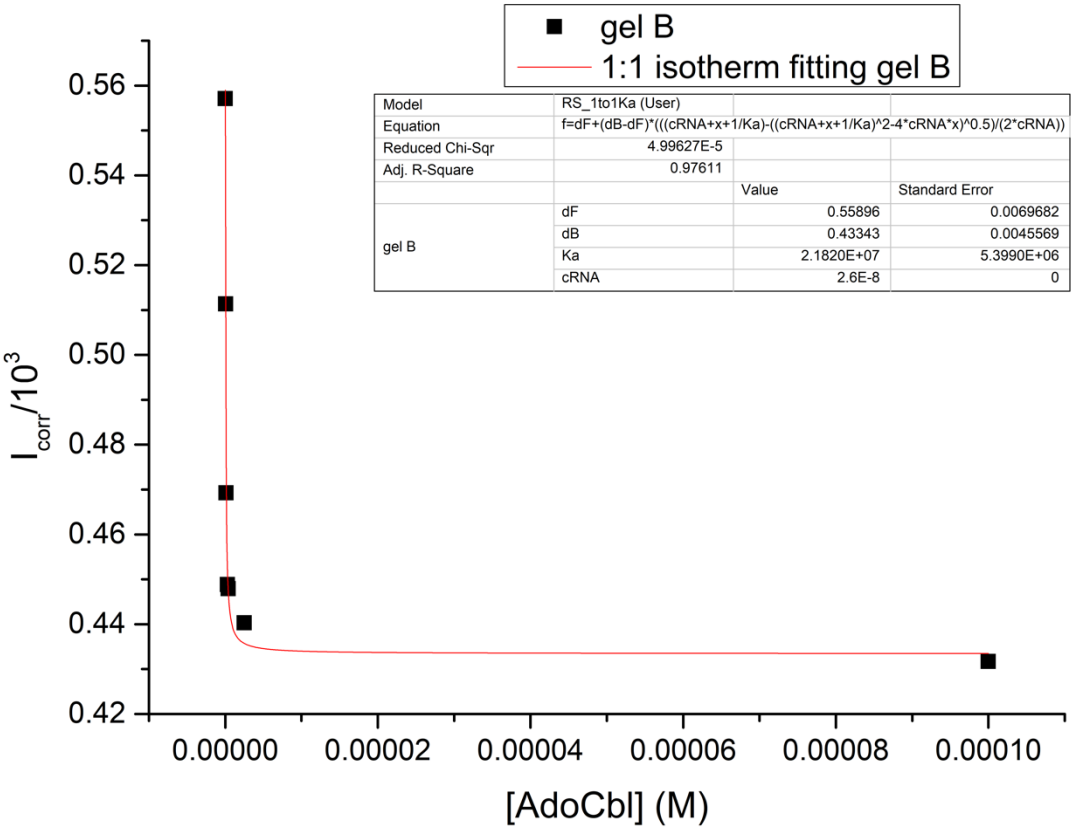

Band 7

Pocket	[AdoCbl] μM	$I_{corrected}$ Gel B	$I_{corrected}$ Gel A	$I_{Corrected}/10^3$ Gel B	$I_{Corrected}/10^3$ Gel A
A	0	820.29	520.72	0.820	0.521
B	0.05	738.44	-	0.738	-
C	0.1	742.03	-	0.742	-
D	0.2	677.72	-	0.678	-
E	0.3	663.90	516.96	0.664	0.517
F	0.4	655.04	503.54	0.655	0.504
G	0.5	664.22	490.28	0.664	0.490
H	1	-	465.34	-	0.465
I	2.5	659.02	435.99	0.659	0.436
J	10	-	406.23	-	0.406
K	100	598.12	396.97	0.598	0.397

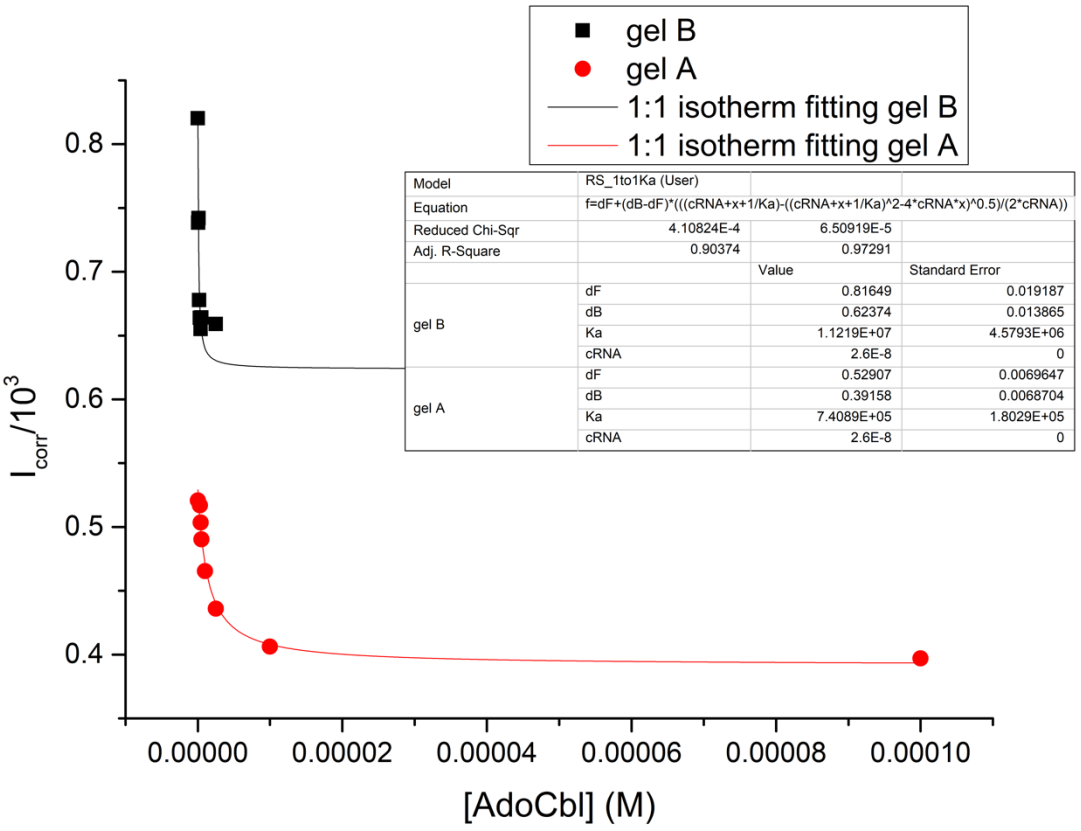

Model	RS_1to1Ka (User)		
Equation	f=dF+(dB-dF)*(((cRNA+x+1/Ka)-((cRNA+x+1/Ka)^2-4*cRNA*x)^0.5)/(2*cRNA))		
Reduced Chi-Sqr	4.10824E-4	6.50919E-5	
Adj. R-Square	0.90374	0.97291	
		Value	Standard Error
gel B	dF	0.81649	0.019187
	dB	0.62374	0.013865
	Ka	1.1219E+07	4.5793E+06
	cRNA	2.6E-8	0
gel A	dF	0.52907	0.0069647
	dB	0.39158	0.0068704
	Ka	7.4089E+05	1.8029E+05
	cRNA	2.6E-8	0

Band 8

Pocket	[AdoCbl] μM	$I_{corrected}$ Gel B	$I_{corregida}$ Gel A	$I_{Corregida}/10^3$ Gel B	$I_{Corregida}/10^3$ Gel A
A	0	381.72	-	0.382	-
B	0.05	428.02	-	0.428	-
C	0.1	438.72	-	0.439	-
D	0.2	464.10	-	0.464	-
E	0.3	507.65	-	0.508	-
F	0.4	515.99	-	0.516	-
G	0.5	479.48	-	0.479	-
H	1	497.63	-	0.498	-
I	2.5	-	-	-	-
J	10	-	-	-	-
K	100	533.07	-	0.533	-

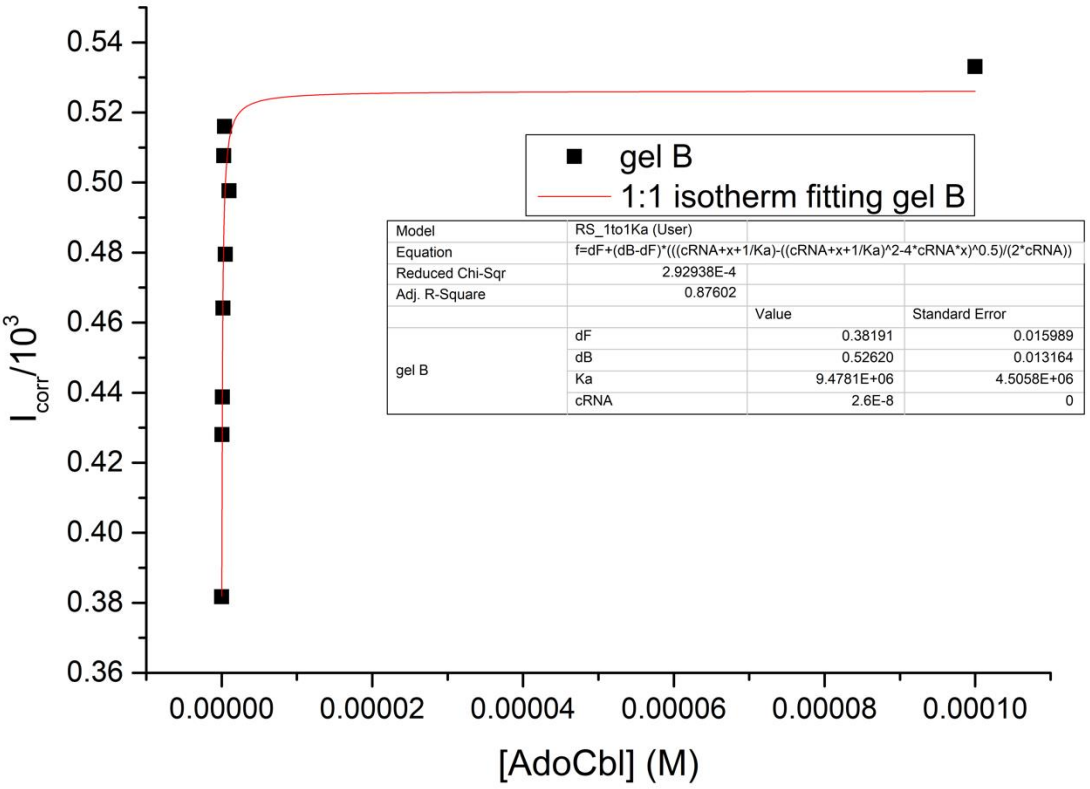

Band 8'

Pocket	[AdoCbl] μM	$I_{corrected}$ Gel B	$I_{corrected}$ Gel A	$I_{Corrected}/10^3$ Gel B	$I_{Corrected}/10^3$ Gel A
A	0	553.07	391.00	0.553	0.391
B	0.05	596.74	-	0.597	-
C	0.1	582.09	446.56	0.582	0.447
D	0.2	608.05	461.73	0.608	0.462
E	0.3	617.40	458.73	0.617	0.459
F	0.4	632.95	-	0.633	-
G	0.5	622.91	462.30	0.623	0.462
H	1	658.18	481.72	0.658	0.482
I	2.5	691.45	485.52	0.691	0.486
J	10	-	-	-	-
K	100	717.68	488.97	0.718	0.489

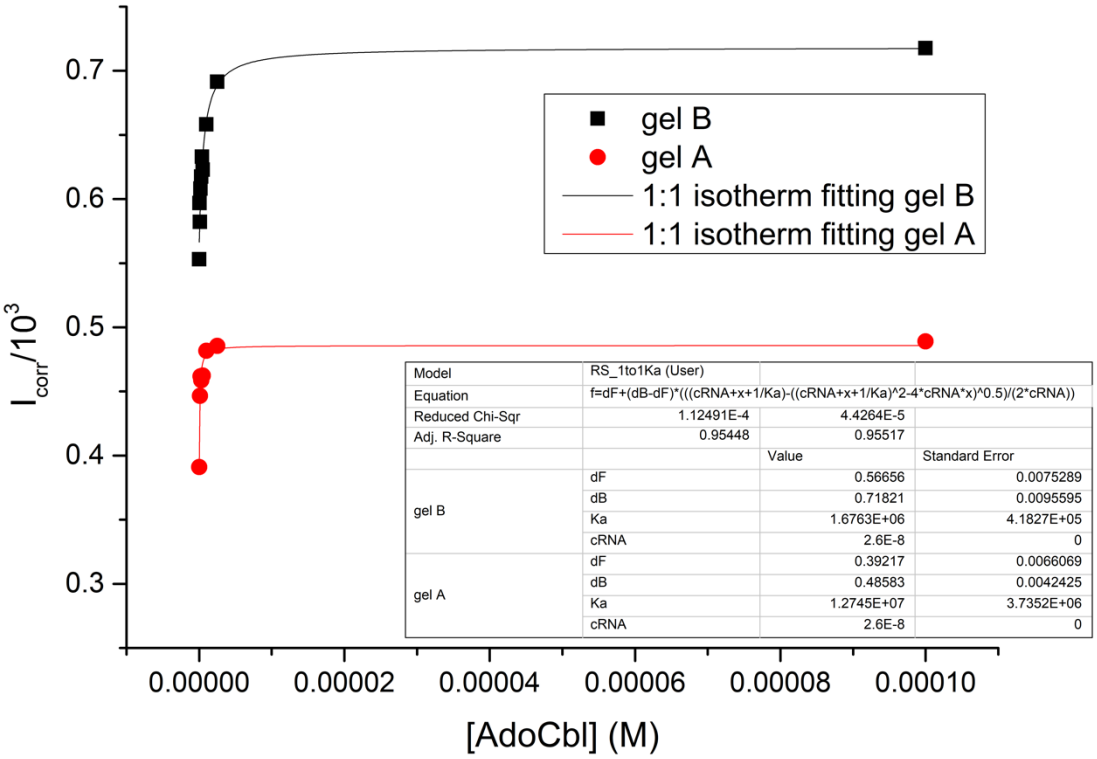

Model	RS_1to1Ka (User)		
Equation	f=dF+(dB-dF)*(((cRNA+x+1/Ka)-((cRNA+x+1/Ka)^2-4*cRNA*x)^0.5)/(2*cRNA))		
Reduced Chi-Sqr	1.12491E-4	4.4264E-5	
Adj. R-Square	0.95448	0.95517	
		Value	Standard Error
gel B	dF	0.56656	0.0075289
	dB	0.71821	0.0095595
	Ka	1.6763E+06	4.1827E+05
	cRNA	2.6E-8	0
gel A	dF	0.39217	0.0066069
	dB	0.48583	0.0042425
	Ka	1.2745E+07	3.7352E+06
	cRNA	2.6E-8	0

Band 9

Pocket	[AdoCbl] μM	$I_{corrected}$ Gel B	$I_{corrected}$ Gel A	$I_{Corrected}/10^3$ Gel B	$I_{Corrected}/10^3$ Gel A
A	0	691.00	556.19	0.691	0.556
B	0.05	616.04	-	0.616	-
C	0.1	609.31	502.60	0.609	0.503
D	0.2	546.63	477.52	0.547	0.478
E	0.3	546.84	412.77	0.547	0.413
F	0.4	560.45	379.04	0.560	0.379
G	0.5	515.68	383.54	0.516	0.384
H	1	463.79	331.67	0.464	0.332
I	2.5	432.60	297.44	0.433	0.297
J	10	-	282.27	-	0.282
K	100	409.47	270.10	0.409	0.270

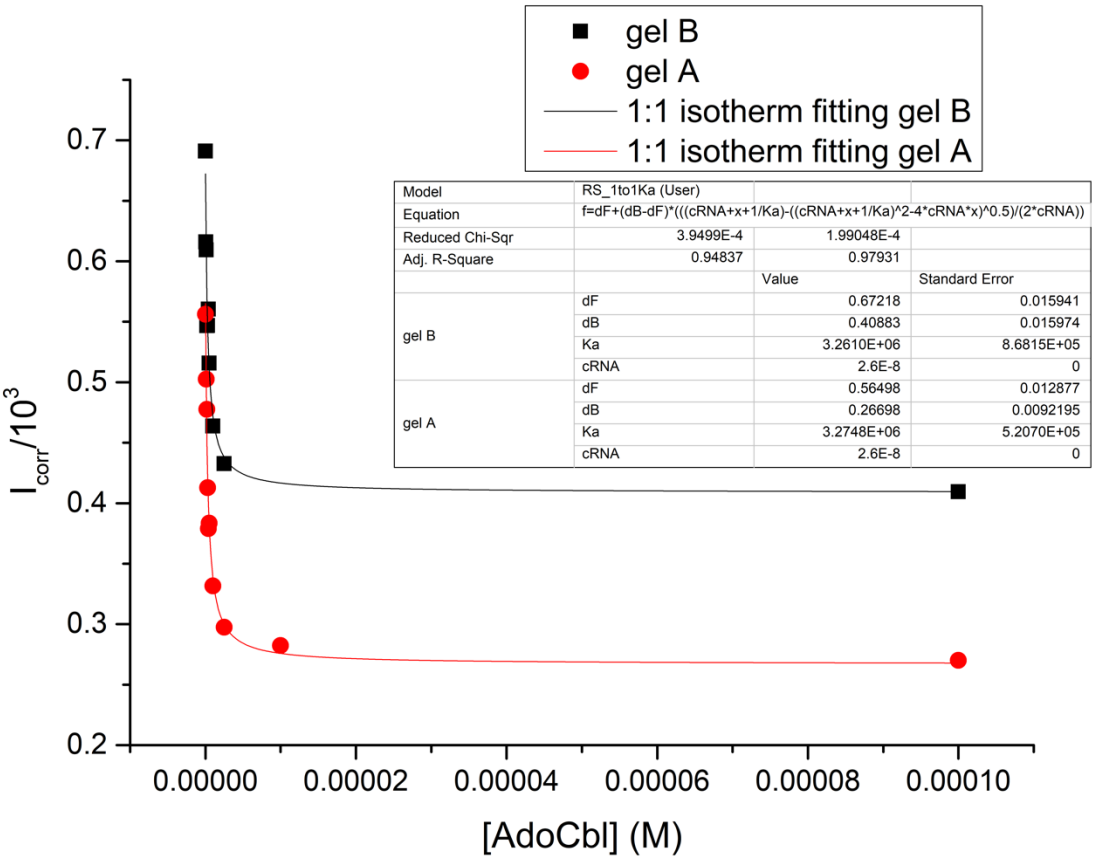

Model	RS_1to1Ka (User)		
Equation	f=dF+(dB-dF)*(((cRNA+x+1/Ka)-((cRNA+x+1/Ka)^2-4*cRNA*x)^0.5)/(2*cRNA))		
Reduced Chi-Sqr	3.9499E-4	1.99048E-4	
Adj. R-Square	0.94837	0.97931	
		Value	Standard Error
gel B	dF	0.67218	0.015941
	dB	0.40883	0.015974
	Ka	3.2610E+06	8.6815E+05
	cRNA	2.6E-8	0
gel A	dF	0.56498	0.012877
	dB	0.26698	0.0092195
	Ka	3.2748E+06	5.2070E+05
	cRNA	2.6E-8	0

Band 10

Pocket	[AdoCbl] μM	$I_{corrected}$ Gel B	$I_{corrected}$ Gel A	$I_{Corrected}/10^3$ Gel B	$I_{Corrected}/10^3$ Gel A
A	0	1150.47	-	1.150	-
B	0.05	1285.20	-	1.285	-
C	0.1	-	-	-	-
D	0.2	1300.22	-	1.300	-
E	0.3	1349.76	-	1.350	-
F	0.4	-	-	-	-
G	0.5	1351.77	-	1.352	-
H	1	1416.57	-	1.417	-
I	2.5	1434.11	-	1.434	-
J	10	-	-	-	-
K	100	1555.53	-	1.556	-

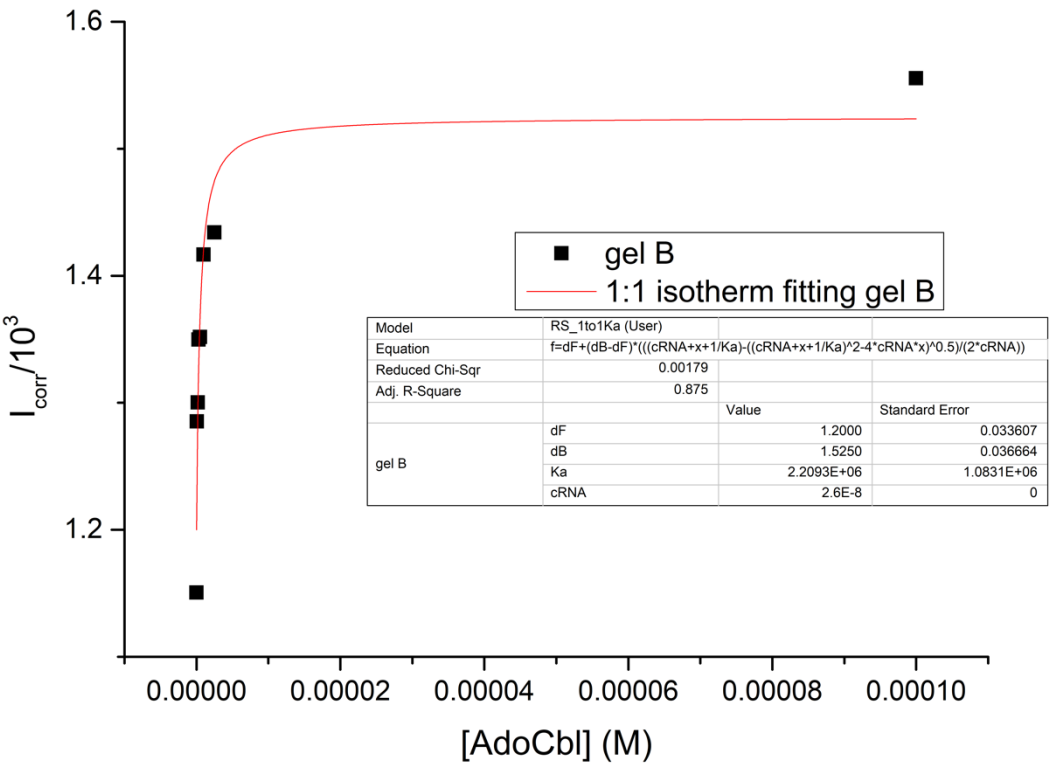

Band 11

Pocket	[AdoCbl] μM	$I_{corrected}$ Gel B	$I_{corrected}$ Gel A	$I_{Corrected}/10^3$ Gel B	$I_{Corrected}/10^3$ Gel A
A	0	2303.55	1938.39	2.304	1.938
B	0.05	2159.68	-	2.160	-
C	0.1	2010.21	1887.15	2.010	1.887
D	0.2	1911.11	1893.81	1.911	1.894
E	0.3	1864.84	1743.39	1.865	1.743
F	0.4	1931.27	-	1.931	-
G	0.5	1857.46	1709.32	1.857	1.709
H	1	-	1589.19	-	1.589
I	2.5	1886.45	1508.94	1.886	1.509
J	10	-	-	-	-
K	100	1825.12	1500.69	1.825	1.501

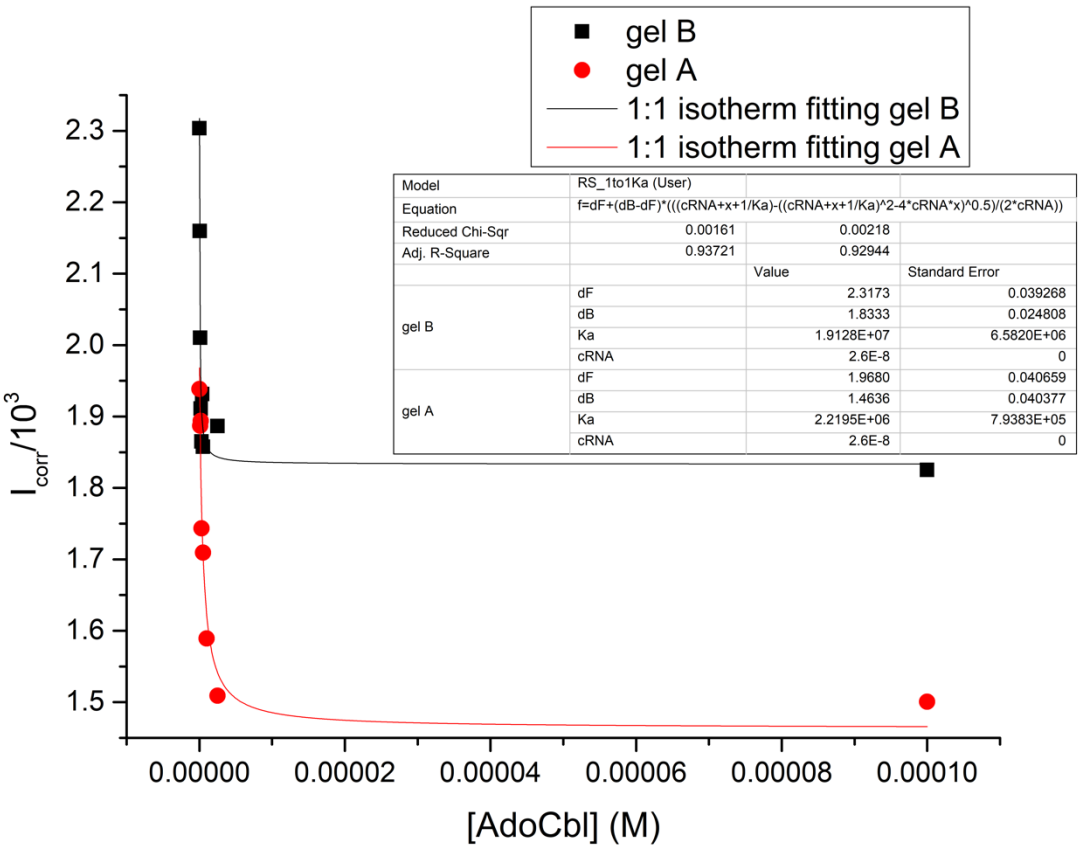

Model	RS_1to1Ka (User)		
Equation	f=dF+(dB-dF)*(((cRNA+x+1/Ka)-((cRNA+x+1/Ka)^2-4*cRNA*x)^0.5)/(2*cRNA))		
Reduced Chi-Sqr	0.00161	0.00218	
Adj. R-Square	0.93721	0.92944	
		Value	Standard Error
gel B	dF	2.3173	0.039268
	dB	1.8333	0.024808
	Ka	1.9128E+07	6.5820E+06
	cRNA	2.6E-8	0
gel A	dF	1.9680	0.040659
	dB	1.4636	0.040377
	Ka	2.2195E+06	7.9383E+05
	cRNA	2.6E-8	0

Band 12

Pocket	[AdoCbl] µM	$I_{corrected}$ Gel B	$I_{corrected}$ Gel A	$I_{Corrected}/10^3$ Gel B	$I_{Corrected}/10^3$ Gel A
A	0	1921.11	1508.31	1.921	1.508
B	0.05	1677.53	-	1.678	-
C	0.1	1702.52	1518.99	1.703	1.519
D	0.2	1505.46	1402.50	1.505	1.403
E	0.3	1432.47	1290.95	1.432	1.291
F	0.4	1306.40	1241.94	1.306	1.242
G	0.5	1282.99	1124.71	1.283	1.125
H	1	1223.45	1047.27	1.223	1.047
I	2.5	-	949.65	-	0.950
J	10	-	864.39	-	0.864
K	100	1028.27	822.86	1.028	0.823

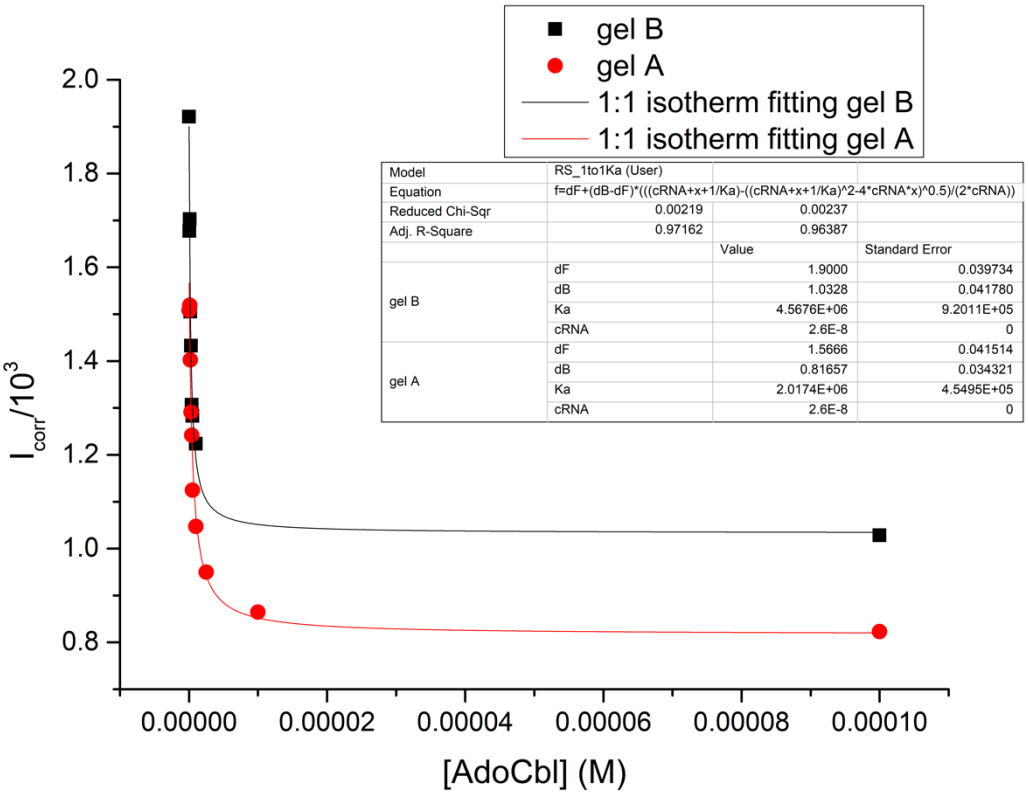

Model	RS_1to1Ka (User)		
Equation	f=dF+(dB-dF)*(((cRNA+x+1/Ka)-((cRNA+x+1/Ka)^2-4*cRNA*x)^0.5)/(2*cRNA))		
Reduced Chi-Sqr	0.00219	0.00237	
Adj. R-Square	0.97162	0.96387	
		Value	Standard Error
gel B	dF	1.9000	0.039734
	dB	1.0328	0.041780
	Ka	4.5676E+06	9.2011E+05
	cRNA	2.6E-8	0
gel A	dF	1.5666	0.041514
	dB	0.81657	0.034321
	Ka	2.0174E+06	4.5495E+05
	cRNA	2.6E-8	0

Band 13

Pocket	[AdoCbl] µM	$I_{correted}$ Gel B	$I_{corrected}$ Gel A	$I_{Corrected}/10^3$ Gel B	$I_{Corrected}/10^3$ Gel A
A	0	2457.70	1808.57	2.458	1.809
B	0.05	2730.45	-	2.730	-
C	0.1	2739.01	1929.68	2.739	1.930
D	0.2	2672.64	2082.28	2.673	2.082
E	0.3	2909.02	2073.66	2.909	2.074
F	0.4	2783.01	-	2.783	-
G	0.5	-	2165.40	-	2.165
H	1	2940.18	2247.09	2.940	2.247
I	2.5	-	2176.39	-	2.176
J	10	3117.62	2311.76	3.118	2.312
K	100	3386.95	2439.30	3.387	2439

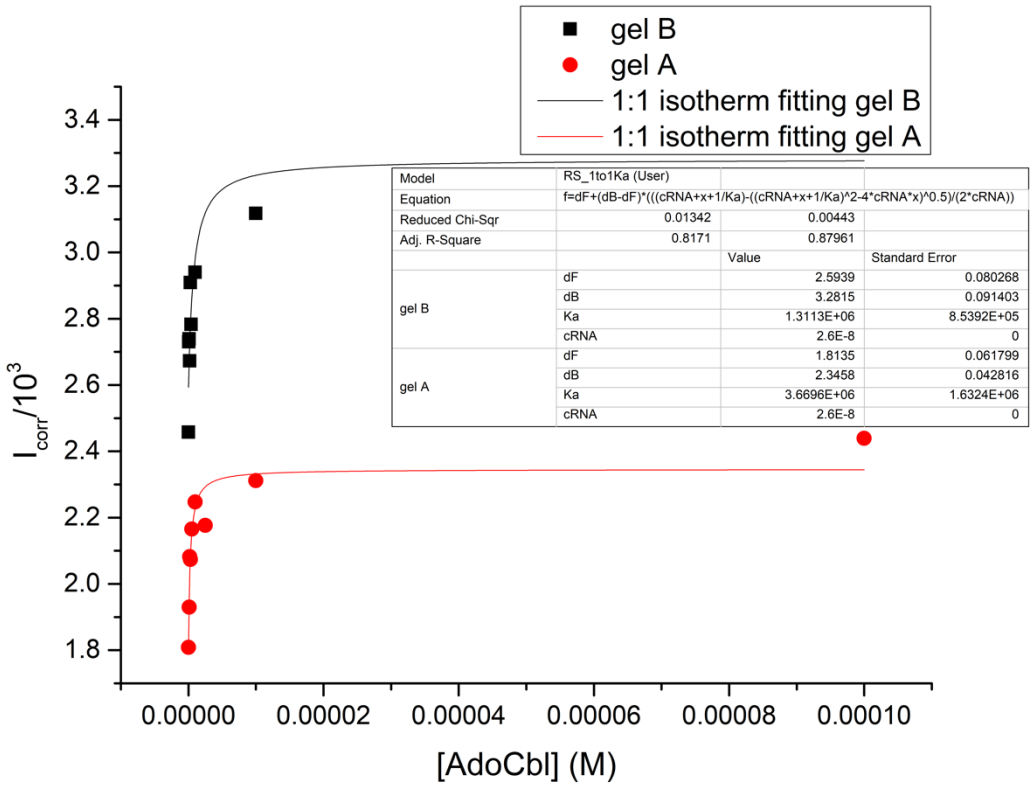

Band 14

Pocket	[AdoCbl] μM	$I_{corrected}$ Gel B	$I_{corrected}$ Gel A	$I_{Corrected}/10^3$ Gel B	$I_{Corrected}/10^3$ Gel A
A	0	3737.16	-	3.737	-
B	0.05	3524.08	-	3.524	-
C	0.1	3374.96	-	3.375	-
D	0.2	3191.43	-	3.191	-
E	0.3	3188.68	-	3.189	-
F	0.4	-	-	-	-
G	0.5	2906.67	-	2.907	-
H	1	2904.54	-	2.905	-
I	2.5	2641.53	-	2.642	-
J	10	2459.16	-	2.459	-
K	100	2409.06	-	2.409	-

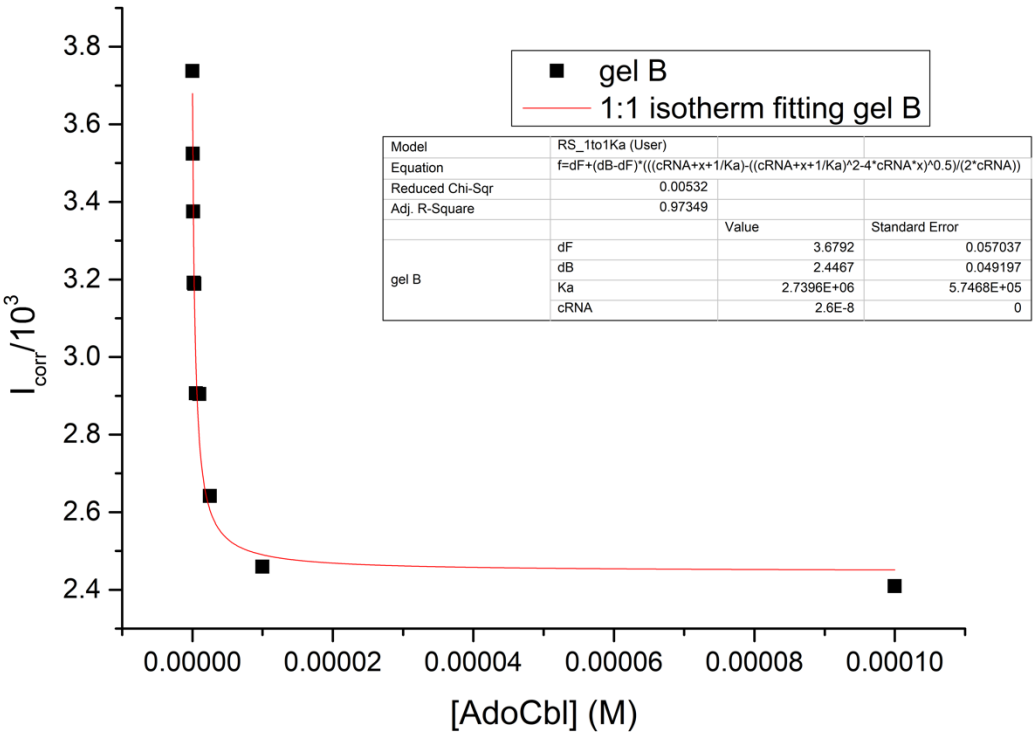

Band 15

Pocket	[AdoCbl] μM	$I_{corrected}$ Gel B	$I_{corrected}$ Gel A	$I_{Corrected}/10^3$ Gel B	$I_{Corrected}/10^3$ Gel A
A	0	-	-	-	-
B	0.05	7105.96	4735.72	7.106	4.736
C	0.1	6552.91	-	6.553	-
D	0.2	7543.01	5769.16	7.543	5.769
E	0.3	8159.16	6566.59	8.159	6.567
F	0.4	7160.25	6765.11	7.160	6.765
G	0.5	7212.64	5849.22	7.213	5.849
H	1	8203.45	6754.62	8.203	6.755
I	2.5	-	7374.93	-	7.375
J	10	8411.59	7199.70	8.412	7.200
K	100	8500.54	7399.22	8.501	7.399

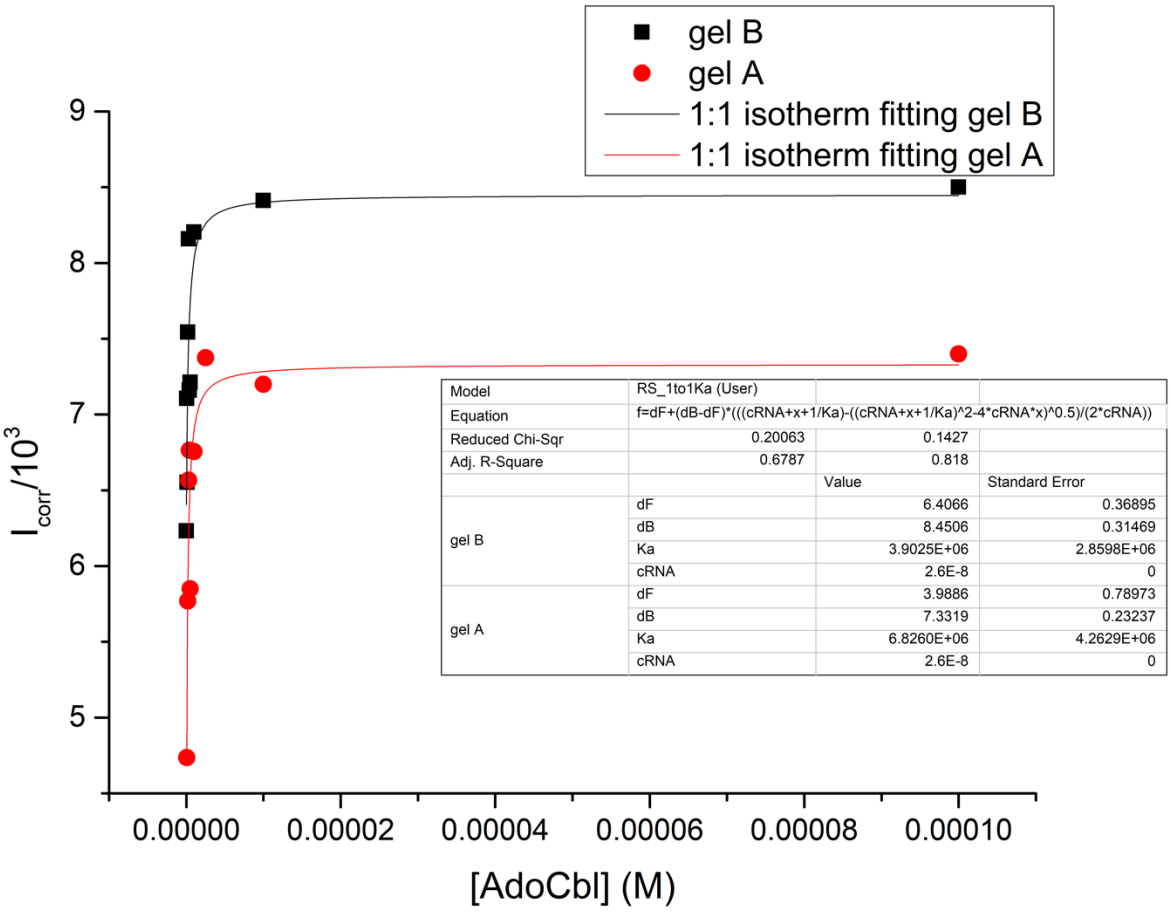

Model	RS_1to1Ka (User)		
Equation	f=dF+(dB-dF)*(((cRNA+x+1/Ka)-((cRNA+x+1/Ka)^2-4*cRNA*x)^0.5)/(2*cRNA))		
Reduced Chi-Sqr	0.20063	0.1427	
Adj. R-Square	0.6787	0.818	
		Value	Standard Error
gel B	dF	6.4066	0.36895
	dB	8.4506	0.31469
	Ka	3.9025E+06	2.8598E+06
	cRNA	2.6E-8	0
gel A	dF	3.9886	0.78973
	dB	7.3319	0.23237
	Ka	6.8260E+06	4.2629E+06
	cRNA	2.6E-8	0

Appendix 3. Isothermal titration calorimetry data

Individual ITC experiments for JP01

T (K)	Ka/10^6	log Ka	ΔH (kJ/mol)	n	ΔS (J/K mol)	K_D (nM)
303.15	1.22	6.09	-131.2	1.002	-316.1	820
303.15	0.97	5.99	-128.3	0.886	-308.7	1026
303.15	0.81	5.91	-137.4	0.853	-340.0	1240
300.65	1.39	6.14	-119.1	0.702	-278.7	722
300.65	1.70	6.23	-142.2	0.844	-353.8	588
300.65	2.00	6.30	-114.5	0.633	-260.0	500
300.65	1.88	6.28	-105.2	0.704	-229.7	531
298.15	1.73	6.24	-119.5	0.808	-281.3	578
298.15	1.82	6.26	-122.2	0.819	-290.2	551
298.15	2.12	6.33	-117.2	1.375	-272.1	472
295.65	2.22	6.35	-101.1	0.779	-220.3	451
295.65	2.44	6.39	-99.1	1.052	-212.8	410
295.65	3.30	6.52	-117.3	0.695	-272.1	303
293.15	4.59	6.66	-86.6	0.923	-167.8	218
293.15	4.76	6.68	-80.9	1.057	-148.1	210
293.15	4.94	6.69	-83.6	0.613	-157.0	202
290.65	4.67	6.67	-65.3	0.681	-96.9	214
290.65	3.06	6.49	-77.7	0.703	-143.1	327
290.65	2.93	6.47	-66.5	0.735	-66.5	342
290.65	2.81	6.45	-93.4	0.696	-198.0	356
290.65	3.73	6.57	-75.7	0.625	-134.5	268
288.15	5.71	6.76	-66.4	0.789	-101.0	175
288.15	5.41	6.73	-55.3	0.835	-63.1	185
288.15	5.16	6.71	-60.3	0.833	-80.7	194

Individual ITC experiments for MB01

T (K)	Ka/10^6	log Ka	ΔH (kJ/mol)	n	ΔS (J/K mol)	K_D (nM)
303.15	1.22	6.09	-131.2	1.002	-316.1	820
303.15	0.97	5.99	-128.3	0.886	-308.7	1026
303.15	0.81	5.91	-137.4	0.853	-340.0	1240
298.15	1.73	6.24	-119.5	0.808	-281.3	578
298.15	1.82	6.26	-122.2	0.819	-290.2	551
298.15	2.12	6.33	-117.2	1.375	-272.1	472
293.15	4.59	6.66	-86.6	0.923	-167.8	218
293.15	4.76	6.68	-80.9	1.057	-148.1	210
293.15	4.94	6.69	-83.6	0.613	-157.0	202
288.15	5.71	6.76	-66.4	0.789	-101.0	175
288.15	5.41	6.73	-55.4	0.835	-63.13	185
288.15	5.16	6.71	-60.3	0.833	-80.71	194